SEMI ANALYTICAL STUDY OF STRESS AND DEFORMATION ANALYSIS OF ANISOTROPIC SHELLS OF REVOLUTION INCLUDING FIRST ORDER TRANSVERSE SHEAR DEFORMATION

A THESIS SUBMITTED TO
THE GRADUATE SCHOOL OF NATURAL AND APPLIED SCIENCES
OF
MIDDLE EAST TECHNICAL UNIVERSITY

BY

ÖZGÜR SİNAN OYGÜR

IN PARTIAL FULFILLMENT OF THE REQUIREMENTS
FOR
THE DEGREE OF MASTER OF SCIENCE
IN
AEROSPACE ENGINEERING

SEPTEMBER 2008

Approval of the thesis:

SEMI ANALYTICAL STUDY OF STRESS AND DEFORMATION ANALYSIS OF ANISOTROPIC SHELLS OF REVOLUTION INCLUDING FIRST ORDER TRANSVERSE SHEAR DEFORMATION

submitted by **ÖZGÜR SİNAN OYGÜR** in partial fulfillment of the requirements for the degree of **Master of Science in Aerospace Engineering Department, Middle East Technical University by,**

Prof. Dr. Canan Özgen _____
Dean, Graduate School of **Natural and Applied Sciences**

Prof. Dr. İsmail Hakkı Tuncer _____
Head of Department, **Aerospace Engineering**

Assoc. Prof. Dr. Altan Kayran
Supervisor, **Aerospace Engineering Dept., METU** _____

Dr. Özge Şen _____
Co-Supervisor, **TÜBİTAK-SAGE**

Examining Committee Members:

Prof. Dr. Ozan Tekinalp _____
Aerospace Engineering Dept., METU

Assoc. Prof. Dr. Altan Kayran _____
Aerospace Engineering Dept., METU

Assist. Prof. Dr. Ferhat Akgül _____
Engineering Sciences Dept., METU

Dr. Güçlü Seber _____
Aerospace Engineering Dept., METU

Dr. Özge Şen _____
TÜBİTAK-SAGE

Date: _____

I hereby declare that all information in this document has been obtained and presented in accordance with academic rules and ethical conduct. I also declare that, as required by these rules and conduct, I have fully cited and referenced all material and results that are not original to this work.

Name, Last name: Özgür Sinan Oygür

Signature :

ABSTRACT

SEMI ANALYTICAL STUDY OF STRESS AND DEFORMATION ANALYSIS OF ANISOTROPIC SHELLS OF REVOLUTION INCLUDING FIRST ORDER TRANSVERSE SHEAR DEFORMATION

Oygür, Özgür Sinan

M.Sc., Department of Aerospace Engineering
Supervisor : Assoc. Prof. Dr. Altan Kayran
Co-Supervisor: Dr. Özge Şen

September 2008, 258 pages

In this study, anisotropic shells of revolution subject to symmetric and unsymmetrical static loads are analysed. In derivation of governing equations to be used in the solution, first order transverse shear effects are included in the formulation. The governing equations can be listed as kinematic equations, constitutive equations, and equations of motion. The equations of motion are derived from Hamilton's principle, the constitutive equations are developed under the assumptions of the classical lamination theory and the kinematic equations are based on the Reissner-Naghdi linear shell theory. In the solution method, these governing equations are manipulated and written as a set called fundamental set of equations. In order to handle anisotropy and first order transverse shear deformations, the fundamental set of equations is transformed into 20 first order ordinary differential equations using finite exponential Fourier decomposition and then solved with multisegment method of integration, after reduction of the two-point boundary value problem to a series of initial value problems. The results are compared with finite element

analysis results for a number of sample cases and good agreement is found. Case studies are performed for circular cylindrical shell and truncated spherical shell geometries. While reviewing the results, effects of temperature and pressure loads, both constant and variable throughout the shell, are discussed. Some drawbacks of the first order transverse shear deformation theory are exhibited.

Keywords: Shell of Revolution, First Order Transverse Shear Deformation, Anisotropy, Finite Exponential Fourier Decomposition, Multisegment Method of Integration

ÖZ

BİRİNCİ DERECEDEN YANAL KESME DEFORMASYONU DAHİL EDİLMİŞ ANİZOTROPİK EKSENEL SİMETRİK KABUK YAPILARININ GERİLME VE DEFORMASYON ANALİZİ YARI ANALİTİK ÇALIŞMASI

Oygür, Özgür Sinan

Yüksek Lisans, Havacılık ve Uzay Mühendisliği Bölümü
Tez Yöneticisi : Doç. Dr. Altan Kayran
Ortak Tez Yöneticisi : Dr. Özge Şen

Eylül 2008, 258 sayfa

Bu tezde simetrik ve simetrik olmayan statik yüklemelere maruz kalan anizotropik eksenel simetrik kabuk yapıları incelenmiştir. Bünye denklemlerinin türetimi sırasında birinci dereceden yanal kesme etkileri formülasyona dahil edilmiştir. Bünye denklemleri, kinematik denklemler, konstitutif denklemler ve hareket denklemlerinden oluşmaktadır. Hareket denklemleri, Hamilton prensibinden yola çıkılarak; konstitütif denklemler klasik katmanlı yapı teorisinin kabullerine dayanılarak; hareket denklemleri de Reissner Naghdi doğrusal kabuk teorisi kullanılarak türetilmiştir. Çözüm sırasında, bünye denklemleri tekrar düzenlenmiş ve temel denklem seti adı verilen bir dizi denklem haline getirilmiştir. Anizotropi ve birinci dereceden yanal kesme etkilerinden dolayı temel denklem seti, sonlu üstel Fourier dönüşüm metodu kullanılarak 20 birinci dereceden bayağı diferansiyel denkleme çevrilmiş ve iki noktalı sınır değeri problemi bir dizi başlangıç değeri problemine dönüştürüldükten sonra çok parçalı integrasyon metodu kullanılarak çözülmüştür. Bir dizi deneme durumu için bulunan sonuçlar sonlu eleman analizinden elde edilen sonuçlarla kıyaslanmış ve iki yöntemden elde edilen

değerlerin birbirine yakın olduğu görülmüştür. Dairesel silindirik kabuk ve kesik küresel kabuk geometrileri için durum çalışmaları yapılmış, sonuçlar incelenirken sabit ve kabuk üzerinde değişken sıcaklık ve basınç yüklemelerinin etkileri belirtilmiştir. Ayrıca birinci dereceden yanal kesme deformasyonu teorisini bazı eksiklikleri ortaya konulmuştur.

Anahtar Kelimeler: Eksenel Simetrik Kabuk Yapıları, Birinci Dereceden Yanal Kesme Deformasyonu, Anizotropi, Sonlu Üstel Fourier Dönüşüm Metodu, Çok Parçalı Integrasyon Metodu

To the family...

ACKNOWLEDGMENTS

First of all I would like to thank Assoc. Prof. Dr. Altan Kayran for his endless and invaluable support, understanding, guidance, help and encouragements throughout the research and writing of this thesis, without which it would be impossible to finish this study.

I would like to express my appreciation to Dr. Özge Şen for his guidance, support and understanding throughout this study. I would also like to thank my coordinator Dr. Serkan Gözübüyük for his support and understanding.

I would like to thank Department of Aerospace Engineering for having provided me with the opportunity for graduate study.

Analyses carried out on Absoft FORTRAN compiler and NASTRAN were performed using the facilities at TÜBİTAK-SAGE, which is gratefully acknowledged.

I would like to thank Mr. Efe Kafdağlı, Mr. İlke Aydıncak and Mr. Emrah Konokman for their advices and motivation. Technical assistance and advices of Mr. Erdem Yavuzbalkan and Ms. Özlem Sümer is also deeply appreciated.

Finally my special thanks go to Ms. Deniz Okay for her heartily support, understanding, and inspiration which helped me very much for the completion of this thesis.

TABLE OF CONTENTS

APPENDICES

LIST OF TABLES

TABLES

LIST OF FIGURES

FIGURES

LIST OF SYMBOLS

1,2,3	: Principal material coordinates
x_1, x_2, x_3	: Rectangular coordinates
ξ, η, ζ	: Curvilinear coordinates
ϕ, θ, ζ	: Shell of revolution coordinates in meridional, tangential and thickness directions, respectively.
g_i	: Metric tensor components
α_ξ, α_η	: Geometric scale factors
R_i	: Radii of curvature in (i) direction
z_i	: Distance from reference surface to the mid-surface of the i^{th} layer in a laminate
h	: Thickness of the shell
l	: Length of the meridian of the shell
ϕ_{in}	: Initial meridional position
ϕ_{final}	: Final meridional position
E_{11}	: Young's modulus in fiber direction
E_{22}	: Young's modulus in transverse to fiber direction
ν_{12}	: Poisson's ratio in 12 plane
G_{12}	: In-plane shear modulus
G_{13}, G_{23}	: Shear modulus in 13 and 23 directions, respectively
α_{11}	: Coefficient of thermal expansion in fiber direction
α_{22}	: Coefficient of thermal expansion in transverse to fiber Direction
ρ	: Ply density

C_{ij} : Compliance matrix

Q_{ij} : Reduced stiffness coefficients $(i, j = 1,2,6)$

$\overline{Q}_{ij}$: Transformed reduced stiffness coefficients

T_{ij} : Transformation matrix

A_{ij} : Extensional stiffness coefficients $(i, j = 1,2,6)$

A_{ij} : Transverse stiffness coefficients $(i, j = 4,5)$

B_{ij} : Bending-stretching stiffness coefficients $(i, j = 1,2,6)$

D_{ij} : Bending stiffness coefficients $(i, j = 1,2,6)$

u_i : Total displacement in a shell in (i) direction

u_i^0 : Mid-surface displacement in a shell in (i) direction

β_i : Rotations of the normal of the mid-surface of the shell with respect to (i) direction

ε_{ii} : Overall normal strain in (ii) direction

γ_{ij} : Overall shear strain in (ij) direction

ε_{ii}^0 : Membrane strain in (ii) direction

κ_{ij} : Bending strain in (ij) direction

γ_{ij}^0 : Mid-plane shear strain in (ij) direction

σ_{ij} : Cauchy stress components

N_{ij} : In-plane force resultant per unit length in (ij) direction

M_{ij} : Moment resultant per unit length in (ij) direction

Q_{ij} : Transverse force resultant per unit length in (ij) direction

N_{ij}^T : In-plane force resultant per unit length in (ij) direction due to thermal loading

M_{ij}^T : Moment resultant per unit length in (ij) direction due to

thermal loading

p_i : Distributed mechanical load in (i) direction

ΔT : Temperature difference

ΔT_1 : Constant term of temperature difference function

ΔT_2 : Linear term of temperature difference function

n : Circumferential wave number

$c_{ij}, cp_{ij}, cdp_{ij}$: Coefficients of fundamental variables

ψ_i : Fundamental variable vector

B_i : Vector of nonhomogeneous coefficients due to loading

CB_{ij} : Non-homogeneous coefficients matrix

K_{ij}, KB_{ij} : Coefficient matrices in two point boundary value Problem

U_a, U_b : Boundary conditions matrices

u_a, u_b : Boundary conditions vectors

C_i : Vector of arbitrary constants

W_{ij} : Homogeneous solution matrix

D_{ij} : Non-homogeneous solution matrix

β : Scale factor in two point boundary value Problem

M : Number of segments

m : Number of fundamental variables

U_s : Strain energy

K : Kinetic energy

W_{in} : Total input energy

E_B : Energy input by boundary force resultants

E_L : Energy input by load components

CHAPTER 1

INTRODUCTION

1.1. Background

The basic theory of the present study is based on shell structures made of composite materials. In the following Sections 1.1.1 and 1.1.2, these two main concepts are introduced.

1.1.1. Shell Structures

All structures are made of three dimensional bodies, regardless of their dimension. However, three dimensional theory of elasticity is not always needed to be used when the stresses and deformations on such a body are calculated. Structural elements are designed to withstand certain types of loads. For example, cables and bars are created to transmit loads in one direction, and therefore they are known as straight two force members [31]. Thus, while deriving the equations that govern these kinds of structures, they are geometrically regarded as lines with cross sections assigned, so that a number of simplifying assumptions can be made instead of solving the full equations of three dimensional elasticity.

Similarly, structures like aircraft panels and cloth hulls of balloons can be described by a plane or curved surface, and accordingly their analysis must be built on the concept of a physical surface capable of transmitting loads from one part to another and of undergoing consequent deformations. When dealing with mathematical models, such structural elements are classified into two types: Plane surfaces are called plates, while curved surfaces are called shells.

In conclusion, shell is defined as an object which may be considered as the materialization of a curved surface. The definition implies that the thickness of a shell is small compared to its other dimensions.

In most cases, a shell is bounded by two curved surfaces, namely its faces. The thickness of the shell may be the same everywhere or it may vary from point to point. The middle surface of the shell is defined as the surface which passes midway between the two faces. If the shape of the middle surface and the thickness of the shell is known for everywhere on the shell, then the shell can geometrically be fully described. Therefore the middle surface and the thickness represent the shell mechanically.

There are many aspects of the use of shells in engineering. For example, pressure vessels and associated pipework are the key components in thermal and nuclear power plants for chemical and power engineering. Some other examples of the use of shell structures in engineering include water cooling towers for power stations, grain silos, armour, arch dams, tunnels, submarines, etc.

Apart from those, shells have a vast usage area in aerospace structures. Many airplane components such as ribs, skin, bulkhead etc., solid rocket motor cases and payloads carried under wings like missiles and fuel tanks are classified as shell structures.

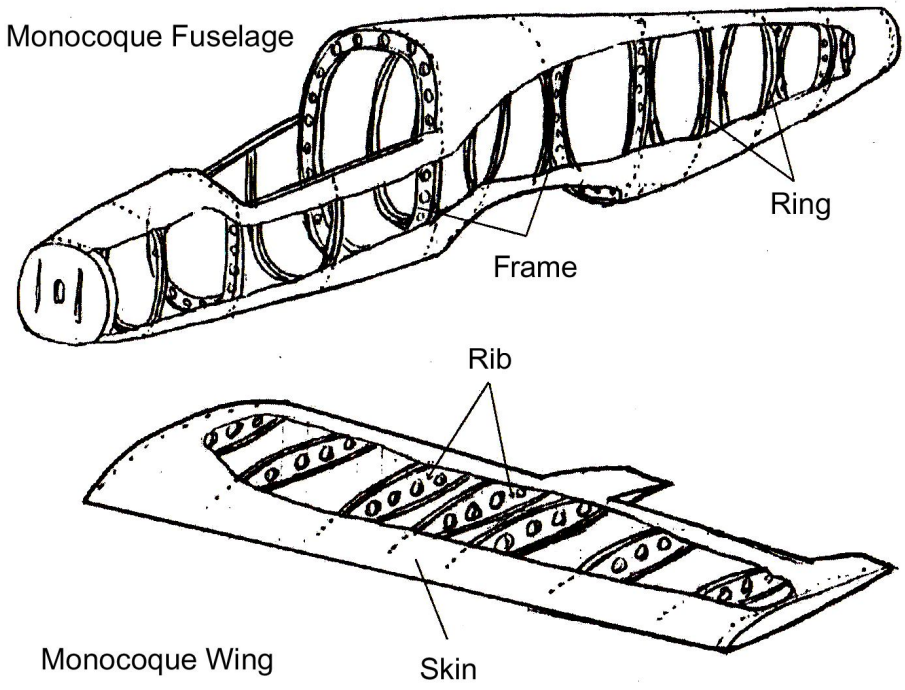

Figure 1.1 Shell Structures Used as Aircraft Components

Shells can be classified in terms of the ratio of the thickness to a characteristic dimension as [34]:

- Very Thick: Three dimensional effects are fully included
- Thick: Stretching, Bending and higher order transverse shear
- Moderately Thick: Stretching, bending and first order transverse shear
- Thin: Stretching and bending energy considered but first order transverse shear neglected
- Very Thin: Dominated by stretching effects. Also called membranes.

1.1.2. Composite Materials

A composite material can be defined as a material that consists of at least two identifiably distinct constituent materials that are combined on a macroscopic scale. If the constituent materials are combined microscopically, the resulting material becomes macroscopically homogeneous. Mechanical properties of materials such as strength, stiffness, corrosion resistance, temperature dependent behaviour and weight can be improved by forming a composite material, because composite materials exhibit the best qualities of their constituents and sometimes qualities that neither of the constituents posses.

Composite parts have both advantages and disadvantages when compared to the metal parts they are being used to replace [36]. Among the advantages of composites

1) A higher performance for a given weight leads to fuel savings in vehicles. Excellent strength to weight ratios can be achieved by composite materials. This is usually expressed as strength divided by density and stiffness modulus divided by density.
2) Laminate patterns and ply build-up in a part can be tailored to give the required mechanical properties in various directions.
3) It is easier to achieve smooth aerodynamic profiles for drag reduction. Complex double-curvature parts with a smooth surface finish can be made in one manufacturing operation.
4) Integration of different parts is simpler in composite structures, and molded composite construction allows for simple strong structures that can be built without requiring expensive equipment and highly skilled assemblers
5) In prototype engineering composites offer various advantages such as ease of repair
6) Composites may be made by a wide range of processes so there are many alternative methods of manufacturing.

7) Composites offer excellent resistance to corrosion, chemical attack and outdoor weathering, as mentioned above.
8) Generally, composites have higher fatigue resistance compared to metals

And among the disadvantages of composites the following can be listed:

1) Failure mechanisms of composite structures are more complex and the design methodologies of structures made of composite materials are not as good standardized as the structures made of metal
2) Repair introduces new problems, for the following reasons:
    a. Materials require refrigerated transport and storage and have limited shelf lives.
    b. Hot curing is necessary in many cases, requiring special equipment.
    c. Curing either hot or cold takes time. The job is not finished when the last rivet has been installed during the montage process.
3) If rivets have been used and must be removed, this presents problems of removal without causing further damage.
4) Repair at the original cure temperature requires tooling and pressure.
5) Composites must be thoroughly cleaned of all contamination before repair.
6) Composites must be dried before repair because all resin matrices and some fibers absorb moisture.

It should be stressed that since one of the main goals to be achieved in aerospace structures is light-weight, the advantages that composite materials offer due to their high strength to weight ratios become more and more important.

Structural classification of composites is performed in three ways:

1) Basic / Elemental Classification
2) Microstructural Classification
3) Macrostructural Classification

In macrostructural classification, composites are generally classified into three main groups according to the types of their constituents [4]:

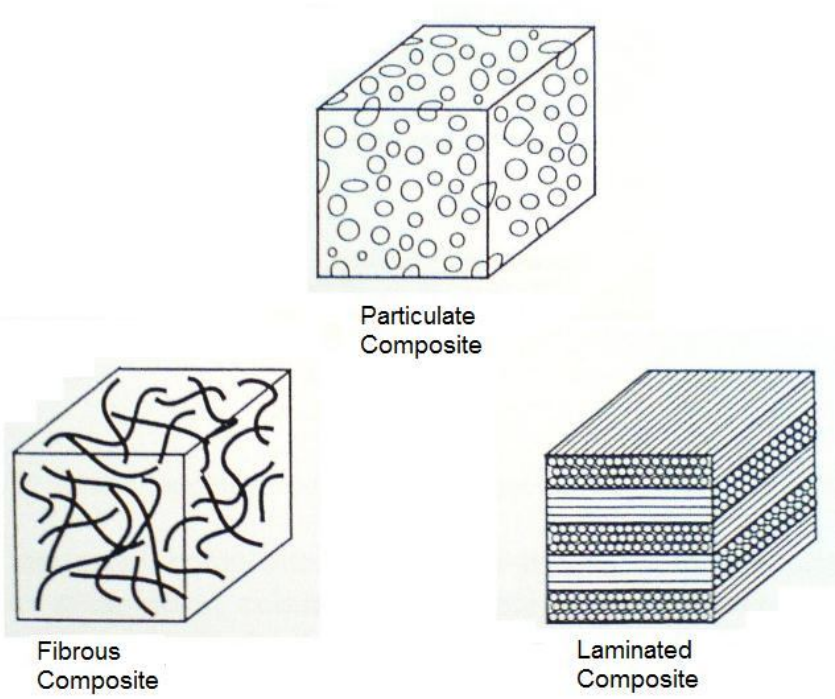

Figure 1.2 Composite Materials with Different Form of Constituents

- Fibrous Composites: Those consist of fibers in a matrix. The fibers in such composites are generally strong and stiff and therefore serve as primary load-carrying constituent. The matrix holds the fibers together and serves as an agent to redistribute the loads from a broken fiber to the adjacent fibers in the material when fibers start failing under excessive loads.
- Particulate Composites: Those composed of particles in a matrix. Particulate composites consist of particles of one or more materials

suspended in a matrix of another material. The particles can either be metallic or non-metallic as can the matrix.

- Laminated Composites: Those consist of layers of at least two different materials that are bonded together.

A lamina is a flat or curved arrangement of unidirectional fibers or woven fibers in a matrix; and a laminate is a stack of laminae with various orientations of principal material directions in the laminae. Lamination is used to combine the best aspects of the constituent layers in order to achieve a more useful material. In laminated composites, the layers of unidirectional fiber reinforced composites are stacked on top of one another. Such laminates are described according to a standard notation called stacking sequence, which lists fiber orientations measured from a reference axis of the laminate. If the orientation is counter clockwise from the reference direction it is considered to be positive. The standard stacking sequence lists orientations of the different layers, starting from the bottom of the laminate to the top in a string separated by slashes. For a laminate with *N* layers, starting from the bottom layer with a fiber orientation θ_1, the laminate is represented as $[\theta_1 / \theta_2 / .../ \theta_N]$. Therefore the total thickness, *h*, of the laminate is $h = t \times N$.

A laminate is symmetric when the fiber orientations of the top half of the laminate are mirror images of the fiber orientations below the mid-plane of the laminate, for example [90°/45°/-60°/-60°/45°/90°]. Laminates that have alternating orientations of 0° and 90° plies are called cross-ply laminates. Another special case is the angle ply laminate. All the layers of an angle ply laminate have the same fiber orientation angle with an alternating sign, such as [45°/-45°/45°/-45°]. Finally, a laminate is antisymmetric if the magnitude of the ply orientation angle above the laminate mid-plane is a mirror image of the ply orientations below the mid-plane with signs reversed. For example, [30/-60/90/-90/60/-30].

1.2. Overview of the Thesis

Axisymmetric shells have considerable practical interest in aerospace engineering. It has been mentioned that thin-walled structures such as plates and shells have a vast usage area in aerospace structures. Among them, shell of revolution is a major body type when aerodynamics and flight mechanics aspects are considered and it is therefore widely used in aerospace components like external fuel tanks or missile, rocket and airframe fuselage.

A shell of revolution is generated by a generating cross section that rotates 360° about an axis of revolution, as illustrated in Figure 1.3. Such structures are said to be rotationally symmetric.

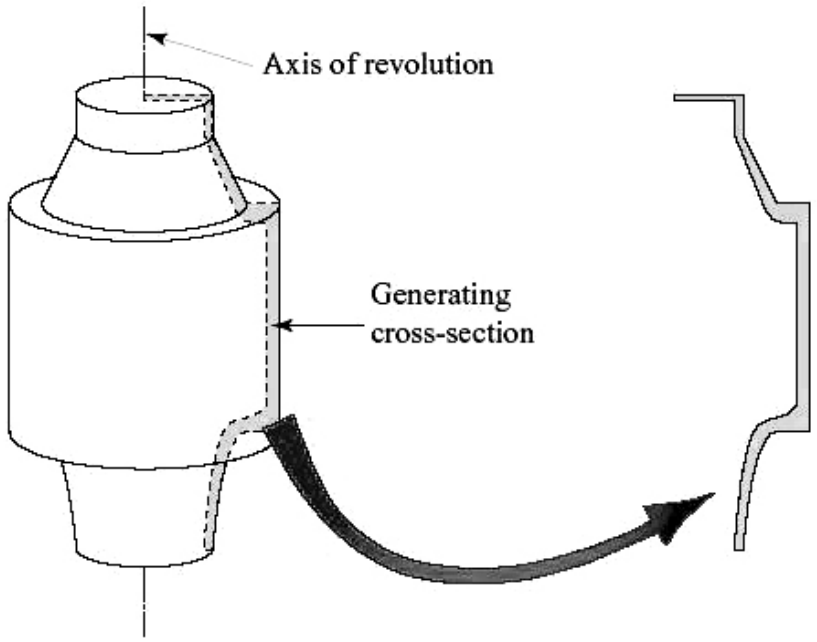

Figure 1.3 A shell of Revolution

The technical importance of shells of revolution is considerable because of the following practical considerations:

- Fabrication: Axisymmetric bodies are usually easier to manufacture than bodies with more complex geometries.
- Strength: axisymmetric configurations are often optimal in terms of strength to weight ratio because of the favourable distribution of the structural material.

The axisymmetric problem deals with the analysis of structures of revolution under axisymmetric loading. However, a shell of revolution under unsymmetrical loading can be treated by the Fourier decomposition method. This involves decomposing the load into a Fourier series in the circumferential direction, calculating the response of the structure to each harmonic term retained in the series, and superposing the results. But if the shell of revolution material is anisotropic, classical Fourier decomposition can not be employed, due to the reasons explained in Section 3.3.

In the present study, macroscopically anisotropic shells of revolution under symmetrical and unsymmetrical loads are analyzed. Since the loads can be unsymmetrical and material is macroscopically anisotropic, finite exponential Fourier transform method is utilized for the analysis.

The present work aims to propose a method for the analysis of anisotropic shells of revolution, with transverse shear deformations taken into account. Unlike variational methods of approximation, this method is based on a semi-analytical method and therefore can be regarded as an alternative to numerical-based methods. As extensively explained in Chapter 3, multisegment method of integration, which was originated by Kalnins [7], is used for the solution of the problems.

As loading, distributed mechanical loads in meridional, tangential and thickness directions of the shell of revolution and temperature difference can be exerted. It has already been mentioned that loads can be unsymmetrical

with respect to the rotation axis, and therefore finite exponential Fourier transform method is utilized in the analysis of anisotropic shells of revolution. In addition to that, the use of multisegment method of integration enables the application of the loads as a function of the meridional coordinate. Furthermore, as exhibited in the succeeding chapters, the method allows the application of temperature difference as a function of the thickness.

In this thesis the Reissner-Naghdi linear shell theory including first order transverse shear deformation is used [9]. It should be noted that other linear shell theories can also be used in the numerical integration based method of analysis as long as the governing equations of those shell theories are used.

As opposed to those listed above, there are a number of limitations in the present study. First of all, as stated above, the theory used in the formulation is linear and therefore only linear static problems can be analyzed.

Furthermore, the thickness of the shell may be same everywhere or it may vary from point to point, as stated previously. In the present study the thickness of the shell is taken as constant. However, the extension of the method to variable thickness shell of revolution can be performed without much labour and it is listed as one of the future work.

In general, in a shell of revolution, orientation of fibers in the laminate may be a function of the meridional direction, which depends on the manufacturing process of the laminate such as filament winding. However, in the present study, in order to demonstrate the application of the multi-segment numerical integration technique to the static analysis of shells of revolution, orientation of the fibers is assumed to be constant in the meridional direction. Similar to the variable thickness problem, meridional change of the winding angle can also be incorporated into the solution method with some extra effort, and this is also listed as one of the future work.

Finally, effects arising from moisture are neglected, although it can easily be included in the analysis since the formulation of loads due to moisture effects is very similar to the formulation of loads due to temperature difference.

CHAPTER 2

GOVERNING EQUATIONS FOR ROTATIONALLY SYMMETRIC SHELLS OF REVOLUTION

The equations that govern the analysis of macroscopically anisotropic shells of revolution are derived from the equations of elasticity. These are frequently grouped into three main sets of equations. The first set, which represents the kinematics of the problem, is called kinematic equations; or the strain displacement relations. The second set, which governs the relations between the stresses and strains, are called constitutive equations; or the stress strain relations. The last set represents the kinetics of the problem and it is called the equations of motion; or the equilibrium equations.

In the following sections, these equations are given for shells of arbitrary shape in the beginning, and subsequently the equations are specialized to shells of revolution. Finally, as an example to commonly occurring shell of revolution geometries, the equations for circular cylinder are derived from general shell of revolution equations. This section begins with description of the shell geometry and coordinate system to be used in the derivation of governing equations, preceded by kinematic equations, constitutive equations and the equations of motion; respectively.

2.1. Shell Geometry and Coordinate System

In this section, general shell geometry and the coordinate system used in the derivation of governing equations for thin shells of arbitrary shape and constant thickness are explained. As explained in Section 2.1.1, a curvilinear coordinate system is used for the derivation of shell equations. It is assumed that the shell is thin with respect to its radii of curvature so that the deflections of the shell are small. The discussion is then specialized on the shell of revolution geometry. In the end, as an example to commonly occurring shell of revolution geometries, relations are further simplified to the circular cylinder geometry.

2.1.1. Curvilinear Coordinates

Let the coordinates of a point P on an arbitrary shell be defined by P(x_1, x_2, x_3) in a three dimensional rectangular coordinate system and ξ, η, ζ be the curvilinear coordinates. If a correspondence can be established between x_1, x_2, x_3 and ξ, η, ζ; then there exists a coordinate transformation between x_1, x_2, x_3 and ξ, η, ζ in the form of three functions

$$x_1 = x_1(\xi, \eta, \zeta) \tag{2.1.1.1}$$

$$x_2 = x_2(\xi, \eta, \zeta) \tag{2.1.1.2}$$

$$x_3 = x_3(\xi, \eta, \zeta) \tag{2.1.1.3}$$

If this correspondence is one to one, then there exists a unique inverse of Equations (2.1.1.1), (2.1.1.2), (2.1.1.3) in the form

$$\xi = \xi(x_1, x_2, x_3) \tag{2.1.1.4}$$

$$\eta = \eta(x_1, x_2, x_3) \tag{2.1.1.5}$$

$$\zeta = \zeta(x_1, x_2, x_3) \tag{2.1.1.6}$$

It is said that point P has curvilinear coordinates ξ, η, ζ. The position vector $\vec{p}$ of the point P has the rectangular coordinates given by Equation 2.1.1.7.

$$\vec{p} = x_1\vec{i}_1 + x_2\vec{i}_2 + x_3\vec{i}_3 \tag{2.1.1.7}$$

The vector increment of the position vector is,

$$d\vec{p} = dx_1\vec{i}_1 + dx_2\vec{i}_2 + dx_3\vec{i}_3 \tag{2.1.1.8}$$

The same position vector increment $d\vec{p}$ can be similarly given in terms of the curvilinear coordinate increments by

$$d\vec{p} = d\xi\ \vec{g}_\xi + d\eta\ \vec{g}_\eta + d\zeta\ \vec{g}_\zeta \tag{2.1.1.9}$$

where the coefficients of the metric tensor g_ξ, g_η, g_ζ are given by [5]

$$g_\xi = \left[\alpha_\xi\left(1 + \frac{\zeta}{R_\xi}\right)\right]^2 \tag{2.1.1.10}$$

$$g_\eta = \left[\alpha_\eta\left(1 + \frac{\zeta}{R_\eta}\right)\right]^2 \tag{2.1.1.11}$$

$$g_\xi = 1 \tag{2.1.1.12}$$

where R_ξ and R_η are the radii of curvature in the ξ and η directions of the shell respectively; α_ξ and α_η are some scale factors, to be explained in the next section.

2.1.2. General Shell Geometry

A shell is defined as a three dimensional body, whose one dimension is smaller than any other characteristic length. For the description of the points of the shell, a reference surface of the shell is defined as the (ξ,η) surface at $\zeta = 0$, and ζ coordinate is taken as a straight line directed along the normal of the reference surface. The length of the ζ coordinate line lying within the shell is called the thickness of the shell.

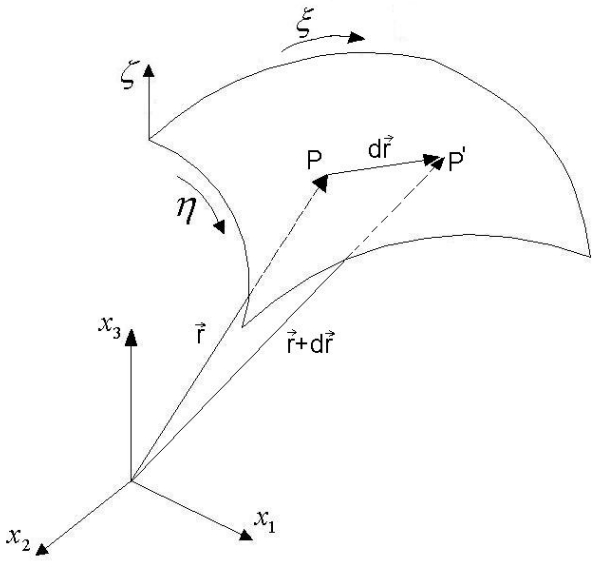

Figure 2.1 General Shell Coordinates

The change of the position vector $\vec{r}$ of a point P on the shell, with coordinates ξ and η are defined as [3]

$$\frac{\partial \vec{r}}{\partial \xi} \cdot \frac{\partial \vec{r}}{\partial \xi} = \left| \frac{\partial \vec{r}}{\partial \xi} \right|^2 = \alpha_\xi^2 \tag{2.1.2.1}$$

$$\frac{\partial \vec{r}}{\partial \eta} \cdot \frac{\partial \vec{r}}{\partial \eta} = \left| \frac{\partial \vec{r}}{\partial \eta} \right|^2 = \alpha_\eta^2 \tag{2.1.2.2}$$

α_ξ and α_η in Equations (2.1.2.1) and (2.1.2.2) are called fundamental form parameters or Lamé parameters.

The deformation of a thin shell is determined by the displacement of its reference surface and there are some relationships about the deformation of this surface. One of them is called Mainardi – Codazzi Equations, which are given in Equations (2.1.2.3) and (2.1.2.4), explain the relation between R_ξ, R_η, α_ξ and α_η [6].

$$\frac{\partial}{\partial \xi}\left[\alpha_\eta\left(1+\frac{\zeta}{R_\eta}\right)\right] = \left(1+\frac{\zeta}{R_\xi}\right)\frac{\partial \alpha_\eta}{\partial \xi} \tag{2.1.2.3}$$

$$\frac{\partial}{\partial \eta}\left[\alpha_\xi\left(1+\frac{\zeta}{R_\xi}\right)\right] = \left(1+\frac{\zeta}{R_\eta}\right)\frac{\partial \alpha_\xi}{\partial \eta} \tag{2.1.2.4}$$

2.1.3. Shell of Revolution Geometry and Coordinate System

Shells whose neutral surface is generated by rotating a line about an axis are called shells of revolution. For such shells, the lines of principal curvature are its meridians and its parallel circles. In shell coordinate system, ξ is replaced

by ϕ and η is replaced by θ, as shown in Figure 2.2 and Figure 2.3. Therefore, for a shell of revolution principal radii of curvature are given by Equations 2.1.3.1 and 2.1.3.2.

$$R_{\xi} = R_{\phi} \tag{2.1.3.1}$$

$$R_{\eta} = R_{\theta} \tag{2.1.3.2}$$

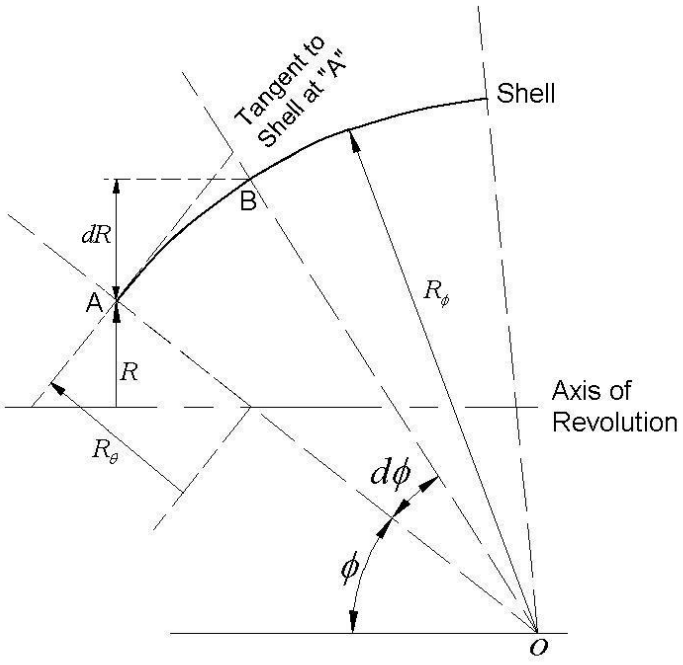

Figure 2.2 General Shell of Revolution Coordinates (2D)

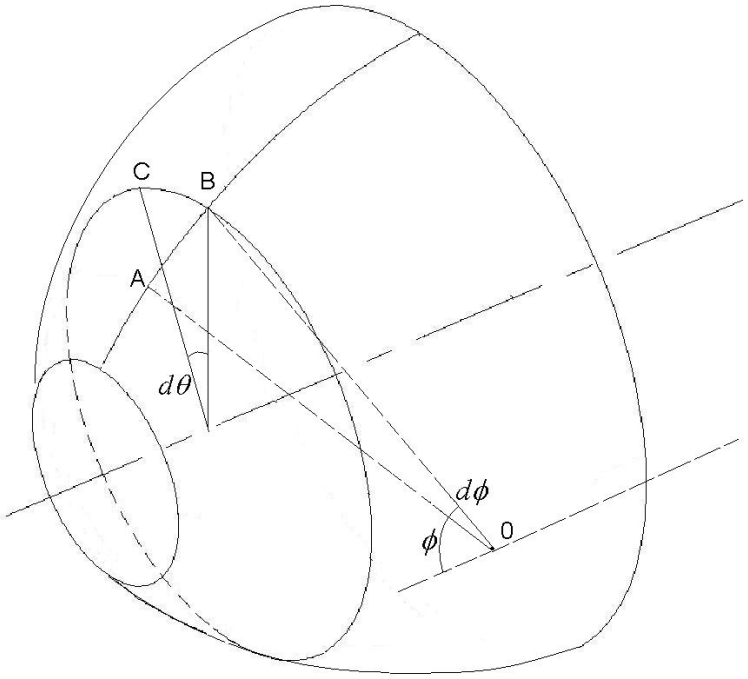

Figure 2.3 General Shell of Revolution Coordinates (3D)

From Figure 2.3, it is clear that the infinitesimal distance between points A and C can be written as

$$dr^2 = \left|AC\right|^2 = \left|AB\right|^2 + \left|BC\right|^2 \tag{2.1.3.3}$$

and Figure 2.2 reveals that

$$\left|AB\right| = R_\phi d\phi \tag{2.1.3.4}$$

And therefore the distance between points B and C is, as can be seen from Figure 2.2 and Figure 2.3,

$$\left|BC\right| = \left(R + dR\right)d\theta \cong Rd\theta = \left(R_\theta \sin\phi\right)d\theta \tag{2.1.3.5}$$

thus

$$dr^2 = R_\phi^2 d\phi^2 + \left(R_\theta \sin\phi\right)^2 d\theta^2 \tag{2.1.3.6}$$

Lamé parameters α_ξ and α_η were defined in Equations (2.1.2.1) and (2.1.2.2). For the shell of revolution they become

$$\frac{\partial \vec{r}}{\partial \phi} \cdot \frac{\partial \vec{r}}{\partial \phi} = \left|\frac{\partial \vec{r}}{\partial \phi}\right|^2 = \alpha_\phi^2 \tag{2.1.3.7}$$

$$\frac{\partial \vec{r}}{\partial \theta} \cdot \frac{\partial \vec{r}}{\partial \theta} = \left|\frac{\partial \vec{r}}{\partial \theta}\right|^2 = \alpha_\theta^2 \tag{2.1.3.8}$$

Substituting Equation (2.1.3.6) into Equations (2.1.3.7) and (2.1.3.8), α_ϕ and α_θ become for shell of revolution

$$\alpha_\phi = R_\phi \tag{2.1.3.9}$$

$$\alpha_\theta = R_\theta \sin\phi \tag{2.1.3.10}$$

In addition to those, from Figure 2.2 it is obvious that

$$R = R_\theta \sin\phi \tag{2.1.3.11}$$

as already been used in Equation (2.1.3.5) and

$$dR = d(R_\theta \sin\phi) = \left(R_\phi d\phi\right)\cos\phi \tag{2.1.3.12}$$

One final issue which is of interest is that since shell of revolution is axisymmetric, geometric properties R_ϕ, R_θ, α_ϕ and α_θ are independent of θ, i.e.

$$\frac{\partial}{\partial\theta}\left[R_\phi, R_\theta, \alpha_\phi, \alpha_\theta\right] = 0 \qquad (2.1.3.13)$$

Further simplifications can be made to the shell of revolution geometry, in order to obtain the equations of some commonly occurring geometries, which can also be classified as shell of revolution. Among them, one of the most commonly occurring and therefore widely used geometry is circular cylinder. (See Figure 2.4)

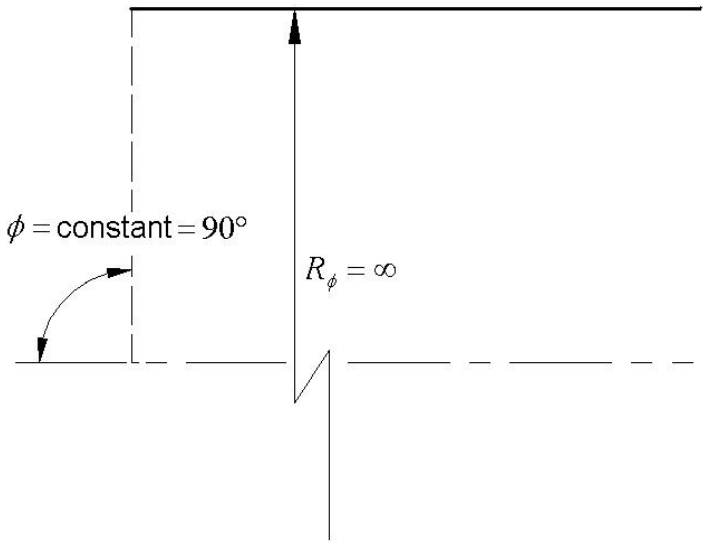

Figure 2.4 Circular Cylinder Coordinates

It is clear from Figure 2.4 that for cylinder,

$$\phi = \text{Constant} = 90° \qquad (2.1.3.14)$$

$$\alpha_\phi = R_\phi \to \infty \qquad (2.1.3.15)$$

For cylindrical shells of revolution, Equations (2.1.3.10) and (2.1.3.11) become

$$\alpha_\theta = R_\theta \sin\phi = R_\theta = R \tag{2.1.3.16}$$

In addition, ϕ coordinate, which is constant along the symmetry axis of the cylinder, is the axial direction of the cylinder and becomes x coordinate. The relation between x and ϕ coordinates can be found utilizing Equation (2.1.3.4). Thus, for cylinder, relation between x and ϕ coordinates becomes:

$$dx = R_\phi d\phi \tag{2.1.3.17}$$

Equation (2.1.3.17) leads to the transformation between the ϕ coordinate of the general shell of revolution and x coordinate of the circular cylinder:

$$\frac{\partial}{\partial x} = \frac{1}{R_\phi}\frac{\partial}{\partial \phi} \tag{2.1.3.18}$$

2.2. Kinematic Equations

In this section, the equations which represent the kinematics of the problem, in other words kinematic equations; or the strain displacement relations are described.

2.2.1. Shell Assumptions

The approach to be used in the expression of the strain displacement relations is based on the thin shell theory with first order transverse shear deformation

effects included. The assumptions to be used in this work are first stated by Reissner [9]. These can be summarized as,

1. Thickness of the shell is small compared to the other dimensions of the shell; as stated in 2.1.2.

2. Strains and displacements are so small that higher than first order terms can be neglected in strain – displacement relations.

3. Normal stress component perpendicular to the reference surface of the shell (transverse normal stress) is small compared to the other normal stresses and may be neglected.

4. A lineal element normal to the undeformed reference surface undergoes at most a translation and a rotation and suffers no elongation.

2.2.2. General Derivation

The displacement field proposed under these assumptions is given by Equations (2.2.1), (2.2.2) and (2.2.3) [9].

$$U_{\xi}(\xi,\eta,\zeta) = u_{\xi}^{0}(\xi,\eta) + \zeta\,\beta_{\xi}(\xi,\eta) \tag{2.2.1}$$

$$U_{\eta}(\xi,\eta,\zeta) = u_{\eta}^{0}(\xi,\eta) + \zeta\,\beta_{\eta}(\xi,\eta) \tag{2.2.2}$$

$$U_{\zeta}(\xi,\eta,\zeta) = u_{\zeta}^{0}(\xi,\eta) \tag{2.2.3}$$

where U_{ξ}, U_{η} and U_{ζ} are the displacements of the shell in ξ, η and ζ coordinates; u_{ξ}^{0}, u_{η}^{0}, u_{ζ}^{0} are the middle surface displacements of the shell in the corresponding directions and β_{ξ} and β_{η} are the rotations of the normal of

the middle surface of the shell with respect to η and ξ directions respectively. The rotations β_ξ and β_η are given by Equations (2.2.4) and (2.2.5).

$$\beta_\xi = \frac{\partial U_\xi(\xi,\eta,\zeta)}{\partial \zeta} \tag{2.2.4}$$

$$\beta_\eta = \frac{\partial U_\eta(\xi,\eta,\zeta)}{\partial \zeta} \tag{2.2.5}$$

The strain displacement equations of three dimensional theory of elasticity is simplified to the following equations under the assumptions of Reissner for thin shell theory with first order transverse shear deformation effects included, and strain-displacement equations are given by Equations (2.2.6) – (2.2.10) [1].

$$\varepsilon_{\xi\xi} = \frac{1}{\alpha_\xi}\frac{\partial U_\xi}{\partial \xi} + \frac{U_\eta}{\alpha_\xi \alpha_\eta}\frac{\partial \alpha_\xi}{\partial \eta} + \frac{U_\zeta}{R_\xi} \tag{2.2.6}$$

$$\varepsilon_{\eta\eta} = \frac{1}{\alpha_\eta}\frac{\partial U_\eta}{\partial \eta} + \frac{U_\xi}{\alpha_\xi \alpha_\eta}\frac{\partial \alpha_\eta}{\partial \xi} + \frac{U_\zeta}{R_\eta} \tag{2.2.7}$$

$$\gamma_{\xi\eta} = \frac{\alpha_\xi}{\alpha_\eta}\frac{\partial}{\partial \eta}\left(\frac{U_\xi}{\alpha_\xi}\right) + \frac{\alpha_\eta}{\alpha_\xi}\frac{\partial}{\partial \xi}\left(\frac{U_\eta}{\alpha_\eta}\right) \tag{2.2.8}$$

$$\gamma_{\xi\zeta} = \alpha_\xi\left(1+\frac{\zeta}{R_\xi}\right)\frac{\partial}{\partial \zeta}\left(\frac{U_\xi}{\alpha_\xi\left(1+\frac{\zeta}{R_\xi}\right)}\right) + \frac{1}{\alpha_\xi\left(1+\frac{\zeta}{R_\xi}\right)}\frac{\partial U_\zeta}{\partial \xi} \tag{2.2.9}$$

$$\gamma_{\eta\zeta} = \alpha_\eta\left(1+\frac{\zeta}{R_\eta}\right)\frac{\partial}{\partial \zeta}\left(\frac{U_\eta}{\alpha_\eta\left(1+\frac{\zeta}{R_\eta}\right)}\right) + \frac{1}{\alpha_\eta\left(1+\frac{\zeta}{R_\eta}\right)}\frac{\partial U_\zeta}{\partial \eta} \tag{2.2.10}$$

Substituting the proposed displacement field into the strain displacement equations, total strains can be represented as the sum of the membrane and bending strains which are also commonly referred to as extensional strains and curvatures:

$$\varepsilon_{\xi\xi} = \varepsilon^0_{\xi\xi} + \zeta\,\kappa_{\xi\xi} \tag{2.2.11}$$

$$\varepsilon_{\eta\eta} = \varepsilon^0_{\eta\eta} + \zeta\,\kappa_{\eta\eta} \tag{2.2.12}$$

$$\gamma_{\xi\eta} = \gamma^0_{\xi\eta} + \zeta\,\kappa_{\xi\eta} \tag{2.2.13}$$

$$\gamma_{\xi\zeta} = \beta_\xi - \frac{u^0_\xi}{R_\xi} + \frac{1}{\alpha_\xi}\frac{\partial u_\zeta}{\partial \xi} \tag{2.2.14}$$

$$\gamma_{\eta\zeta} = \beta_\eta - \frac{u^0_\eta}{R_\eta} + \frac{1}{\alpha_\eta}\frac{\partial u_\zeta}{\partial \eta} \tag{2.2.15}$$

where

$$\varepsilon^0_{\xi\xi} = \frac{1}{\alpha_\xi}\frac{\partial u^0_\xi}{\partial \xi} + \frac{u^0_\eta}{\alpha_\xi\alpha_\eta}\frac{\partial \alpha_\xi}{\partial \eta} + \frac{u^0_\zeta}{R_\xi} \tag{2.2.16}$$

$$\varepsilon^0_{\eta\eta} = \frac{1}{\alpha_\eta}\frac{\partial u^0_\eta}{\partial \eta} + \frac{u^0_\xi}{\alpha_\xi\alpha_\eta}\frac{\partial \alpha_\eta}{\partial \xi} + \frac{u^0_\zeta}{R_\eta} \tag{2.2.17}$$

$$\gamma^0_{\xi\eta} = \frac{\alpha_\xi}{\alpha_\eta}\frac{\partial}{\partial \eta}\left(\frac{u^0_\xi}{\alpha_\xi}\right) + \frac{\alpha_\eta}{\alpha_\xi}\frac{\partial}{\partial \eta}\left(\frac{u^0_\eta}{\alpha_\eta}\right) \tag{2.2.18}$$

$$\kappa_{\xi\xi} = \frac{1}{\alpha_\xi}\frac{\partial \beta_\xi}{\partial \xi} + \frac{\beta_\eta}{\alpha_\xi\alpha_\eta}\frac{\partial \alpha_\xi}{\partial \eta} \tag{2.2.19}$$

$$\kappa_{\eta\eta} = \frac{1}{\alpha_\eta}\frac{\partial \beta_\eta}{\partial \eta} + \frac{\beta_\xi}{\alpha_\xi\alpha_\eta}\frac{\partial \alpha_\eta}{\partial \xi} \tag{2.2.20}$$

$$\kappa_{\xi\eta} = \frac{\alpha_\eta}{\alpha_\xi}\frac{\partial}{\partial \xi}\left(\frac{\beta_\eta}{\alpha_\eta}\right) + \frac{\alpha_\xi}{\alpha_\eta}\frac{\partial}{\partial \eta}\left(\frac{\beta_\xi}{\alpha_\xi}\right) \tag{2.2.21}$$

2.2.3. Reduction to Shell of Revolution

Strain displacement relations given in Equations (2.2.11) through (2.2.21) are derived for shells of arbitrary shape. In order to obtain the kinematic relations for shells of revolution, modifications discussed in 2.1.3 have to be made. Substituting Equations (2.1.3.9), (2.1.3.10) and (2.1.3.13) into Equations (2.2.11) through (2.2.21) and changing the shell coordinates to ϕ and θ, midstrains and curvatures terms become:

$$\varepsilon_{\phi\phi}^{0} = \frac{1}{R_\phi}\left[\frac{\partial u_\phi^0}{\partial \phi} + u_\zeta^0\right] \tag{2.2.3.1}$$

$$\varepsilon_{\theta\theta}^{0} = \frac{1}{R_\theta \sin\phi}\left[u_\phi^0 \cos\phi + \frac{\partial u_\theta^0}{\partial \theta} + u_\zeta^0 \sin\phi\right] \tag{2.2.3.2}$$

$$\gamma_{\phi\theta}^{0} = \frac{1}{R_\theta \sin\phi}\frac{\partial u_\phi^0}{\partial \theta} + \frac{1}{R_\phi}\frac{\partial u_\theta^0}{\partial \phi} - \frac{\cot\phi}{R_\theta}u_\theta^0 \tag{2.2.3.3}$$

$$\kappa_{\phi\phi} = \frac{1}{R_\phi}\frac{\partial \beta_\phi}{\partial \phi} \tag{2.2.3.4}$$

$$\kappa_{\theta\theta} = \frac{1}{R_\theta \sin\phi}\left[\beta_\phi \cos\phi + \frac{\partial \beta_\theta}{\partial \theta}\right] \tag{2.2.3.5}$$

$$\kappa_{\phi\theta} = \frac{1}{R_\theta \sin\phi}\frac{\partial \beta_\phi}{\partial \theta} + \frac{1}{R_\phi}\frac{\partial \beta_\theta}{\partial \phi} - \frac{\cot\phi}{R_\theta}\beta_\theta \tag{2.2.3.6}$$

For a general shell of revolution, the overall (total) strains are given by:

$$\varepsilon_{\phi\phi}(\phi,\theta,\zeta) = \varepsilon_{\phi\phi}^{0}(\phi,\theta) + \zeta\,\kappa_{\phi\phi}(\phi,\theta) \tag{2.2.3.7}$$

$$\varepsilon_{\theta\theta}(\phi,\theta,\zeta) = \varepsilon_{\theta\theta}^{0}(\phi,\theta) + \zeta\kappa_{\theta\theta}(\phi,\theta) \tag{2.2.3.8}$$

$$\gamma_{\phi\theta}(\phi,\theta,\zeta) = \gamma_{\phi\theta}^{0}(\phi,\theta) + \zeta\,\kappa_{\phi\theta}(\phi,\theta) \tag{2.2.3.9}$$

$$\gamma_{\phi\zeta} = \beta_\phi - \frac{u_\phi^0}{R_\phi} + \frac{1}{R_\phi}\frac{\partial u_\zeta^0}{\partial \phi} \tag{2.2.3.10}$$

$$\gamma_{\theta\zeta} = \beta_\theta - \frac{u_\theta^0}{R_\theta} + \frac{1}{R_\theta \sin\phi}\frac{\partial u_\zeta^0}{\partial \theta} \tag{2.2.3.11}$$

If one utilizes the Equations (2.1.3.14) to (2.1.3.16) and (2.1.3.18), and substituting ϕ with x , kinematic relations given above for general shells of revolution can further be specialized to circular cylindrical shells. For circular cylindrical shells mid plane strains and curvatures are given by Equations (2.2.3.12) – (2.2.3.17).

$$\varepsilon_{xx}^0 = \frac{\partial u_x^0}{\partial x} \tag{2.2.3.12}$$

$$\varepsilon_{\theta\theta}^0 = \frac{1}{R}\left[\frac{\partial u_\theta^0}{\partial \theta} + u_\zeta^0\right] \tag{2.2.3.13}$$

$$\gamma_{x\theta}^0 = \frac{1}{R}\frac{\partial u_x^0}{\partial \theta} + \frac{\partial u_\theta^0}{\partial x} \tag{2.2.3.14}$$

$$\kappa_{xx} = \frac{\partial \beta_x}{\partial x} \tag{2.2.3.15}$$

$$\kappa_{\theta\theta} = \frac{1}{R}\frac{\partial \beta_\theta}{\partial \theta} \tag{2.2.3.16}$$

$$\kappa_{x\theta} = \frac{1}{R}\frac{\partial \beta_x}{\partial \theta} + \frac{\partial \beta_\theta}{\partial x} \tag{2.2.3.17}$$

For a cylindrical shell of revolution, the overall strains are given by:

$$\varepsilon_{xx}(x,\theta,\zeta) = \varepsilon_x^0(x,\theta) + \zeta\,\kappa_{xx}(x,\theta) \tag{2.2.3.18}$$

$$\varepsilon_{\theta\theta}(x,\theta,\zeta) = \varepsilon_{\theta\theta}^0(x,\theta) + \zeta\,\kappa_{\theta\theta}(x,\theta) \tag{2.2.3.19}$$

$$\gamma_{x\theta}(x,\theta,\zeta) = \gamma_{x\theta}^0(x,\theta) + \zeta\,\kappa_{x\theta}(x,\theta) \tag{2.2.3.20}$$

$$\gamma_{x\zeta} = \beta_x + \frac{\partial u_\zeta^0}{\partial x} \tag{2.2.3.21}$$

$$\gamma_{\theta\zeta} = \beta_\theta - \frac{u_\theta^0}{R} + \frac{1}{R}\frac{\partial u_\zeta^0}{\partial \theta} \tag{2.2.3.22}$$

2.3. Constitutive Equations

Constitutive equations described in this section govern the relations between the stresses and strains arisen due to the external effects in a laminate. Since a laminate is defined as two or more laminae (layers) bonded together to construct a complete structural member, there are a number of theories which explain the bonding between these layers. Among these, one of the most widely known and used theories is *Classical Lamination Theory* [4], [12]. The constitutive equations explained in this section are developed under the assumptions of this Classical Lamination Theory. Most of these assumptions are identical to the thin shell theory with first order transverse shear deformation effects included, which are given in Section 2.2.1. The only difference is in the material properties. In classical lamination theory, Perfect bonding between layers is assumed. The bonding itself is infinitesimally small (there is no flaw or gap between layers); and non-shear-deformable (no lamina can slip relative to another). The strength of bonding is as strong as it needs to be (the laminate acts as a single lamina with special integrated properties).

The laminae principal material directions are oriented to produce a structural element capable of resisting load in several directions. Therefore, since the material directions and the geometric directions of the structure do not overlap for this reason, transformation between the coordinates of the material and the structure is necessary. The following section deals with this subject.

2.3.1. Transformations of Stresses and Strains

In materials of any kind, there is always a need for establishing transformation relations among stresses and strains in one coordinate system to corresponding quantities in another coordinate system.

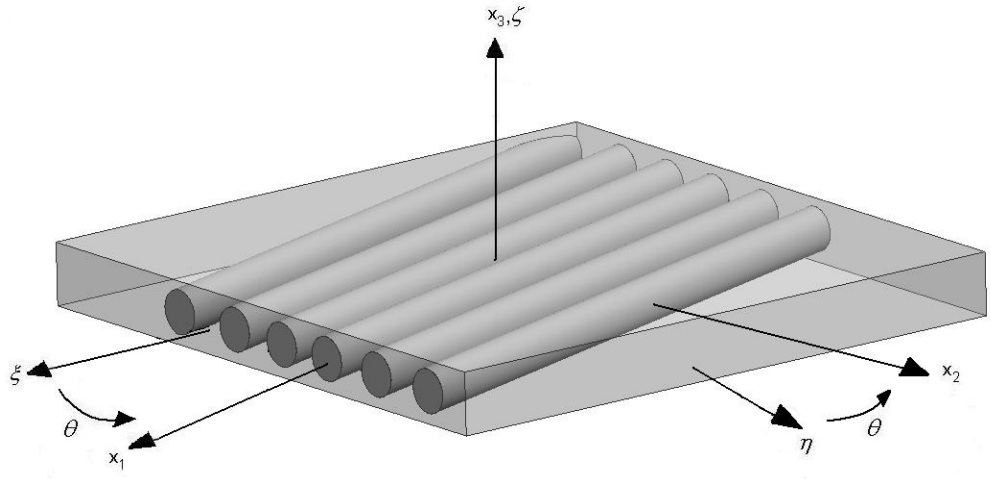

Figure 2.5 Material and Geometric Coordinates

For a fiber reinforced composite layer, which is schematically shown in Figure 2.5, let x_1, x_2 and x_3 represent principal material coordinates, x_1 being the fiber direction, x_2 the transverse to fiber direction and x_3 the thickness direction; and ξ, η, ζ represent the geometric coordinates. From Figure 2.5, it can be devised that

$$\begin{Bmatrix} x_1 \\ x_2 \\ x_3 \end{Bmatrix} = \begin{bmatrix} \cos\theta & \sin\theta & 0 \\ \sin\theta & \cos\theta & 0 \\ 0 & 0 & 1 \end{bmatrix} \begin{Bmatrix} \xi \\ \eta \\ \zeta \end{Bmatrix} \tag{2.3.1.1}$$

and

$$\begin{Bmatrix} \xi \\ \eta \\ \zeta \end{Bmatrix} = \begin{bmatrix} \cos\theta & \sin\theta & 0 \\ \sin\theta & \cos\theta & 0 \\ 0 & 0 & 1 \end{bmatrix}^T \begin{Bmatrix} x_1 \\ x_2 \\ x_3 \end{Bmatrix} \tag{2.3.1.2}$$

since

$$\begin{bmatrix} \cos\theta & \sin\theta & 0 \\ \sin\theta & \cos\theta & 0 \\ 0 & 0 & 1 \end{bmatrix}^{-1} = \begin{bmatrix} \cos\theta & \sin\theta & 0 \\ \sin\theta & \cos\theta & 0 \\ 0 & 0 & 1 \end{bmatrix}^T \tag{2.3.1.3}$$

Using Equation (2.3.1.1), transformation of stresses between material coordinate system and geometric coordinate system can be written as

$$\begin{bmatrix} \sigma_{11} & \sigma_{12} & \sigma_{13} \\ \sigma_{21} & \sigma_{22} & \sigma_{23} \\ \sigma_{31} & \sigma_{32} & \sigma_{33} \end{bmatrix} = \begin{bmatrix} \cos\theta & \sin\theta & 0 \\ \sin\theta & \cos\theta & 0 \\ 0 & 0 & 1 \end{bmatrix} \begin{bmatrix} \sigma_{\xi\xi} & \sigma_{\xi\eta} & \sigma_{\xi\zeta} \\ \sigma_{\eta\xi} & \sigma_{\eta\eta} & \sigma_{\eta\zeta} \\ \sigma_{\zeta\xi} & \sigma_{\zeta\eta} & \sigma_{\zeta\zeta} \end{bmatrix} \begin{bmatrix} \cos\theta & \sin\theta & 0 \\ \sin\theta & \cos\theta & 0 \\ 0 & 0 & 1 \end{bmatrix}^T \tag{2.3.1.4}$$

For symmetric stress tensor, one can write the elements of the stress tensor in vector form. Thus, Equation (2.3.1.4) can be re-arranged as in Equation (2.3.1.5) [12].

$$\begin{Bmatrix}\sigma_{11}\\ \sigma_{22}\\ \sigma_{33}\\ \sigma_{23}\\ \sigma_{13}\\ \sigma_{12}\end{Bmatrix}=\begin{bmatrix} m^2 & n^2 & 0 & 0 & 0 & 2mn \\ n^2 & m^2 & 0 & 0 & 0 & -2mn \\ 0 & 0 & 1 & 0 & 0 & 0 \\ 0 & 0 & 0 & m & -n & 0 \\ 0 & 0 & 0 & n & m & 0 \\ -mn & mn & 0 & 0 & 0 & \left(m^2-n^2\right) \end{bmatrix}\begin{Bmatrix}\sigma_{\xi\xi}\\ \sigma_{\eta\eta}\\ \sigma_{\zeta\zeta}\\ \sigma_{\eta\zeta}\\ \sigma_{\xi\zeta}\\ \sigma_{\xi\eta}\end{Bmatrix} \tag{2.3.1.5}$$

where

$$m=\cos\theta \ , \ n=\sin\theta \tag{2.3.1.6}$$

For plane stress situation, Equation (2.3.1.5) becomes

$$\begin{Bmatrix}\sigma_{11}\\ \sigma_{22}\\ \sigma_{12}\end{Bmatrix}=\begin{bmatrix} m^2 & n^2 & 2mn \\ n^2 & m^2 & -2mn \\ -mn & mn & \left(m^2-n^2\right) \end{bmatrix}\begin{Bmatrix}\sigma_{\xi\xi}\\ \sigma_{\eta\eta}\\ \sigma_{\xi\eta}\end{Bmatrix} \tag{2.3.1.7}$$

Similarly, for the strains,

$$\begin{Bmatrix}\varepsilon_{11}\\ \varepsilon_{22}\\ \varepsilon_{33}\\ 2\cdot\varepsilon_{23}\\ 2\cdot\varepsilon_{13}\\ 2\cdot\varepsilon_{12}\end{Bmatrix}=\begin{bmatrix} m^2 & n^2 & 0 & 0 & 0 & mn \\ n^2 & m^2 & 0 & 0 & 0 & -mn \\ 0 & 0 & 1 & 0 & 0 & 0 \\ 0 & 0 & 0 & m & -n & 0 \\ 0 & 0 & 0 & n & m & 0 \\ -2mn & 2mn & 0 & 0 & 0 & \left(m^2-n^2\right) \end{bmatrix}\begin{Bmatrix}\varepsilon_{\xi\xi}\\ \varepsilon_{\eta\eta}\\ \varepsilon_{\zeta\zeta}\\ 2\varepsilon_{\eta\zeta}\\ 2\varepsilon_{\xi\zeta}\\ 2\varepsilon_{\xi\eta}\end{Bmatrix} \tag{2.3.1.8}$$

For plane stress,

$$\begin{Bmatrix}\varepsilon_{11}\\ \varepsilon_{22}\\ \gamma_{12}\end{Bmatrix}=\begin{bmatrix} m^2 & n^2 & mn \\ n^2 & m^2 & -mn \\ -2mn & 2mn & \left(m^2-n^2\right) \end{bmatrix}\begin{Bmatrix}\varepsilon_{\xi\xi}\\ \varepsilon_{\eta\eta}\\ \gamma_{\xi\eta}\end{Bmatrix} \tag{2.3.1.9}$$

Note that $2\varepsilon_{ij} = \gamma_{ij}$.

2.3.2. Macromechanical Behaviour of Lamina and Laminate

The Generalized Hooke's Law relating stresses to strains in the material coordinate system can be written in contracted notation as [4]:

$$\begin{Bmatrix} \sigma_1 \\ \sigma_2 \\ \sigma_3 \\ \sigma_4 \\ \sigma_5 \\ \sigma_6 \end{Bmatrix} = \begin{bmatrix} C_{11} & C_{12} & C_{13} & C_{14} & C_{15} & C_{16} \\ C_{21} & C_{22} & C_{23} & C_{24} & C_{25} & C_{26} \\ C_{31} & C_{32} & C_{33} & C_{34} & C_{35} & C_{36} \\ C_{41} & C_{42} & C_{43} & C_{44} & C_{45} & C_{46} \\ C_{51} & C_{52} & C_{53} & C_{54} & C_{55} & C_{56} \\ C_{61} & C_{62} & C_{63} & C_{64} & C_{65} & C_{66} \end{bmatrix} \begin{Bmatrix} \varepsilon_1 \\ \varepsilon_2 \\ \varepsilon_3 \\ 2\varepsilon_4 \\ 2\varepsilon_5 \\ 2\varepsilon_6 \end{Bmatrix} \qquad (2.3.2.1)$$

Note that $\sigma_4 = \sigma_{23}$, $\sigma_5 = \sigma_{13}$, $\sigma_6 = \sigma_{12}$; and $\varepsilon_4 = \varepsilon_{23}$, $\varepsilon_5 = \varepsilon_{13}$, $\varepsilon_6 = \varepsilon_{12}$. Matrix C_{ij} is symmetric, that is $C_{ij} = C_{ji}$, so for fully anisotropic materials there are 21 independent material constants. For monoclinic materials, i.e. the materials which exhibit single plane of elastic symmetry, the number of independent constants reduces to 13 and for orthotropic materials, the materials which exhibit three planes of elastic symmetry, this number reduces to 9.

Since laminates are generally composed of layers of fiber-reinforced laminae, and lamina is a flat or curved arrangement of unidirectional fibers or woven fibers in a matrix, stress strain relations should be investigated for plane stress behaviour in orthotropic materials. For a lamina, plane stress state is defined by setting $\sigma_3 = 0$ $\sigma_{23} = 0$ $\sigma_{13} = 0$ in Equation (2.3.2.1). For orthotropic materials, plane stress assumption leads to $\varepsilon_{23} = 0$ and $\varepsilon_{13} = 0$. Therefore, for the plane stress case, Generalized Hooke's Law can be written as:

$$\begin{Bmatrix}\sigma_1\\ \sigma_2\\ \sigma_{12}\end{Bmatrix}=\begin{bmatrix}Q_{11} & Q_{12} & 0\\ Q_{12} & Q_{22} & 0\\ 0 & 0 & Q_{66}\end{bmatrix}\begin{Bmatrix}\varepsilon_1\\ \varepsilon_2\\ \gamma_{12}\end{Bmatrix} \tag{2.3.2.2}$$

The material constants Q_{ij} in Equation (2.3.2.2) are called the reduced stiffnesses and are given, in terms of engineering constants, as [4]

$$\begin{aligned}Q_{11} &= \frac{E_1}{1-\nu_{12}\nu_{21}}\\ Q_{12} &= \frac{\nu_{12}E_2}{1-\nu_{12}\nu_{21}} = \frac{\nu_{21}E_1}{1-\nu_{12}\nu_{21}}\\ Q_{11} &= \frac{E_2}{1-\nu_{12}\nu_{21}}\\ Q_{11} &= G_{12}\end{aligned} \tag{2.3.2.3}$$

For a lamina of arbitrary orientation, stress strain relations are transformed using the approach explained in Section 2.3.1. Let the transformation matrix given in Equation (2.3.1.7) denoted with T_1 and the transformation matrix given in Equation (2.3.1.9) with T_2, so that

$$T_1=\begin{bmatrix}m^2 & n^2 & 2mn\\ n^2 & m^2 & -2mn\\ -mn & mn & \left(m^2-n^2\right)\end{bmatrix} \tag{2.3.2.4}$$

$$T_2=\begin{bmatrix}m^2 & n^2 & mn\\ n^2 & m^2 & -mn\\ -2mn & 2mn & \left(m^2-n^2\right)\end{bmatrix} \tag{2.3.2.5}$$

In geometric coordinates, stresses can be related to strains using the Equations (2.3.1.7), (2.3.1.9) and (2.3.2.2). Substituting the stress and strains

expressions for geometric coordinates given in Equations (2.3.1.7) and (2.3.1.9) into Equation (2.3.2.2) yields,

$$\begin{Bmatrix}\sigma_{\xi\xi}\\ \sigma_{\eta\eta}\\ \sigma_{\xi\eta}\end{Bmatrix} = T_1^{-1}\begin{bmatrix}Q_{11} & Q_{12} & 0\\ Q_{12} & Q_{22} & 0\\ 0 & 0 & Q_{66}\end{bmatrix} T_2 \begin{Bmatrix}\varepsilon_{\xi\xi}\\ \varepsilon_{\eta\eta}\\ \gamma_{\xi\eta}\end{Bmatrix} \tag{2.3.2.6}$$

Rewriting Equation (2.3.2.6) one gets,

$$\begin{Bmatrix}\sigma_{\xi\xi}\\ \sigma_{\eta\eta}\\ \sigma_{\xi\eta}\end{Bmatrix} = \begin{bmatrix}\overline{Q}_{11} & \overline{Q}_{12} & \overline{Q}_{16}\\ \overline{Q}_{12} & \overline{Q}_{22} & \overline{Q}_{26}\\ \overline{Q}_{16} & \overline{Q}_{26} & \overline{Q}_{66}\end{bmatrix} \begin{Bmatrix}\varepsilon_{\xi\xi}\\ \varepsilon_{\eta\eta}\\ \gamma_{\xi\eta}\end{Bmatrix} \tag{2.3.2.7}$$

where

$$\begin{aligned}
\overline{Q}_{11} &= Q_{11}\cos^4\theta + 2\left(Q_{12}+2Q_{66}\right)\cdot\sin^2\cos^2 + Q_{22}\sin^4\theta\\
\overline{Q}_{12} &= \left(Q_{11}+Q_{22}-4Q_{66}\right)\cos^2\theta\sin^2\theta + Q_{12}\left(\cos^4\theta+\sin^4\theta\right)\\
\overline{Q}_{22} &= Q_{11}\sin^4\theta + 2\left(Q_{12}+2Q_{66}\right)\cdot\sin^2\cos^2 + Q_{22}\cos^4\theta\\
\overline{Q}_{16} &= \left(Q_{11}-Q_{12}-2Q_{66}\right)\cos^3\theta\sin\theta + \left(Q_{11}-Q_{22}+2Q_{66}\right)\cos\theta\sin^3\theta\\
\overline{Q}_{26} &= \left(Q_{11}-Q_{12}-2Q_{66}\right)\cos\theta\sin^3\theta + \left(Q_{11}-Q_{22}+2Q_{66}\right)\cos^3\theta\sin\theta\\
\overline{Q}_{66} &= \left(Q_{11}+Q_{22}-2Q_{12}-2Q_{66}\right)\cos^2\theta\sin^2\theta + Q_{66}\left(\cos^4\theta+\sin^4\theta\right)
\end{aligned} \tag{2.3.2.8}$$

When transverse shear effects are not neglected, the terms $\gamma_{\xi\zeta}$ and $\gamma_{\eta\zeta}$ are non-zero and should appear in the constitutive equations. This is discussed further in Section 2.3.3. The relation between transverse shear stresses and transverse shear strains for geometric coordinates are given by [11]:

$$\begin{Bmatrix}\sigma_{\eta\zeta}\\ \sigma_{\xi\zeta}\end{Bmatrix} = \begin{bmatrix}\overline{Q}_{44} & \overline{Q}_{45}\\ \overline{Q}_{45} & \overline{Q}_{55}\end{bmatrix} \begin{Bmatrix}\gamma_{\eta\zeta}\\ \gamma_{\xi\zeta}\end{Bmatrix} \tag{2.3.2.9}$$

Note that the coordinate transformation is carried out the same way. So $\overline{Q}_{ij}$ $(i, j = 4,5)$ coefficients are given, in terms of material stiffness coefficients, by

$$\begin{aligned}
\overline{Q}_{44} &= Q_{44}\cos^2\theta + Q_{55}\sin^2\theta \\
\overline{Q}_{55} &= Q_{55}\cos^2\theta + Q_{44}\sin^2\theta \\
\overline{Q}_{45} &= (Q_{55} - Q_{44})\cos\theta\sin\theta
\end{aligned} \tag{2.3.2.10}$$

The material stiffness coefficients in transformation Equations (2.3.2.10) are given in terms of engineering constants, by

$$\begin{aligned}
Q_{44} &= C_{44} = G_{23} \\
Q_{55} &= C_{55} = G_{13}
\end{aligned} \tag{2.3.2.11}$$

Stress and strain variation in a laminate is essential for determining the extensional and bending stiffness of the laminate. In the classical lamination theory, the laminate is assumed to be consisting of perfectly bonded laminae. Displacements u_ξ and u_η are assumed to vary linearly through the thickness of the laminate. Similarly, strains $\varepsilon_{\xi\xi}$, $\varepsilon_{\eta\eta}$ and $\gamma_{\xi\eta}$ also vary linearly through the thickness of the laminate. Since the strains are related to the stresses through the Equation (2.3.2.7), stresses acting on each layer of the laminate can be integrated through the shell thickness to obtain the force and moment resultants per unit length for the shell which has a total thickness of h. For the face perpendicular to ξ direction, in-plane force resultants are given as [1]

$$\begin{Bmatrix} N_{\xi\xi} \\ N_{\xi\eta} \end{Bmatrix} = \int_{-h/2}^{h/2} \begin{Bmatrix} \sigma_{\xi\xi} \\ \sigma_{\xi\eta} \end{Bmatrix} \left(1 + \frac{\zeta}{R_\eta}\right) d\zeta \tag{2.3.2.12}$$

and for the face perpendicular to η direction,

$$\begin{Bmatrix} N_{\eta\eta} \\ N_{\eta\xi} \end{Bmatrix} = \int_{-h/2}^{h/2} \begin{Bmatrix} \sigma_{\eta\eta} \\ \sigma_{\eta\xi} \end{Bmatrix} \left(1 + \frac{\zeta}{R_\xi} \right) d\zeta \tag{2.3.2.13}$$

Similarly, the moment resultants are given by:

$$\begin{Bmatrix} M_{\xi\xi} \\ M_{\xi\eta} \end{Bmatrix} = \int_{-h/2}^{h/2} \begin{Bmatrix} \sigma_{\xi\xi} \\ \sigma_{\xi\eta} \end{Bmatrix} \left(1 + \frac{\zeta}{R_\eta} \right) \zeta \, d\zeta \tag{2.3.2.14}$$

$$\begin{Bmatrix} M_{\eta\eta} \\ M_{\eta\xi} \end{Bmatrix} = \int_{-h/2}^{h/2} \begin{Bmatrix} \sigma_{\eta\eta} \\ \sigma_{\eta\xi} \end{Bmatrix} \left(1 + \frac{\zeta}{R_\xi} \right) \zeta \, d\zeta \tag{2.3.2.15}$$

As mentioned in Section 2.2.1, one of the major assumptions made by Reissner for shell theory is that thickness of the shell is small compared to the other dimensions of the shell, so that ζ / R_ξ and ζ / R_η can be neglected.

Furthermore, although due to the symmetry of the stress tensor $\sigma_{\xi\eta} = \sigma_{\eta\xi}$, it is clear from Equations (2.3.2.12) and (2.3.2.13) that $N_{\xi\eta} \neq N_{\eta\xi}$ unless $R_\xi = R_\eta$ or ζ / R_ξ and ζ / R_η terms are cancelled from the equations. Since based on the assumptions of Reissner's shell theory ζ / R_ξ and ζ / R_η terms can be neglected, it can be said that for the current study, which is based on Reissner Shell Theory, the force resultants are also symmetric, $N_{\xi\eta} = N_{\eta\xi}$. Symmetry is also valid for the moment resultants, $M_{\xi\eta} = M_{\eta\xi}$. As a result, Equations (2.3.2.12) - (2.3.2.15) become, after regrouping,

$$\begin{Bmatrix} N_\xi \\ N_\eta \\ N_{\xi\eta} \end{Bmatrix} = \int_{-h/2}^{h/2} \begin{Bmatrix} \sigma_{\xi\xi} \\ \sigma_{\eta\eta} \\ \sigma_{\xi\eta} \end{Bmatrix} d\zeta \tag{2.3.2.16}$$

$$\begin{Bmatrix} M_\xi \\ M_\eta \\ M_{\xi\eta} \end{Bmatrix} = \int_{-h/2}^{h/2} \begin{Bmatrix} \sigma_{\xi\xi} \\ \sigma_{\eta\eta} \\ \sigma_{\xi\eta} \end{Bmatrix} \zeta \, d\zeta \tag{2.3.2.17}$$

Stresses are integrated over the laminate by integrating over each lamina separately. Since the laminae are assumed to be bonded perfectly, displacements are continuous through the thickness, but integrations for each lamina should be summed up.

$$\begin{Bmatrix} N_\xi \\ N_\eta \\ N_{\xi\eta} \end{Bmatrix} = \sum_{k=1}^{N} \int_{Z_{k-1}}^{Z_k} \begin{Bmatrix} \sigma_{\xi\xi} \\ \sigma_{\eta\eta} \\ \sigma_{\xi\eta} \end{Bmatrix}_k d\zeta \qquad (2.3.2.18)$$

$$\begin{Bmatrix} M_\xi \\ M_\eta \\ M_{\xi\eta} \end{Bmatrix} = \sum_{k=1}^{N} \int_{Z_{k-1}}^{Z_k} \begin{Bmatrix} \sigma_{\xi\xi} \\ \sigma_{\eta\eta} \\ \sigma_{\xi\eta} \end{Bmatrix}_k \zeta \, d\zeta \qquad (2.3.2.19)$$

In these equations, *N* is the total number of lamina and as shown in Figure 2.6, Z is the vectorial quantity defining the distance between the mid-surface and any layer; k is the dummy variable for the summation of values for each layer. It should be noted that although reference plane is usually taken as the mid plane of the shell or laminate wall, in theory reference surface can be taken anywhere within the laminate.

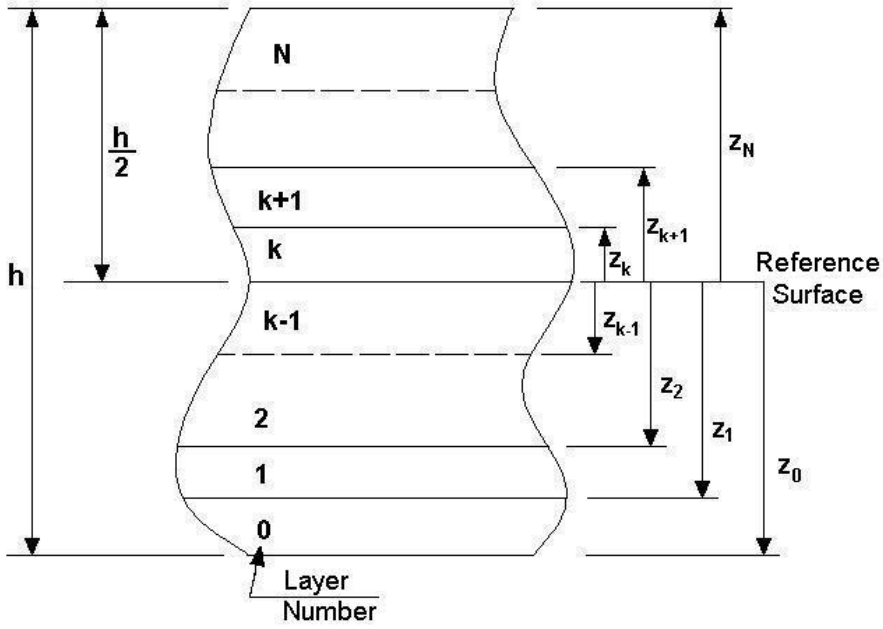

Figure 2.6 Stacking of Layers through the Shell Thickness

Substituting Hooke's Law given by Equation (2.3.2.7) into Equation (2.3.2.18) and Equation (2.3.2.19), and writing the total strains as the sum of membrane and bending strains as explained in Section 2.2, one gets:

$$\begin{Bmatrix} N_\xi \\ N_\eta \\ N_{\xi\eta} \end{Bmatrix} = \sum_{k=1}^{N} \begin{bmatrix} \overline{Q}_{11} & \overline{Q}_{12} & \overline{Q}_{16} \\ \overline{Q}_{12} & \overline{Q}_{22} & \overline{Q}_{26} \\ \overline{Q}_{16} & \overline{Q}_{26} & \overline{Q}_{66} \end{bmatrix}_k \left\{ \int_{Z_{k-1}}^{Z_k} \begin{Bmatrix} \varepsilon^0_{\xi\xi} \\ \varepsilon^0_{\eta\eta} \\ \varepsilon^0_{\xi\eta} \end{Bmatrix}_k d\zeta + \int_{Z_{k-1}}^{Z_k} \begin{Bmatrix} \kappa_{\xi\xi} \\ \kappa_{\eta\eta} \\ \kappa_{\xi\eta} \end{Bmatrix}_k \zeta \, d\zeta \right\} \qquad (2.3.2.20)$$

$$\begin{Bmatrix} M_\xi \\ M_\eta \\ M_{\xi\eta} \end{Bmatrix} = \sum_{k=1}^{N} \begin{bmatrix} \overline{Q}_{11} & \overline{Q}_{12} & \overline{Q}_{16} \\ \overline{Q}_{12} & \overline{Q}_{22} & \overline{Q}_{26} \\ \overline{Q}_{16} & \overline{Q}_{26} & \overline{Q}_{66} \end{bmatrix}_k \left\{ \int_{Z_{k-1}}^{Z_k} \begin{Bmatrix} \varepsilon^0_{\xi\xi} \\ \varepsilon^0_{\eta\eta} \\ \varepsilon^0_{\xi\eta} \end{Bmatrix}_k \zeta \, d\zeta + \int_{Z_{k-1}}^{Z_k} \begin{Bmatrix} \kappa_{\xi\xi} \\ \kappa_{\eta\eta} \\ \kappa_{\xi\eta} \end{Bmatrix}_k \zeta^2 d\zeta \right\} \qquad (2.3.2.21)$$

Performing the integrations, Equations (2.3.2.20) and (2.3.2.21) can be rewritten as:

$$\begin{Bmatrix} N_\xi \\ N_\eta \\ N_{\xi\eta} \end{Bmatrix} = \begin{bmatrix} A_{11} & A_{12} & A_{16} \\ A_{12} & A_{22} & A_{26} \\ A_{16} & A_{26} & A_{66} \end{bmatrix} \begin{Bmatrix} \varepsilon^0_{\xi\xi} \\ \varepsilon^0_{\eta\eta} \\ \varepsilon^0_{\xi\eta} \end{Bmatrix} + \begin{bmatrix} B_{11} & B_{12} & B_{16} \\ B_{12} & B_{22} & B_{26} \\ B_{16} & B_{26} & B_{66} \end{bmatrix} \begin{Bmatrix} \kappa_{\xi\xi} \\ \kappa_{\eta\eta} \\ \kappa_{\xi\eta} \end{Bmatrix} \quad (2.3.2.22)$$

$$\begin{Bmatrix} M_\xi \\ M_\eta \\ M_{\xi\eta} \end{Bmatrix} = \begin{bmatrix} B_{11} & B_{12} & B_{16} \\ B_{12} & B_{22} & B_{26} \\ B_{16} & B_{26} & B_{66} \end{bmatrix} \begin{Bmatrix} \varepsilon^0_{\xi\xi} \\ \varepsilon^0_{\eta\eta} \\ \varepsilon^0_{\xi\eta} \end{Bmatrix} + \begin{bmatrix} D_{11} & D_{12} & D_{16} \\ D_{12} & D_{22} & D_{26} \\ D_{16} & D_{26} & D_{66} \end{bmatrix} \begin{Bmatrix} \kappa_{\xi\xi} \\ \kappa_{\eta\eta} \\ \kappa_{\xi\eta} \end{Bmatrix} \quad (2.3.2.23)$$

where

$$A_{ij} = \sum_{k=1}^{N} \left(\overline{Q}_{ij}\right)_k \left(z_k - z_{k-1}\right) \qquad i, j = 1,2,6 \quad (2.3.2.24)$$

$$B_{ij} = \frac{1}{2} \sum_{k=1}^{N} \left(\overline{Q}_{ij}\right)_k \left(z_k^2 - z_{k-1}^2\right) \qquad i, j = 1,2,6 \quad (2.3.2.25)$$

$$D_{ij} = \frac{1}{3} \sum_{k=1}^{N} \left(\overline{Q}_{ij}\right)_k \left(z_k^3 - z_{k-1}^3\right) \qquad i, j = 1,2,6 \quad (2.3.2.26)$$

In Equations (2.3.2.24) – (2.3.2.26), A_{ij} terms are the extensional stiffness coefficients, B_{ij} terms are the bending stretching coupling stiffness coefficients, and D_{ij} terms are the bending stiffness coefficients.

In the case of the analysis of laminates that have not been cured at operational design temperatures, thermal stresses arise and final stress distribution is given by the superposition of stresses due to mechanical effects and thermal effects. To deal with the real world of polymer composites, strain stress relations must be modified as in Equations (2.3.2.27) and (2.3.2.28) [4].

$$\varepsilon_i = S_{ij}\sigma_j + \alpha_i \Delta T \quad (i = 1,2,3) \quad (2.3.2.27)$$

$$\varepsilon_i = S_{ij}\sigma_j \quad (i = 4,5,6) \quad (2.3.2.28)$$

It should be noted that coefficients of thermal expansion affect only extensional strains, not the shearing strain. The total normal strain ε_i is the sum of the mechanical strain $S_{ij}\sigma_j$ and the thermal strain $\alpha_i \Delta T$. Inverting the Equations (2.3.2.27) and (2.3.2.28), stress strain relations for plane stress for an orthotropic lamina are obtained.

$$\begin{Bmatrix} \sigma_1 \\ \sigma_2 \\ \sigma_{12} \end{Bmatrix} = \begin{bmatrix} Q_{11} & Q_{12} & 0 \\ Q_{12} & Q_{22} & 0 \\ 0 & 0 & Q_{66} \end{bmatrix} \begin{Bmatrix} \varepsilon_1 - \alpha_1 \Delta T \\ \varepsilon_2 - \alpha_2 \Delta T \\ \gamma_{12} \end{Bmatrix} \tag{2.3.2.29}$$

Stresses in laminate coordinates, or geometric coordinates, for the kth layer are obtained by transformation of coordinates. Transformation yields:

$$\begin{Bmatrix} \sigma_{\xi\xi} \\ \sigma_{\eta\eta} \\ \sigma_{\xi\eta} \end{Bmatrix}_k = \begin{bmatrix} \overline{Q}_{11} & \overline{Q}_{12} & \overline{Q}_{16} \\ \overline{Q}_{12} & \overline{Q}_{22} & \overline{Q}_{26} \\ \overline{Q}_{16} & \overline{Q}_{26} & \overline{Q}_{66} \end{bmatrix}_k \begin{Bmatrix} \varepsilon_{\xi\xi} - \alpha_\xi \Delta T \\ \varepsilon_{\eta\eta} - \alpha_\eta \Delta T \\ \gamma_{\xi\eta} - \alpha_{\xi\eta} \Delta T \end{Bmatrix}_k \tag{2.3.2.30}$$

where

$$\begin{aligned} \alpha_\xi &= \alpha_1 \cos^2\theta + \alpha_2 \sin^2\theta \\ \alpha_\eta &= \alpha_1 \sin^2\theta + \alpha_2 \cos^2\theta \\ \alpha_{\xi\eta} &= 2(\alpha_1 - \alpha_2)\cos\theta \sin\theta \end{aligned} \tag{2.3.2.31}$$

Substituting Equation (2.3.2.7) with Equation (2.3.2.30) and carrying out the same procedure for force and moment resultants, one gets:

$$\begin{Bmatrix} N_\xi \\ N_\eta \\ N_{\xi\eta} \end{Bmatrix} = \begin{bmatrix} A_{11} & A_{12} & A_{16} \\ A_{12} & A_{22} & A_{26} \\ A_{16} & A_{26} & A_{66} \end{bmatrix} \begin{Bmatrix} \varepsilon^0_{\xi\xi} \\ \varepsilon^0_{\eta\eta} \\ \varepsilon^0_{\xi\eta} \end{Bmatrix} + \begin{bmatrix} B_{11} & B_{12} & B_{16} \\ B_{12} & B_{22} & B_{26} \\ B_{16} & B_{26} & B_{66} \end{bmatrix} \begin{Bmatrix} \kappa_{\xi\xi} \\ \kappa_{\eta\eta} \\ \kappa_{\xi\eta} \end{Bmatrix} - \begin{Bmatrix} N^T_\xi \\ N^T_\eta \\ N^T_{\xi\eta} \end{Bmatrix} \tag{2.3.2.32}$$

$$\begin{Bmatrix} M_\xi \\ M_\eta \\ M_{\xi\eta} \end{Bmatrix} = \begin{bmatrix} B_{11} & B_{12} & B_{16} \\ B_{12} & B_{22} & B_{26} \\ B_{16} & B_{26} & B_{66} \end{bmatrix} \begin{Bmatrix} \varepsilon^0_{\xi\xi} \\ \varepsilon^0_{\eta\eta} \\ \varepsilon^0_{\xi\eta} \end{Bmatrix} + \begin{bmatrix} D_{11} & D_{12} & D_{16} \\ D_{12} & D_{22} & D_{26} \\ D_{16} & D_{26} & D_{66} \end{bmatrix} \begin{Bmatrix} \kappa_{\xi\xi} \\ \kappa_{\eta\eta} \\ \kappa_{\xi\eta} \end{Bmatrix} - \begin{Bmatrix} M^T_\xi \\ M^T_\eta \\ M^T_{\xi\eta} \end{Bmatrix} \quad (2.3.2.33)$$

where thermal force and moment resultants are given by Equations (2.3.2.34) and (2.3.2.35).

$$\begin{Bmatrix} N^T_\xi \\ N^T_\eta \\ N^T_{\xi\eta} \end{Bmatrix} = \sum_{k=1}^{N} \int_{Z_{k-1}}^{Z_k} \begin{bmatrix} \overline{Q}_{11} & \overline{Q}_{12} & \overline{Q}_{16} \\ \overline{Q}_{12} & \overline{Q}_{22} & \overline{Q}_{26} \\ \overline{Q}_{16} & \overline{Q}_{26} & \overline{Q}_{66} \end{bmatrix}_k \begin{Bmatrix} \alpha_\xi \\ \alpha_\eta \\ \alpha_{\xi\eta} \end{Bmatrix}_k \Delta T \, d\zeta \quad (2.3.2.34)$$

$$\begin{Bmatrix} M^T_\xi \\ M^T_\eta \\ M^T_{\xi\eta} \end{Bmatrix} = \sum_{k=1}^{N} \int_{Z_{k-1}}^{Z_k} \begin{bmatrix} \overline{Q}_{11} & \overline{Q}_{12} & \overline{Q}_{16} \\ \overline{Q}_{12} & \overline{Q}_{22} & \overline{Q}_{26} \\ \overline{Q}_{16} & \overline{Q}_{26} & \overline{Q}_{66} \end{bmatrix}_k \begin{Bmatrix} \alpha_\xi \\ \alpha_\eta \\ \alpha_{\xi\eta} \end{Bmatrix}_k \Delta T\zeta \, d\zeta \quad (2.3.2.35)$$

For constant spatial temperature difference between the operational temperature and cure temperature of the composite, thermal force and moment resultants can be obtained as:,

$$\begin{Bmatrix} N^T_\xi \\ N^T_\eta \\ N^T_{\xi\eta} \end{Bmatrix} = \sum_{k=1}^{N} \begin{bmatrix} \overline{Q}_{11} & \overline{Q}_{12} & \overline{Q}_{16} \\ \overline{Q}_{12} & \overline{Q}_{22} & \overline{Q}_{26} \\ \overline{Q}_{16} & \overline{Q}_{26} & \overline{Q}_{66} \end{bmatrix}_k \begin{Bmatrix} \alpha_\xi \\ \alpha_\eta \\ \alpha_{\xi\eta} \end{Bmatrix}_k \Delta T\left(z_k - z_{k-1}\right) \quad (2.3.2.36)$$

$$\begin{Bmatrix} M^T_\xi \\ M^T_\eta \\ M^T_{\xi\eta} \end{Bmatrix} = \frac{1}{2} \sum_{k=1}^{N} \begin{bmatrix} \overline{Q}_{11} & \overline{Q}_{12} & \overline{Q}_{16} \\ \overline{Q}_{12} & \overline{Q}_{22} & \overline{Q}_{26} \\ \overline{Q}_{16} & \overline{Q}_{26} & \overline{Q}_{66} \end{bmatrix}_k \begin{Bmatrix} \alpha_\xi \\ \alpha_\eta \\ \alpha_{\xi\eta} \end{Bmatrix}_k \Delta T\left(z_k^2 - z_{k-1}^2\right) \quad (2.3.2.37)$$

For shells of revolution it is very probable that the temperature across the thickness may vary depending on the exposure of the shell to external environment. For instance, a cylindrical pipe, which is subject to different temperatures inside and outside the cylinder, will definitely have a varying temperature distribution across the thickness of the shell. For thin walled shells, linear variation of the temperature distribution across the thickness can

be assumed in most engineering problems. If the temperature difference is allowed to vary linearly across the thickness in the form given by Equation (2.3.2.38),

$$\Delta T(\zeta) = \Delta T_1 + \Delta T_2\,\zeta \tag{2.3.2.38}$$

then the expressions should be modified accordingly. Note that $\zeta = 0$ plane is the middle surface of the laminate. Substituting Equation (2.3.2.38) into Equations (2.3.2.34) and (2.3.2.35),

$$\begin{Bmatrix} N_\xi^T \\ N_\eta^T \\ N_{\xi\eta}^T \end{Bmatrix} = \sum_{k=1}^{N} \int_{Z_{k-1}}^{Z_k} \begin{bmatrix} \overline{Q}_{11} & \overline{Q}_{12} & \overline{Q}_{16} \\ \overline{Q}_{12} & \overline{Q}_{22} & \overline{Q}_{26} \\ \overline{Q}_{16} & \overline{Q}_{26} & \overline{Q}_{66} \end{bmatrix}_k \begin{Bmatrix} \alpha_\xi \\ \alpha_\eta \\ \alpha_{\xi\eta} \end{Bmatrix}_k (\Delta T_1 + \Delta T_2 \zeta) d\zeta \tag{2.3.2.39}$$

$$\begin{Bmatrix} M_\xi^T \\ M_\eta^T \\ M_{\xi\eta}^T \end{Bmatrix} = \sum_{k=1}^{N} \int_{Z_{k-1}}^{Z_k} \begin{bmatrix} \overline{Q}_{11} & \overline{Q}_{12} & \overline{Q}_{16} \\ \overline{Q}_{12} & \overline{Q}_{22} & \overline{Q}_{26} \\ \overline{Q}_{16} & \overline{Q}_{26} & \overline{Q}_{66} \end{bmatrix}_k \begin{Bmatrix} \alpha_\xi \\ \alpha_\eta \\ \alpha_{\xi\eta} \end{Bmatrix}_k (\Delta T_1 + \Delta T_2 \zeta) \zeta\, d\zeta \tag{2.3.2.40}$$

Evaluation of the integrals yields:

$$\begin{Bmatrix} N_\xi^T \\ N_\eta^T \\ N_{\xi\eta}^T \end{Bmatrix} = \sum_{k=1}^{N} \begin{bmatrix} \overline{Q}_{11} & \overline{Q}_{12} & \overline{Q}_{16} \\ \overline{Q}_{12} & \overline{Q}_{22} & \overline{Q}_{26} \\ \overline{Q}_{16} & \overline{Q}_{26} & \overline{Q}_{66} \end{bmatrix}_k \begin{Bmatrix} \alpha_\xi \\ \alpha_\eta \\ \alpha_{\xi\eta} \end{Bmatrix}_k \left(\Delta T_1 (z_k - z_{k-1}) + \frac{\Delta T_2}{2} \left(z_k^2 - z_{k-1}^2 \right) \right) \tag{2.3.2.41}$$

$$\begin{Bmatrix} M_\xi^T \\ M_\eta^T \\ M_{\xi\eta}^T \end{Bmatrix} = \sum_{k=1}^{N} \begin{bmatrix} \overline{Q}_{11} & \overline{Q}_{12} & \overline{Q}_{16} \\ \overline{Q}_{12} & \overline{Q}_{22} & \overline{Q}_{26} \\ \overline{Q}_{16} & \overline{Q}_{26} & \overline{Q}_{66} \end{bmatrix}_k \begin{Bmatrix} \alpha_\xi \\ \alpha_\eta \\ \alpha_{\xi\eta} \end{Bmatrix}_k \left(\frac{\Delta T_1}{2} \left(z_k^2 - z_{k-1}^2 \right) + \frac{\Delta T_2}{3} \left(z_k^3 - z_{k-1}^3 \right) \right) \tag{2.3.2.42}$$

Thus, the thermal force and moment resultants caused by linearly varying temperature difference across the laminate thickness are obtained. Note that in Equation (2.3.2.38), setting $\Delta T_2 = 0$ reduces the Equations (2.3.2.41) and

(2.3.2.42) to the Equations (2.3.2.36) and (2.3.2.37), which are derived for constant temperature difference across the thickness. In total, constitutive equations can be written as

$$\begin{Bmatrix} N_{\xi\xi} \\ N_{\eta\eta} \\ N_{\xi\eta} \\ M_{\xi\xi} \\ M_{\eta\eta} \\ M_{\xi\eta} \end{Bmatrix} = \begin{bmatrix} A_{11} & A_{12} & A_{16} & B_{11} & B_{12} & B_{16} \\ A_{12} & A_{22} & A_{26} & B_{12} & B_{22} & B_{26} \\ A_{16} & A_{26} & A_{66} & B_{16} & B_{26} & B_{66} \\ B_{11} & B_{12} & B_{16} & D_{11} & D_{12} & D_{16} \\ B_{12} & B_{22} & B_{26} & D_{12} & D_{22} & D_{26} \\ B_{16} & B_{26} & B_{66} & D_{16} & D_{26} & D_{66} \end{bmatrix} \begin{Bmatrix} \varepsilon^0_{\xi\xi} \\ \varepsilon^0_{\eta\eta} \\ \gamma^0_{\xi\eta} \\ \kappa_{\xi\xi} \\ \kappa_{\eta\eta} \\ \kappa_{\xi\eta} \end{Bmatrix} - \begin{Bmatrix} N^T_{\xi\xi} \\ N^T_{\eta\eta} \\ N^T_{\xi\eta} \\ M^T_{\xi\xi} \\ M^T_{\eta\eta} \\ M^T_{\xi\eta} \end{Bmatrix} \qquad (2.3.2.43)$$

Substituting ϕ for ξ and θ for η, and bearing in mind that the strain displacement relations are given by Equations (2.2.3.1) – (2.2.3.6), in-plane constitutive equations for shells of revolution can be written as in Equation 2.3.2.44.

$$\begin{Bmatrix} N_{\phi\phi} \\ N_{\theta\theta} \\ N_{\phi\theta} \\ M_{\phi\phi} \\ M_{\theta\theta} \\ M_{\phi\theta} \end{Bmatrix} = \begin{bmatrix} A_{11} & A_{12} & A_{16} & B_{11} & B_{12} & B_{16} \\ A_{12} & A_{22} & A_{26} & B_{12} & B_{22} & B_{26} \\ A_{16} & A_{26} & A_{66} & B_{16} & B_{26} & B_{66} \\ B_{11} & B_{12} & B_{16} & D_{11} & D_{12} & D_{16} \\ B_{12} & B_{22} & B_{26} & D_{12} & D_{22} & D_{26} \\ B_{16} & B_{26} & B_{66} & D_{16} & D_{26} & D_{66} \end{bmatrix} \begin{Bmatrix} \varepsilon^0_{\phi\phi} \\ \varepsilon^0_{\theta\theta} \\ \gamma^0_{\phi\theta} \\ \kappa_{\phi\phi} \\ \kappa_{\theta\theta} \\ \kappa_{\phi\theta} \end{Bmatrix} - \begin{Bmatrix} N^T_{\phi\phi} \\ N^T_{\theta\theta} \\ N^T_{\phi\theta} \\ M^T_{\phi\phi} \\ M^T_{\theta\theta} \\ M^T_{\phi\theta} \end{Bmatrix} \qquad (2.3.2.44)$$

Constitutive equations for the circular cylindrical shells of revolution can be written by substituting x in place of ϕ in Equation (2.3.2.44), and keeping in mind that strain displacement relations are given by Equations (2.2.3.12) – (2.2.3.17).

$$\begin{Bmatrix} N_{xx} \\ N_{\theta\theta} \\ N_{x\theta} \\ M_{xx} \\ M_{\theta\theta} \\ M_{x\theta} \end{Bmatrix} = \begin{bmatrix} A_{11} & A_{12} & A_{16} & B_{11} & B_{12} & B_{16} \\ A_{12} & A_{22} & A_{26} & B_{12} & B_{22} & B_{26} \\ A_{16} & A_{26} & A_{66} & B_{16} & B_{26} & B_{66} \\ B_{11} & B_{12} & B_{16} & D_{11} & D_{12} & D_{16} \\ B_{12} & B_{22} & B_{26} & D_{12} & D_{22} & D_{26} \\ B_{16} & B_{26} & B_{66} & D_{16} & D_{26} & D_{66} \end{bmatrix} \begin{Bmatrix} \varepsilon^0_{xx} \\ \varepsilon^0_{\theta\theta} \\ \gamma^0_{x\theta} \\ \kappa_{xx} \\ \kappa_{\theta\theta} \\ \kappa_{x\theta} \end{Bmatrix} - \begin{Bmatrix} N^T_{xx} \\ N^T_{\theta\theta} \\ N^T_{x\theta} \\ M^T_{xx} \\ M^T_{\theta\theta} \\ M^T_{x\theta} \end{Bmatrix} \quad (2.3.2.45)$$

2.3.3. Transverse Shear Resultants

In order to include the transverse shear effects in the formulation, assumptions of classical shell theory should be modified such that transverse shear strains $\gamma_{\xi\zeta}$ and $\gamma_{\eta\zeta}$ should be taken as non-zero. When the transverse shear deformation is non-zero, surfaces normal to the middle surface before deformation will not remain normal after deformation. In case of first order transverse shear deformation theory, it is assumed that normals to the mid surface before deformation at most undergoes a rotation leading to two more unknowns compared to the unknowns present in classical shell theory equations.

Since the top and bottom surfaces of the laminates composite shell are free surfaces and therefore force and moment resultants should be equal to zero on these faces, assuming constant transverse shear stresses do not satisfy the boundary conditions on the top and bottom surfaces of the shell. However, according to the elementary beam theory, the transverse shear stress varies parabolically through the beam thickness and is zero at the top and bottom surfaces. In order to satisfy these conditions, Equation (2.3.3.1) is used as a weighing function, so that the transverse shear stress distribution is parabolic through the thickness and equals to zero at the top and bottom surfaces of the shell [12].

$$f(\zeta)=\frac{5}{4}\left\{1-\left[\frac{\zeta}{h/2}\right]^2\right\} \tag{2.3.3.1}$$

In Equation (2.3.3.1), h is the total thickness of the laminated composite shell and the coefficient $5/4$ is called as the shear correction factor, as suggested by Mindlin and Reissner for the isotropic case [10], [13]. It should be noted that a factor of 5/4 multiplies the distribution function used by Whitney [14] so that the shear factor calculated for the layered anisotropic shell wall can be consistent with the established shear factor from the previous work of Mindlin [10] and Reissner [13] for the homogenous case.

The relation between transverse shear stresses and transverse shear strains were given by Equation (2.3.2.9). By multiplying the transverse shear stresses by the weighing function, Equation (2.3.3.1), and carrying out integration through the thickness of the laminated shell wall, the transverse force resultants can be calculated as given Equations (2.3.3.2) and (2.3.3.3) [1].

$$Q_{\eta\zeta}=\sum_{k=1}^{N}\int_{Z_{k-1}}^{Z_k}\left(\sigma_{\eta\zeta}\right)_k\left(1+\frac{\zeta}{R_\xi}\right)f(\zeta)\,d\zeta \tag{2.3.3.2}$$

$$Q_{\xi\zeta}=\sum_{k=1}^{N}\int_{Z_{k-1}}^{Z_k}\left(\sigma_{\xi\zeta}\right)_k\left(1+\frac{\zeta}{R_\eta}\right)f(\zeta)\,d\zeta \tag{2.3.3.3}$$

Again utilizing the basic Reissner Shell Theory assumption that the thickness of the shell is small compared to the other dimensions of the shell, so that ζ/R_ξ and ζ/R_η can be neglected, as explained in Section 2.3.2, Equations (2.3.3.2) and (2.3.3.3) become

$$\begin{Bmatrix}Q_{\eta\zeta}\\ Q_{\xi\zeta}\end{Bmatrix}=\sum_{k=1}^{N}\int_{Z_{k-1}}^{Z_k}\begin{Bmatrix}\sigma_{\eta\zeta}\\ \sigma_{\xi\zeta}\end{Bmatrix}_k f(\zeta)d\zeta \tag{2.3.3.4}$$

Substituting Equation (2.3.2.9) into (2.3.3.4), one gets Equation (2.3.3.5).

$$\begin{Bmatrix} Q_{\eta\zeta} \\ Q_{\xi\zeta} \end{Bmatrix} = \begin{bmatrix} A_{44} & A_{45} \\ A_{45} & A_{55} \end{bmatrix} \begin{Bmatrix} \gamma_{\eta\zeta} \\ \gamma_{\xi\zeta} \end{Bmatrix} \tag{2.3.3.5}$$

where A_{ij} $(i, j = 4,5)$ terms, which are defined as transverse shear stiffness coefficients, are given by

$$A_{ij} = \frac{5}{4}\sum_{k=1}^{N}\left(\overline{Q}_{ij}\right)_k \left[z_k - z_{k-1} - \frac{4}{3}\left(z_k^3 - z_{k-1}^3\right)\frac{1}{h^2} \right] \quad (i, j = 4,5) \tag{2.3.3.6}$$

In Equation (2.3.3.6), $\overline{Q}_{ij}$ $(i, j = 4,5)$ terms are given by Equation (2.3.2.10).

For a general shell of revolution, by switching the coordinate notation, $\xi \leftrightarrow \phi$ and $\eta \leftrightarrow \theta$, one can rewrite 2.3.3.5 as:

$$\begin{Bmatrix} Q_{\theta\zeta} \\ Q_{\phi\zeta} \end{Bmatrix} = \begin{bmatrix} A_{44} & A_{45} \\ A_{45} & A_{55} \end{bmatrix} \begin{Bmatrix} \gamma_{\theta\zeta} \\ \gamma_{\phi\zeta} \end{Bmatrix} \tag{2.3.3.7}$$

In addition, for a circular cylindrical shell of revolution, after switching the coordinates ($\phi \leftrightarrow x$) one can rewrite Equation (2.3.3.7) as:

$$\begin{Bmatrix} Q_{\theta\zeta} \\ Q_{x\zeta} \end{Bmatrix} = \begin{bmatrix} A_{44} & A_{45} \\ A_{45} & A_{55} \end{bmatrix} \begin{Bmatrix} \gamma_{\theta\zeta} \\ \gamma_{x\zeta} \end{Bmatrix} \tag{2.3.3.8}$$

2.4. Equations of Motion

In this section the equations representing the kinetics of the problem, which are called the equations of motion; or the equilibrium equations are described.

2.4.1. General Derivation

Equations of motion for shells of arbitrary shape is derived from Hamilton's Principle, which states that while there are several possible paths along which a dynamic system may move from one point to another in space and time, the path which is actually followed is the one that minimizes the time integral of the difference between the kinetic and potential energies.

Hamilton's Principle can be written as in Equation (2.4.1.1) [3].

$$\delta \int_{t_0}^{t_1} (U_s - K - W_{in}) dt = 0 \qquad (2.4.1.1)$$

where U_s is the strain energy, K is the kinetic energy and W_{in} is the total input energy, which is defined as the sum of the energy input by the boundary force resultants (E_B) and the energy input by the applied load components (E_L). By taking the variation symbol inside the integral one can re-express the Hamilton's principle as:

$$\int_{t_0}^{t_1} (\delta U_s - \delta K - \delta E_B - \delta E_L) dt = 0 \qquad (2.4.1.2)$$

In Equation (2.4.1.2), if the variations are examined one by one and evaluated separately, after substituting them back to Equation (2.4.1.2), Equation

(2.4.1.3) is obtained for a general shell. The full derivation of Equation 2.4.1.3 is skipped since it is given in many previous works such as [1], [2]. In Equation (2.4.1.3) translatory and rotatory inertia terms are also included for the sake of generality.

$$
\begin{aligned}
&\int_{t_0}^{t_1}\int_{\eta}\int_{\xi}\Bigg[\Bigg(-\frac{\partial\left(N_{\xi\xi}\alpha_{\eta}\right)}{\partial\xi}-\frac{\partial\left(N_{\xi\eta}\alpha_{\xi}\right)}{\partial\eta}-N_{\xi\eta}\frac{\partial\alpha_{\xi}}{\partial\eta}+N_{\eta\eta}\frac{\partial\alpha_{\eta}}{\partial\xi}-\frac{Q_{\xi\zeta}}{R_{\xi}}\alpha_{\xi}\alpha_{\eta}\\
&-p_{\xi}\alpha_{\xi}\alpha_{\eta}+\rho h\ddot{u}_{\xi}\alpha_{\xi}\alpha_{\eta}\Bigg)\delta u_{\xi}\\
&+\Bigg(-\frac{\partial\left(N_{\xi\eta}\alpha_{\eta}\right)}{\partial\xi}-\frac{\partial\left(N_{\eta\eta}\alpha_{\xi}\right)}{\partial\eta}-N_{\xi\eta}\frac{\partial\alpha_{\eta}}{\partial\xi}+N_{\xi\xi}\frac{\partial\alpha_{\xi}}{\partial\eta}-\frac{Q_{\eta\zeta}}{R_{\eta}}\alpha_{\xi}\alpha_{\eta}\\
&-p_{\eta}\alpha_{\xi}\alpha_{\eta}+\rho h\ddot{u}_{\eta}\alpha_{\xi}\alpha_{\eta}\Bigg)\delta u_{\eta}\\
&+\Bigg(-\frac{\partial\left(Q_{\eta\zeta}\alpha_{\xi}\right)}{\partial\eta}-\frac{\partial\left(Q_{\xi\zeta}\alpha_{\eta}\right)}{\partial\xi}+\left(\frac{N_{\xi\xi}}{R_{\xi}}+\frac{N_{\eta\eta}}{R_{\eta}}\right)\alpha_{\xi}\alpha_{\eta}\\
&-p_{\zeta}\alpha_{\xi}\alpha_{\eta}+\rho h\ddot{u}_{\zeta}\alpha_{\xi}\alpha_{\eta}\Bigg)\delta u_{\zeta}\\
&+\Bigg(-\frac{\partial\left(M_{\xi\xi}\alpha_{\eta}\right)}{\partial\xi}-\frac{\partial\left(M_{\xi\eta}\alpha_{\xi}\right)}{\partial\eta}-M_{\xi\eta}\frac{\partial\alpha_{\xi}}{\partial\eta}+M_{\eta\eta}\frac{\partial\alpha_{\eta}}{\partial\xi}+Q_{\xi\zeta}\alpha_{\xi}\alpha_{\eta}\\
&+\rho\frac{h^{3}}{12}\ddot{\beta}_{\xi}\alpha_{\xi}\alpha_{\eta}\Bigg)\delta\beta_{\xi}\\
&+\Bigg(-\frac{\partial\left(M_{\xi\eta}\alpha_{\eta}\right)}{\partial\xi}-\frac{\partial\left(M_{\eta\eta}\alpha_{\xi}\right)}{\partial\eta}-M_{\xi\eta}\frac{\partial\alpha_{\eta}}{\partial\xi}+M_{\xi\xi}\frac{\partial\alpha_{\xi}}{\partial\eta}+Q_{\eta\zeta}\alpha_{\xi}\alpha_{\eta}\\
&+\rho\frac{h^{3}}{12}\ddot{\beta}_{\eta}\alpha_{\xi}\alpha_{\eta}\Bigg)\delta\beta_{\eta}\Bigg]d\xi\,d\eta\,d\zeta\\
&+\int_{t_0}^{t_1}\int_{\xi}\Big[\left(N_{\xi\eta}-N_{\xi\eta}^{*}\right)\delta u_{\xi}+\left(N_{\eta\eta}-N_{\eta\eta}^{*}\right)\delta u_{\eta}+\left(Q_{\eta\zeta}-Q_{\eta\zeta}^{*}\right)\delta u_{\zeta}\\
&+\left(M_{\xi\eta}-M_{\xi\eta}^{*}\right)\delta\beta_{\xi}+\left(M_{\eta\eta}-M_{\eta\eta}^{*}\right)\delta\beta_{\eta}\Big]\cdot\alpha_{\xi}\,d\xi\,dt
\end{aligned}
\tag{2.4.1.3}
$$

$$+\int_{t_0}^{t_1}\int_{\eta}\left[\left(N_{\xi\xi}-N_{\xi\xi}^{*}\right)\delta u_{\xi}+\left(N_{\xi\eta}-N_{\xi\eta}^{*}\right)\delta u_{\eta}+\left(Q_{\xi\zeta}-Q_{\xi\zeta}^{*}\right)\delta u_{\zeta}\right.$$
$$\left.+\left(M_{\xi\xi}-M_{\xi\xi}^{*}\right)\delta\beta_{\xi}+\left(M_{\xi\eta}-M_{\xi\eta}^{*}\right)\delta\beta_{\eta}\right]\alpha_{\eta}\,d\eta\,dt=0$$

Equation (2.4.1.3) can be satisfied only if each of the triple and double integrals is zero individually. Moreover, since the variational displacements are arbitrary, each integral equation can only be satisfied if the coefficients of the variational displacements are zero. Thus, by setting the coefficients of the triple integral to zero, one gets the following five equations of motion for a shell of arbitrary shape.

$$\frac{\partial(N_{\xi\xi}\alpha_{\eta})}{\partial\xi}+\frac{\partial(N_{\xi\eta}\alpha_{\xi})}{\partial\eta}+N_{\xi\eta}\frac{\partial\alpha_{\xi}}{\partial\eta}-N_{\eta\eta}\frac{\partial\alpha_{\eta}}{\partial\xi}+\frac{Q_{\xi\zeta}}{R_{\xi}}\alpha_{\xi}\alpha_{\eta}$$
$$+p_{\xi}\alpha_{\xi}\alpha_{\eta}=\rho h\ddot{u}_{\xi}\alpha_{\xi}\alpha_{\eta} \qquad (2.4.1.4)$$

$$\frac{\partial(N_{\xi\eta}\alpha_{\eta})}{\partial\xi}+\frac{\partial(N_{\eta\eta}\alpha_{\xi})}{\partial\eta}+N_{\xi\eta}\frac{\partial\alpha_{\eta}}{\partial\xi}-N_{\xi\xi}\frac{\partial\alpha_{\xi}}{\partial\eta}+\frac{Q_{\eta\zeta}}{R_{\eta}}\alpha_{\xi}\alpha_{\eta}$$
$$+p_{\eta}\alpha_{\xi}\alpha_{\eta}=\rho h\ddot{u}_{\eta}\alpha_{\xi}\alpha_{\eta} \qquad (2.4.1.5)$$

$$\frac{\partial(Q_{\xi\zeta}\alpha_{\eta})}{\partial\xi}+\frac{\partial(Q_{\eta\zeta}\alpha_{\xi})}{\partial\eta}+-\left(\frac{N_{\xi\xi}}{R_{\xi}}+\frac{N_{\eta\eta}}{R_{\eta}}\right)\alpha_{\xi}\alpha_{\eta}-p_{\zeta}\alpha_{\xi}\alpha_{\eta}=\rho h\ddot{u}_{\zeta}\alpha_{\xi}\alpha_{\eta} \qquad (2.4.1.6)$$

$$\frac{\partial(M_{\xi\xi}\alpha_{\eta})}{\partial\xi}+\frac{\partial(M_{\xi\eta}\alpha_{\xi})}{\partial\eta}+M_{\xi\eta}\frac{\partial\alpha_{\xi}}{\partial\eta}-M_{\eta\eta}\frac{\partial\alpha_{\eta}}{\partial\xi}$$
$$-Q_{\xi\zeta}\alpha_{\xi}\alpha_{\eta}=\rho\frac{h^{3}}{12}\ddot{\beta}_{\xi}\alpha_{\xi}\alpha_{\eta} \qquad (2.4.1.7)$$

$$\frac{\partial(M_{\xi\eta}\alpha_{\eta})}{\partial\xi}+\frac{\partial(M_{\eta\eta}\alpha_{\xi})}{\partial\eta}+M_{\xi\eta}\frac{\partial\alpha_{\eta}}{\partial\xi}-M_{\xi\xi}\frac{\partial\alpha_{\xi}}{\partial\eta}$$
$$-Q_{\eta\zeta}\alpha_{\xi}\alpha_{\eta}=\rho\frac{h^{3}}{12}\ddot{\beta}_{\eta}\alpha_{\xi}\alpha_{\eta} \qquad (2.4.1.8)$$

If one traces the derivation of these equations from their beginning at Hamilton's Principle to the ending at equilibrium equations, It will be revealed that in these equations, p_ξ, p_η and p_ζ terms are caused by the distributed forces applied to shell externally. Among them, since p_ζ is the distributed force in the thickness direction, it is always normal to the surface and therefore can be treated as pressure. Furthermore, p_ξ and p_η can be considered as the applied shearing stresses in the ξ and η directions, respectively.

2.4.2. Boundary Conditions

Each of the double integrals given in (2.4.1.3) is equal to zero only if the coefficients of the variational displacements, variational displacements or one of the two for each term are zero. Since variational displacements are only zero at all times when the boundary displacements are prescribed, this translates into the following possible boundary conditions for a constant ξ edge.

Either $N_{\xi\xi} = N^*_{\xi\xi}$ or $u_\xi = u^*_\xi$ (2.4.2.1)

Either $N_{\xi\eta} = N^*_{\xi\eta}$ or $u_\eta = u^*_\eta$ (2.4.2.2)

Either $Q_{\xi\zeta} = Q^*_{\xi\zeta}$ or $u_\zeta = u^*_\zeta$ (2.4.2.3)

Either $M_{\xi\xi} = M^*_{\xi\xi}$ or $\beta_\xi = \beta^*_\xi$ (2.4.2.4)

Either $M_{\xi\eta} = M^*_{\xi\eta}$ or $\beta_\eta = \beta^*_\eta$ (2.4.2.5)

This states the intuitively obvious fact that at a boundary one has to prescribe either force resultants (moments) or displacements (rotations). Thus, at a constant ξ edge, five conditions have to be specified. Similarly, examining

Equation (2.4.3) along a constant η edge, the five boundary conditions have to be given by Equations (2.4.2.6) – (2.4.2.10).

Either $N_{\xi\eta} = N^*_{\xi\eta}$ or $u_\xi = u^*_\xi$ (2.4.2.6)

Either $N_{\eta\eta} = N^*_{\eta\eta}$ or $u_\eta = u^*_\eta$ (2.4.2.7)

Either $Q_{\eta\zeta} = Q^*_{\eta\zeta}$ or $u_\zeta = u^*_\zeta$ (2.4.2.8)

Either $M_{\xi\eta} = M^*_{\xi\eta}$ or $\beta_\xi = \beta^*_\xi$ (2.4.2.9)

Either $M_{\eta\eta} = M^*_{\eta\eta}$ or $\beta_\eta = \beta^*_\eta$ (2.4.2.10)

It should be noted that the terms given with asterisk (*) are the prescribed values of the boundary conditions.

2.4.3. Reduction to Shells of Revolution

Equations (2.4.1.4) – (2.4.1.8) along with boundary conditions (2.4.2.1) – (2.4.2.10) constitute the equations of equilibrium for an arbitrary shaped shell. Therefore, some simplifications should be made to obtain the equations of motion for shells of revolution. Substituting Equations (2.1.3.9), (2.1.3.10) and (2.1.3.13) into Equations (2.4.1.4) through (2.4.1.8), and changing the variables used for the shell coordinates $\phi \leftrightarrow \xi$ and $\theta \leftrightarrow \eta$ one gets the equations of equilibrium for a general shell of revolution.

$$\frac{\partial N_{\phi\phi}}{\partial \phi} R_\theta \sin\phi + (N_{\phi\phi} - N_{\theta\theta}) R_\phi \cos\phi + \frac{\partial N_{\phi\theta}}{\partial \theta} R_\phi + Q_{\phi\zeta} R_\theta \sin\phi + p_\phi R_\phi R_\theta \sin\phi = \rho h \ddot{u}^0_\phi R_\theta R_\phi \sin\phi \quad (2.4.3.1)$$

$$\frac{\partial N_{\phi\theta}}{\partial \phi} R_\theta \sin\phi + 2N_{\phi\theta} R_\phi \cos\phi + \frac{\partial N_{\theta\theta}}{\partial \theta} R_\phi + Q_{\theta\zeta} R_\phi \sin\phi + p_\theta R_\phi R_\theta \sin\phi = \rho h \ddot{u}^0_\theta R_\theta R_\phi \sin\phi \quad (2.4.3.2)$$

$$\frac{\partial Q_{\theta\zeta}}{\partial\theta}R_\phi+\frac{\partial Q_{\phi\zeta}}{\partial\phi}R_\theta\sin\phi+Q_\phi R_\phi\cos\phi-N_{\theta\theta}R_\phi\sin\phi-N_{\phi\phi}R_\theta\sin\phi$$
$$+p_\xi R_\phi R_\theta\sin\phi=\rho h\ddot{w}^0R_\theta R_\phi\sin\phi \qquad (2.4.3.3)$$

$$\frac{\partial M_{\phi\phi}}{\partial\phi}R_\theta\sin\phi+\frac{\partial M_{\phi\theta}}{\partial\theta}R_\phi+(M_{\phi\phi}-M_{\theta\theta})R_\phi\cos\phi-Q_{\phi\zeta}R_\phi R_\theta\sin\phi$$
$$=\frac{1}{12}\rho h^3\ddot{\beta}_\phi R_\theta R_\phi\sin\phi \qquad (2.4.3.4)$$

$$\frac{\partial M_{\phi\theta}}{\partial\phi}R_\theta\sin\phi+\frac{\partial M_{\theta\theta}}{\partial\theta}R_\phi+2M_{\phi\theta}R_\phi\cos\phi-Q_{\theta\zeta}R_\phi R_\theta\sin\phi$$
$$=\frac{1}{12}\rho h^3\ddot{\beta}_\theta R_\theta R_\phi\sin\phi \qquad (2.4.3.5)$$

For a shell of revolution, circumferential coordinate θ changes from 0 to 2π; so it traverses a full circle. Therefore, there is no boundary at a constant θ edge, meaning that only possible boundary is constant $\phi=$ edge, where a boundary condition can be applied. So, the applicable boundary conditions are given by Equations (2.4.2.1) – (2.4.2.5). Since for shell of revolution $\xi\leftrightarrow\phi$ and $\eta\leftrightarrow\theta$, these equations can be re-written as:

Either $N_{\phi\phi}=N^*_{\phi\phi}$ or $u_\phi=u^*_\phi$ (2.4.3.6)

Either $N_{\phi\theta}=N^*_{\phi\theta}$ or $u_\theta=u^*_\theta$ (2.4.3.7)

Either $Q_{\phi\zeta}=Q^*_{\phi\zeta}$ or $u_\zeta=u^*_\zeta$ (2.4.3.8)

Either $M_{\phi\phi}=M^*_{\phi\phi}$ or $\beta_\phi=\beta^*_\phi$ (2.4.3.9)

Either $M_{\phi\theta}=M^*_{\phi\theta}$ or $\beta_\theta=\beta^*_\theta$ (2.4.3.10)

It should be noted that for a shell of revolution the first double integral in Equation (2.4.1.3) vanishes. This is because in the derivation of Equation (2.4.1.3) at the intermediate steps integration by parts is applied. When the integration by parts is applied to η derivative terms, the first integral which emerges is a definite integral which has to be evaluated at the η boundaries.

Since for a shell of revolution η boundaries coincide the force and moment resultant terms (N and M) coming from the strain energy expression vanishes. In addition, since not constant η boundary exists the energy input into the shell by the applied boundary force and moment resultants (N^* and M^*) along a constant η boundary also does not exist. Thus, the first double integral in Equation (2.4.1.3) vanishes.

Furthermore, since the current study is limited to static conditions, terms involving the change of quantities with time (i.e. derivatives with respect to time) necessarily happen to be zero and drop from the equations. Therefore, Equations (2.4.3.1) to (2.4.3.5) become:

$$\frac{\partial N_{\phi\phi}}{\partial \phi} R_\theta \sin\phi + (N_{\phi\phi} - N_{\theta\theta}) R_\phi \cos\phi + \frac{\partial N_{\phi\theta}}{\partial \theta} R_\phi + Q_{\phi\zeta} R_\theta \sin\phi + p_\phi R_\phi R_\theta \sin\phi = 0 \quad (2.4.3.11)$$

$$\frac{\partial N_{\phi\theta}}{\partial \phi} R_\theta \sin\phi + 2N_{\phi\theta} R_\phi \cos\phi + \frac{\partial N_{\theta\theta}}{\partial \theta} R_\phi + Q_{\theta\zeta} R_\phi \sin\phi + p_\theta R_\phi R_\theta \sin\phi = 0 \quad (2.4.3.12)$$

$$\frac{\partial Q_{\theta\zeta}}{\partial \theta} R_\phi + \frac{\partial Q_{\phi\zeta}}{\partial \phi} R_\theta \sin\phi + Q_\phi R_\phi \cos\phi - N_{\theta\theta} R_\phi \sin\phi - N_{\phi\phi} R_\theta \sin\phi + p_\xi R_\phi R_\theta \sin\phi = 0 \quad (2.4.3.13)$$

$$\frac{\partial M_{\phi\phi}}{\partial \phi} R_\theta \sin\phi + \frac{\partial M_{\phi\theta}}{\partial \theta} R_\phi + (M_{\phi\phi} - M_{\theta\theta}) R_\phi \cos\phi - Q_{\phi\zeta} R_\phi R_\theta \sin\phi = 0 \quad (2.4.3.14)$$

$$\frac{\partial M_{\phi\theta}}{\partial \phi} R_\theta \sin\phi + \frac{\partial M_{\theta\theta}}{\partial \theta} R_\phi + 2M_{\phi\theta} R_\phi \cos\phi - Q_{\theta\zeta} R_\phi R_\theta \sin\phi = 0 \quad (2.4.3.15)$$

Equilibrium equations for circular cylindrical shell of revolution can be obtained by substituting Equations (2.3.1.14) to (2.3.1.16) and (2.3.1.18), with the change of coordinate ϕ to coordinate x, into these equilibrium Equations (2.4.3.11) to (2.4.3.15) given for general shell of revolution above. Thus, the

equilibrium equations for a circular cylindrical shell of revolution reduce to Equations (2.4.3.16) – (2.4.3.20).

$$\frac{\partial N_{xx}}{\partial x}R+\frac{\partial N_{x\theta}}{\partial \theta}+p_x R=0 \tag{2.4.3.16}$$

$$\frac{\partial N_{x\theta}}{\partial x}R+\frac{\partial N_{\theta\theta}}{\partial \theta}+Q_{\theta\zeta}+p_\theta R=0 \tag{2.4.3.17}$$

$$\frac{\partial Q_{\theta\zeta}}{\partial \theta}+\frac{\partial Q_{x\zeta}}{\partial x}R-N_{\theta\theta}R+p_\xi R=0 \tag{2.4.3.18}$$

$$\frac{\partial M_{xx}}{\partial x}R+\frac{\partial M_{x\theta}}{\partial \theta}-Q_{\phi\zeta}R=0 \tag{2.4.3.19}$$

$$\frac{\partial M_{x\theta}}{\partial x}R+\frac{\partial M_{\theta\theta}}{\partial \theta}-Q_{\theta\zeta}R=0 \tag{2.4.3.20}$$

And obviously the boundary conditions are re-written with x substitution in place of ϕ:

Either $N_{xx}=N_{xx}^*$ or $u_x=u_x^*$ (2.4.3.21)

Either $N_{x\theta}=N_{x\theta}^*$ or $u_\theta=u_\theta^*$ (2.4.3.22)

Either $Q_{x\zeta}=Q_{x\zeta}^*$ or $u_\zeta=u_\zeta^*$ (2.4.3.23)

Either $M_{xx}=M_{xx}^*$ or $\beta_x=\beta_x^*$ (2.4.3.24)

Either $M_{x\theta}=M_{x\theta}^*$ or $\beta_\theta=\beta_\theta^*$ (2.4.3.25)

CHAPTER 3

METHOD OF SOLUTION

3.1. General Description of the Method of Solution

In Chapter 2, governing equations required for the static analysis of shells of revolution are explained. In this chapter, a solution methodology will be defined in order to exhibit how these equations are handled. First in Section 3.2, the governing equations are reduced to a system of equations called fundamental set of equations by some algebraic formulations and manipulations. In Section 3.3, Finite Exponential Fourier Transform of the fundamental system of equations [8] is performed in order to eliminate the circumferential coordinate from the fundamental set of equations. Having completed this operation, the physical shell variables are transformed and the solution method is applied on the fundamental system of equations written in terms of transformed shell variables. In Sections 3.4 and 3.5, these transformed unknown variables of fundamental set of equations, which are derived in Section 3.3, are solved by the methods named as *reduction of a two-point boundary value problem to a number of initial value problems* and *multisegment method of integration,* respectively [7]. After the solution, these variables are back-transformed to actual physical variables with the method described in Section 3.6, and in Section 3.7 stresses and strains are extracted by post processing on the fundamental shell variables which are found by applying the solution methodology.

3.2. Formulation of Fundamental System of Equations

In Chapter 2, governing equations for rotationally symmetric shells of revolution are given. In summary, there are 21 equations, of which eight are kinematic equations (Equations (2.2.3.1) – (2.2.3.6), (2.2.3.10), (2.2.3.11)), there are eight constitutive equations (Equations (2.3.2.44), (2.3.3.7)) and there are five equilibrium equations (Equations (2.4.3.11) – (2.4.3.15)). In these equations there are 21 unknowns, which are eight force and moment resultants ($N_\phi, N_\theta, N_{\phi\theta}, Q_{\phi\zeta}, Q_{\theta\zeta}, M_\phi, M_\theta, M_{\phi\theta}$), five displacement and rotation terms ($u_\phi^0, u_\theta^0, u_\zeta^0, \beta_\phi, \beta_\theta$), three middle surface in-plane strains ($\varepsilon_{\phi\phi}^0$, $\varepsilon_{\theta\theta}^0$, $\gamma_{\phi\theta}^0$), two transverse shear strains ($\gamma_{\phi\zeta}$, $\gamma_{\theta\zeta}$), three middle surface curvatures ($\kappa_{\phi\phi}$, $\kappa_{\theta\theta}$, $\kappa_{\phi\theta}$).

These 21 equations with 21 unknowns can be reduced to 10 equations with 10 unknowns by formulating some of the unknowns in terms of others. When the formulation is completed, the obtained 10 equations are called as the fundamental system of equations, and these can be written in the following form:

$$\frac{\partial\{\psi(\phi,\theta)\}}{\partial\phi} = f\left(\{\psi(\phi,\theta)\}, \frac{\partial}{\partial\theta}\left(\{\psi(\phi,\theta)\}\right), \frac{\partial^2}{\partial^2\theta}\left(\{\psi(\phi,\theta)\}\right)\right) + \{B(\phi,\theta)\}_{10x1} \tag{3.2.1}$$

where $\{B(\phi,\theta)\}$ is a vector which includes all the non-homogeneous terms due to loading and $\{\psi(\phi,\theta)\}$ is a vector representing the fundamental shell variables that enter into the appropriate boundary conditions on a rotationally symmetric edge of the shell of revolution, and for the Reissner-Naghdi improved shell theory they are given by

$$\{\psi(\phi,\theta)\} = \left\{u_\zeta^0, u_\phi^0, u_\theta^0,\ \beta_\phi, \beta_\theta, Q_\phi, N_{\phi\phi}, N_{\phi\theta}, M_{\phi\phi}, M_{\phi\theta}\right\}^T \tag{3.2.2}$$

The unknown variables in Equation (3.2.1) are called as the fundamental variables, and the first half consists of the reference plane displacements and the second half consist of the stress and moment resultants which are defined in appropriate manner (Soedel [3], Vinson and Sierakowski [12], Toorani and Lakis [25]).

Fundamental system of equations given by Equation (3.2.1) are obtained by deriving expressions for the first derivative of the fundamental shell variables with respect to meridional coordinate ϕ. In the following, the fundamental system of equations is obtained in terms of fundamental variables. While deriving the fundamental system of equations, a similar method to the one used in a previous study [2] will be followed. As it can be seen in Equation (3.2.2), fundamental set of equations begin with the term lateral displacement u_ζ^0. Substituting Equations (2.2.3.10) and (2.2.3.11) into (2.3.3.7), one gets

$$Q_{\phi\zeta} = A_{45}\left(\beta_\theta - \frac{u_\theta^0}{R_\theta} + \frac{1}{R_\theta \sin\theta}\frac{\partial u_\zeta^0}{\partial\theta}\right) + A_{55}\left(\beta_\phi - \frac{u_\phi^0}{R_\phi} + \frac{1}{R_\phi}\frac{\partial u_\zeta^0}{\partial\phi}\right) \tag{3.2.3}$$

writing in a similar form of Equation (3.2.1),

$$\frac{\partial u_\zeta^0}{\partial\phi} = \frac{R_\phi}{A_{55}}Q_{\phi\zeta} - \frac{A_{45}R_\phi}{A_{55}}\beta_\theta + \frac{A_{45}}{R_\theta}\frac{R_\phi}{A_{55}}u_\theta^0 - R_\phi\beta_\phi - \frac{A_{45}}{A_{55}}\frac{R_\phi}{R_\theta\sin\theta}\frac{\partial u_\zeta^0}{\partial\theta} + u_\phi^0 \tag{3.2.4}$$

or in a more compact form Equation (3.2.4) can be rewritten as in Equation (3.2.5) in terms of coefficients which are defined in terms of parameters given in Equation (3.2.4).

$$\frac{\partial u_{\zeta}^{0}}{\partial \phi} = cp_{11}\frac{\partial u_{\zeta}^{0}}{\partial \theta} + c_{12}u_{\phi}^{0} + c_{13}u_{\theta}^{0} + c_{14}\beta_{\phi} + c_{15}\beta_{\theta} + c_{16}Q_{\phi\zeta} \tag{3.2.5}$$

Coefficients of the fundamental variables c_{ij}, and cp_{ij} are given also in Appendix A.

Similarly, first, third, fourth and sixth rows of Equation set (2.3.2.44) can be used to derive the necessary coefficients for $\partial u_{\phi}^{0}/\partial\phi$, $\partial u_{\theta}^{0}/\partial\phi$, $\partial\beta_{\phi}/\partial\phi$ and $\partial\beta_{\theta}/\partial\phi$ by substituting the strain-displacement relations given in (2.2.3.1) – (2.2.3.6). After the completion of necessary algebraic operations and manipulations, these equations can be brought to the following form:

$$\begin{bmatrix} h_{11} & h_{12} & h_{13} & h_{14} \\ h_{21} & h_{22} & h_{23} & h_{24} \\ h_{31} & h_{32} & h_{33} & h_{34} \\ h_{41} & h_{42} & h_{43} & h_{44} \end{bmatrix} \begin{Bmatrix} \partial u_{\phi}^{0}/\partial\phi \\ \partial u_{\theta}^{0}/\partial\phi \\ \partial \beta_{\phi}^{0}/\partial\phi \\ \partial \beta_{\theta}^{0}/\partial\phi \end{Bmatrix} = \begin{Bmatrix} j_1 \\ j_2 \\ j_3 \\ j_4 \end{Bmatrix} \tag{3.2.6}$$

In Equation (3.2.6), the components of the 4x4 coefficient matrix *h* depend on stiffness coefficients (A_{ij}, B_{ij}, D_{ij}; $i,j = 1,2,6$), and radii of curvature of the shell (R_{ϕ}, R_{θ}). The components of the vector *j* on the right hand side of Equation (3.2.6), comprise of the fundamental variables, θ derivatives of the fundamental variables, meridional coordinate ϕ, stiffness coefficients (A_{ij}, B_{ij}, D_{ij}; $i,j = 1,2,6$), and radii of curvature of the shell (R_{ϕ}, R_{θ}).

Equation (3.2.6), is solved symbolically by MATLAB, which is a numerical computing environment and programming language [26], for the first ϕ derivatives of $u_{\phi}^{0}, u_{\theta}^{0}, \beta_{\phi}$ and β_{θ}. By taking the inverse of Equation (3.2.6), fundamental system of equations giving $\partial u_{\phi}^{0}/\partial\phi$, $\partial u_{\theta}^{0}/\partial\phi$, $\partial\beta_{\phi}/\partial\phi$ and $\partial\beta_{\theta}/\partial\phi$ are written in the desired form:

$$\begin{Bmatrix} \partial u_{\phi}^{0}/\partial\phi \\ \partial u_{\theta}^{0}/\partial\phi \\ \partial \beta_{\phi}^{0}/\partial\phi \\ \partial \beta_{\theta}^{0}/\partial\phi \end{Bmatrix} = \begin{bmatrix} h_{11} & h_{12} & h_{13} & h_{14} \\ h_{21} & h_{22} & h_{23} & h_{24} \\ h_{31} & h_{32} & h_{33} & h_{34} \\ h_{41} & h_{42} & h_{43} & h_{44} \end{bmatrix}^{-1} \begin{Bmatrix} j_1 \\ j_2 \\ j_3 \\ j_4 \end{Bmatrix} \tag{3.2.7}$$

Re-arranging Equation (3.2.7) so that it can be written in terms of the fundamental variables and their first and second θ derivatives, as shown by Equation (3.2.1), one can express the meridional coordinate (ϕ) derivative of the displacement and rotation terms as in Equations (3.2.8 - 3.2.11).

$$\frac{\partial u_{\phi}^{0}}{\partial\phi} = c_{21}u_{\zeta}^{0} + c_{22}u_{\phi}^{0} + cp_{22}\frac{\partial u_{\phi}^{0}}{\partial\theta} + c_{23}u_{\theta}^{0} + cp_{23}\frac{\partial u_{\theta}^{0}}{\partial\theta} + c_{24}\beta_{\phi} + cp_{24}\frac{\partial\beta_{\phi}}{\partial\theta}$$
$$+ c_{25}\beta_{\theta} + cp_{25}\frac{\partial\beta_{\theta}}{\partial\theta} + c_{27}N_{\phi\phi} + c_{28}N_{\phi\theta} + c_{29}M_{\phi\phi} + c_{210}M_{\phi\theta} + B_2 \tag{3.2.8}$$

$$\frac{\partial u_{\theta}^{0}}{\partial\phi} = c_{31}u_{\zeta}^{0} + c_{32}u_{\phi}^{0} + cp_{32}\frac{\partial u_{\phi}^{0}}{\partial\theta} + c_{33}u_{\theta}^{0} + cp_{33}\frac{\partial u_{\theta}^{0}}{\partial\theta} + c_{34}\beta_{\phi} + cp_{34}\frac{\partial\beta_{\phi}}{\partial\theta}$$
$$+ c_{35}\beta_{\theta} + cp_{35}\frac{\partial\beta_{\theta}}{\partial\theta} + c_{37}N_{\phi\phi} + c_{38}N_{\phi\theta} + c_{39}M_{\phi\phi} + c_{310}M_{\phi\theta} + B_3 \tag{3.2.9}$$

$$\frac{\partial\beta_{\phi}}{\partial\phi} = c_{41}u_{\zeta}^{0} + c_{42}u_{\phi}^{0} + cp_{42}\frac{\partial u_{\phi}^{0}}{\partial\theta} + c_{43}u_{\theta}^{0} + cp_{43}\frac{\partial u_{\theta}^{0}}{\partial\theta} + c_{44}\beta_{\phi} + cp_{44}\frac{\partial\beta_{\phi}}{\partial\theta}$$
$$+ c_{45}\beta_{\theta} + cp_{45}\frac{\partial\beta_{\theta}}{\partial\theta} + c_{47}N_{\phi\phi} + c_{48}N_{\phi\theta} + c_{49}M_{\phi\phi} + c_{410}M_{\phi\theta} + B_4 \tag{3.2.10}$$

$$\frac{\partial \beta_\theta}{\partial \phi} = c_{51}u_\zeta^0 + c_{52}u_\phi^0 + cp_{52}\frac{\partial u_\phi^0}{\partial \theta} + c_{53}u_\theta^0 + cp_{53}\frac{\partial u_\theta^0}{\partial \theta} + c_{54}\beta_\phi$$
$$+ cp_{54}\frac{\partial \beta_\phi}{\partial \theta} cp_{55}\frac{\partial \beta_\theta}{\partial \theta} + c_{55}\beta_\theta + c_{57}N_{\phi\phi} + c_{58}N_{\phi\theta} + c_{59}M_{\phi\phi} + c_{510}M_{\phi\theta} + B_5$$

(3.2.11)

In Equations (3.2.8) – (3.2.11) the coefficients multiplying the fundamental variables and circumferential coordinate (θ) derivatives of the fundamental variables are given in detail in Appendix A, and the components of the load vector B_i are given in Appendix B.

For the derivation of equations corresponding to the meridional coordinate derivative of force and moment resultants, $\partial Q_{\phi\zeta}/\partial\phi$, $\partial N_{\phi\phi}/\partial\phi$, $\partial N_{\phi\theta}/\partial\phi$, $\partial M_{\phi\phi}/\partial\phi$ and $\partial M_{\phi\theta}/\partial\phi$, equilibrium Equations (2.4.3.13), (2.4.3.11), (2.4.3.12), (2.4.3.14) and (2.4.3.15) are utilized, respectively. Primarily, $N_{\theta\theta}$ and $M_{\theta\theta}$ terms in these equations are substituted by the second and fourth rows of Equation set (2.3.2.44), since they do not appear in the fundamental variables. Utilizing kinematic relations given by Equations (2.2.3.1) – (2.2.3.6) and the recently derived Equations (3.2.5), (3.2.8) – (3.2.11) in the second and fourth rows of Equation set (2.3.2.44) where necessary, $\partial Q_{\phi\zeta}/\partial\phi$, $\partial N_{\phi\phi}/\partial\phi$, $\partial N_{\phi\theta}/\partial\phi$, $\partial M_{\phi\phi}/\partial\phi$ and $\partial M_{\phi\theta}/\partial\phi$ terms are obtained in terms of other fundamental variables and their first and second θ derivatives:

$$\frac{\partial Q_\phi}{\partial \phi} = c_{61}u_\zeta^0 + cdp_{61}\frac{\partial^2 u_\zeta^0}{\partial \theta^2} + c_{62}u_\phi^0 + cp_{62}\frac{\partial u_\phi^0}{\partial \theta} + c_{63}u_\theta^0 + cp_{63}\frac{\partial u_\theta^0}{\partial \theta} + c_{64}\beta_\phi$$
$$+ cp_{64}\frac{\partial \beta_\phi}{\partial \theta} + c_{65}\beta_\theta + cp_{65}\frac{\partial \beta_\theta}{\partial \theta} + c_{66}Q_\phi + cp_{66}\frac{\partial Q_\phi}{\partial \theta} + c_{67}N_{\phi\phi}$$
$$+ c_{68}N_{\phi\theta} + c_{69}M_{\phi\phi} + c_{610}M_{\phi\theta} + B_6$$

(3.2.12)

$$\frac{\partial N_{\phi\phi}}{\partial \phi} = c_{71}u_{\zeta}^{0} + c_{72}\,u_{\phi}^{0} + cp_{72}\,\frac{\partial u_{\phi}^{0}}{\partial \theta} + c_{73}\,u_{\theta}^{0} + cp_{73}\,\frac{\partial u_{\theta}^{0}}{\partial \theta} + c_{74}\beta_{\phi}$$
$$+ cp_{74}\,\frac{\partial \beta_{\phi}}{\partial \theta} + c_{75}\beta_{\theta} + cp_{75}\,\frac{\partial \beta_{\theta}}{\partial \theta} + c_{76}Q_{\phi} + c_{77}N_{\phi\phi} + c_{78}N_{\phi\theta}$$
$$+ cp_{78}\,\frac{\partial N_{\phi\theta}}{\partial \theta} + c_{79}M_{\phi\phi} + c_{710}M_{\phi\theta} + B_{7}$$

(3.2.13)

$$\frac{\partial N_{\phi\theta}}{\partial \phi} = cp_{81}\,\frac{\partial u_{\zeta}^{0}}{\partial \theta} + c_{82}\,u_{\phi}^{0} + cp_{82}\,\frac{\partial u_{\phi}^{0}}{\partial \theta} + cdp_{82}\,\frac{\partial^{2} u_{\phi}^{0}}{\partial \theta^{2}} + c_{83}\,u_{\theta}^{0} + cp_{83}\,\frac{\partial u_{\theta}^{0}}{\partial \theta}$$
$$+ cdp_{83}\,\frac{\partial^{2} u_{\theta}^{0}}{\partial \theta^{2}} + c_{84}\beta_{\phi} + cp_{84}\,\frac{\partial \beta_{\phi}}{\partial \theta} + cdp_{84}\,\frac{\partial^{2} \beta_{\phi}}{\partial \theta^{2}} + c_{85}\beta_{\theta}$$
$$+ cp_{85}\,\frac{\partial \beta_{\theta}}{\partial \theta} + cdp_{85}\,\frac{\partial^{2} \beta_{\theta}}{\partial \theta^{2}} + c_{86}Q_{\phi} + cp_{87}\,\frac{\partial N_{\phi\phi}}{\partial \theta} + c_{88}N_{\phi\theta}$$
$$+ cp_{88}\,\frac{\partial N_{\phi\theta}}{\partial \theta} + cp_{89}\,\frac{\partial M_{\phi\phi}}{\partial \theta} + cp_{810}\,\frac{\partial M_{\phi\theta}}{\partial \theta} + B_{8}$$

(3.2.14)

$$\frac{\partial M_{\phi\phi}}{\partial \phi} = c_{91}u_{\zeta}^{0} + c_{92}\,u_{\phi}^{0} + cp_{92}\,\frac{\partial u_{\phi}^{0}}{\partial \theta} + c_{93}\,u_{\theta}^{0} + cp_{93}\,\frac{\partial u_{\phi}^{0}}{\partial \theta} + c_{94}\beta_{\phi}$$
$$+ cp_{94}\,\frac{\partial \beta_{\phi}}{\partial \theta} + c_{95}\beta_{\theta} + cp_{95}\,\frac{\partial \beta_{\theta}}{\partial \theta} + c_{96}Q_{\phi} + c_{97}N_{\phi\phi} + c_{98}N_{\phi\theta}$$
$$+ c_{99}M_{\phi\phi} + c_{910}M_{\phi\theta} + cp_{910}\,\frac{\partial M_{\phi\theta}}{\partial \theta} + B_{9}$$

(3.2.15)

$$\frac{\partial M_{\phi\theta}}{\partial \phi} = cp_{101}\frac{\partial w^0}{\partial \theta} + c_{102}\,u_\phi^0 + cp_{102}\frac{\partial u_\phi^0}{\partial \theta} + cdp_{102}\frac{\partial^2 u_\phi^0}{\partial \theta^2} + c_{103}\,u_\theta^0$$
$$+ cp_{103}\frac{\partial u_\theta^0}{\partial \theta} + cdp_{103}\frac{\partial^2 u_\theta^0}{\partial \theta^2} + c_{104}\,\beta_\phi + cp_{104}\frac{\partial \beta_\phi}{\partial \theta}$$
$$+ cdp_{104}\frac{\partial^2 \beta_\phi}{\partial \theta^2} + c_{105}\,\beta_\theta + cp_{105}\frac{\partial \beta_\theta}{\partial \theta} + cdp_{105}\frac{\partial^2 \beta_\theta}{\partial \theta^2} + c_{106}Q_\phi$$
$$+ cp_{107}\frac{\partial N_{\phi\phi}}{\partial \theta} + cp_{108}\frac{\partial N_{\phi\theta}}{\partial \theta} + cp_{109}\frac{\partial M_{\phi\phi}}{\partial \theta} + c_{1010}M_{\phi\theta}$$
$$+ cp_{1010}\frac{\partial M_{\phi\theta}}{\partial \theta} + B_{10}$$

(3.2.16)

B_i vector contains the non-homogeneous terms of the fundamental system of equations and they are given in Appendix B. Coefficients c_{ij}, cp_{ij} and cdp_{ij} of the homogeneous part are given in Appendix A.

Equation (3.2.5) and Equations (3.2.8) - (3.2.16) are the fundamental system of partial differential equations in ϕ and θ. In the following, reduction of these equations to first order system of ordinary differential equations will be discussed. The reduction process makes use of the rotational symmetry of the shell of revolution.

3.3. Finite Exponential Fourier Transform of the Fundamental System of Equations

The fundamental set of equations derived in Section 3.2 also contains the first and second θ derivatives of fundamental variables, as well as the fundamental variables themselves. Therefore, the fundamental system of equations given by Equation (3.2.5) and Equations (3.2.8) - (3.2.16) are partial

differential equations. In order to utilize the multisegment numerical integration technique for the solution of this set, one needs to transform the partial differential equation set into a system of ordinary differential equations. This is achieved by eliminating θ derivatives from the equations, and expressing the meridional coordinate (ϕ) derivatives of the fundamental shell variables only in terms of the fundamental variables and the load vector, which includes all the non-homogeneous terms due to loading. For the elimination of the circumferential coordinate (θ) derivatives in the fundamental system of equations, Finite Exponential Fourier Transform Method is employed.

For the classical shell theory, which neglects transverse shear deformation, when the full anisotropic form of constitutive relations given by Equations (2.3.2.44) and (2.3.3.7) are utilized, the uncoupling of the governing equations describing the symmetric and antisymmetric responses, with respect to circumferential coordinate, cannot be achieved by the classical Fourier decomposition of the fundamental shell variables in which each variable is expressed by either a cosine series or sine series exploiting the rotational symmetry of the shell of revolution. Therefore, multisegment numerical integration technique cannot be employed due to the existence of coupling stiffness coefficients. The same restriction also exists for the first order shear deformation shell theory [1]. Vanishing of coupling stiffness coefficients with subscripts 16, 26, and 45 imply laminates with specially orthotropic layers. Thus, with the classical Fourier decomposition of the fundamental variables in the circumferential direction, it is not possible to treat shells of revolution with full anisotropic constitutive relations, which allow for arbitrary orientation of fibres with respect to the curvilinear coordinate system of the shell of revolution.

For laminated shells of revolution, which include the effects of extensional shear $\left(A_{16}, A_{26}\right)$, extensional bending $\left(B_{16}, B_{26}\right)$, bending twisting $\left(D_{16}, D_{26}\right)$ and transverse shear $\left(A_{45}\right)$ coupling stiffness terms in constitutive equations, uncoupling of the governing equations, describing the symmetric and

antisymmetric responses with respect to circumferential coordinate θ is achieved by Finite Exponential Fourier Transform.

In the previous works of Lestingi and Padovan such as [8] and [17], the applicability of the technique of multisegment method of integration is extended to include the solution of general macroscopically anisotropic multilayered shells of revolution through the use of Finite Exponential Fourier Transform Method. Prior to their works, for shells of revolution, this technique was limited to the special case of orthotropic materials.

In Reference 8, this method was applied for the static loading solution of governing equations of classical shell theory, which includes eight fundamental variables; and the solution is carried out by reduction of the equations to sixteen first order ordinary differential equations. In [2] this method is used to reduce the governing equations for free vibration analysis of anisotropic laminated composite shells of revolution to twenty first order homogeneous ordinary differential equations. In the present study, the method of Finite Exponential Fourier Transform is utilized for the reduction of the governing equations of macroscopically anisotropic shells of revolution, including first order transverse shear deformation, to twenty first order nonhomogeneous ordinary differential equations.

Through the use of Finite Exponential Fourier Transform, the partial differential equations with independent variables ϕ and θ are converted into ordinary differential equations with ϕ being the only independent variable. Considering the first fundamental variable of the fundamental variable vector ψ, complex Fourier series representation can be shown as [15]

$$\mathrm{u}_{\zeta}^{0}(\phi,\theta) = \sum_{n=-\infty}^{+\infty} \left(\mathrm{u}_{\zeta}^{0}(\phi)\right)_{n} e^{\mathrm{i}n\theta} \tag{3.3.1}$$

where

$$\left(\mathrm{u}_{\zeta}^{0}(\phi)\right)_{n}=\frac{1}{2\pi}\int_{0}^{2\pi}\mathrm{u}_{\zeta}^{0}(\phi,\theta)\,e^{-\mathrm{i}n\theta}d\theta=\left(\mathrm{u}_{\zeta}^{0}(\phi)\right)_{nc}-\mathrm{i}\left(\mathrm{u}_{\zeta}^{0}(\phi)\right)_{ns} \tag{3.3.2}$$

and

$$\left(\mathrm{u}_{\zeta}^{0}(\phi)\right)_{nc}=\frac{1}{2\pi}\int_{0}^{2\pi}\mathrm{u}_{\zeta}^{0}(\phi,\theta)\cos n\theta\,d\theta \tag{3.3.3}$$

$$\left(\mathrm{u}_{\zeta}^{0}(\phi)\right)_{ns}=\frac{1}{2\pi}\int_{0}^{2\pi}\mathrm{u}_{\zeta}^{0}(\phi,\theta)\sin n\theta\,d\theta \tag{3.3.4}$$

It should be noted that in getting Equations (3.3.3) and (3.3.4), $e^{\pm in\theta}$ is expanded using Euler's formula [15]

$$e^{\pm in\theta}=\cos n\theta\pm i\sin n\theta \tag{3.3.5}$$

If Finite Exponential Fourier Transform is applied to the first fundamental equation (Equation (3.2.5)), it can be written in terms of real and imaginary parts as in Equation (3.3.2). During this operation, integration by parts is employed to perform the integration in Equation (3.3.2). Since the integral boundaries are 0 and 2π, and the geometry is a shell of revolution, all the variables are periodic in the circumferential direction, so that $u_{\zeta}^{0}(\phi,0)=u_{\zeta}^{0}(\phi,2\pi)$. Thus, all the initial terms, which emerge after the integration by parts is performed, disappear. Application of Finite Exponential Fourier Transform to Equation (3.2.5) yields

$$\left(\frac{\partial u_\zeta^0}{\partial \phi}\right)_{nc} - i\left(\frac{\partial u_\zeta^0}{\partial \phi}\right)_{ns} = cp_{11} n\left[i\left(\mathrm{u}_\zeta^0(\phi)\right)_{nc} + \left(\mathrm{u}_\zeta^0(\phi)\right)_{ns}\right] +$$
$$c_{12}\left[\left(\mathrm{u}_\phi^0(\phi)\right)_{nc} - i\left(\mathrm{u}_\phi^0(\phi)\right)_{ns}\right] + c_{13}\left[\left(\mathrm{u}_\theta^0(\phi)\right)_{nc} - i\left(\mathrm{u}_\theta^0(\phi)\right)_{ns}\right] + \quad (3.3.6)$$
$$c_{14}\left[\left(\beta_\phi^0(\phi)\right)_{nc} - i\left(\beta_\phi^0(\phi)\right)_{ns}\right] + c_{15}\left[\left(\beta_\theta^0(\phi)\right)_{nc} - i\left(\beta_\theta^0(\phi)\right)_{ns}\right] +$$
$$c_{16}\left[\left(Q_{\phi\zeta}^0(\phi)\right)_{nc} - i\left(Q_{\phi\zeta}^0(\phi)\right)_{ns}\right]$$

and since $a + ib = c + id$ implies $a = c$ and $b = d$, we can write real and imaginary parts separately:

$$\left(\frac{\partial u_\zeta^0}{\partial \phi}\right)_{nc} = cp_{11} n\left(\mathrm{u}_\zeta^0(\phi)\right)_{ns} + c_{12}\left(\mathrm{u}_\phi^0(\phi)\right)_{nc} + c_{13}\left(\mathrm{u}_\theta^0(\phi)\right)_{nc} + c_{14}\left(\beta_\phi^0(\phi)\right)_{nc} \quad (3.3.7)$$
$$+ c_{15}\left(\beta_\theta^0(\phi)\right)_{nc} + c_{16}\left(Q_{\phi\zeta}^0(\phi)\right)_{nc}$$

$$\left(\frac{\partial u_\zeta^0}{\partial \phi}\right)_{ns} = -cp_{11} n\left(\mathrm{u}_\zeta^0(\phi)\right)_{nc} + c_{12}\left(\mathrm{u}_\phi^0(\phi)\right)_{ns} + c_{13}\left(\mathrm{u}_\theta^0(\phi)\right)_{ns} + c_{14}\left(\beta_\phi^0(\phi)\right)_{ns} \quad (3.3.8)$$
$$+ c_{15}\left(\beta_\theta^0(\phi)\right)_{ns} + c_{16}\left(Q_{\phi\zeta}^0(\phi)\right)_{ns}$$

It is clearly seen that application of finite exponential Fourier transform results in doubling of the number of fundamental variables.

However, one important issue has to be mentioned here. First fundamental equation, Equation (3.2.5) differs from the rest of the fundamental equations because of the non-existence of a nonhomogeneous load vector term, that is $B_1 = 0$. Therefore, in order to investigate the Finite Exponential Fourier Transform of nonhomogeneous terms, another fundamental equation has to be analyzed. To demonstrate the application of Finite Exponential Fourier Transform to an equation which includes nonhomogeneous loading terms, sixth fundamental equation is considered. In Equation (3.2.12), the loading term B_6, as explained in Appendix B, is given by,

$$B_6 = CB_{61} p_\zeta + CB_{64} N_\phi^T + CB_{65} N_\theta^T + CB_{66} N_{\phi\theta}^T + CB_{67} M_\phi^T + CB_{69} M_{\phi\theta}^T \quad (3.3.9)$$

If Finite Exponential Fourier Transform is applied to the sixth fundamental equation (Equation (3.2.12)), it can be written in terms of real and imaginary parts like in Equation (3.3.2). During this operation, in Equation (3.2.12), all the terms appearing except B_6, i.e. the terms of the homogeneous part, are handled in the same manner as it has been done for the first fundamental equation. In Equation (3.3.9) p_ζ (pressure loading in the thickness direction of the shell ζ), which is the first term in B_6, can be expanded by using Finite Exponential Fourier Transform as:

$$p_\zeta(\phi,\theta) = \sum_{n=-\infty}^{+\infty} \left(p_\zeta(\phi)\right)_n e^{\mathrm{i}n\theta} \tag{3.3.10}$$

where

$$\left(p_\zeta(\phi)\right)_n = \frac{1}{2\pi}\int_0^{2\pi} p_\zeta(\phi,\theta)\, e^{-\mathrm{i}n\theta}\, d\theta = \left(p_\zeta(\phi)\right)_{nc} - \mathrm{i}\left(p_\zeta(\phi)\right)_{ns} \tag{3.3.11}$$

and

$$\left(p_\zeta(\phi)\right)_{nc} = \frac{1}{2\pi}\int_0^{2\pi} p_\zeta(\phi,\theta)\cos n\theta\, d\theta \tag{3.3.12}$$

$$\left(p_\zeta(\phi)\right)_{ns} = \frac{1}{2\pi}\int_0^{2\pi} p_\zeta(\phi,\theta)\sin n\theta\, d\theta \tag{3.3.13}$$

Equation (3.3.10) can be rewritten as

$$p_\zeta(\phi,\theta) = p_{\zeta 0} + \sum_{n=1}^{+\infty} \left(p_\zeta(\phi)\right)_n e^{\mathrm{i}n\theta} + \sum_{n=-1}^{-\infty} \left(p_\zeta(\phi)\right)_n e^{\mathrm{i}n\theta} \tag{3.3.14}$$

or

$$p_\zeta(\phi,\theta) = p_{\zeta 0} + \sum_{n=1}^{+\infty} \left(p_\zeta(\phi)\right)_n e^{\mathrm{i}n\theta} + \sum_{n=1}^{+\infty} \left(p_\zeta(\phi)\right)_{-n} e^{-\mathrm{i}n\theta} \tag{3.3.15}$$

In Equations (3.3.14) and (3.3.15), $p_{\zeta 0}$ term corresponds to the coefficient of the series when $n = 0$. Therefore,

$$p_{\zeta 0} = \frac{1}{2\pi} \int_0^{2\pi} p_\zeta(\phi,\theta)\, d\theta \tag{3.3.16}$$

Considering the first part of Equation (3.3.11), it can be written that

$$\left(p_\zeta(\phi)\right)_{-n} = \frac{1}{2\pi} \int_0^{2\pi} p_\zeta(\phi,\theta)\, e^{\mathrm{i}n\theta} d\theta \tag{3.3.17}$$

Comparing Equations (3.3.11) and (3.3.17), it is obvious that $\left(p_\zeta(\phi)\right)_n$ and $\left(p_\zeta(\phi)\right)_{-n}$ are complex conjugates. Therefore,

$$\left(p_\zeta(\phi)\right)_{-n} = \left(p_\zeta(\phi)\right)_n^* \tag{3.3.18}$$

Rewriting Equation (3.3.15),

$$p_\zeta(\phi,\theta) = p_{\zeta 0} + \sum_{n=1}^{+\infty} \left[\left(p_\zeta(\phi)\right)_n e^{\mathrm{i}n\theta} + \left(p_\zeta(\phi)\right)_n^* e^{-\mathrm{i}n\theta}\right] \tag{3.3.19}$$

Substituting Euler's formula given with Equation (3.3.5) and using the second part of the Equation (3.3.11), Equation (3.3.19) can be written as

$$\begin{aligned} p_\zeta(\phi,\theta) = p_{\zeta 0} + \sum_{n=1}^{+\infty} &\left[\left(p_\zeta(\phi)\right)_{nc} - \mathrm{i}\left(p_\zeta(\phi)\right)_{ns}\right]\left[\cos n\theta + i\sin n\theta\right] + \\ &\left[\left(p_\zeta(\phi)\right)_{nc} + \mathrm{i}\left(p_\zeta(\phi)\right)_{ns}\right]\left[\cos n\theta - i\sin n\theta\right] \end{aligned} \tag{3.3.20}$$

It is clear from Equation (3.3.11) that the terms $\left(p_\zeta(\phi)\right)_{nc}$ and $\left(p_\zeta(\phi)\right)_{ns}$ expanded in Equations (3.3.12) and (3.3.13) are necessarily the real and imaginary parts of $\left(p_\zeta(\phi)\right)_n$. Rearranging Equation (3.3.20), one gets:

$$p_\zeta(\phi,\theta) = p_{\zeta 0} + 2\sum_{n=1}^{+\infty}\left[\left(p_\zeta(\phi)\right)_{nc}\cos n\theta + \left(p_\zeta(\phi)\right)_{ns}\sin n\theta\right] \tag{3.3.21}$$

Equation (3.3.21) shows how p_ζ, the first term in B_6, can be expanded by using Finite Exponential Fourier Transform. The other load terms $\left(p_\phi, p_\theta, N_\phi^T, N_\theta^T, N_{\phi\theta}^T, M_\phi^T, M_\theta^T, M_{\phi\theta}^T\right)$ in the load vector B_i $(i = 1,...10)$ can be expanded using the same procedure. Thus, all the loading terms can be expressed as:

$$p_\phi(\phi,\theta) = p_{\phi 0} + 2\sum_{n=1}^{+\infty}\left[\left(p_\phi(\phi)\right)_{nc}\cos n\theta + \left(p_\phi(\phi)\right)_{ns}\sin n\theta\right] \tag{3.3.22}$$

$$p_\theta(\phi,\theta) = p_{\theta 0} + 2\sum_{n=1}^{+\infty}\left[\left(p_\theta(\phi)\right)_{nc}\cos n\theta + \left(p_\theta(\phi)\right)_{ns}\sin n\theta\right] \tag{3.3.23}$$

$$N_\phi^T(\phi,\theta) = \left(N_\phi^T\right)_0 + 2\sum_{n=1}^{+\infty}\left[\left(N_\phi^T(\phi)\right)_{nc}\cos n\theta + \left(N_\phi^T(\phi)\right)_{ns}\sin n\theta\right] \tag{3.3.24}$$

$$N_\theta^T(\phi,\theta) = \left(N_\theta^T\right)_0 + 2\sum_{n=1}^{+\infty}\left[\left(N_\theta^T(\phi)\right)_{nc}\cos n\theta + \left(N_\theta^T(\phi)\right)_{ns}\sin n\theta\right] \tag{3.3.25}$$

$$N_{\phi\theta}^T(\phi,\theta) = \left(N_{\phi\theta}^T\right)_0 + 2\sum_{n=1}^{+\infty}\left[\left(N_{\phi\theta}^T(\phi)\right)_{nc}\cos n\theta + \left(N_{\phi\theta}^T(\phi)\right)_{ns}\sin n\theta\right] \tag{3.3.26}$$

$$M_\phi^T(\phi,\theta) = \left(M_\phi^T\right)_0 + 2\sum_{n=1}^{+\infty}\left[\left(M_\phi^T(\phi)\right)_{nc}\cos n\theta + \left(M_\phi^T(\phi)\right)_{ns}\sin n\theta\right] \tag{3.3.27}$$

$$M_\theta^T(\phi,\theta) = \left(M_\theta^T\right)_0 + 2\sum_{n=1}^{+\infty}\left[\left(M_\theta^T(\phi)\right)_{nc}\cos n\theta + \left(M_\theta^T(\phi)\right)_{ns}\sin n\theta\right] \tag{3.3.28}$$

$$M^{T}_{\phi\theta}(\phi,\theta) = \left(M^{T}_{\phi\theta}\right)_0 + 2\sum_{n=1}^{+\infty}\left[\left(M^{T}_{\phi\theta}(\phi)\right)_{nc}\cos n\theta + \left(M^{T}_{\phi\theta}(\phi)\right)_{ns}\sin n\theta\right] \quad (3.3.29)$$

This implies that any function, which can be expanded as a Fourier series, can be applied as the loading (distributed force in any direction or temperature) to the shell of revolution. This is the explanation of how the axisymmetric loads (i.e. the loads constant in circumferential direction θ) and the unsymmetrical loads (i.e. the loads given as a function of circumferential direction θ) are handled mathematically.

Physically, if the loading is axisymmetric, this implies that circumferential wave number n is zero and the load is defined by only the first term of Equations (3.3.21) – (3.3.29). On the other hand, if the loading is unsymmetrical, first the function defining the load is expanded as a Fourier series by incorporating finite number of terms defined by n, then the real and imaginary parts of the series are expressed as the coefficients of $\cos n\theta$ and $\sin n\theta$ of the corresponding circumferential wave number n in Equations (3.3.21) – (3.3.29), respectively. For the function defining the unsymmetrical load, if there is a constant term in the Fourier series of that function, this is also represented by the constant term in the Equations (3.3.21) – (3.3.29). In order this to be better understood, Finite Exponential Fourier Transform is applied to the Equation (3.2.12) in Appendix C, as an exhibition of how the procedure is carried out.

Equations involving the temperature loading, i.e. Equations (3.3.25) – (3.3.29) should further be investigated. Substituting ϕ for ξ and θ for η in Equations (2.3.2.34) and (2.3.2.35), force and moment resultants due to temperature loading, either constant temperature difference throughout the thickness or linearly varying temperature difference through the thickness respectively, can be obtained for a shell of revolution:

$$\begin{Bmatrix} N_{\phi}^{T} \\ N_{\theta}^{T} \\ N_{\phi\theta}^{T} \end{Bmatrix} = \sum_{k=1}^{N} \begin{bmatrix} \overline{Q}_{11} & \overline{Q}_{12} & \overline{Q}_{16} \\ \overline{Q}_{12} & \overline{Q}_{22} & \overline{Q}_{26} \\ \overline{Q}_{16} & \overline{Q}_{26} & \overline{Q}_{66} \end{bmatrix}_{k} \begin{Bmatrix} \alpha_{\phi} \\ \alpha_{\theta} \\ \alpha_{\phi\theta} \end{Bmatrix}_{k} \Delta T\left(z_{k} - z_{k-1}\right) \tag{3.3.30}$$

$$\begin{Bmatrix} M_{\phi}^{T} \\ M_{\theta}^{T} \\ M_{\phi\theta}^{T} \end{Bmatrix} = \frac{1}{2} \sum_{k=1}^{N} \begin{bmatrix} \overline{Q}_{11} & \overline{Q}_{12} & \overline{Q}_{16} \\ \overline{Q}_{12} & \overline{Q}_{22} & \overline{Q}_{26} \\ \overline{Q}_{16} & \overline{Q}_{26} & \overline{Q}_{66} \end{bmatrix}_{k} \begin{Bmatrix} \alpha_{\phi} \\ \alpha_{\theta} \\ \alpha_{\phi\theta} \end{Bmatrix}_{k} \Delta T\left(z_{k}^{2} - z_{k-1}^{2}\right) \tag{3.3.31}$$

$$\begin{Bmatrix} N_{\phi}^{T} \\ N_{\theta}^{T} \\ N_{\phi\theta}^{T} \end{Bmatrix} = \sum_{k=1}^{N} \begin{bmatrix} \overline{Q}_{11} & \overline{Q}_{12} & \overline{Q}_{16} \\ \overline{Q}_{12} & \overline{Q}_{22} & \overline{Q}_{26} \\ \overline{Q}_{16} & \overline{Q}_{26} & \overline{Q}_{66} \end{bmatrix}_{k} \begin{Bmatrix} \alpha_{\phi} \\ \alpha_{\theta} \\ \alpha_{\phi\theta} \end{Bmatrix}_{k} \left(\Delta T_{1}\left(z_{k} - z_{k-1}\right) + \frac{\Delta T_{2}}{2}\left(z_{k}^{2} - z_{k-1}^{2}\right) \right) \tag{3.3.32}$$

$$\begin{Bmatrix} M_{\phi}^{T} \\ M_{\theta}^{T} \\ M_{\phi\theta}^{T} \end{Bmatrix} = \sum_{k=1}^{N} \begin{bmatrix} \overline{Q}_{11} & \overline{Q}_{12} & \overline{Q}_{16} \\ \overline{Q}_{12} & \overline{Q}_{22} & \overline{Q}_{26} \\ \overline{Q}_{16} & \overline{Q}_{26} & \overline{Q}_{66} \end{bmatrix}_{k} \begin{Bmatrix} \alpha_{\phi} \\ \alpha_{\theta} \\ \alpha_{\phi\theta} \end{Bmatrix}_{k} \left(\frac{\Delta T_{1}}{2}\left(z_{k}^{2} - z_{k-1}^{2}\right) + \frac{\Delta T_{2}}{3}\left(z_{k}^{3} - z_{k-1}^{3}\right) \right) \tag{3.3.33}$$

Equations (3.3.30) and (3.3.31) give the thermal force and moment resultants for constant temperature difference, and Equations (3.3.32) and (3.3.33) give the thermal force and moment resultants for linearly varying temperature difference through the thickness.

These equations give the relation between the temperature difference exerted as the loading and its effects as force and moment resultants on a shell of revolution. Let Equations (3.3.30) – (3.3.33) be rewritten as

$$\begin{Bmatrix} N_{\phi}^{T} \\ N_{\theta}^{T} \\ N_{\phi\theta}^{T} \end{Bmatrix} = \Delta T \begin{Bmatrix} Th1_{\phi} \\ Th1_{\theta} \\ Th1_{\phi\theta} \end{Bmatrix} \tag{3.3.34}$$

$$\begin{Bmatrix} M_{\phi}^{T} \\ M_{\theta}^{T} \\ M_{\phi\theta}^{T} \end{Bmatrix} = \Delta T \begin{Bmatrix} Th2_{\phi} \\ Th2_{\theta} \\ Th2_{\phi\theta} \end{Bmatrix} \tag{3.3.35}$$

$$\begin{Bmatrix} N_\phi^T \\ N_\theta^T \\ N_{\phi\theta}^T \end{Bmatrix} = \Delta T_1 \begin{Bmatrix} Th1_\phi \\ Th1_\theta \\ Th1_{\phi\theta} \end{Bmatrix} + \Delta T_2 \begin{Bmatrix} Th2_\phi \\ Th2_\theta \\ Th2_{\phi\theta} \end{Bmatrix} \tag{3.3.36}$$

$$\begin{Bmatrix} M_\phi^T \\ M_\theta^T \\ M_{\phi\theta}^T \end{Bmatrix} = \Delta T_1 \begin{Bmatrix} Th2_\phi \\ Th2_\theta \\ Th2_{\phi\theta} \end{Bmatrix} + \Delta T_2 \begin{Bmatrix} Th3_\phi \\ Th3_\theta \\ Th3_{\phi\theta} \end{Bmatrix} \tag{3.3.37}$$

where

$$\begin{Bmatrix} Th1_\phi \\ Th1_\theta \\ Th1_{\phi\theta} \end{Bmatrix} = \sum_{k=1}^{N} \begin{bmatrix} \overline{Q}_{11} & \overline{Q}_{12} & \overline{Q}_{16} \\ \overline{Q}_{12} & \overline{Q}_{22} & \overline{Q}_{26} \\ \overline{Q}_{16} & \overline{Q}_{26} & \overline{Q}_{66} \end{bmatrix}_k \begin{Bmatrix} \alpha_\phi \\ \alpha_\theta \\ \alpha_{\phi\theta} \end{Bmatrix}_k \left(z_k - z_{k-1}\right) \tag{3.3.38}$$

$$\begin{Bmatrix} Th2_\phi \\ Th2_\theta \\ Th2_{\phi\theta} \end{Bmatrix} = \frac{1}{2} \sum_{k=1}^{N} \begin{bmatrix} \overline{Q}_{11} & \overline{Q}_{12} & \overline{Q}_{16} \\ \overline{Q}_{12} & \overline{Q}_{22} & \overline{Q}_{26} \\ \overline{Q}_{16} & \overline{Q}_{26} & \overline{Q}_{66} \end{bmatrix}_k \begin{Bmatrix} \alpha_\phi \\ \alpha_\theta \\ \alpha_{\phi\theta} \end{Bmatrix}_k \left(z_k^2 - z_{k-1}^2\right) \tag{3.3.39}$$

$$\begin{Bmatrix} Th3_\phi \\ Th3_\theta \\ Th3_{\phi\theta} \end{Bmatrix} = \frac{1}{3} \sum_{k=1}^{N} \begin{bmatrix} \overline{Q}_{11} & \overline{Q}_{12} & \overline{Q}_{16} \\ \overline{Q}_{12} & \overline{Q}_{22} & \overline{Q}_{26} \\ \overline{Q}_{16} & \overline{Q}_{26} & \overline{Q}_{66} \end{bmatrix}_k \begin{Bmatrix} \alpha_\phi \\ \alpha_\theta \\ \alpha_{\phi\theta} \end{Bmatrix}_k \left(z_k^3 - z_{k-1}^3\right) \tag{3.3.40}$$

As stated in Section 2.3.2, letting $\Delta T_2 = 0$ in Equations (3.3.36) and (3.3.37), which are derived for linear variation of temperature difference through the thickness, leads to the Equations (3.3.34) and (3.3.35), which are derived for constant temperature difference throughout the thickness. This shows that Equations (3.3.36) and (3.3.37) are general forms of Equations (3.3.34) and (3.3.35). Therefore only Equations (3.3.36) and (3.3.37) will be used from now on.

As it is seen above, coefficients of Equations (3.3.36) and (3.3.37) are given by Equations (3.3.38) – (3.3.40). They consist of transformed material coefficients $\overline{Q}_{ij}$, thermal expansion coefficients α_i, and the position vectors of

layers in the thickness direction ζ with respect to the reference surface of the laminate z_i, none of which are functions of the circumferential direction θ. And since these coefficients are not θ dependent, they do not need to be expanded with Finite exponential Fourier Transform. Therefore, only ΔT_1 and ΔT_2 are expanded with Finite exponential Fourier Transform:

$$\Delta T_1(\phi,\theta) = \left(\Delta T_1(\phi)\right)_0 + 2\sum_{n=1}^{+\infty}\left[\left(\Delta T_1(\phi)\right)_{nc}\cos n\theta + \left(\Delta T_1(\phi)\right)_{ns}\sin n\theta\right] \quad (3.3.41)$$

where $\left(\Delta T_1\right)_{nc}$, $\left(\Delta T_1\right)_{ns}$ and $\left(\Delta T_1\right)_0$ are given in the same manner as Equations (3.3.12), (3.3.13) and (3.3.16)

$$\left(\Delta T_1(\phi)\right)_{nc} = \frac{1}{2\pi}\int_0^{2\pi}\Delta T_1(\phi,\theta)\cos n\theta\, d\theta \quad (3.3.42)$$

$$\left(\Delta T_1(\phi)\right)_{ns} = \frac{1}{2\pi}\int_0^{2\pi}\Delta T_1(\phi,\theta)\sin n\theta\, d\theta \quad (3.3.43)$$

$$\left(\Delta T_1(\phi)\right)_0 = \frac{1}{2\pi}\int_0^{2\pi}\Delta T_1(\phi,\theta)\, d\theta \quad (3.3.44)$$

Similarly,

$$\Delta T_2(\phi,\theta) = \left(\Delta T_2(\phi)\right)_0 + 2\sum_{n=1}^{+\infty}\left[\left(\Delta T_2(\phi)\right)_{nc}\cos n\theta + \left(\Delta T_2(\phi)\right)_{ns}\sin n\theta\right] \quad (3.3.45)$$

where

$$\left(\Delta T_2(\phi)\right)_{nc} = \frac{1}{2\pi}\int_0^{2\pi}\Delta T_2(\phi,\theta)\cos n\theta\, d\theta \quad (3.3.46)$$

$$\left(\Delta T_2(\phi)\right)_{ns} = \frac{1}{2\pi}\int_0^{2\pi} \Delta T_2(\phi,\theta)\sin n\theta\, d\theta \tag{3.3.47}$$

$$\left(\Delta T_2(\phi)\right)_0 = \frac{1}{2\pi}\int_0^{2\pi} \Delta T_2(\phi,\theta)\, d\theta \tag{3.3.48}$$

Note that ΔT can also vary in the ϕ direction since ΔT_1 and ΔT_2 can be defined as a function of ϕ. How this can be accomplished will be explained in the succeeding sections. However, it should be emphasized that, using Finite Exponential Fourier Transform and defining temperature difference ΔT as $\left(\Delta T_1 + \Delta T_2\,\zeta\right)$ in Equation (2.3.2.38) so that it can vary linearly through the thickness, allow the temperature difference ΔT be defined as a function of all three ϕ, θ, and ζ directions.

We can now get the expressions for the thermal stress and moment resultants by first substituting Equations (3.3.41) and (3.3.45) into (3.3.36) and (3.3.37); and then Equations (3.3.36) and (3.3.37) into Equations (3.3.24) – (3.3.29).

$$\begin{aligned} N_\phi^T(\phi,\theta) = {} & \left\{Th1_\phi\right\}\left\{\left(\Delta T_1(\phi)\right)_0 + 2\sum_{n=1}^{+\infty}\begin{bmatrix}\left(\Delta T_1(\phi)\right)_{nc}\cos n\theta \\ +\left(\Delta T_1(\phi)\right)_{ns}\sin n\theta\end{bmatrix}\right\} \\ & + \left\{Th2_\phi\right\}\left\{\left(\Delta T_2(\phi)\right)_0 + 2\sum_{n=1}^{+\infty}\begin{bmatrix}\left(\Delta T_2(\phi)\right)_{nc}\cos n\theta \\ +\left(\Delta T_2(\phi)\right)_{ns}\sin n\theta\end{bmatrix}\right\} \end{aligned} \tag{3.3.49}$$

$$\begin{aligned} N_\theta^T(\phi,\theta) = {} & \left\{Th1_\theta\right\}\left\{\left(\Delta T_1(\phi)\right)_0 + 2\sum_{n=1}^{+\infty}\begin{bmatrix}\left(\Delta T_1(\phi)\right)_{nc}\cos n\theta \\ +\left(\Delta T_1(\phi)\right)_{ns}\sin n\theta\end{bmatrix}\right\} \\ & + \left\{Th2_\theta\right\}\left\{\left(\Delta T_2(\phi)\right)_0 + 2\sum_{n=1}^{+\infty}\begin{bmatrix}\left(\Delta T_2(\phi)\right)_{nc}\cos n\theta \\ +\left(\Delta T_2(\phi)\right)_{ns}\sin n\theta\end{bmatrix}\right\} \end{aligned} \tag{3.3.50}$$

$$\begin{aligned} N_{\phi\theta}^T(\phi,\theta) = {} & \left\{Th1_{\phi\theta}\right\}\left\{\left(\Delta T_1(\phi)\right)_0 + 2\sum_{n=1}^{+\infty}\begin{bmatrix}\left(\Delta T_1(\phi)\right)_{nc}\cos n\theta \\ +\left(\Delta T_1(\phi)\right)_{ns}\sin n\theta\end{bmatrix}\right\} \\ & + \left\{Th2_{\phi\theta}\right\}\left\{\left(\Delta T_2(\phi)\right)_0 + 2\sum_{n=1}^{+\infty}\begin{bmatrix}\left(\Delta T_2(\phi)\right)_{nc}\cos n\theta \\ +\left(\Delta T_2(\phi)\right)_{ns}\sin n\theta\end{bmatrix}\right\} \end{aligned} \tag{3.3.51}$$

$$M_{\phi}^{T}(\phi,\theta) = \{Th2_{\phi}\}\left\{(\Delta T_1(\phi))_0 + 2\sum_{n=1}^{+\infty}\begin{bmatrix}(\Delta T_1(\phi))_{nc}\cos n\theta \\ +(\Delta T_1(\phi))_{ns}\sin n\theta\end{bmatrix}\right\} + \{Th3_{\phi}\}\left\{(\Delta T_2(\phi))_0 + 2\sum_{n=1}^{+\infty}\begin{bmatrix}(\Delta T_2(\phi))_{nc}\cos n\theta \\ +(\Delta T_2(\phi))_{ns}\sin n\theta\end{bmatrix}\right\} \tag{3.3.52}$$

$$M_{\theta}^{T}(\phi,\theta) = \{Th2_{\theta}\}\left\{(\Delta T_1(\phi))_0 + 2\sum_{n=1}^{+\infty}\begin{bmatrix}(\Delta T_1(\phi))_{nc}\cos n\theta \\ +(\Delta T_1(\phi))_{ns}\sin n\theta\end{bmatrix}\right\} + \{Th3_{\theta}\}\left\{(\Delta T_2(\phi))_0 + 2\sum_{n=1}^{+\infty}\begin{bmatrix}(\Delta T_2(\phi))_{nc}\cos n\theta \\ +(\Delta T_2(\phi))_{ns}\sin n\theta\end{bmatrix}\right\} \tag{3.3.53}$$

$$M_{\phi\theta}^{T}(\phi,\theta) = \{Th2_{\phi\theta}\}\left\{(\Delta T_1(\phi))_0 + 2\sum_{n=1}^{+\infty}\begin{bmatrix}(\Delta T_1(\phi))_{nc}\cos n\theta \\ +(\Delta T_1(\phi))_{ns}\sin n\theta\end{bmatrix}\right\} + \{Th3_{\phi\theta}\}\left\{(\Delta T_2(\phi))_0 + 2\sum_{n=1}^{+\infty}\begin{bmatrix}(\Delta T_2(\phi))_{nc}\cos n\theta \\ +(\Delta T_2(\phi))_{ns}\sin n\theta\end{bmatrix}\right\} \tag{3.3.54}$$

Comparing Equations (3.3.24) – (3.3.29) and (3.3.49) – (3.3.54), it is seen that

$$\begin{Bmatrix}(N_{\phi}^{T}(\phi))_{nc} \\ (N_{\theta}^{T}(\phi))_{nc} \\ (N_{\phi\theta}^{T}(\phi))_{nc}\end{Bmatrix} = \begin{Bmatrix}Th1_{\phi} \\ Th1_{\theta} \\ Th1_{\phi\theta}\end{Bmatrix}(\Delta T_1(\phi))_{nc} + \begin{Bmatrix}Th2_{\phi} \\ Th2_{\theta} \\ Th2_{\phi\theta}\end{Bmatrix}(\Delta T_2(\phi))_{nc} \tag{3.3.55}$$

$$\begin{Bmatrix}(N_{\phi}^{T}(\phi))_{ns} \\ (N_{\theta}^{T}(\phi))_{ns} \\ (N_{\phi\theta}^{T}(\phi))_{ns}\end{Bmatrix} = \begin{Bmatrix}Th1_{\phi} \\ Th1_{\theta} \\ Th1_{\phi\theta}\end{Bmatrix}(\Delta T_1(\phi))_{ns} + \begin{Bmatrix}Th2_{\phi} \\ Th2_{\theta} \\ Th2_{\phi\theta}\end{Bmatrix}(\Delta T_2(\phi))_{ns} \tag{3.3.56}$$

$$\begin{Bmatrix}(M_{\phi}^{T}(\phi))_{nc} \\ (M_{\theta}^{T}(\phi))_{nc} \\ (M_{\phi\theta}^{T}(\phi))_{nc}\end{Bmatrix} = \begin{Bmatrix}Th2_{\phi} \\ Th2_{\theta} \\ Th2_{\phi\theta}\end{Bmatrix}(\Delta T_1(\phi))_{nc} + \begin{Bmatrix}Th3_{\phi} \\ Th3_{\theta} \\ Th3_{\phi\theta}\end{Bmatrix}(\Delta T_2(\phi))_{nc} \tag{3.3.57}$$

$$\begin{Bmatrix}(M_{\phi}^{T}(\phi))_{ns} \\ (M_{\theta}^{T}(\phi))_{ns} \\ (M_{\phi\theta}^{T}(\phi))_{ns}\end{Bmatrix} = \begin{Bmatrix}Th2_{\phi} \\ Th2_{\theta} \\ Th2_{\phi\theta}\end{Bmatrix}(\Delta T_1(\phi))_{ns} + \begin{Bmatrix}Th3_{\phi} \\ Th3_{\theta} \\ Th3_{\phi\theta}\end{Bmatrix}(\Delta T_2(\phi))_{ns} \tag{3.3.58}$$

After the application of Finite Exponential Fourier Transform, first and second derivatives of the fundamental variables with respect to θ are eliminated from the fundamental set of equations. However, this causes the number of fundamental variables and elements of the load vector to be doubled; all consisting of real and imaginary parts now. This results in a system of 20 first order nonhomogeneous ordinary differential equations, which is represented by the following matrix equation:

$$\frac{d\psi}{d\phi}=\frac{d}{d\phi}\begin{Bmatrix}\psi^{(1)}(\phi)\\ \psi^{(2)}(\phi)\end{Bmatrix}_{20x1}=\left[\mathrm{K}(n,\phi)\right]_{20x20}\begin{Bmatrix}\psi^{(1)}(\phi)\\ \psi^{(2)}(\phi)\end{Bmatrix}_{20x1}+\begin{Bmatrix}B^{(1)}(\phi)\\ B^{(2)}(\phi)\end{Bmatrix}_{20x1} \tag{3.3.59}$$

where n is the circumferential wave number and

$$\psi^{(1)}(\phi)=\begin{bmatrix}\left(u_{\zeta}^{0}\right)_{nc},\left(u_{\zeta}^{0}\right)_{ns},\left(u_{\phi}^{0}\right)_{nc},\left(u_{\phi}^{0}\right)_{ns},\left(u_{\theta}^{0}\right)_{nc},\left(u_{\theta}^{0}\right)_{ns},\left(\beta_{\phi}^{0}\right)_{nc},\\ \left(\beta_{\phi}^{0}\right)_{ns},\left(\beta_{\theta}^{0}\right)_{nc},\left(\beta_{\theta}^{0}\right)_{ns}\end{bmatrix}^{T}_{10x1} \tag{3.3.60}$$

$$\psi^{(2)}(\phi)=\begin{bmatrix}\left(Q_{\phi\zeta}^{0}\right)_{nc},\left(Q_{\phi\zeta}^{0}\right)_{ns},\left(N_{\phi}^{0}\right)_{nc},\left(N_{\phi}^{0}\right)_{ns},\left(N_{\phi\theta}^{0}\right)_{nc},\left(N_{\phi\theta}^{0}\right)_{ns}\\ ,\left(M_{\phi}^{0}\right)_{nc},\left(M_{\phi}^{0}\right)_{ns},\left(M_{\phi\theta}^{0}\right)_{nc},\left(M_{\phi\theta}^{0}\right)_{ns}\end{bmatrix}^{T}_{10x1} \tag{3.3.61}$$

and

$$\begin{Bmatrix}B^{(1)}(\phi)\\ B^{(2)}(\phi)\end{Bmatrix}_{20x1}=\left[KB\right]_{20x18}\left\{BL(\phi)\right\}_{18x1} \tag{3.3.62}$$

where

$$BL(\phi)=\begin{bmatrix}\left(p_{\zeta}\right)_{nc},\left(p_{\zeta}\right)_{ns},\left(p_{\phi}\right)_{nc},\left(p_{\phi}\right)_{ns},\left(p_{\theta}\right)_{nc},\left(p_{\theta}\right)_{ns},\\ \left(N_{\phi}^{T}\right)_{nc},\left(N_{\phi}^{T}\right)_{ns},\left(N_{\theta}^{T}\right)_{nc},\left(N_{\theta}^{T}\right)_{ns},\left(N_{\phi\theta}^{T}\right)_{nc},\left(N_{\phi\theta}^{T}\right)_{ns},\\ \left(M_{\phi}^{T}\right)_{nc},\left(M_{\phi}^{T}\right)_{ns},\left(M_{\theta}^{T}\right)_{nc},\left(M_{\theta}^{T}\right)_{ns},\left(M_{\phi\theta}^{T}\right)_{nc},\left(M_{\phi\theta}^{T}\right)_{ns}\end{bmatrix}^{T}_{18x1} \tag{3.3.63}$$

The elements of the coefficient matrix K and KB are given in Appendix D and Appendix E, respectively in detail.

It should be remembered that the fundamental variables given by the fundamental set of Equations (3.3.59), are not the actual physical variables but they are the transformed variables. For the fundamental variable u_ζ^0 they are given by Equations (3.3.3) and (3.3.4). Generalizing these equations to all fundamental variables,

$$\{\psi(\phi,\theta)\} = \sum_{n=-\infty}^{+\infty} \left(\{\psi(\phi)\}\right)_n e^{\mathrm{i}n\theta} \tag{3.3.64}$$

where

$$\left(\{\psi(\phi)\}\right)_n = \frac{1}{2\pi}\int_0^{2\pi} \{\psi(\phi,\theta)\} e^{-\mathrm{i}n\theta} d\theta = \left(\{\psi(\phi)\}\right)_{nc} - \mathrm{i}\left(\{\psi(\phi)\}\right)_{ns} \tag{3.3.65}$$

and

$$\left(\{\psi(\phi)\}\right)_{nc} = \frac{1}{2\pi}\int_0^{2\pi} \{\psi(\phi,\theta)\} \cos n\theta \, d\theta \tag{3.3.66}$$

$$\left(\{\psi(\phi)\}\right)_{ns} = \frac{1}{2\pi}\int_0^{2\pi} \{\psi(\phi,\theta)\} \sin n\theta \, d\theta \tag{3.3.67}$$

The transformed variables used in Equation (3.3.59) are given by Equations (3.3.66) and (3.3.67).

In order to be compatible with the equation (3.3.59), the boundary conditions, given by Equations (2.4.3.6) – (2.4.3.10), should also be expressed in terms of the transformed variables. If the Finite Exponential Fourier Transform is applied to the fundamental variables at the boundary of the shell of revolution,

then the boundary conditions at an edge of the shell of revolution can be expressed in terms of the transformed shell variables as:

Either $\left(N_{\phi nc}, N_{\phi ns}\right) = \left(N^{*}_{\phi nc}, N^{*}_{\phi ns}\right)$ or $(u^{0}_{\phi nc}, u^{0}_{\phi ns}) = \left(\left(u^{0}_{\phi nc}\right)^{*}, \left(u^{0}_{\phi ns}\right)^{*}\right)$

(3.3.68)

Either $\left(N_{\phi\theta nc}, N_{\phi\theta ns}\right) = \left(N^{*}_{\phi\theta nc}, N^{*}_{\phi\theta ns}\right)$ or $(u^{0}_{\theta nc}, u^{0}_{\theta ns}) = \left(\left(u^{0}_{\theta nc}\right)^{*}, \left(u^{0}_{\theta ns}\right)^{*}\right)$

(3.3.69)

Either $\left(Q_{\phi\zeta nc}, Q_{\phi\zeta ns}\right) = \left(Q^{*}_{\phi\zeta nc}, Q^{*}_{\phi\zeta ns}\right)$ or $(u^{0}_{\zeta nc}, u^{0}_{\zeta ns}) = \left(\left(u^{0}_{\zeta nc}\right)^{*}, \left(u^{0}_{\zeta ns}\right)^{*}\right)$

(3.3.70)

Either $\left(M_{\phi nc}, M_{\phi ns}\right) = \left(M^{*}_{\phi nc}, M^{*}_{\phi ns}\right)$ or $\left(\beta_{\phi nc}, \beta_{\phi ns}\right) = \left(\beta^{*}_{\phi nc}, \beta^{*}_{\phi ns}\right)$

(3.3.71)

Either $\left(M_{\phi\theta nc}, M_{\phi\theta ns}\right) = \left(M^{*}_{\phi\theta nc}, M^{*}_{\phi\theta ns}\right)$ or $\left(\beta_{\theta nc}, \beta_{\theta ns}\right) = \left(\beta^{*}_{\theta nc}, \beta^{*}_{\theta ns}\right)$

(3.3.72)

Fundamental system of equations (Equation (3.3.59)), together with the boundary conditions (Equations (3.3.68) – (3.3.72)) specified at the two boundary edges of an anisotropic shell of revolution form a two point boundary value problem for the solution of the fundamental shell variables which are the transformed displacements, and stress and moment resultants.

3.4. Reduction to Initial Value Problems

This section is concerned with the reduction of a two-point boundary value problem given by

$$\left\{\frac{d\psi(\phi)}{d\phi}\right\}_{mx\,1} = \left[K(\phi)\right]_{mxm}\left\{\psi(\phi)\right\}_{mx1} + \left\{B(\phi)\right\}_{mx1} \tag{3.4.1}$$

in Equation (3.3.59) to a series of initial value problems by the method proposed by Kalnins [7]. In Equation (3.4.1), $\psi(\phi)$ is the vector which represents m unknown functions, $K(\phi)$ denotes the coefficient matrix, and $B(\phi)$ is the vector of nonhomogeneous terms. For the present study, as shown in the preceding section, m is twenty for the first order transverse shear deformation theory.

The object is to determine $\psi(\phi)$ in the interval $\phi_{\min} \le \phi \le \phi_{\max}$ subject to $m/2$ boundary conditions at each end of the shell of revolution in the form

$$\left[U_a(\phi_{\min})\right]_{mxm} \left\{\psi(\phi_{\min})\right\}_{mx1} = \left\{u_a\right\}_{mx1} \tag{3.4.2}$$

$$\left[U_b(\phi_{\max})\right]_{mxm} \left\{\psi(\phi_{\max})\right\}_{mx1} = \left\{u_b\right\}_{mx1} \tag{3.4.3}$$

The elements of U_a and U_b matrices and u_a and u_b vectors are determined by the boundary conditions. These Equations (3.4.2) and (3.4.3) enable any linear combination of the elements of ψ vector to be prescribed at the boundaries.

It must be emphasized that the governing Equation set (3.4.1) and the boundary conditions (3.4.2) and (3.4.3) are given in the form of governing Equations (3.3.59) and boundary conditions (3.3.68) – (3.3.72) which are derived for the static analysis of the shell of revolution subject to symmetrical and unsymmetrical loads.

Equations (3.4.1), (3.4.2) and (3.4.3) represent the two-point boundary value problem which is going to be to reduced to a number of initial value problems. The solution proposed for the ordinary differential Equation set (3.4.1) can be written as [7]:

$$\left\{\psi(\phi)\right\}_{mx1} = \left[W(\phi)\right]_{mxm} \left\{C\right\}_{mx1} + \left\{D(\phi)\right\}_{mx1} \tag{3.4.4}$$

where $\{C\}$ represents vector of arbitrary constants, $[W(\phi)]$ and $\{D(\phi)\}$ are the homogeneous and particular solutions of Equation (3.4.1). In order to determine the vector of arbitrary constants, Equation (3.4.4) is evaluated at $\phi = \phi_{\min}$, i.e. at the boundary:

$$\{\psi(\phi_{\min})\} = [W(\phi_{\min})]\{C\} + \{D(\phi_{\min})\} \tag{3.4.5}$$

Solving Equation (3.4.5) for $\{C\}$,

$$\{C\} = [W(\phi_{\min})]^{-1}\{\psi(\phi_{\min})\} + [W(\phi_{\min})]^{-1}\{D(\phi_{\min})\}_{mx1} \tag{3.4.6}$$

and substituting $\{C\}$ given by Equation (3.4.6) into Equation (3.4.4),

$$\{\psi(\phi)\} = [SH(\phi)]\{\psi(\phi_{\min})\} + \{SP(\phi)\} \tag{3.4.7}$$

where

$$[SH(\phi)] = [W(\phi)]\,[W(\phi_{\min})]^{-1} \tag{3.4.8}$$

$$\{SP(\phi)\} = -[W(\phi)]\,[W(\phi_{\min})]^{-1}\{D(\phi_{\min})\} + \{D(\phi)\} \tag{3.4.9}$$

Substituting Equation (3.4.7) into Equation (3.4.1),

$$\frac{d}{d\phi}\left([SH(\phi)]\{\psi(\phi_{\min})\} + \{SP(\phi)\}\right) = [K(\phi)]\left([SH(\phi)]\{\psi(\phi_{\min})\} + \{SP(\phi)\}\right) + \{B(\phi)\} \tag{3.4.10}$$

Opening the parenthesis,

$$\{\psi(\phi_{\min})\}\frac{d}{d\phi}[SH(\phi)]+\frac{d}{d\phi}(\{SP(\phi)\})=[K(\phi)][SH(\phi)]\{\psi(\phi_{\min})\}+ \\ [K(\phi)]\{SP(\phi)\}+\{B(\phi)\} \tag{3.4.11}$$

This equation can be separated by regrouping the first terms on the left hand side and right hand side together in one equation, and second terms on the left hand side and right hand side in another equation. Since $\{\psi(\phi_{\min})\}$ appears in both sides of the first equation, it drops out. The first and second equations mentioned are written as

$$\left[\frac{dSH(\phi)}{d\phi}\right]_{mxm}=[K(\phi)]_{mxm}[SH(\phi)]_{mxm} \tag{3.4.12}$$

$$\left\{\frac{dSP(\phi)}{d\phi}\right\}_{mx1}=[K(\phi)]_{mxm}\{SP(\phi)\}_{mx1}+\{B(\phi)\}_{mx1} \tag{3.4.13}$$

The matrix $[SH(\phi)]$ is also named as transfer matrix, because it relates the fundamental shell variables at one end of the shell of revolution to the fundamental shell variables at the other end of the shell of revolution.

In order to find out the initial conditions, Equations (3.4.8) and (3.4.9) are evaluated at $\phi=\phi_{\min}$:

$$[SH(\phi_{\min})]=[W(\phi_{\min})][W(\phi_{\min})]^{-1}=[I] \tag{3.4.14}$$

$$\{SP(\phi_{\min})\}=-[W(\phi_{\min})][W(\phi_{\min})]^{-1}\{D(\phi_{\min})\}+\{D(\phi_{\min})\} \\ =-[I]\{D(\phi_{\min})\}+\{D(\phi_{\min})\}=\{0\} \tag{3.4.15}$$

Therefore, the initial condition required for the determination of homogeneous solution $[SH(\phi)]$ is the unity matrix and that for the determination of the particular solution $\{SP(\phi)\}$ is zero, i.e.

$$\left[SH\left(\phi_{\min}\right)\right]=\left[I\right] \tag{3.4.16}$$

$$\left[SP\left(\phi_{\min}\right)\right]=\left[0\right] \tag{3.4.17}$$

In addition, evaluation of the Equation (3.4.7) at the other boundary, i.e. at $\phi=\phi_{\max}$, provides the continuity between $\phi_{\min}$ and $\phi_{\max}$ as:

$$\left\{\psi\left(\phi_{\max}\right)\right\}_{mx1}=\left[SH\left(\phi_{\max}\right)\right]_{mxm}\left\{\psi\left(\phi_{\min}\right)\right\}_{mx1}+\left\{SP\left(\phi_{\max}\right)\right\}_{mx1} \tag{3.4.18}$$

Equation set (3.4.18) constitutes a system of 2m linear algebraic equations with 2m unknowns, with the boundary conditions prescribed by Equations (3.4.2) and (3.4.3). Of these 2m unknowns, m are to be determined at $\phi=\phi_{\min}$, which are represented as $\left\{\psi\left(\phi_{\min}\right)\right\}$, and m are to be determined at $\phi=\phi_{\max}$, which are represented as $\left\{\psi\left(\phi_{\max}\right)\right\}$. Once $\left\{\psi\left(\phi_{\min}\right)\right\}$ is known, the solution at any value of ϕ can be obtained using Equation (3.4.7), as long as $\left[SH\right]$ and $\left\{SP\right\}$ for the ϕ value of interest are known. Thus, the reduction of a two point boundary value problem defined by Equations (3.4.1), (3.4.2) and (3.4.3) to $m+1$ initial value problems given by Equations (3.4.12), (3.4.13), (3.4.16) and (3.4.17) is now completed.

During the solution of the initial value problem defined above, elements of the $\left[SH\right]$ matrix and $\left\{SP\right\}$ vector are observed to increase in magnitude in such a way that if the length of the interval $\left(\phi_{\min},\phi_{\max}\right)$ is increased by a factor of x, the magnitude of the solutions of $\left[SH\right]$ matrix and $\left\{SP\right\}$ vector increase approximately exponentially with x [7]. Increasing x on the other hand physically means that the meridional dimension of the shell becomes longer. And naturally, as the shell gets longer in the meridional direction, the effects of the applied loads on one end of the shell is perceived less on the other end. Therefore, as opposed to $\left[SH\right]$ matrix and $\left\{SP\right\}$ vector, the elements of $\psi\left(\phi_{\max}\right)$ are expected to decrease with increasing x.

If the Equation (3.4.18) is examined carefully, in the light of the mathematical and physical facts explained in the above paragraph, it is expected that $\{\psi(\phi_{\max})\}$ should decrease, while $[SH(\phi_{\max})]$ and $\{SP(\phi_{\max})\}$ increase and $\{\psi(\phi_{\min})\}$ is kept constant with increasing x, which represents $(\phi_{\min}, \phi_{\max})$ interval. However, if the length of the interval $(\phi_{\min}, \phi_{\max})$ exceeds a critical value, loss of accuracy occurs in Equation (3.4.18), which involve matrix multiplication and addition operations. Loss of accuracy occurs because after a certain value of the interval $(\phi_{\min}, \phi_{\max})$, all significant digits of $[SH(\phi_{\max})]$ are lost when $[SH(\phi_{\max})]$ is multiplied by $\{\psi(\phi_{\min})\}$. The only way that the matrix product of Equation (3.4.18) can give small values of $\{\psi(\phi_{\max})\}$ is that a number of significant digits of the large values of $[SH(\phi_{\max})]$ subtract out.

Therefore, drawback of this using a single shell interval is the loss of accuracy that is encountered when the length of the interval $(\phi_{\min}, \phi_{\max})$ exceeds a critical value.

In order to overcome this problem and estimate the critical length of a shell approximately, a convenient length factor is defined by Kalnins [7]:

$$\beta = \frac{l\left[3\left(1-\upsilon^2\right)\right]^{0.25}}{(Rh)^{0.5}} \tag{3.4.19}$$

where l is the length of the meridian of the shell, R is a minimum radius of curvature, and h is the thickness of the shell.

However, the loss of accuracy can be avoided completely and shells of revolution with larger values of β can be analyzed by means of the direct integration technique if the multisegment method given in the next section is employed.

3.5. Multisegment Method of Integration

This method is the continuation of the method described in the previous section and has been used widely after it was first developed by Kalnins [7] in many studies such as [1] and [2]. Let the shell be divided into M segments denoted by S_i, where $i = 1,2,...,M$. (See Figure 3.1) These M segments can be arbitrary in length, but all should be less or equal to β so that loss of accuracy that was described above does not occur. A generic shell segment S_i is defined between the meridional coordinates ϕ_i and ϕ_{i+1}.

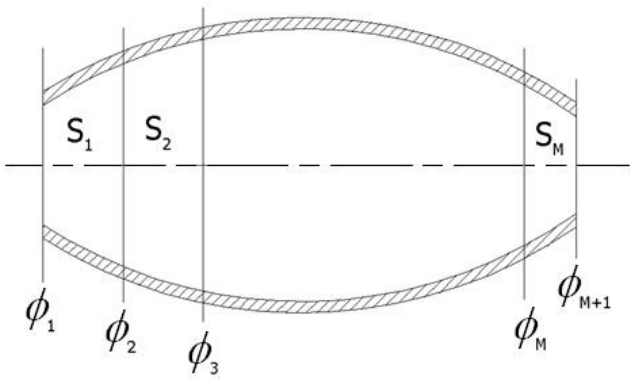

Figure 3.1 Notation for Division of Total Interval into Segments

The equations derived for the whole interval $(\phi_{\min}, \phi_{\max})$ in the previous section is now used for each segment. Therefore, analogous to Equations (3.4.7), (3.4.12), (3.4.13), (3.4.16) and (3.4.17), one can write:

$$\{\psi(\phi)\}_{mx1} = [SH_i(\phi)]_{mxm} \{\psi(\phi_i)\}_{mx1} + \{SP_i(\phi)\}_{mx1} \tag{3.5.1}$$

$$\left[\frac{dSH_i(\phi)}{d\phi}\right]_{mxm} = \left[K(\phi)\right]_{mxm}\left[SH_i(\phi)\right]_{mxm} \tag{3.5.2}$$

$$\left\{\frac{dSP_i(\phi)}{d\phi}\right\}_{mx1} = \left[K(\phi)\right]_{mxm}\left\{SP_i\ (\phi)\right\}_{mx1} + \left\{B(\phi)\right\}_{mx1} \tag{3.5.3}$$

$$\left[SH_i(\phi_i)\right] = \left[I\right] \tag{3.5.4}$$

$$\left[SP_i(\phi_i)\right] = \left[0\right] \tag{3.5.5}$$

Requiring the continuity of all elements of $\{\psi(\phi)\}$ at the ends of each segment, using Equation (3.4.18)

$$\left\{\psi(\phi_{i+1})\right\}_{mx1} = \left[SH_i(\phi_{i+1})\right]_{mxm}\left\{\psi(\phi_i)\right\}_{mx1} + \left\{SP_i(\phi_{i+1})\right\}_{mx1} \tag{3.5.6}$$

As seen in Equation set (3.5.6), the unknown vector $\{\psi(\phi)\}$ has m elements. Since the equation is solved at the beginning and end points of each segment, and there are a total number of M segments and $M+1$ points in the interval $(\phi_{\min}, \phi_{\max})$ as shown in Figure 3.1, the total number of variables is $m(M+1)$. Of these variables, $2m$ exist at the boundaries, that is at ϕ_1 and ϕ_{m+1} ($\phi_{\min}$ and $\phi_{\max}$). As explained in Section 2.4.2, only half of the variables existing at the boundaries can be known (either force terms or the corresponding displacements can be prescribed in any direction). Therefore, of the $2m$ variables existing at ϕ_1 and ϕ_{m+1}, $m/2$ are known at one end and $m/2$ are known at the other end. Consequently, as the calculation in Equation (3.5.7) shows, the matrix equation involves exactly $m \times M$ number of unknowns.

$$m(M+1) - \frac{m}{2} - \frac{m}{2} = mM \tag{3.5.7}$$

It has been shown in Equations (3.4.2) and (3.4.3) that the boundary conditions can be given as a linear combination of any of the variables. Since

$\phi_{\min} = \phi_1$ and $\phi_{\max} = \phi_{M+1}$ for the multisegment method of integration, these equations can be rewritten as

$$\left[U_a(\phi_{\min})\right]_{mxm} \left\{\psi(\phi_1)\right\}_{mx1} = \left\{u_a\right\}_{mx1} \tag{3.5.8}$$

$$\left[U_b(\phi_{\max})\right]_{mxm} \left\{\psi(\phi_{M+1})\right\}_{mx1} = \left\{u_b\right\}_{mx1} \tag{3.5.9}$$

where $m/2$ elements of u_a and $m/2$ elements of u_b are assumed to be prescribed. It is convenient to arrange the rows of the given boundary condition matrices U_a and U_b in such a way that, the prescribed elements of u_a appear as the first $m/2$ elements and the prescribed elements of u_b are the last $m/2$ elements. Writing the continuity Equation (3.5.1) for the first point using Equation (3.5.8),

$$\left\{\psi(\phi_2)\right\}_{mx1} = \left[SH_1(\phi_2)\right]_{mxm} \left[U_a(\phi_{\min})\right]^{-1}_{mxm} \left\{u_a\right\}_{mx1} + \left\{SP_1(\phi_2)\right\}_{mx1} \tag{3.5.10}$$

and for the last point, using Equation (3.5.9),

$$\left\{u_b\right\}_{mx1} = \left[U_b(\phi_{M+1})\right]_{mxm} \left[SH_M(\phi_{M+1})\right]_{mxm} \left\{\psi(\phi_M)\right\}_{mx1} + \left[U_b(\phi_{M+1})\right]_{mxm} \left\{SP_M(\phi_{M+1})\right\}_{mx1} \tag{3.5.11}$$

For the first and last segments respectively, the following transformations are performed:

$$\left[SH_M(\phi_2)\right]_{mxm} \left[U_a(\phi_1)\right]^{-1}_{mxm} \Rightarrow \left[SH_M(\phi_2)\right]_{mxm} \tag{3.5.12}$$

$$\left[U_B(\phi_{m+1})\right]_{mxm} \left[SH_M(\phi_{m+1})\right]_{mxm} \Rightarrow \left[SH_M(\phi_{m+1})\right]_{mxm} \tag{3.5.13}$$

$$\left[U_B(\phi_{m+1})\right]_{mxm} \left[SP_M(\phi_{m+1})\right]_{mxm} \Rightarrow \left[SP_M(\phi_{m+1})\right]_{mxm} \tag{3.5.14}$$

Matrix Equation (3.5.6) contains both known variables, which are prescribed at the boundaries, and unknown variables together. In order to solve the

equation to find out the unknown variables properly, first known and unknown variables should be separated. As stated above, for convenience, the first $m/2$ elements of u_a and last $m/2$ elements of u_b are assumed to be prescribed. Therefore, the first $m/2$ elements of $\{\psi(\phi_1)\}$, denoted by $\{\psi_1(\phi_1)\}$ are assumed to be known and the last $m/2$ elements of $\{\psi(\phi_1)\}$, denoted by $\{\psi_2(\phi_1)\}$ are assumed to be unknown. On the other hand, for the other end, the first $m/2$ elements of $\{\psi(\phi_{M+1})\}$, denoted by $\{\psi_1(\phi_{M+1})\}$ are unknown and the last $m/2$ elements of $\{\psi(\phi_{M+1})\}$, denoted by $\{\psi_2(\phi_{M+1})\}$ are known. If the rearrangement of the columns in the matrix Equation (3.5.6) is performed, the continuity equations can be rewritten as a partitioned matrix product in the form given by Equation (3.5.15).

$$\begin{Bmatrix}\psi_1(\phi_{i+1})\\ \psi_2(\phi_{i+1})\end{Bmatrix}=\begin{bmatrix}SH_i^{(1)}(\phi_{i+1}) & SH_i^{(2)}(\phi_{i+1})\\ SH_i^{(3)}(\phi_{i+1}) & SH_i^{(4)}(\phi_{i+1})\end{bmatrix}\begin{Bmatrix}\psi_1(\phi_i)\\ \psi_2(\phi_i)\end{Bmatrix}+\begin{Bmatrix}SP_i^{(1)}(\phi_{i+1})\\ SP_i^{(2)}(\phi_{i+1})\end{Bmatrix} \tag{3.5.15}$$

In each shell segment $(i=1,2,...,M)$, Equation (3.5.15) can be written as

$$\left[SH_i^{(1)}(\phi_{i+1})\right]\{\psi_1(\phi_i)\}+\left[SH_i^{(2)}(\phi_{i+1})\right]\{\psi_2(\phi_i)\}-\{\psi_1(\phi_{i+1})\}=-\left\{SP_i^{(1)}(\phi_{i+1})\right\} \tag{3.5.16}$$

$$\left[SH_i^{(3)}(\phi_{i+1})\right]\{\psi_1(\phi_i)\}+\left[SH_i^{(4)}(\phi_{i+1})\right]\{\psi_2(\phi_i)\}-\{\psi_2(\phi_{i+1})\}=-\left\{SP_i^{(2)}(\phi_{i+1})\right\} \tag{3.5.17}$$

The result is a system of $2M$ linear algebraic matrix equations with known coefficient matrices $\left[SH_i^{(j)}(\phi_{i+1})\right]$ $(j=1,2,3,4\ ;\ i=1,2,...M)$ and vectors of nonhomogeneous coefficients $\left\{SP_i^{(j)}(\phi_{i+1})\right\}$ $(j=1,2\ \ ;\ i=1,2,...,M)$. It should be noted that in Equation (3.5.16), $\{\psi_1(\phi_1)\}$; and in Equation (3.5.17), $\{\psi_2(\phi_{M+1})\}$ are known. Therefore, the unknowns partitioned vectors are given by $\{\psi_1(\phi_i)\}$ with $(i=2,3...,M+1)$ and $\{\psi_2(\phi_i)\}$ with $(i=1,2,3...,M)$. Thus, there are exactly $2M$ unknowns.

System of Equations (3.5.16) and (3.5.17) is brought into the following form by means of Gaussian elimination.

$$\begin{bmatrix} E_1 & -I & 0 & 0 & . & . & 0 & 0 \\ 0 & C_1 & -I & 0 & . & . & 0 & 0 \\ 0 & 0 & E_2 & -I & . & . & 0 & 0 \\ 0 & 0 & 0 & C_2 & . & . & 0 & 0 \\ . & . & . & . & . & . & 0 & 0 \\ . & . & . & . & . & . & -I & 0 \\ 0 & 0 & 0 & 0 & 0 & 0 & E_M & -I \\ 0 & 0 & 0 & 0 & 0 & 0 & 0 & C_M \end{bmatrix} \cdot \begin{Bmatrix} \psi_2(\phi_1) \\ \psi_1(\phi_2) \\ \psi_2(\phi_2) \\ \psi_1(\phi_3) \\ . \\ . \\ \psi_2(\phi_M) \\ \psi_1(\phi_{M+1}) \end{Bmatrix} = \begin{Bmatrix} VA_1 \\ VB_1 \\ VA_2 \\ VB_2 \\ . \\ . \\ VA_M \\ VB_M \end{Bmatrix} \tag{3.5.18}$$

where the dots indicate the equations for $i = 3,..M-1$. The $(m/2 \times m/2)$ matrices E_i and C_i are defined for $i = 1$ as

$$E_1 = SH_1^{(2)} \tag{3.5.19}$$

$$C_1 = SH_1^{(4)} E_1^{-1} \tag{3.5.20}$$

and for $i = 2,3,..M$, as

$$E_i = SH_i^{(2)} + SH_i^{(1)} C_{i-1}^{-1} \tag{3.5.21}$$

$$C_i = \left(SH_i^{(4)} + SH_i^{(3)} C_{i-1}^{-1}\right) E_i^{-1} \tag{3.5.22}$$

The $(m/2 \times 1)$ vectors VA_i and VB_i are defined for $i = 1$ as

$$VA_1 = -SP_1^{(1)} - SH_1^{(1)} \psi_1\left(\phi_1\right) \tag{3.5.23}$$

$$VB_1 = -SP_1^{(2)} - SH_1^{(3)} \psi_1\left(\phi_1\right) - SH_1^{(4)} E_1^{-1} VA_1 \tag{3.5.24}$$

for $i = 2,3,..M-1$, as

$$VA_i = -SP_i^{(1)} - SH_1^{(1)} C_{i-1}^{-1} VB_{i-1} \tag{3.5.25}$$

$$VB_i = -SP_i^{(2)} - SH_i^{(3)} C_{i-1}^{-1} VB_{i-1} - \left(SH_i^{(4)} + SH_i^{(3)} C_{i-1}^{-1}\right) E_i^{-1} VA_i \tag{3.5.26}$$

and for the M^{th} segment

$$VA_M = -SP_M^{(1)} - SH_M^{(1)} C_{M-1}^{-1} VB_{M-1} \tag{3.5.27}$$

$$VB_M = \psi_2\left(\phi_{M+1}\right) - SP_M^{(2)} - SH_M^{(3)} C_{M-1}^{-1} VB_{M-1} - \left(SH_M^{(4)} + SH_M^{(3)} C_{M-1}^{-1}\right) E_M^{-1} VA_M \tag{3.5.28}$$

In the relations given above, for brevity, in place of $SH_i^{(j)}\left(\phi_{i+1}\right)$ and $SP_i^{(j)}\left(\phi_{i+1}\right)$, the symbols $SH_i^{(j)}$ and $SP_i^{(j)}$ have been used and square brackets representing the matrices and curly brackets representing the vectors are dropped.

Following this procedure, by the use of Equations (3.5.19) – (3.5.28), the unknown variables are found by

$$\psi_1\left(\phi_{M+1}\right) = C_M^{-1} VB_M \tag{3.5.29}$$

$$\psi_2\left(\phi_M\right) = E_M^{-1}\left[\psi_1\left(\phi_{M+1}\right) + VA_M\right] \tag{3.5.30}$$

and for $i = 1,2,...M-1$,

$$\psi_1\left(\phi_{M-i+1}\right) = C_{M-i}^{-1}\left[\psi_2\left(\phi_{M-i+1}\right) + VB_{M-i}\right] \tag{3.5.31}$$

$$\psi_2\left(\phi_{M-i}\right) = E_{M-i}^{-1}\left[\psi_1\left(\phi_{M-i+1}\right) + VA_{M-i}\right] \tag{3.5.32}$$

It should be noted that the transformed fundamental variables will be determined for a particular circumferential wave number, and depending on the definition of loading the solution process must be repeated for a certain

number of circumferential wave numbers which are used to define any unsymmetrical load with sufficient accuracy in the Fourier series representation. Once all the unknowns $\{\psi(\phi_i)\}$ are found, fundamental variables can be determined using Equation (3.5.1) at any desired values of ϕ at which the solutions $[SH_i(\phi)]$.and $\{SP_i(\phi)\}$ are stored during the integration of the initial value problem defined by Equations (3.5.2) and (3.5.3).

However, it should be remembered that the number of segments that the interval is divided into can be chosen at will, Thus, if the number of segments are sufficiently large, then the solution is obtained at sufficient number of intermediate points and use of Equation (3.5.1) will not be necessary to obtain the fundamental variables at intermediate meridional coordinates; because enough resolution will have been obtained in terms of the meridional coordinates, where the output is given.

The integration of Equations (3.5.2) and (3.5.3) can be accomplished by means of any direct integration method. The description of the integration method used in the present study will be explained in the succeeding sections.

In Section 3.3 it has been stated that loading can also be defined as a function of ϕ. It should be noted that the known vector of nonhomogeneous terms $\{B(\phi)\}_{mx1}$ consist of loading terms, and this vector is calculated at the end points of each of the segments forming the whole interval. Therefore, by specifying mechanical and thermal loads at the end points of the shell segments, one can define of the loads as a function of the meridional coordinate ϕ.

3.6. Back Transformation

Another issue that should be mentioned is that by following the method described above, the results will have been found only for a particular circumferential wave number n. Therefore, for a complete solution, as it was stresses before, solution should be carried out for each circumferential wave number n separately, and finally be summed up to obtain the final result. Furthermore, for each circumferential wave number n, fundamental variables determined are the transformed variables, not the actual physical variables. Therefore, these transformed variables should be back-transformed to the actual physical variables. Back transformation of transformed variables and summation of the solutions for each circumferential wave number n is achieved by Equation (3.6.1) where $\{\psi(\phi,\theta)\}$ represents the vector of fundamental shell variables. The solution process gives the cosine and sine parts of fundamental variables $(\{\psi(\phi)\})_{nc}$ and $(\{\psi(\phi)\})_{ns}$, and once these Fourier components are determined the actual physical variables are calculated by the summation operation over the range of circumferential wave numbers.

$$\{\psi(\phi,\theta)\} = (\{\psi(\phi)\})_0 + 2\sum_{n=1}^{+\infty}\left[(\{\psi(\phi)\})_{nc}\cos n\theta + (\{\psi(\phi)\})_{ns}\sin n\theta\right] \quad (3.6.1)$$

where

$$(\{\psi(\phi)\})_{nc} = \frac{1}{2\pi}\int_0^{2\pi}\{\psi(\phi,\theta)\}\cos n\theta\, d\theta \quad (3.6.2)$$

$$(\{\psi(\phi)\})_{ns} = \frac{1}{2\pi}\int_0^{2\pi}\{\psi(\phi,\theta)\}\sin n\theta\, d\theta \quad (3.6.3)$$

$$(\{\psi(\phi)\})_0 = \frac{1}{2\pi}\int_0^{2\pi}\{\psi(\phi,\theta)\}d\theta \quad (3.6.4)$$

3.7. Post Processing

After back transformation is performed in Section 3.6, all fundamental variables in their actual physical form $\left(\{\psi(\phi,\theta)\}_{10x1}\right)$ have now been calculated. Using these results, it is possible to calculate stresses and strains using the governing equations given in Chapter 2. It should be noted that the fundamental variable vector consists of displacements and rotations and stress and moment resultants. Therefore, for a layered composite structure to calculate the layer stresses and strains one needs to process on the fundamental shell variables to get the strains and stresses through the shell of revolution.

Strain – displacement relations for shells of revolution are given in Chapter 2 by the Equations (2.2.3.1) – (2.2.3.11). For the sake of completeness and ease of explanation, these equations are reminded here again. Overall (total) in-plane strains are given by

$$\varepsilon_{\phi\phi}(\phi,\theta,\zeta)=\varepsilon^0_{\phi\phi}(\phi,\theta)+\zeta\,\kappa_{\phi\phi}(\phi,\theta) \tag{3.7.1}$$

$$\varepsilon_{\theta\theta}(\phi,\theta,\zeta)=\varepsilon^0_{\theta\theta}(\phi,\theta)+\zeta\kappa_{\theta\theta}(\phi,\theta) \tag{3.7.2}$$

$$\gamma_{\phi\theta}(\phi,\theta,\zeta)=\gamma^0_{\phi\theta}(\phi,\theta)+\zeta\,\kappa_{\phi\theta}(\phi,\theta) \tag{3.7.3}$$

where, the midstrains (membrane strains) and bending strains are given by

$$\varepsilon^0_{\phi\phi}=\frac{1}{R_\phi}\left[\frac{\partial u^0_\phi}{\partial\phi}+u^0_\zeta\right] \tag{3.7.4}$$

$$\varepsilon^0_{\theta\theta}=\frac{1}{R_\theta\sin\phi}\left[u^0_\phi\cos\phi+\frac{\partial u^0_\theta}{\partial\theta}+u^0_\zeta\sin\phi\right] \tag{3.7.5}$$

$$\gamma^0_{\phi\theta}=\frac{1}{R_\theta\sin\phi}\frac{\partial u^0_\phi}{\partial\theta}+\frac{1}{R_\phi}\frac{\partial u^0_\theta}{\partial\phi}-\frac{\cot\phi}{R_\theta}u^0_\theta \tag{3.7.6}$$

$$\kappa_{\phi\phi} = \frac{1}{R_\phi}\frac{\partial \beta_\phi}{\partial \phi} \tag{3.7.7}$$

$$\kappa_{\theta\theta} = \frac{1}{R_\theta \sin\phi}\left[\beta_\phi \cos\phi + \frac{\partial \beta_\theta}{\partial \theta}\right] \tag{3.7.8}$$

$$\kappa_{\phi\theta} = \frac{1}{R_\theta \sin\phi}\frac{\partial \beta_\phi}{\partial \theta} + \frac{1}{R_\phi}\frac{\partial \beta_\theta}{\partial \phi} - \frac{\cot\phi}{R_\theta}\beta_\theta \tag{3.7.9}$$

and transverse shear strains are given by

$$\gamma_{\phi\zeta} = \beta_\phi - \frac{u_\phi^0}{R_\phi} + \frac{1}{R_\phi}\frac{\partial u_\zeta^0}{\partial \phi} \tag{3.7.10}$$

$$\gamma_{\theta\zeta} = \beta_\theta - \frac{u_\theta^0}{R_\theta} + \frac{1}{R_\theta \sin\phi}\frac{\partial u_\zeta^0}{\partial \theta} \tag{3.7.11}$$

As it is seen clearly, in order to calculate the total in-plane strains, midstrains (membrane strains) and bending strains should be known, and these are given by Equations (3.7.4) – (3.7.9). In Equations (3.7.4) – (3.7.11), for the calculation of midstrains, bending strains and transverse shear strains; mid-plane displacements u_ϕ^0, u_θ^0, u_ζ^0 and rotations β_ϕ, β_θ should be known, all of which appear in the fundamental variable vector $\{\psi(\phi,\theta)\}_{10x1}$. However, their derivatives with respect to ϕ and with respect to θ also need to be calculated. Since the fundamental variables are given by the Equation (3.6.1) in generic form, mid-plane displacements and rotations u_ϕ^0, u_θ^0, u_ζ^0, β_ϕ and β_θ can be expressed as:

$$\{\psi_d(\phi,\theta)\} = \left(\{\psi(\phi)\}\right)_0 + 2\sum_{n=1}^{+\infty}\left[\left(\{\psi_d(\phi)\}\right)_{nc}\cos n\theta + \left(\{\psi_d(\phi)\}\right)_{ns}\sin n\theta\right] \tag{3.7.12}$$

where

$$\{\psi_d(\phi,\theta)\} = \left\{u_\phi^0(\phi,\theta) \quad u_\theta^0(\phi,\theta) \quad u_\zeta^0(\phi,\theta) \quad \beta_\phi(\phi,\theta) \quad \beta_\theta(\phi,\theta)\right\}^T \tag{3.7.13}$$

Thus, based on Equation (3.7.12), the derivatives of u_ϕ^0, u_θ^0, u_ζ^0, β_ϕ and β_θ with respect to θ can be found as:

$$\frac{\partial\{\psi_d(\phi,\theta)\}}{\partial\theta} = 2\sum_{n=1}^{+\infty}\left[-n\left(\{\psi_d(\phi)\}\right)_{nc}\sin n\theta + n\left(\{\psi_d(\phi)\}\right)_{ns}\cos n\theta\right] \tag{3.7.14}$$

For the calculation of derivatives with respect to ϕ, finite difference method will be employed. To calculate the meridional coordinate derivatives of the fundamental variables at the initial point of the first segment, i.e. at $\phi_i = \phi_1 = \phi_{\min}$, forward difference of first order is used [16]:

$$\frac{\partial\{\psi_d(\phi_1,\theta)\}}{\partial\phi} = \frac{\{\psi_d(\phi_2,\theta)\} - \{\psi_d(\phi_1,\theta)\}}{\Delta\phi} \tag{3.7.15}$$

for the second point and the point one before the last point, i.e. for $\phi_i = \phi_2$ and $\phi_i = \phi_M$, central difference of first order is used [16]:

$$\frac{\partial\{\psi_d(\phi_i,\theta)\}}{\partial\phi} = \frac{\{\psi_d(\phi_{i+1},\theta)\} - \{\psi_d(\phi_{i-1},\theta)\}}{2\Delta\phi} \tag{3.7.16}$$

for the points in between, i.e. for ϕ_i $(i = 3,...,M-1)$ central difference of second order is used in order to improve accuracy [16]:

$$\frac{\partial\{\psi_d(\phi_i,\theta)\}}{\partial\phi} = \frac{-\{\psi_d(\phi_{i+2},\theta)\} + 8\{\psi_d(\phi_{i+1},\theta)\} - 8\{\psi_d(\phi_{i-1},\theta)\} + \{\psi_d(\phi_{i-2},\theta)\}}{12\Delta\phi} \tag{3.7.17}$$

and for the last point, i.e. $\phi_i = \phi_{M+1} = \phi_{\max}$, backward difference of first order is used [16]:

$$\frac{\partial\{\psi_d(\phi_{M+1},\theta)\}}{\partial\phi} = \frac{\{\psi_d(\phi_{M+1},\theta)\} - \{\psi_d(\phi_M,\theta)\}}{\Delta\phi} \tag{3.7.18}$$

Once the mid-plane strains are calculated, one can calculate the total in-plane strains strain from Equations (3.7.1) – (3.7.3) and transverse shear strains from Equations (3.7.10) – (3.7.11). In-plane stresses and transverse shear stresses at each layer can then be calculated from Equation (3.7.19) and (3.7.21), respectively.

$$\begin{Bmatrix}\sigma_{\phi\phi}\\ \sigma_{\theta\theta}\\ \sigma_{\phi\theta}\end{Bmatrix}_k = \begin{bmatrix}\overline{Q}_{11} & \overline{Q}_{12} & \overline{Q}_{16}\\ \overline{Q}_{12} & \overline{Q}_{22} & \overline{Q}_{26}\\ \overline{Q}_{16} & \overline{Q}_{26} & \overline{Q}_{66}\end{bmatrix}_k \begin{Bmatrix}\varepsilon_{\phi\phi} - \alpha_\phi \Delta T\\ \varepsilon_{\theta\theta} - \alpha_\theta \Delta T\\ \gamma_{\phi\theta} - \alpha_{\phi\theta}\Delta T\end{Bmatrix}_k \tag{3.7.19}$$

where

$$\begin{aligned}\alpha_\phi &= \alpha_1 \cos^2\theta + \alpha_2 \sin^2\theta\\ \alpha_\theta &= \alpha_1 \sin^2\theta + \alpha_2 \cos^2\theta\\ \alpha_{\phi\theta} &= 2(\alpha_1 - \alpha_2)\cos\theta\sin\theta\end{aligned} \tag{3.7.20}$$

$$\begin{Bmatrix}\sigma_{\theta\zeta}\\ \sigma_{\phi\zeta}\end{Bmatrix} = \begin{bmatrix}\overline{Q}_{44} & \overline{Q}_{45}\\ \overline{Q}_{45} & \overline{Q}_{55}\end{bmatrix}\begin{Bmatrix}\gamma_{\theta\zeta}\\ \gamma_{\phi\zeta}\end{Bmatrix} \tag{3.7.21}$$

It should be noted that as an alternative method, the mid-plane strains, curvatures and transverse shear strains can also be calculated from the stress/moment resultant strain/curvatures relations. One should recall that the relation of in-plane forces and moments with midstrains (membrane strains) and bending strains is given in Chapter 2 by the Equation (2.3.2.44); and the relation between transverse shear strains and transverse force resultants is given by the Equation (2.3.3.7). To calculate mid-plane strains, bending

strains (curvatures) and transverse shear strains one has to invert Equations (2.3.2.44) and (2.3.3.7) as in Equation (3.7.22) and (3.7.23).

$$\begin{Bmatrix} \varepsilon^0_{\phi\phi} \\ \varepsilon^0_{\theta\theta} \\ \gamma^0_{\phi\theta} \\ \kappa_{\phi\phi} \\ \kappa_{\theta\theta} \\ \kappa_{\phi\theta} \end{Bmatrix} = \begin{bmatrix} A_{11} & A_{12} & A_{16} & B_{11} & B_{12} & B_{16} \\ A_{12} & A_{22} & A_{26} & B_{12} & B_{22} & B_{26} \\ A_{16} & A_{26} & A_{66} & B_{16} & B_{26} & B_{66} \\ B_{11} & B_{12} & B_{16} & D_{11} & D_{12} & D_{16} \\ B_{12} & B_{22} & B_{26} & D_{12} & D_{22} & D_{26} \\ B_{16} & B_{26} & B_{66} & D_{16} & D_{26} & D_{66} \end{bmatrix}^{-1} \left[\begin{Bmatrix} N_{\phi\phi} \\ N_{\theta\theta} \\ N_{\phi\theta} \\ M_{\phi\phi} \\ M_{\theta\theta} \\ M_{\phi\theta} \end{Bmatrix} + \begin{Bmatrix} N^T_{\phi\phi} \\ N^T_{\theta\theta} \\ N^T_{\phi\theta} \\ M^T_{\phi\phi} \\ M^T_{\theta\theta} \\ M^T_{\phi\theta} \end{Bmatrix} \right] \tag{3.7.22}$$

$$\begin{Bmatrix} \gamma_{\theta\zeta} \\ \gamma_{\phi\zeta} \end{Bmatrix} = \begin{bmatrix} A_{44} & A_{45} \\ A_{45} & A_{55} \end{bmatrix}^{-1} \begin{Bmatrix} Q_{\theta\zeta} \\ Q_{\phi\zeta} \end{Bmatrix} \tag{3.7.23}$$

Note that in Equation (3.7.22), the matrix containing the stiffness coefficients A_{ij}, B_{ij} and D_{ij} $(i,j=1,2,6)$ terms is calculated before and therefore known. In addition, the thermal load vector $\{N^T_{\phi\phi} \quad N^T_{\theta\theta} \quad N^T_{\phi\theta} \quad M^T_{\phi\phi} \quad M^T_{\theta\theta} \quad M^T_{\phi\theta}\}^T$ is also known. However, in vector $\{N_{\phi\phi} \quad N_{\theta\theta} \quad N_{\phi\theta} \quad M_{\phi\phi} \quad M_{\theta\theta} \quad M_{\phi\theta}\}^T$; $N_{\phi\phi}$, $N_{\phi\theta}$, $M_{\phi\phi}$ and $M_{\phi\theta}$ terms are known since they are among the fundamental variables and calculated during the solution process. But $N_{\theta\theta}$ and $M_{\theta\theta}$ have not been calculated previously because they are not among the fundamental shell variables. Similarly, in Equation (3.7.23), the matrix containing the transverse shear stiffness coefficients A_{ij} $(i,j=4,5)$ is calculated before and therefore known. Transverse shear stress resultant $Q_{\phi\zeta}$ is also known since it appears in the fundamental variable vector, but $Q_{\theta\zeta}$ is unknown for the time being. Therefore, in order to be able to calculate the midplane strains, bending strains and transverse shear strains from Equations (3.7.22) and (3.7.23) one needs to know the stress and moment resultants $N_{\theta\theta}$, $M_{\theta\theta}$ and transverse shear stress resultant $Q_{\theta\zeta}$. Two methods of calculating $N_{\theta\theta}$ and $M_{\theta\theta}$ are presented below.

In the first method, $N_{\theta\theta}$ and $M_{\theta\theta}$ can be extracted from two of the equations of motion, Equations (2.4.3.11) and (2.4.3.14) as

$$N_{\theta\theta} = \frac{R_\theta}{R_\phi}\frac{\sin\phi}{\cos\phi}\frac{\partial N_{\phi\phi}}{\partial\phi} + N_{\phi\phi} + \frac{1}{\cos\phi}\frac{\partial N_{\phi\theta}}{\partial\theta} + \frac{R_\theta}{R_\phi}\frac{\sin\phi}{\cos\phi}Q_{\phi\zeta} + R_\theta\frac{\sin\phi}{\cos\phi}p_\phi \quad (3.7.24)$$

$$M_{\theta\theta} = \frac{R_\theta}{R_\phi}\frac{\sin\phi}{\cos\phi}\frac{\partial M_{\phi\phi}}{\partial\phi} + M_{\phi\phi} + \frac{1}{\cos\phi}\frac{\partial M_{\phi\theta}}{\partial\theta} - R_\theta\frac{\sin\phi}{\cos\phi}Q_{\phi\zeta} \quad (3.7.25)$$

In these equations, terms involving θ derivatives, i.e. $\partial N_{\phi\theta}/\partial\theta$ and $\partial M_{\phi\theta}/\partial\theta$ are calculated using Equation (3.7.14); and terms involving ϕ derivatives, i.e. $\partial N_{\phi\phi}/\partial\phi$ and $\partial M_{\phi\phi}/\partial\phi$ are calculated using finite difference method given by Equations (3.7.15) – (3.7.18).

In the second method, $N_{\theta\theta}$ and $M_{\theta\theta}$ are calculated using Equation (2.3.3.7) as

$$N_{\theta\theta} = A_{12}\varepsilon^0_{\phi\phi} + A_{22}\varepsilon^0_{\theta\theta} + A_{26}\varepsilon^0_{\phi\theta} + B_{12}\kappa_{\phi\phi} + B_{22}\kappa_{\theta\theta} + B_{26}\kappa_{\phi\theta} \quad (3.7.26)$$

$$M_{\theta\theta} = B_{12}\varepsilon^0_{\phi\phi} + B_{22}\varepsilon^0_{\theta\theta} + B_{26}\varepsilon^0_{\phi\theta} + D_{12}\kappa_{\phi\phi} + D_{22}\kappa_{\theta\theta} + D_{26}\kappa_{\phi\theta} \quad (3.7.27)$$

respectively. But in Equations (3.7.26) and (3.7.27), in order to find $N_{\theta\theta}$ and $M_{\theta\theta}$, midstrains and bending strains should be known, and they are already the unknowns that need to be found.

On the other hand, Equations (3.7.4) – (3.7.9), which use finite difference method for the calculation of midstrains and bending strains, could be used to get an initial estimate of those strain values for the calculation of $N_{\theta\theta}$ and $M_{\theta\theta}$, during the process of midstrain and bending strain calculation.

In order to achieve this, first, midstrains and bending strains are calculated using Equations (3.7.4) – (3.7.9). During these calculations, finite difference method given by Equations (3.7.15) – (3.7.18) is used when derivatives of midsurface displacements and rotations with respect to ϕ need to be found. Second, $N_{\theta\theta}$ and $M_{\theta\theta}$ are calculated by Equations (3.7.26) and (3.7.27), using the strain values just been found.

Then, having found all in-plane force and moment resultants, either by the first method using Equations (3.7.24) and (3.7.25) or by the second method using Equations (3.7.26) and (3.7.27), Equation (3.7.22) can now be used to calculate midstrains (membrane strains) and bending strains.
However, although both methods can be used to calculate $N_{\theta\theta}$ and $M_{\theta\theta}$ for a general shell of revolution, there is a restriction for the special case of circular cylinder. It is shown in Section 2.1.3 that $\phi = 90°$ and therefore $\cos\phi = 0$ for circular cylinder. Hence Equations (3.7.24) and (3.7.25) cannot be used for the calculation of $N_{\theta\theta}$ and $M_{\theta\theta}$, meaning that Equations (3.7.26) and (3.7.27) are used instead for circular cylinder.

It should be emphasized that since in Equation (3.7.22) four of the six variables of the stress/moment resultant vector are known as a result of multisegment numerical integration solution method, exploiting Equation (3.7.22) to determine midplane strains and curvatures could also give accurate results. Because in either of these methods, finite differencing will have been used only for the calculation of the stress and moment resultants $N_{\theta\theta}$ and $M_{\theta\theta}$.

To calculate transverse shear stress resultant $Q_{\theta\zeta}$, transverse shear strain $\gamma_{\theta\zeta}$ has to be calculated. To calculate transverse shear strain $\gamma_{\theta\zeta}$, if equation (3.7.11) is examined carefully, it is seen that use of finite difference method is not necessary since no derivative with respect to ϕ appear in the

equation, and derivative with respect to θ can be calculated by series solution as given by Equation (3.7.14).

Finite difference method is used only once in Equation (3.7.10), and when it is used, central difference of second order given by Equation (3.7.17) is employed at most points, therefore it can be concluded that using Equation (3.7.10) for the calculation of $\gamma_{\phi\zeta}$ causes very little loss of accuracy due to the use of higher order finite differencing. As a result, Equations (3.7.10) and (3.7.11) are used for the calculation of transverse shear strains.

Having found midstrains and bending strains, one can calculate overall (total) in-plane strains by employing Equations (3.7.1) – (3.7.3). Using these equations, overall strains are found at each layer separately throughout the thickness of the laminate.

In plane stresses for a general shell can then be calculated by Equation (2.3.2.30). Since for shell of revolution $\xi \leftrightarrow \phi$ and $\eta \leftrightarrow \theta$, this equation can be re-written as

$$\begin{Bmatrix} \sigma_{\phi\phi} \\ \sigma_{\theta\theta} \\ \sigma_{\phi\theta} \end{Bmatrix}_k = \begin{bmatrix} \overline{Q}_{11} & \overline{Q}_{12} & \overline{Q}_{16} \\ \overline{Q}_{12} & \overline{Q}_{22} & \overline{Q}_{26} \\ \overline{Q}_{16} & \overline{Q}_{26} & \overline{Q}_{66} \end{bmatrix}_k \begin{Bmatrix} \varepsilon_{\phi\phi} - \alpha_\phi \Delta T \\ \varepsilon_{\theta\theta} - \alpha_\theta \Delta T \\ \gamma_{\phi\theta} - \alpha_{\phi\theta} \Delta T \end{Bmatrix}_k \tag{3.7.28}$$

where

$$\begin{aligned} \alpha_\phi &= \alpha_1 \cos^2\theta + \alpha_2 \sin^2\theta \\ \alpha_\theta &= \alpha_1 \sin^2\theta + \alpha_2 \cos^2\theta \\ \alpha_{\phi\theta} &= 2(\alpha_1 - \alpha_2)\cos\theta \sin\theta \end{aligned} \tag{3.7.29}$$

Using Equation (3.7.28), in-plane stresses can be calculated at each layer separately throughout the thickness of the laminate

Transverse shear stresses for a general shell can be calculated by Equation (2.3.2.9). Since for shell of revolution $\xi \leftrightarrow \phi$ and $\eta \leftrightarrow \theta$, this equation can be re-written as

$$\begin{Bmatrix} \sigma_{\theta\zeta} \\ \sigma_{\phi\zeta} \end{Bmatrix} = \begin{bmatrix} \overline{Q}_{44} & \overline{Q}_{45} \\ \overline{Q}_{45} & \overline{Q}_{55} \end{bmatrix} \begin{Bmatrix} \gamma_{\theta\zeta} \\ \gamma_{\phi\zeta} \end{Bmatrix} \tag{3.7.30}$$

where $\gamma_{\phi\zeta}$ and $\gamma_{\theta\zeta}$ are given by Equations (3.7.10) and (3.7.11), respectively. Using Equation (3.7.30), transverse shear stresses can be calculated.

Thus, the post processing of the solution which aims to calculate stresses and strains is now completed. Note that since the fundamental variables are found as functions of ϕ and θ in the preceding section, all stresses and strains calculated in this section are also functions of ϕ and θ. In addition to that, since overall in-plane strains and stresses are found at each layer, these variables, apart from being functions of ϕ and θ, are also functions of the thickness direction of the shell ζ.

CHAPTER 4

IMPLEMENTATION OF THE SOLUTION METHODOLOGY

4.1. Description of the Computer Code Developed

For the analysis of shells of revolution, an algorithm is created following the instructions of the solution methodology described in Chapter 3. In order to implement the algorithm created, a computer code is developed using FORTRAN 77 programming language. The code consists of a main program, thirteen subroutines and an external subroutine used during the execution. Double precision storage format is used in the code in order to improve accuracy.

4.1.1. Description of the Main Program

The algorithm of the main program is graphically represented by the flowchart shown in Figure 4.1. As it can be seen, main program is basically the general router which manages the data flow between the subroutines. Three subroutines are mentioned in the flowchart of the main program. Among them, subroutine “Backtrans” simply follows the instructions on how to perform the back transformation described in Section 3.6. However, subroutines “Nuint”

and “Postprocess” include complicated sequence of instructions for the solution and post processing of the problem, respectively. Therefore, in the following flowcharts describing their algorithms are given individually.

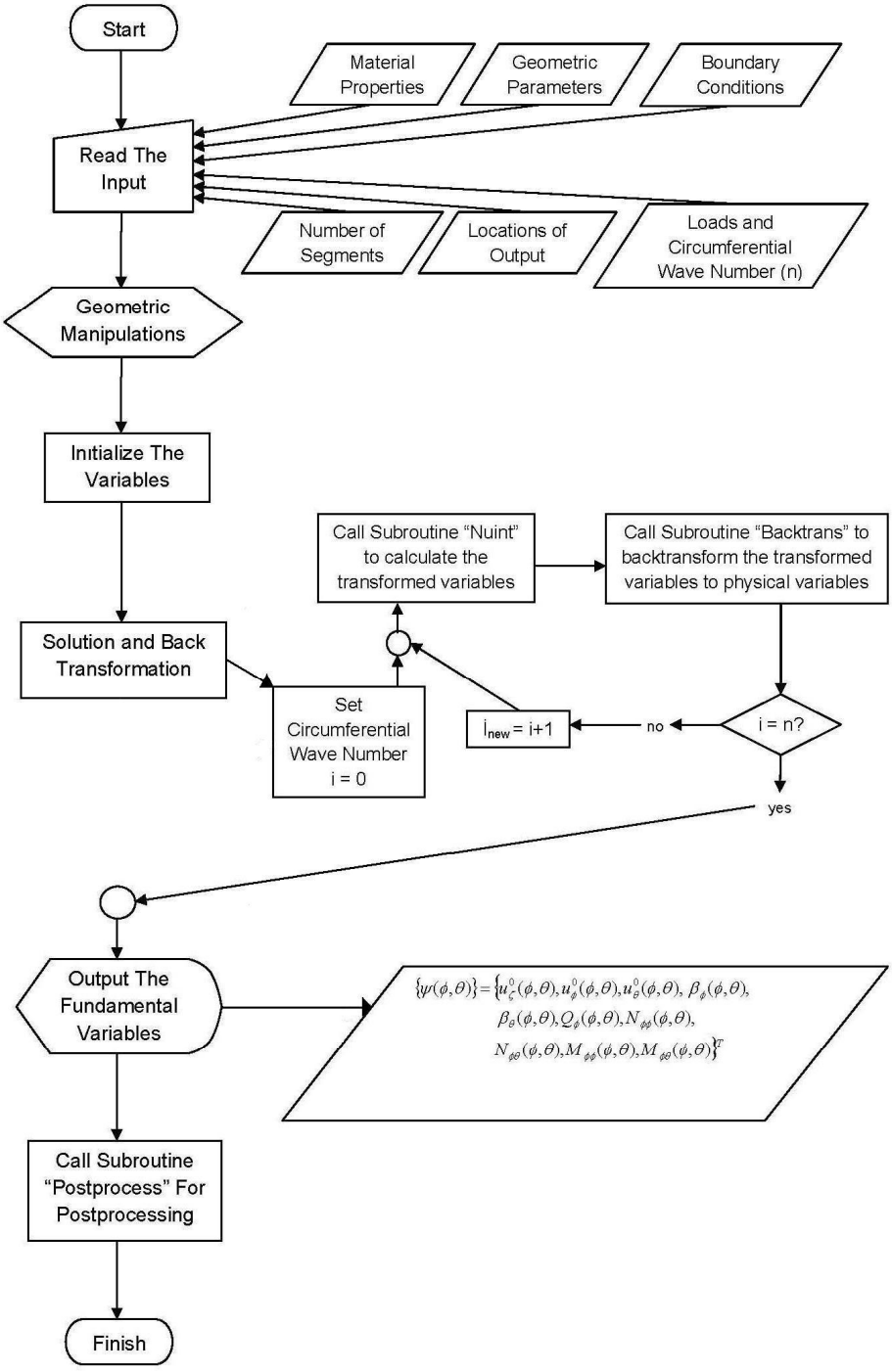

Figure 4.1 Flowchart for the Main Program

4.1.2. Description of the Subroutine “Nuint”

The algorithm of the subroutine “Nuint” is graphically represented by the flowchart shown in Figure 4.2. This subroutine implements the procedures given in Section 3.5, i.e. it applies the multisegment method of integration.

As previously discussed in Section 3.7, an integration scheme needs to be used for the solution of Equations (3.5.2) and (3.5.3), and in the present study, the integration of these equations is performed using the IMSL numerical integration routine DIVPAG, which is the double precision version of the routine IVPAG. It is used to solve the initial value problems for ordinary differential equations using either Adam-Moulton’s or Gear’s BDF method. In the present study, Adam-Moulton’s method is chosen.

Therefore, the external subroutine “DIVPAG” is called during the execution of subroutine “Nuint”. This is one of the routines in the international mathematics and statistics library “IMSL”, which is a comprehensive set of mathematical and statistical functions that programmers can embed into their software applications. The IMSL Libraries are provided by Visual Numerics Inc [18].

The other subroutines called during the execution of subroutine “Nuint” are the subroutines FCN, FCN2, Loadvector and ABD. The sequence of calling these subroutines and their functions are described in Figure 4.2. In addition to these, subroutines INV, Det10X10 and Det9X9 are called for the inversion and determinant finding of matrices when necessary.

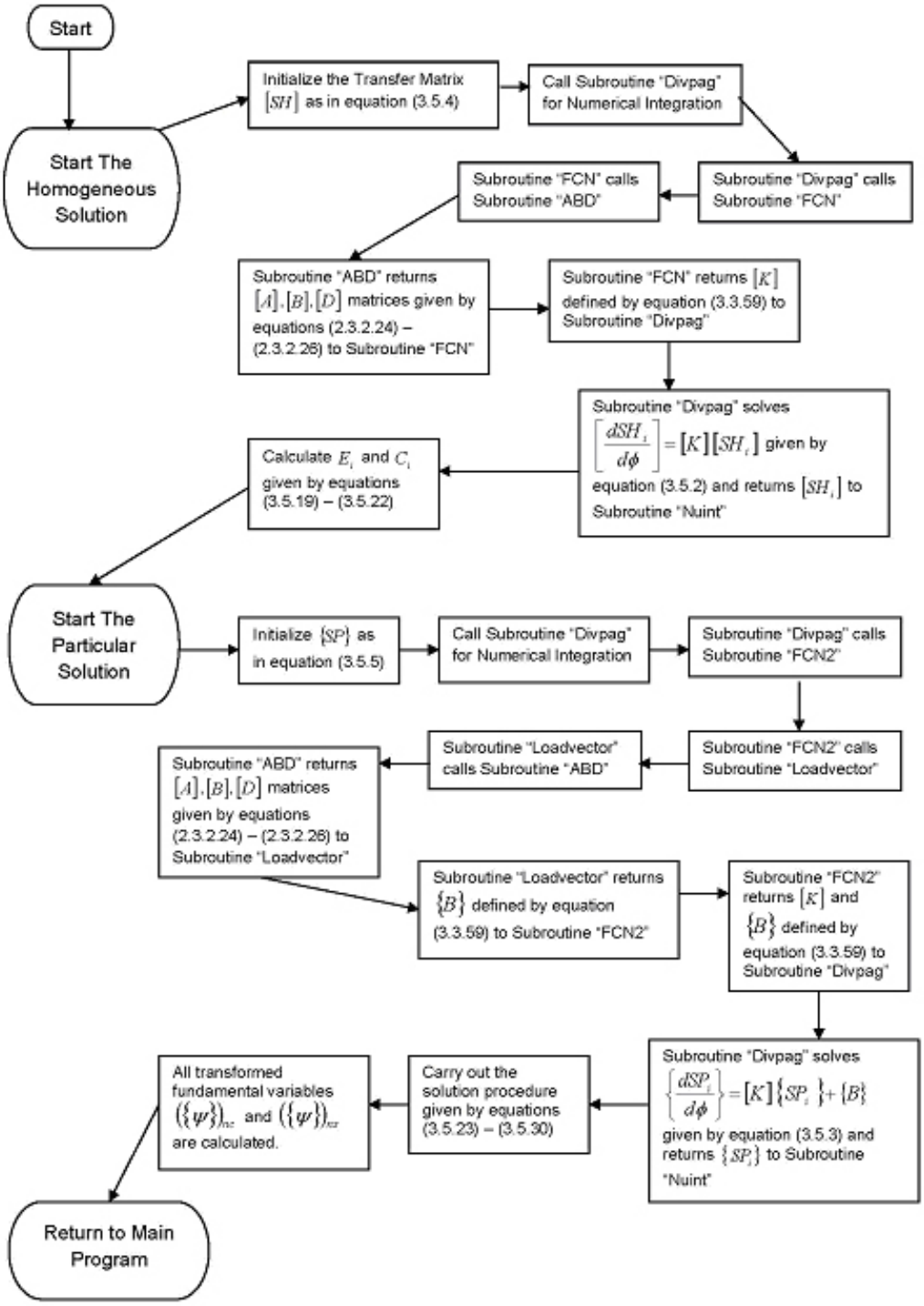

Figure 4.2 Flowchart of the Subroutine Nuint

4.1.3. Description of the Subroutine “Postprocess”

The algorithm of the subroutine “Postprocess” is graphically represented by the flowchart shown in Figure 4.3. This subroutine implements the procedures given in Section 3.7, i.e. it performs the post processing.

Subroutines INV6, Det6X6 and Det5X5 are called during the execution of subroutine “Postprocess” for the inversion and finding the determinant of the matrices when necessary.

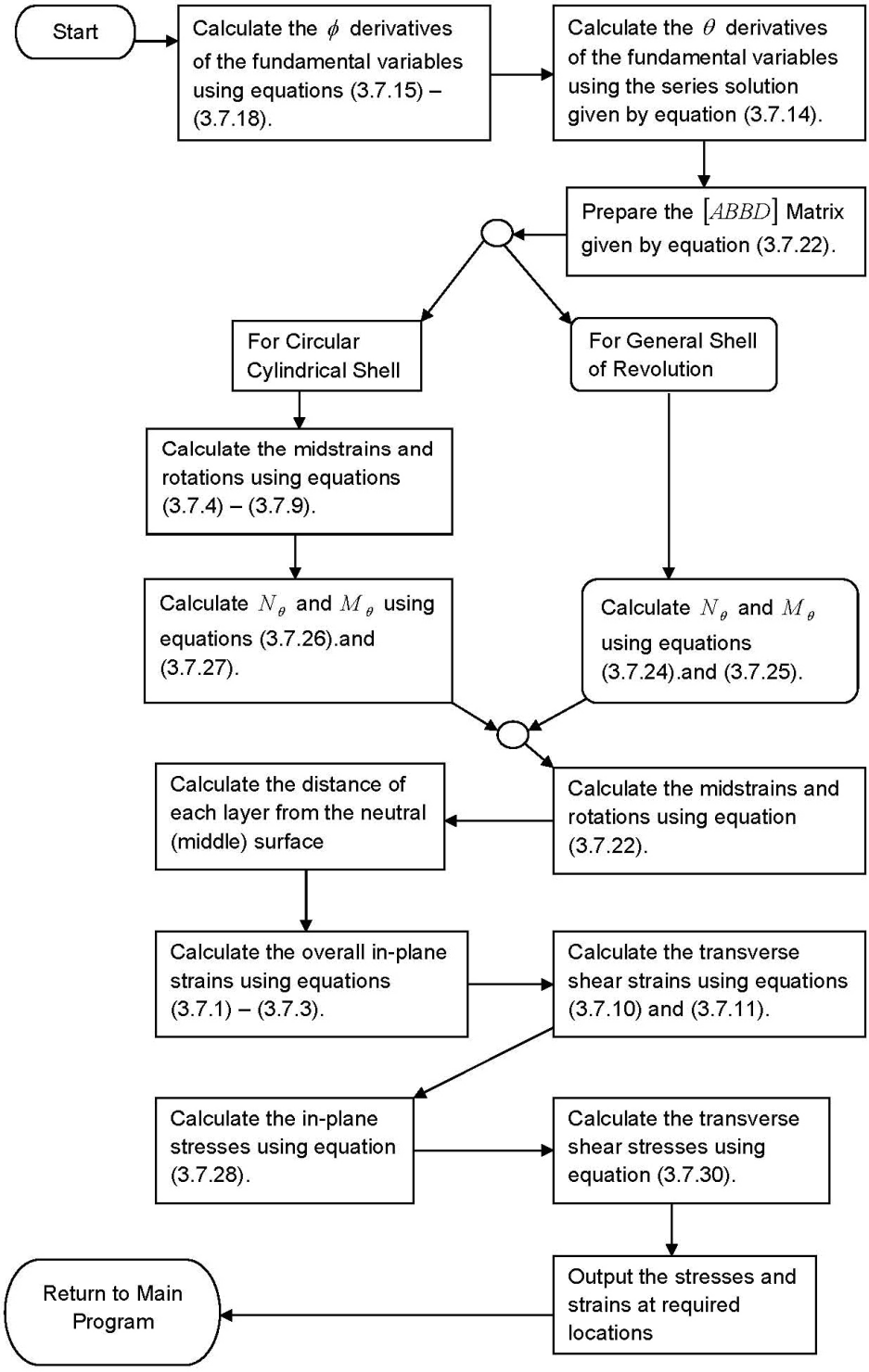

Figure 4.3 Flowchart for the Subroutine Postprocess

4.2. Verification of the Code

In Section 4.1, the computer code developed is described in detail. In this section, the results generated by the code are compared with the results generated by MSC NASTRAN.

MSC NASTRAN is a general purpose finite element analysis solver used for small to complex assemblies [19]. Nastran was initially developed by NASA for the space program in the 1960's and the term NASTRAN is actually an acronym for NASA Structural Analysis. Today, NASTRAN is widely used throughout the world in the aerospace, automotive and maritime industries. It has been claimed in many studies such as [20], [21] and [22] that NASTRAN is the industry standard for analysis of aerospace structures. Therefore, comparison of the results generated by the code developed in the present study with the results generated by MSC NASTRAN is a convenient method for the verification of the code.

MSC NASTRAN is closely linked with MSC Patran. MSC Patran is a comprehensive pre and post processing environment for finite element analysis [19]. Therefore, it is used for the preparation of the model to be solved in MSC NASTRAN and the results are post processed using again MSC Patran.

The following sample problems are analyzed using both the code developed in this study and MSC NASTRAN. Then the results obtained from these solvers are compared.

4.2.1. Sample Problem 1

Consider a laminated circular cylinder clamped at two ends is exposed to a temperature difference of 1000° C, which is uniformly distributed throughout the cylinder. In addition to that, an internal pressure of 100 kPa is applied to the cylinder. Here a temperature difference of 1000° C is used just for demonstration purposes. A high temperature difference is selected on purpose to get high thermal stresses The cylinder is made of MR50/LTM25 Carbon Epoxy Unidirectional Prepreg [23]. The material data used, geometric properties, loads and boundary conditions are given in Table 4.1.

Table 4.1 Analysis Data for the Sample Problem 1

Geometry	**Circular Cylinder**
Radius	0.2 m
Axial Length	1.0 m
Number of segments	300
Material	
Ply Material	MR50/LTM25 Carbon Epoxy
E_{11}	155 GPa
E_{22}	7.31 GPa
υ_{12}	0.345
G_{12}	4.19 GPa
G_{13}	4.19 GPa
G_{23}	3 GPa
Ply thickness	0.146 mm
Ply density (ρ)	1520 kg/m^3

Table 4.1 (continued)

α_{11}	-0.43 x 10^{-6} 1/°C
α_{22}	37.4 x 10^{-6} 1/°C
Laminate	
Number of Layers	4
Ply Orientation	[0°/45°/90°/0°]
Loads	
ΔT (constant along x, θ and ζ)	1000°C
p_ζ (constant along x and θ)	100 kPa
Boundary Conditions	clamped-clamped
left end	$\left(u_\zeta^0\right)_c, \left(u_\zeta^0\right)_s, \left(u_x^0\right)_c, \left(u_x^0\right)_s, \left(u_\theta^0\right)_c, \left(u_\theta^0\right)_s, \left(\beta_x^0\right)_c, \left(\beta_x^0\right)_s, \left(\beta_\theta^0\right)_c, \left(\beta_\theta^0\right)_s = 0$
right end	$\left(u_\zeta^0\right)_c, \left(u_\zeta^0\right)_s, \left(u_x^0\right)_c, \left(u_x^0\right)_s, \left(u_\theta^0\right)_c, \left(u_\theta^0\right)_s, \left(\beta_x^0\right)_c, \left(\beta_x^0\right)_s, \left(\beta_\theta^0\right)_c, \left(\beta_\theta^0\right)_s = 0$

As it can be seen from Table 4.1, in the multisegment integration method the cylinder is divided into 300 segments. In order to overlap the nodes of finite element mesh used in MSC NASTRAN with the grid points of the segments used in the multisegment method of integration in the axial direction, the nodes of finite element mesh which is created in the axial direction of the cylinder are equally spaced and the total number is also 300 The fundamental variables obtained from the code and NASTRAN are compared at these points.

It is stated in many references such as [27] and [28] that in displacement based finite element solvers, stresses, which are calculated during the post processing, are obtained more accurately at element centroids. NASTRAN is

also a displacement based finite element solver. Since stresses and strains are calculated during post processing, stress and strain values at the element centroids are used for the comparison with the results obtained from the code developed in this thesis. Therefore, end points of the shell segments are arranged such that they coincided with the finite element centroids when stresses and strains are compared.

Finite element mesh of the circular cylinder created in MSC Patran is given in Figure 4.4. Among the elements available for the analysis of standard laminated shells in MSC NASTRAN element library, first order shell elements with 4 nodes (CQUAD4 type elements) are used to create the finite element mesh. There are a total number of 37800 elements and 37926 nodes in the finite element model. Loads and boundary conditions applied to the model and material properties used are already given in Table 4.1.

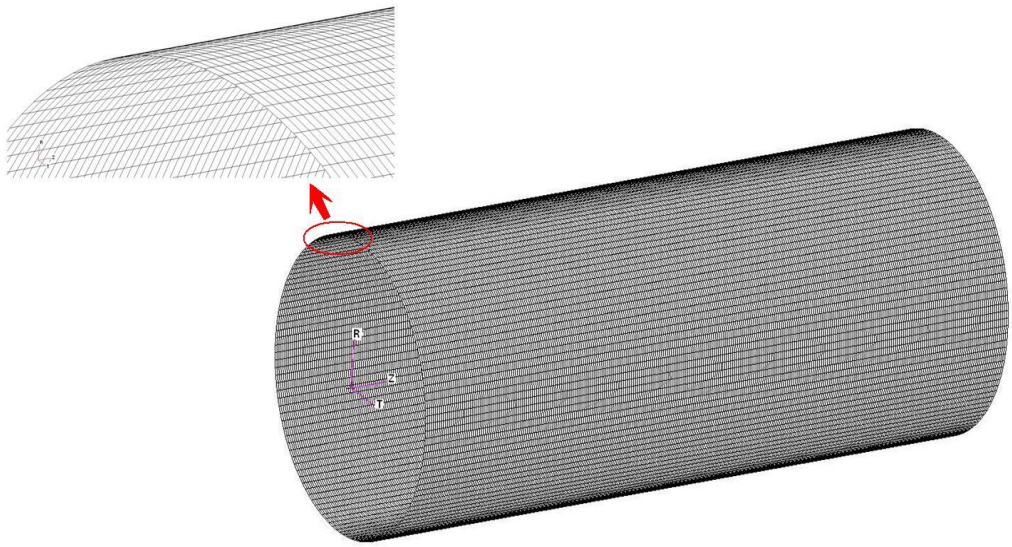

Figure 4.4 Finite Element Mesh for Circular Cylinder

Since the shell equations used in the present study assumes small strain / small displacement (see Section 2.2.1), and the materials are considered to be linearly elastic in the analysis domain, that is they are not functions of strain or strain rate, linear static solution type with sol 101 solution sequence is chosen in MSC NASTRAN.

The analysis is run using both the computer code developed in the present thesis and NASTRAN solver. Following the completion of the analyses, the results are presented.

In Figure 4.5, variation of the mid-surface displacement in the thickness direction u_{ζ}^{0} with axial (meridional) coordinate at $\theta = 0$ is given. It should be emphasized that for the present problem, since the loading is axisymmetric, the problem is completely axisymmetric and the results are not functions of the circumferential coordinate θ, therefore the results would be the same for any value of θ. The results of both NASTRAN and the code are given in this figure for comparison.

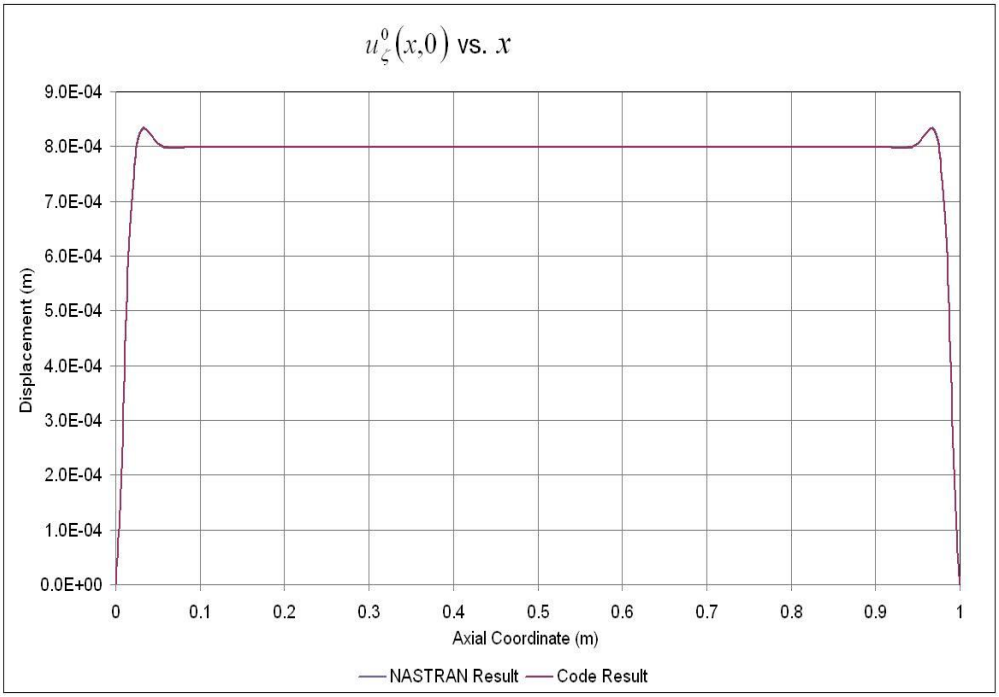

Figure 4.5 Comparison of Solutions for variation of u_ζ^0 with x for Sample Problem 1

In Figure 4.5 one can clearly see the bending boundary layer extending a short distance away from the edges.

In the figure, the results of NASTRAN and the code overlap and are seen as one curve. In order to compare the results more clearly, percent difference is calculated for each grid point in the axial direction:

$$\%\,Difference = \frac{AbsoluteValue\left(NASTRAN\ result - Code\ result\right)}{NASTRAN\ result} \times 100 \tag{4.2.1.1}$$

The variation of percent difference with the axial coordinate x is given in Figure 4.6:

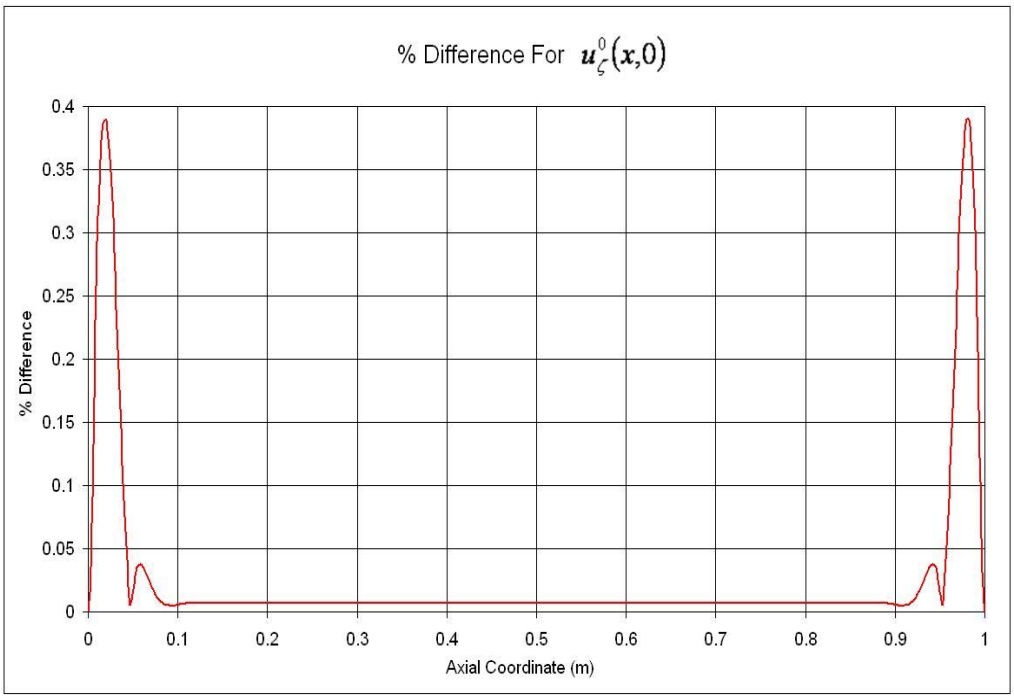

Figure 4.6 Change of Percent Difference with Axial Coordinate for u_ζ^0 for Sample Problem 1

This graph shows that maximum difference between NASTRAN results and code results occur near the boundaries with a value of nearly 0.4%. Away from the boundaries, this value is less than 0.02%, meaning that two methods find almost exactly the same values.

These results given above are for u_ζ^0, which is a fundamental variable. The percent differences between code results and NASTRAN results for other fundamental variables are similar; therefore they are not given here for brevity.

Stresses and strains are also calculated by postprocessing the results found directly from the solution, both for the method used in the present study and

for the finite element method. In Figure 4.7, variation of the stress in the axial direction (σ_{xx}) with axial (meridional) coordinate at $\theta = 0$ and for layer 1 (first layer inside the cylinder) is given. The results of both NASTRAN and the code are given in this figure for comparison.

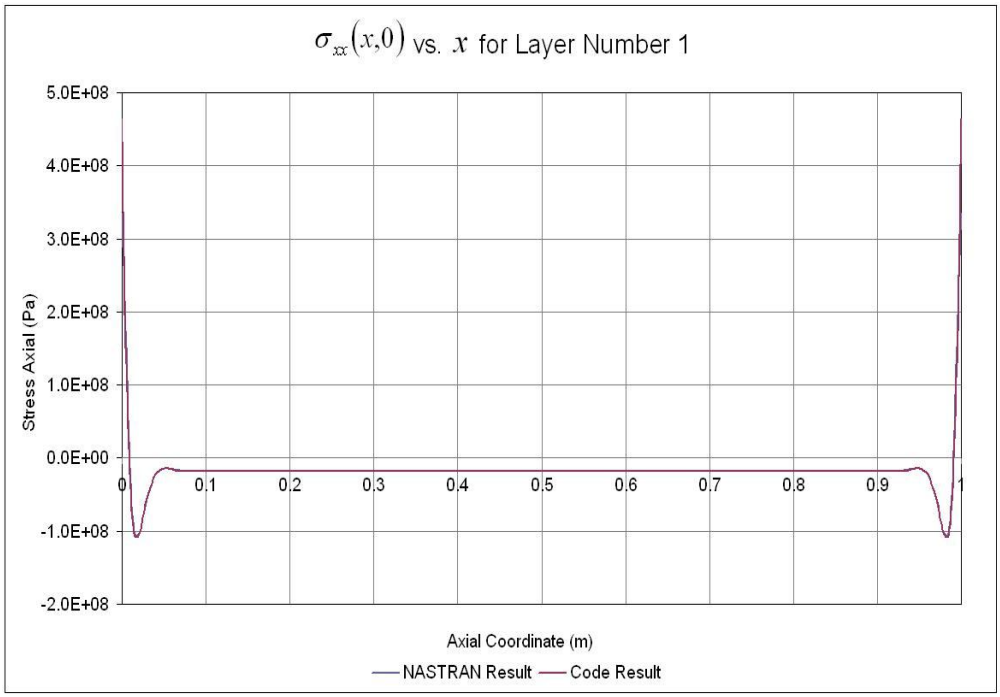

Figure 4.7 Comparison of Solutions for Variation of σ_{xx} with x for Sample Problem 1

Again in the figure, the results of NASTRAN and the code overlap and are seen as one curve, so the percent difference given by Equation (4.2.1.1) is calculated. The behaviour of change of percent difference with axial coordinate is similar to the one given above for u_{ζ}^{0}. The difference is symmetrical and reaches a stable value at some distance away from the boundary. This stable value is 0.02%, and reached around $x = 0.07$ m. The

variation of percent difference with axial coordinate in the interval [0, 0.1] is given in Figure 4.8.

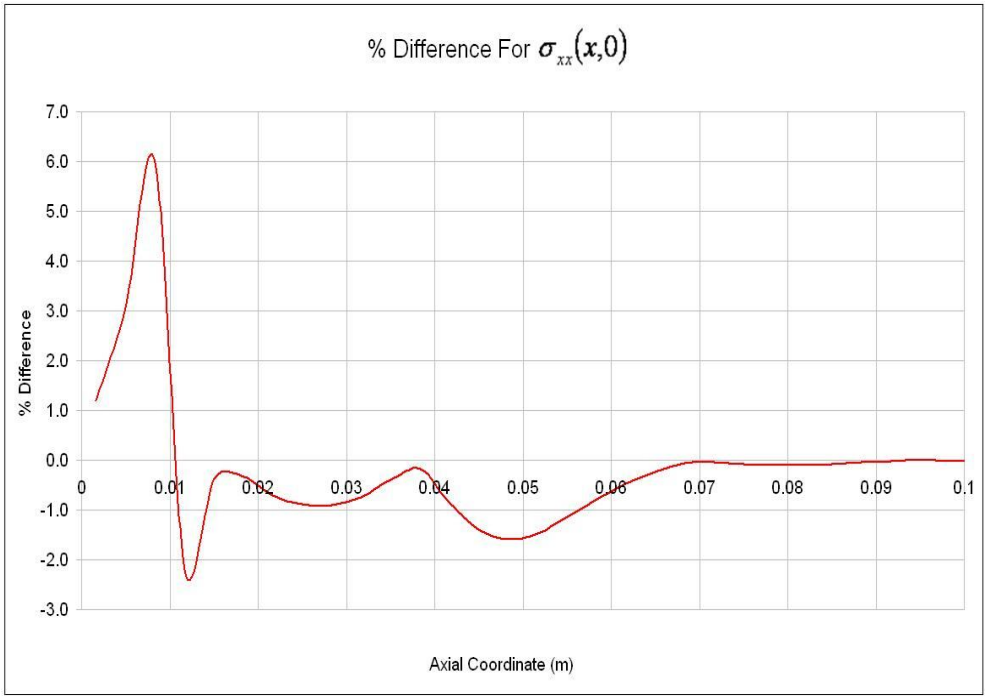

Figure 4.8 Change of Percent Difference with Axial Coordinate for σ_{xx} for Sample Problem 1

The percent difference is highest at the end of the first shell segment, with a value of 6.%, oscillating and getting smaller away from the boundary, eventually reaching the stable value mentioned above. As it is explained in Section 3.7, stresses are calculated using the fundamental variables by postprocessing. During this process, different orders of finite difference method are involved. Central difference of second order is used between 3rd and (m-1)th points, where m is the number of shell segments used in the multi-segment method of integration. Forward difference is used for the first point and backward difference is used for the last ((m+1)th) point. The use of forward

and backward difference at the boundary edges of the shell of revolution may cause loss of accuracy in the calculation of stresses at these points to some extent. It can be seen from Figure 4.8 that the percent difference decreases rapidly and its final value of 0.04% reveals that NASTRAN and the code calculates almost the same axial stress values during the postprocessing. It should also be noted that the axial stress results calculated by the developed code are greater than the axial stress results calculated by NASTRAN in magnitude. As it has been stated above, for the comparison of stresses, NASTRAN element centroids are used.

Force and moment resultants are also among the fundamental variables, and they are calculated during multisegment method of integration, in addition to the displacements and rotations, as it is explained in Section 3.5. For this problem, variation of the mid-surface axial force resultant per unit length $\left(N_{xx}^{0}\right)$ with axial coordinate is calculated as constant throughout the cylinder, as expected. The result obtained from the code is -44170.8 N/m and the result obtained from the NASTRAN solution is -44168.5 N/m. Therefore the percent difference between two solutions is also constant, and calculated as

$$\%\,Difference = \frac{\left|-44170.8+44168.5\right|}{-44168.5}\times 100 = -0.00522\% \qquad (4.2.1.2)$$

Result given by Equation (4.2.1.2) reveal that axial force resultant per unit length is found almost the same by two solvers. The variation of the mid-surface in-plane shear force resultant per unit length $\left(N_{x\theta}^{0}\right)$ with axial coordinate is also constant along the axial direction over most of the cylinder length, with a value of -39146.5 N/m for the code and -39136.3 N/m for NASTRAN.

The percent difference of results between two solvers for this fundamental variable is given in Figure 4.9. The variation is symmetrical with respect to the cylinder cross section at $x = 0.5\,\text{m}$ and is constant over most of the cylinder

since $N^0_{x\theta}$ itself is constant at those points. Therefore, the result is given in the interval [0, 0.1] where the variation starts from its initial value and reaches the constant value.

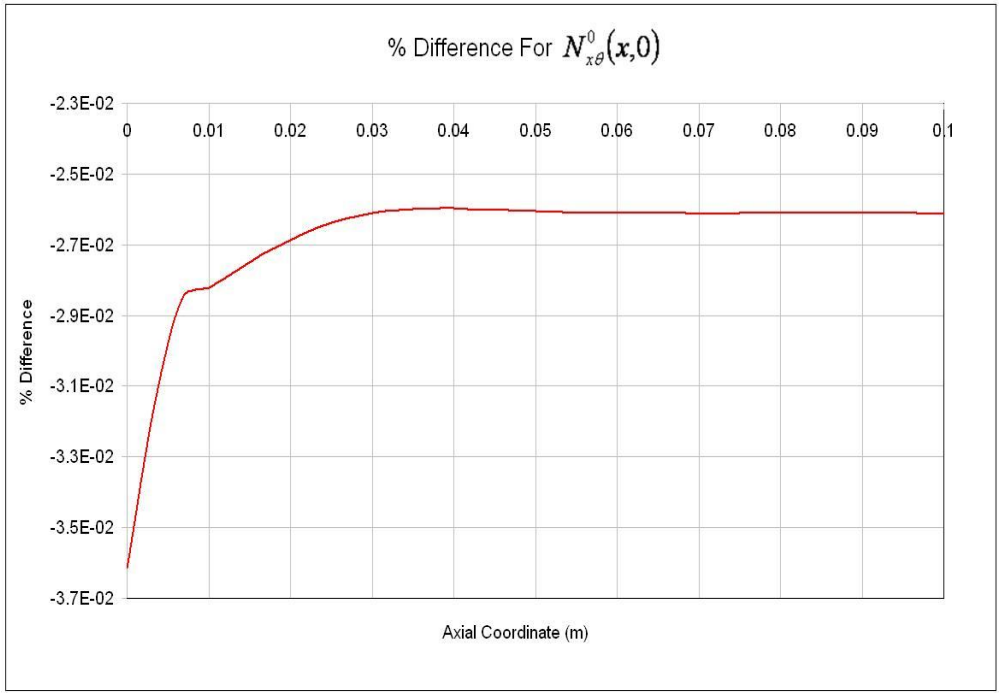

Figure 4.9 Change of Percent Difference with Axial Coordinate for $N_{x\theta}$ for Sample Problem 1

Maximum percent difference is at the boundary with a value of 0.036 %. Therefore it can be said that NASTRAN and the code developed in this thesis both calculate the same results also for the in-plane shear force resultant per unit length.

One final comparison is made for the solution times of the two solvers. On a computer with a 2.40 GHz CPU and 1 GB of RAM, the analysis is run on the code developed, and total time elapsed is 9.953 seconds. When the same

analysis is run on NASTRAN with the finite element mesh described above, it is completed in 490.906 seconds. The solution time for NASTRAN solver does not include the preparation of the NASTRAN input file (*.bdf) from the finite element model by the pre and post-processor Patran. From this data, it can be deduced that the code developed in this study solves this problem about 49 times faster if the shell is divided into 300 segments along the meridian of the shell. Obviously, one should keep in mind that in the finite element model when 300 elements are placed along the meridian of the shell, the element length in the circumferential direction can not be arbitrary in order not to end up with an element configuration with a high aspect ratio. Therefore, finite element model becomes very crowded in terms of element and node numbers. For a particular problem one could get reliable results with a much coarser mesh, and in that case the solution times of the present method and finite element method could approach each other. However, in this example the comparison is made for 300 segments along the meridian of the shell, and for this size the present method is much faster than the finite element method.

4.2.2. Sample Problem 2

Consider again a laminated circular cylinder clamped at two ends. This time, a variable external pressure is applied to it. The cylinder is made of MR50/LTM25 Carbon Epoxy Unidirectional Prepreg [23]. The material data used, geometric properties, loads and boundary conditions are given in Table 4.2

Table 4.2 Analysis Data for the Sample Problem 2

Geometry	**Circular Cylinder**
Radius	0.2 m
Axial Length	1.0 m
Number of segments	300
Material	
Ply Material	MR50/LTM25 Carbon Epoxy
E_{11}	155 GPa
E_{22}	7.31 GPa
υ_{12}	0.345
G_{12}	4.19 GPa
G_{13}	4.19 GPa
G_{23}	3 GPa
Ply thickness	0.146 mm
Ply density (ρ)	1520 kg/m^3
α_{11}	-0.43 x 10^{-6} 1/°C
α_{22}	37.4 x 10^{-6} 1/°C
Laminate	
Number of Layers	4
Ply Orientation	[0°/45°/90°/0°]
Loads	
p_ζ (constant along θ and variable in x)	$p_\zeta = 0$ at $x = 0$, $= 100$ kPa at $x = 1$, changing linearly in between

Table 4.2 (continued)

Boundary Conditions	clamped-clamped
left end	$\left(u_\zeta^0\right)_c, \left(u_\zeta^0\right)_s, \left(u_x^0\right)_c, \left(u_x^0\right)_s, \left(u_\theta^0\right)_c, \left(u_\theta^0\right)_s, \left(\beta_x^0\right)_c, \left(\beta_x^0\right)_s, \left(\beta_\theta^0\right)_c, \left(\beta_\theta^0\right)_s = 0$
right end	$\left(u_\zeta^0\right)_c, \left(u_\zeta^0\right)_s, \left(u_x^0\right)_c, \left(u_x^0\right)_s, \left(u_\theta^0\right)_c, \left(u_\theta^0\right)_s, \left(\beta_x^0\right)_c, \left(\beta_x^0\right)_s, \left(\beta_\theta^0\right)_c, \left(\beta_\theta^0\right)_s = 0$

Finite element mesh used in NASTRAN and number of segments used in the multisegment method of integration are the same as those used in 4.2.1. The variation of p_ζ with axial direction is defined using *fields* option in Patran for the finite element solution. Sol 101 is used again as the solution type in NASTRAN.

In Figure 4.10, variation of the mid-surface displacement in the thickness direction u_ζ^0 with axial (meridional) coordinate at $\theta = 0$ is given. The results of both NASTRAN and the code are given in this figure for comparison.

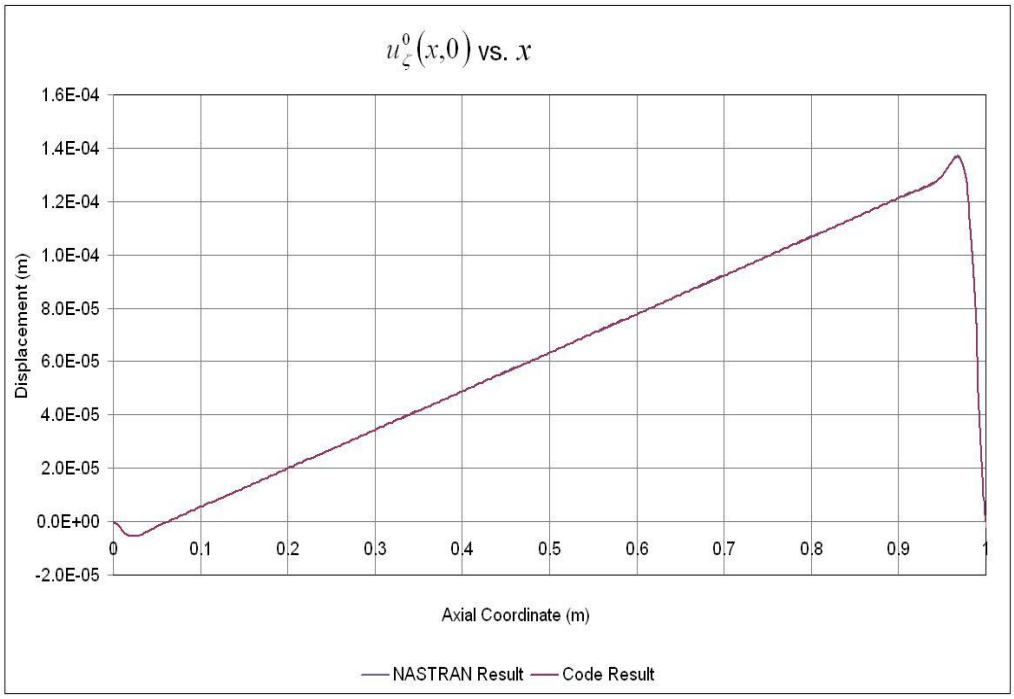

Figure 4.10 Comparison of Solutions for Variation of u_ζ^0 with x for Sample Problem 2

As it can be seen, the displacement in the thickness direction increases linearly as one moves from one boundary to another, with linearly increasing internal pressure. In the figure, the results of NASTRAN and the code overlap and they are seen as one curve. In order to compare the results more clearly, percent difference given by Equation (4.2.1.1) is calculated at each grid point in the axial direction. The variation of percent difference with the axial coordinate x is given in Figure 4.11:

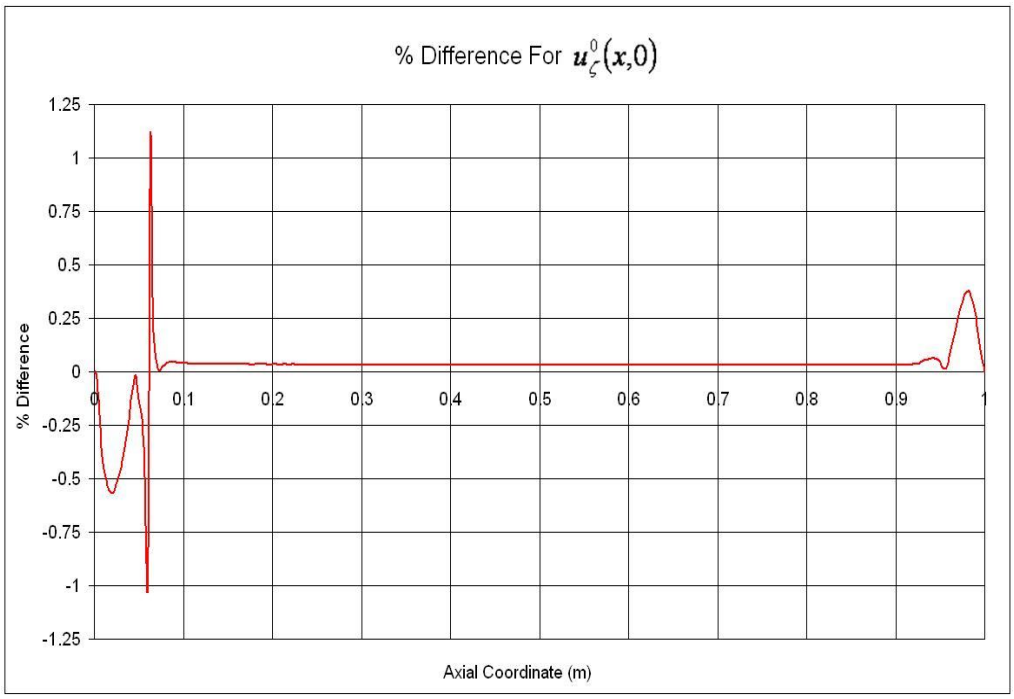

Figure 4.11 Change of Percent Difference with Axial Coordinate for u_ζ^0 for Sample Problem 2

This graph shows that maximum difference between NASTRAN results and code results occur near the boundaries with a value of 1.1%. Away from the boundaries, this value is approximately than 0.03%, meaning that two methods find almost exactly the same values.

These results given above are for u_ζ^0, which is a fundamental variable. The percent differences between code results and NASTRAN results for other fundamental variables are similar; therefore they are not given here for brevity.

In Figure 4.12, the variation of the stress in the axial direction (σ_{xx}) with axial (meridional) coordinate at $\theta = 0$ and for layer 1 (first layer in the cylinder) is given. The results of both NASTRAN and the code are given in this figure for comparison.

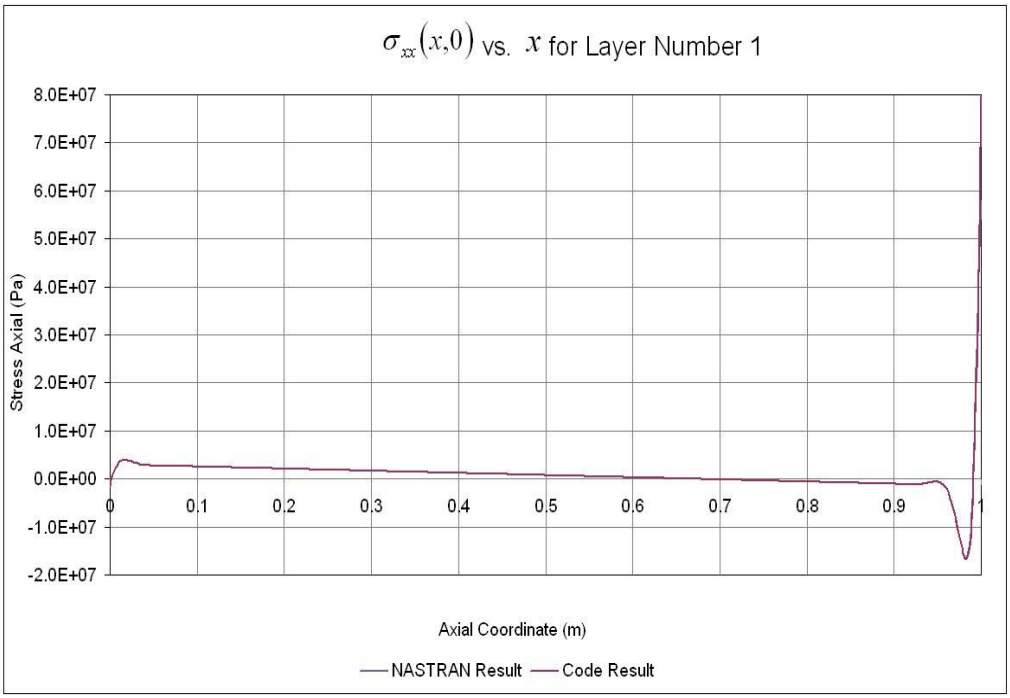

Figure 4.12 Comparison of Solutions for Variation of σ_{xx} with x for Sample Problem 2

Again in Figure 4.12, the results of NASTRAN and the code overlap and they are seen as one curve, so percent difference given by Equation (4.2.1.1) is calculated. The behaviour of variation of the percent difference with the axial direction is not symmetrical as opposed to the previous sample problem, since loading in axial direction is not symmetrical, but it also reaches a stable value at some distance from the boundary. This value is 0.1%, and it is reached at around $x = 0.05$ m. The variation of percent difference with axial coordinate throughout the cylinder is given in Figure 4.13.

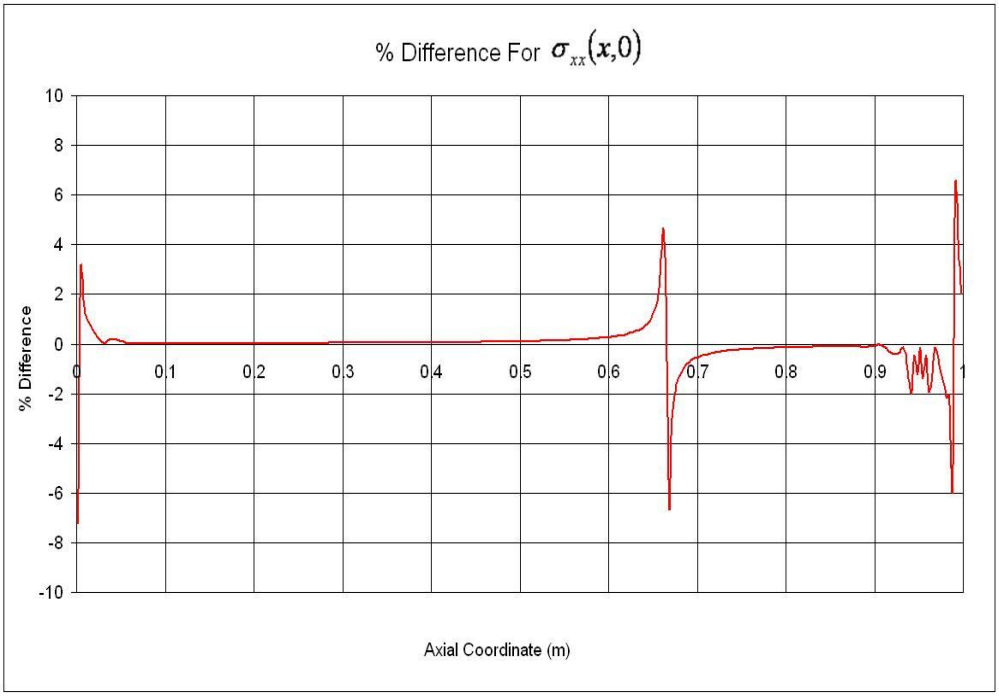

Figure 4.13 Change of Percent Difference with Axial Coordinate for σ_{xx} for Sample Problem 2

The percent difference is highest at the first point, with a value of 7%, getting smaller away from the boundary, eventually reaching a stable value as mentioned above. Its behaviour is similar near the other boundary; however not exactly the same since the problem is not symmetrical, as mentioned before. Away from the boundaries percent difference is about 0.1%, which reveals that the code developed and NASTRAN calculates reasonably close results for axial stress. Relatively higher percent differences near the boundaries can be explained by loss of accuracy due to the reasons stated at the end of Section 4.2.1.

Furthermore, a sudden change in percent difference is observed at about $x = 0.65$ - 0.67. Figure 4.12 shows that axial stress changes sign in the same interval, where the axial stress becomes smaller in magnitude, eventually

reaches zero and increases again. Percent difference is defined in Equation (4.2.1.1) as the absolute value of the difference of results of the code and NASTRAN, divided by the results of NASTRAN. If the code results and NASTRAN results do not become zero at exactly the same point, and they have the same slopes so that one curve is shifted up or down with respect to the other, then the denominator of the percent difference definition becomes smaller and smaller without much change in the numerator, as the axial stresses approach zero. This results in much higher percent differences in the neighbourhood of the point where stress values change sign. Therefore, it is obvious that this phenomenon occurs due to the definition of the percent difference and it affects a considerably small interval. Besides, percent difference converges to its value before the sign change of stress results.

In order to exhibit this more clearly, variation of the stress in the tangential direction $(\sigma_{\theta\theta})$ with axial (meridional) coordinate at $\theta = 0$ and for layer 1 (first layer in the cylinder) is given in Figure 4.14:

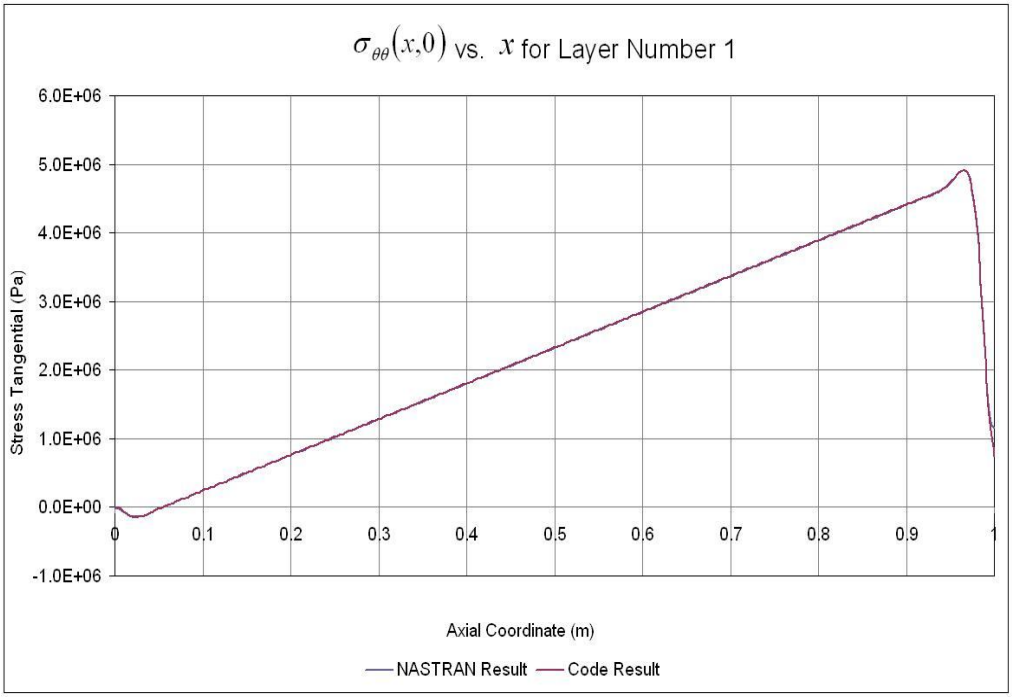

Figure 4.14 Comparison of Solutions for Variation of $\sigma_{\theta\theta}$ with x for Sample Problem 2

As it is seen from Figure 4.14, tangential stress values change sign nearby the left boundary, where the percent difference is already high due to accuracy issues mentioned at the end of Section 4.2.1. The effect of this is seen more clearly in Figure 4.15 which gives the change of percent difference of tangential stresses with axial coordinate:

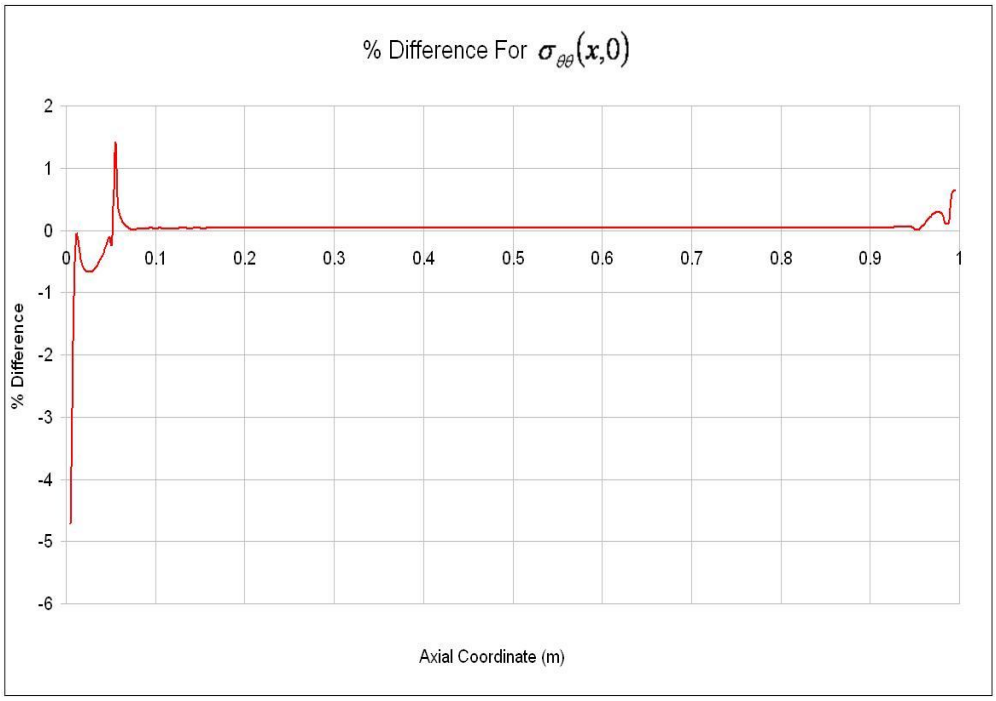

Figure 4.15 Change of Percent Difference with Axial Coordinate for $\sigma_{\theta\theta}$ for Sample Problem 2

The percent difference is highest at the boundaries, again due to the reasons stated at the end of Section 4.2.1, but the difference gets smaller away from the boundaries, and eventually reaches the stable value of 0.1%. Also it is seen that no jumps and peak values occur in the percent difference away from the boundaries, since tangential stress values do not change sign. Therefore, it can be deduced that the results do not deviate significantly from each other, but a numerical error arises from the definition of percent difference in the neighbourhood of the points where the results change sign. Like in Section 4.2.1, stresses are calculated at the NASTRAN element centroids and the comparisons are made at these points.

The variation of the mid-surface axial force resultant per unit length $\left(N_{xx}^{0}\right)$ with axial coordinate is again constant throughout the cylinder for the code with a

value of 2059.413 N/m and it is also constant for NASTRAN solution with a value of 2059.057 N/m, with slight deviations from a constant value near the boundaries. Therefore the percent difference between two solutions is also constant, and calculated as

$$\%\,Differeence = \frac{|2059.057 + 2059.413|}{2059.057} \times 100 = 0.017\% \qquad (4.2.2.1)$$

It is obvious that axial force resultant per unit length is found almost the same by two solvers. In Figure 4.16, variation of the mid-surface in-plane shear force resultant per unit length $\left(N^0_{x\theta}\right)$ with axial coordinate at $\theta = 0$ is given. The results of both NASTRAN and the code are given in this figure for comparison.

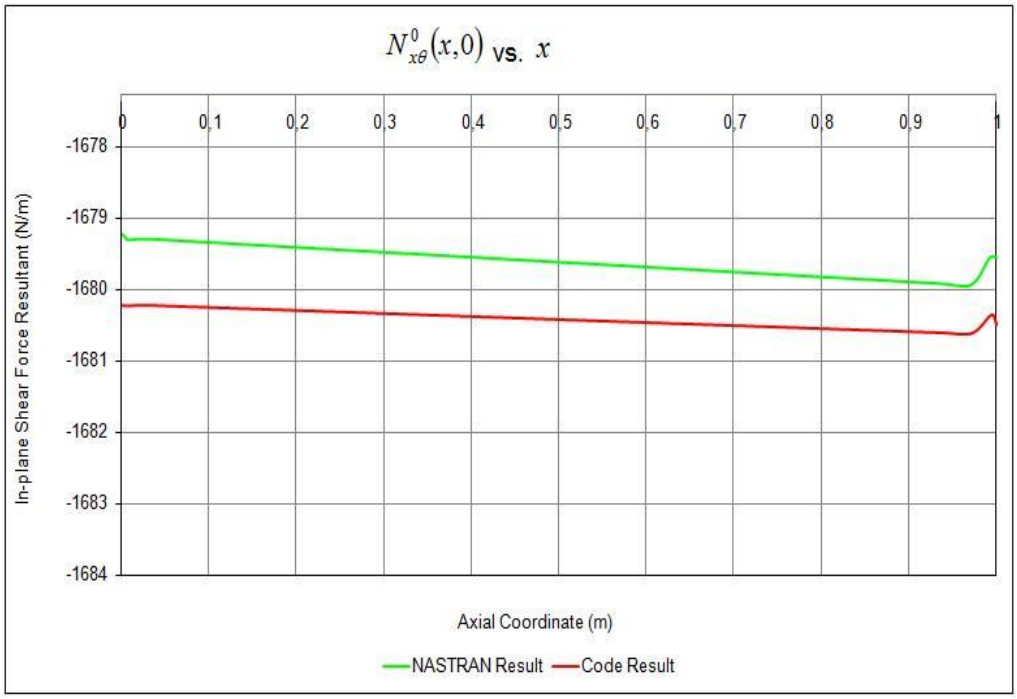

Figure 4.16 Comparison of Solutions for variation of $N^0_{x\theta}$ with x for Sample Problem 2

The in-plane shear force resultant per unit length variations show similar behaviours in two solutions, both increasing in magnitude while going from one boundary to the other. Although graphically the two solution curves do not seem to overlap, percent difference variation in the next figure reveals that they are very close numerically and the reason for the curves not overlapping is that the force resultant values are given in a short range to distinguish the results from each other. The percent difference of results between two solvers for $N_{x\theta}^{0}$ is given in Figure 4.17.

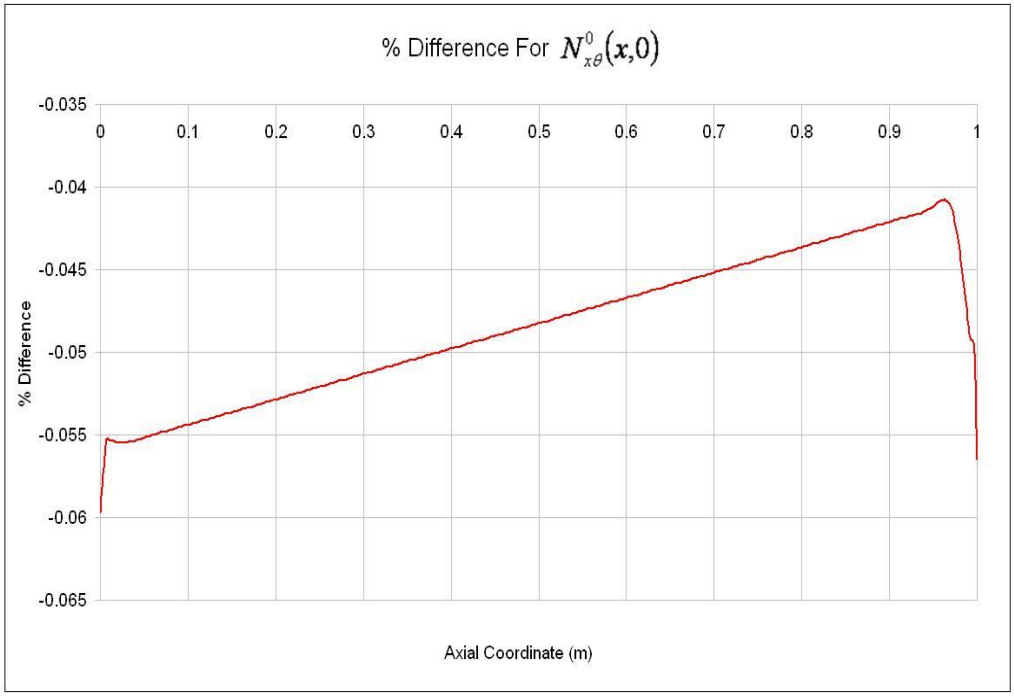

Figure 4.17 Change of Percent Difference with Axial Coordinate for $N_{x\theta}^{0}$ for Sample Problem 2

The maximum percent difference occurs at a boundary with a value of less than 0.06%. Therefore, once again it can be said that NASTRAN and the code developed in this thesis calculate almost the same results also for in-plane shear force resultant per unit length.

Furthermore, it should be noted that there are no jumps and sharp peaks in the percent difference variation, since $N^0_{x\theta}$ values do not change sign along the cylinder. This justifies the explanations on the percent difference variations for the previous displacement and stress results.

One final comparison is again made for the solution times of two solvers. On a computer with a 2.40 GHz CPU and 1 GB of RAM, the analysis is run on the code developed, and total time elapsed is 10.109 real seconds. When the same analysis is run on NASTRAN with the finite element mesh described in Section 4.2.1, it is completed in 497.347 real seconds. This result shows for this problem, the code developed in this study is about 50 times faster than NASTRAN. Again it should be emphasized that NASTRAN solution time does not include the preparation of the NASTRAN input file (*.bdf) from the finite element model by the pre and post-processor Patran. Similar to the previous problem, it should be kept in mind that in the finite element model when 300 elements are placed along the meridian of the shell, the element length in the circumferential direction can not be arbitrary in order not to end up with an element configuration with a high aspect ratio. Therefore, finite element model becomes very crowded in terms of element and node numbers, which increases the solution time for NASTRAN.

4.2.3. Comparison of Methods for Calculating Strain

In Section 3.7, two alternative methods are described for calculating midstrains and bending strains. Strains could either be found by using

Equation (3.7.22), i.e. by the inversion of constitutive equations (method 1); or by using kinematic equations and differentiating displacements and rotations with the finite difference method (method 2). In Figure 4.18, variation of ε_{xx}^{0} with axial coordinate at $\theta = 0$ obtained by using method 1 and method 2 are compared. For the analysis, problem described in 4.2.1 is used and comparison is made at the end points of the shell segments.

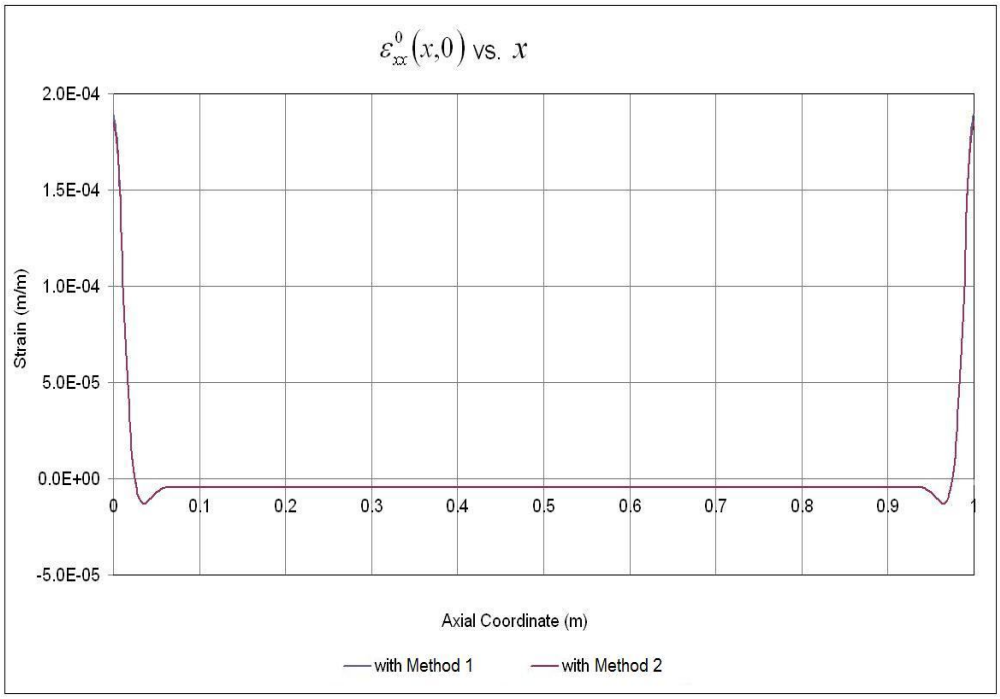

Figure 4.18 Comparison of Solutions for Variation of ε_{xx}^{0} with x for Sample Problem 1

In Figure 4.18, the results obtained by methods 1 and 2 overlap and are seen as one curve. In order to compare the results more clearly, a percent difference is calculated, in a similar way to Equation (4.2.1.1), at each grid point in the axial direction:

$$\%\,Difference = \frac{AbsoluteValue\left(method\,1\ result - method\,2\ result\right)}{method\,1\ result} \times 100$$

(4.2.3.1)

The variation of percent difference with the axial coordinate is given in Figure 4.19:

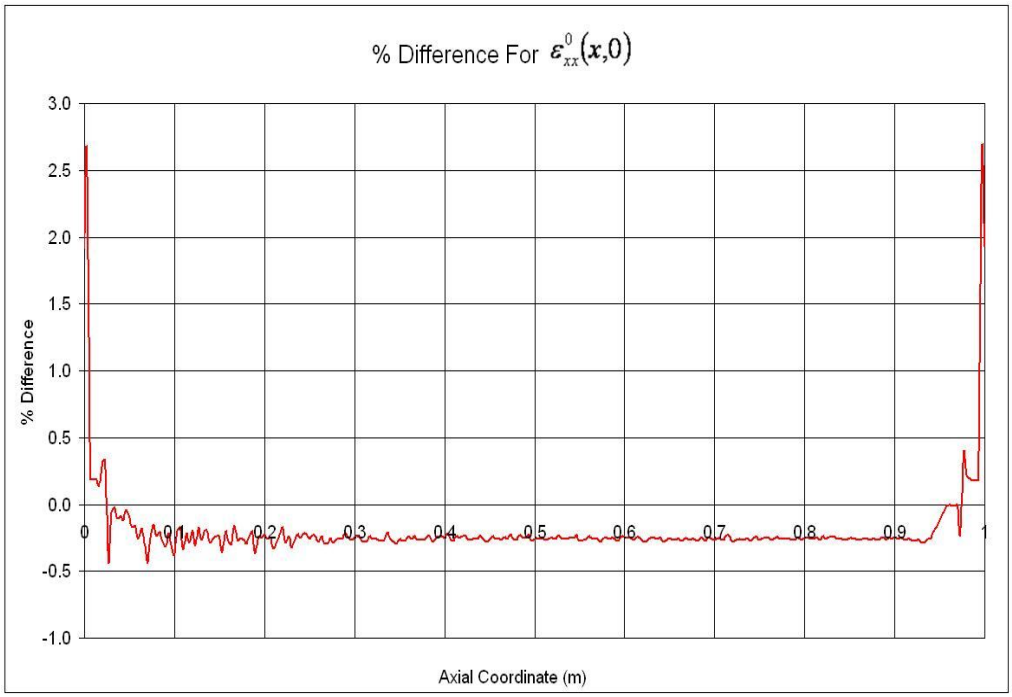

Figure 4.19 Change of Percent Difference with Axial Coordinate for ε^0_{xx} in Sample Problem 1

This graph shows that, maximum percent difference between the results of two methods occur near the boundaries with a value of 2.6%. As moving away from the boundaries, this value reduces below 0.5%, which reveals that either of these methods can be used as an alternative to the other.

Furthermore, calculation of overall (total) strains is discussed in Sections 2.2.3 and 3.7. Variation of overall strain in the x direction (ε_{xx}) with axial coordinate at $\theta = 0$ and for layer 1 (first layer in the cylinder) are calculated by using method 1, method 2 and NASTRAN. In Figure 4.20, the results are given for comparison. For the analysis, problem described in 4.2.1 is used and comparison of two methods with NASTRAN results are made at the NASTRAN element centroids, as explained for the stress calculation in Section 4.2.1.

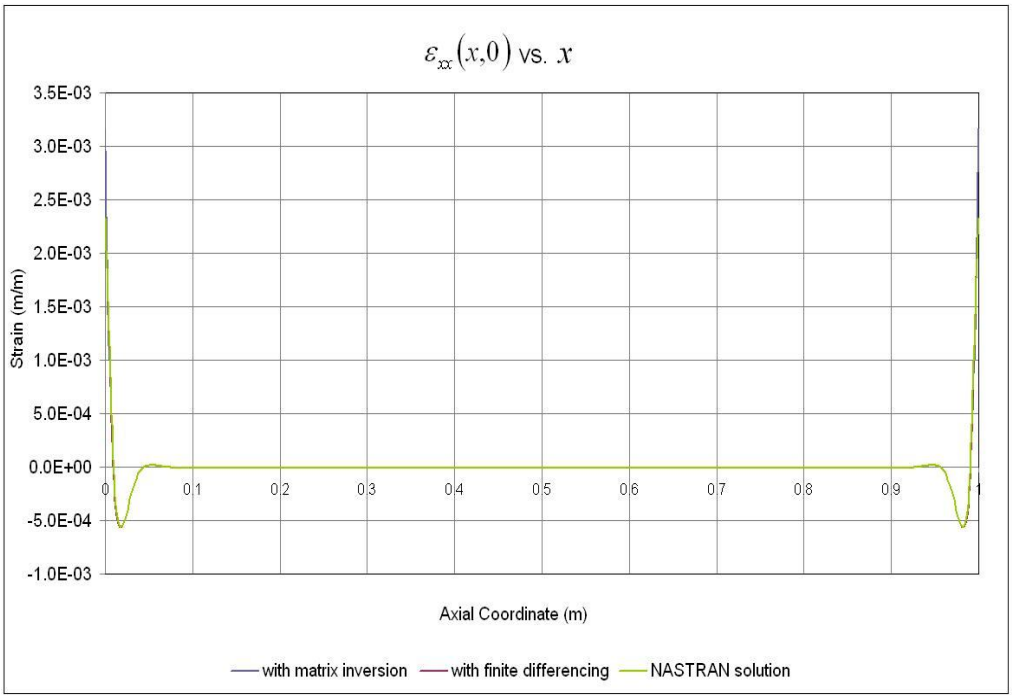

Figure 4.20 Comparison of Solutions for Variation of ε_{xx} with x for Sample Problem 1

In Figure 4.20, again similar to the previous results, the overall strains obtained from method 1, method 2 and NASTRAN overlap. In order to compare the results of the two methods with NASTRAN results, two percent

differences are calculated, in a similar way to the Equation (4.2.1.1), for each grid point in the axial direction:

$$\%\,Difference\ 1 = \frac{Abs.Value\left(method\,1\ result - NASTRAN\ result\right)}{NASTRAN\ result} \times 100 \tag{4.2.4.1}$$

$$\%\,Difference\ 2 = \frac{Abs.Value\left(method\,2\ result - NASTRAN\ result\right)}{NASTRAN\ result} \times 100 \tag{4.2.4.2}$$

The variations of the percent differences with axial coordinate are very much similar to each other. The variation is symmetrical with respect to the mid-span and reaches stable values at some distance away from the boundary. These stable values are both below 1%, and reached around $x = 0.1$ m. The variation of percent differences with axial coordinate in the interval [0, 0.12] is given in Figure 4.21:

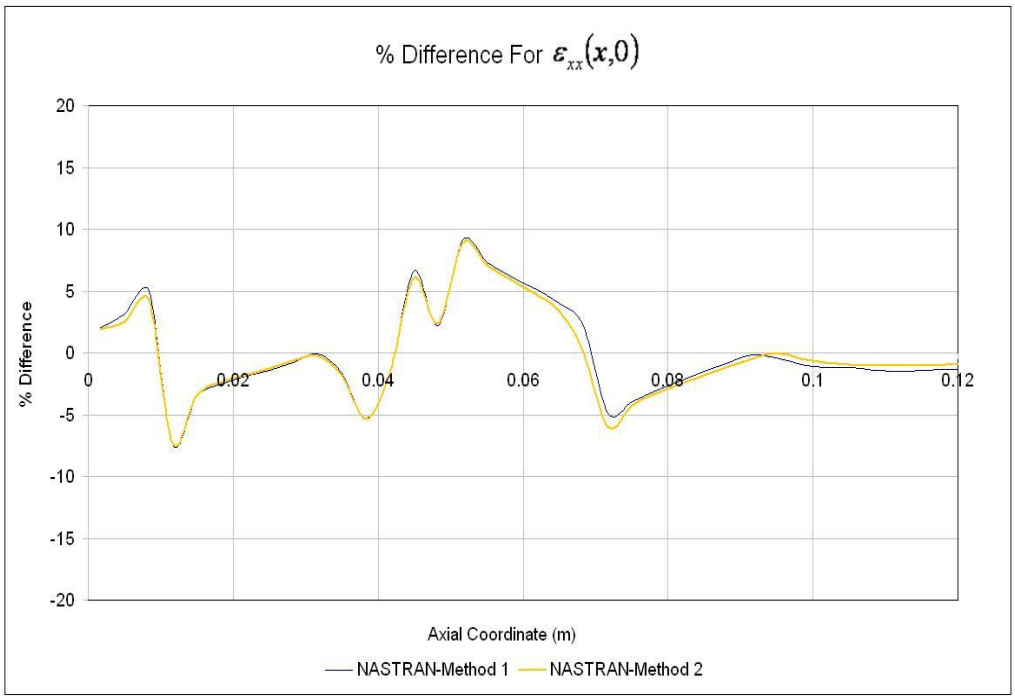

Figure 4.21 Change of Percent Differences with Axial Coordinate for ε_{xx} in Sample Problem 1

The percent differences are around 5% at the first point, oscillate as one moves away from the boundary, and eventually reach stable values below 1%. It is seen from Figure 4.21 that method 1 and method 2 results deviate almost by the same amount from the NASTRAN results, except for slight differences at around $x = 0.07$. This result is expected, since it is shown in Figure 4.19 that two methods deviate very little (less than 0.5 %) from each other. As seen from Figure 4.21, for this particular example, method 2 deviates less from NASTRAN solution than method 1.

In addition, it is explained in Section 2.3.2 that stresses are related to strains through the transformed material constants $\overline{Q}_{ij}$. Furthermore, percent change

of σ_{xx} variation with axial coordinate is less than 1%, as shown in Figure 4.8. Therefore, the percent difference of ε_{xx} also being less than 1% is justifiable.

Since stresses are calculated using strains as explained in Section 3.7, the results shown in this section are similar for stresses.

4.2.4. Effect of Number of Segments on the Results

In Sections 4.2.1 and 4.2.2, the solutions are performed for 300 segments when the code is used and similarly, cylinder is divided into 300 elements in the axial direction when NASTRAN is used. In this section, in order to investigate the effect of number of segment on the results, the problem in Section 4.2.2 is re-solved with various numbers of segments using the code developed in the thesis.

In Figure 4.22, variations of the mid-surface displacements in the thickness direction $\left(u_{\zeta}^{0}\right)$ with axial coordinate at $\theta = 0$ are given for 300, 400, 600 and 900 segments (M).

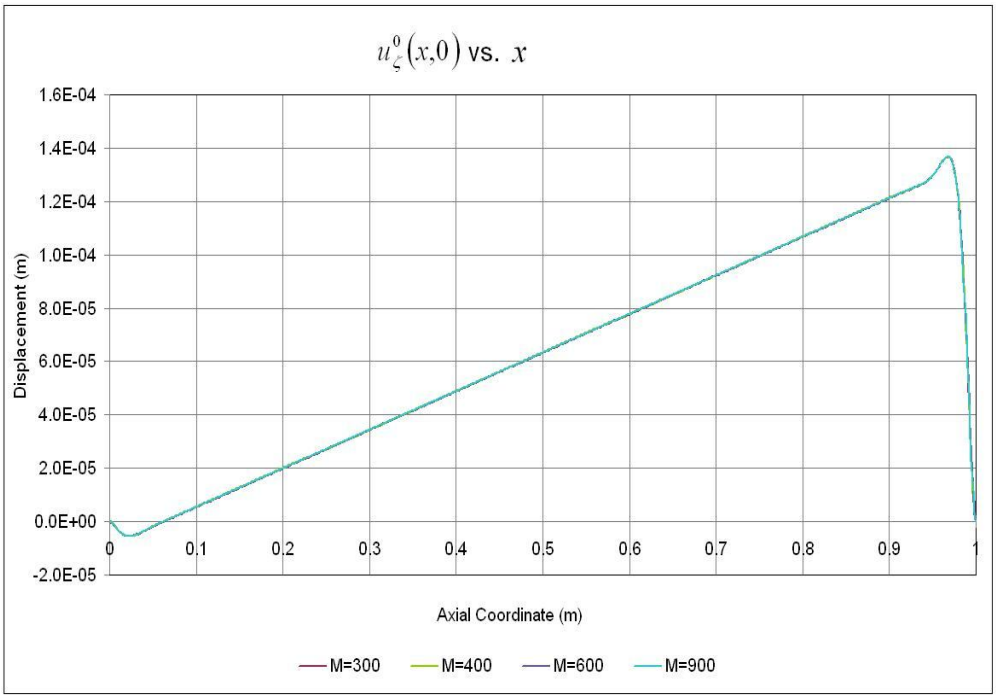

Figure 4.22 Variation of u_ζ^0 with x for Various Segments Numbers

Similar to the results obtained in Sections 4.2.1 and 4.2.2, the results overlap such that they cannot be distinguished from each other visually. Therefore, percent differences are again defined in order to estimate the deviations of results from each other. In percent difference calculation, reference is chosen to be the solution with 900 segments, which is the most accurate result case. Consequently, the percent difference definitions appear as

$$\%\,Difference_X = \frac{Absolute Value\left[\begin{pmatrix} results\ for \\ M=900 \end{pmatrix} - \begin{pmatrix} results\ for \\ M=X \end{pmatrix}\right]}{\begin{pmatrix} results\ for \\ M=900 \end{pmatrix}} \times 100 \quad (4.2.4.1)$$

where $(X = 300,400,600)$

In Figure 4.23, percent differences of u_ζ calculated using Equation (4.2.4.1) for the given number of segments are shown as a variation of the axial coordinate x.

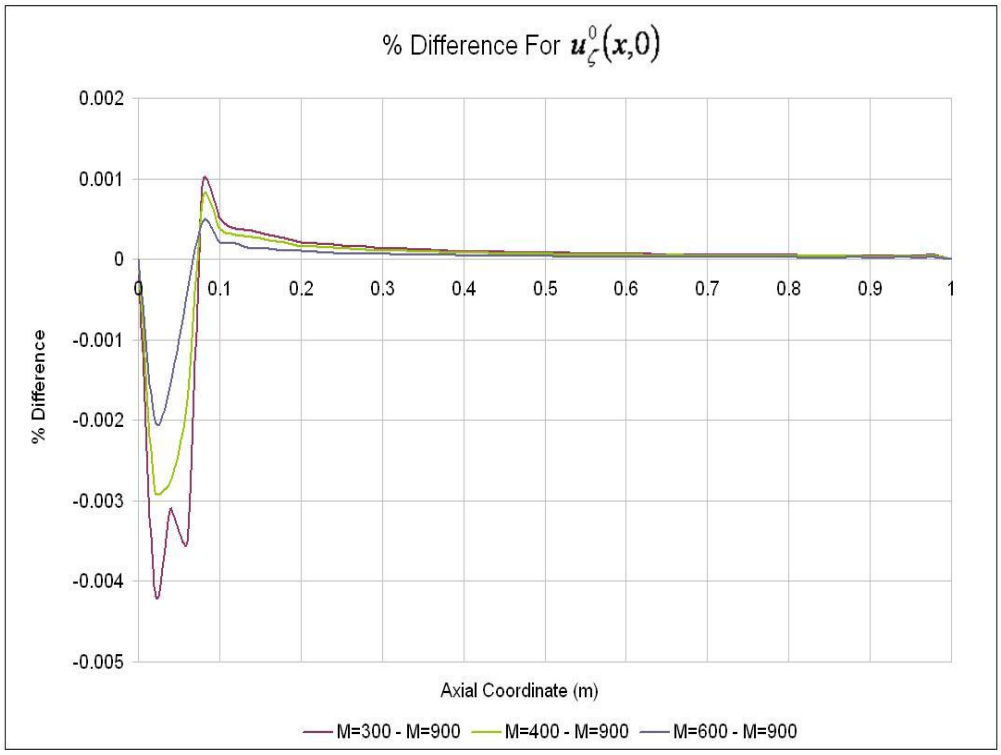

Figure 4.23 Percent Difference Results of u_ζ^0 vs. Axial Coordinate for Various Segments Numbers

The deviations decrease expectedly as the number of segments approach 900 which is the reference number of segments. Still, even for the smallest segments number 300, the maximum difference is 0.004%; and it gets even smaller as the axial coordinate x increases. This shows that results do not exhibit significant changes for this problem as the segments number exceeds 300, which means that sufficient accuracy is reached. Another point of interest

is the position where the maximum percent difference occurs, and this will be elaborated soon.

In Figure 4.24, variations of the axial stress (σ_{xx}) with axial coordinate at $\theta = 0$ are given for 300, 400, 600 and 900 segments (M) at layer 1 (first layer in the cylinder).

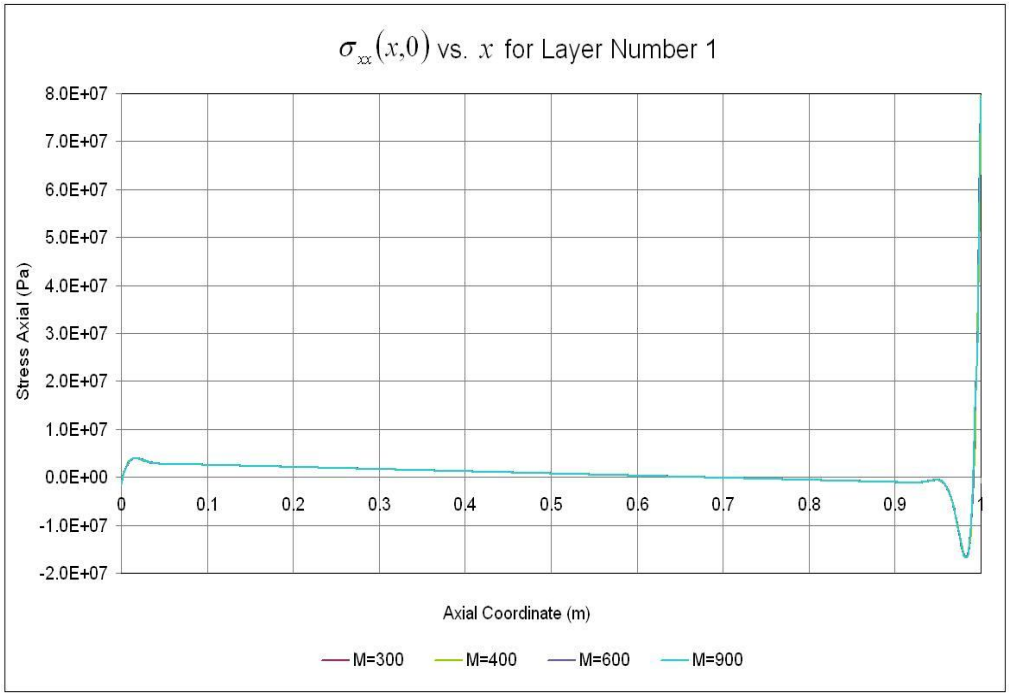

Figure 4.24 Variation of σ_{xx} with x for Various Segments Numbers

Again in order to distinguish the deviations of results from each other, percent differences given by Equation (4.2.4.1) are calculated. In Figure 4.25, percent differences are given as a function of axial coordinate for the same number of segments

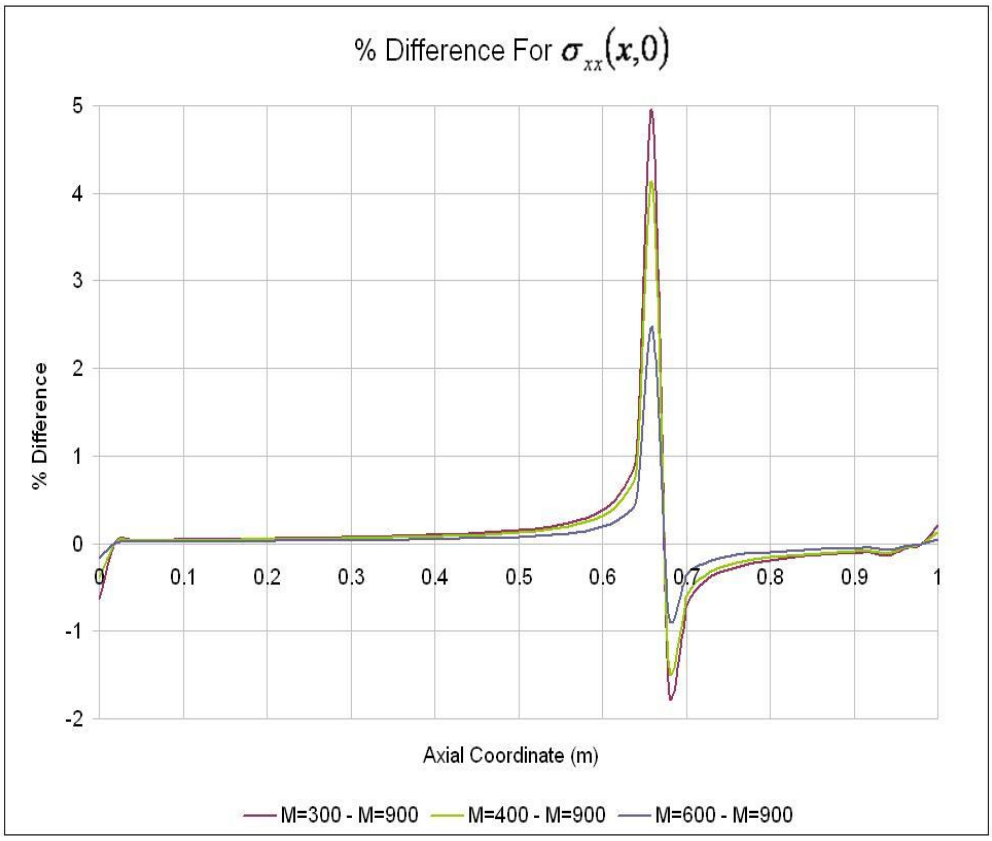

Figure 4.25 Percent Difference Results of σ_{xx} vs. Axial Coordinate for Various Segments Numbers

It can be seen from Figure 4.25 that percent differences are generally below 0.1%, and again the deviations decrease as the number of segments approach the reference value of 900

However, in Figure 4.25, there is a special point of interest which is at $x = 0.66$. It can be seen from Figure 4.24 that this point is the coordinate where σ_{xx} values change sign, going from positive values to negative values. Furthermore, if Figure 4.22 and Figure 4.23 are examined carefully, percent differences of u_ζ results for all segments numbers reach their maximum values also at the point where u_ζ values move from negative values to

positive values. This phenomenon was also observed when viewing the results in Section 4.2.2 and the reasons were explained in detail. The same discussion will not be given here in order to avoid repetition. However, it should be emphasized once again that the results do not deviate significantly from each other, but the difference is a result of the numerical error arising from the definition of percent difference.

It can be concluded that the results obtained by the multisegment integration method do not change significantly beyond a particular number of segments. For the current problem, sufficient accuracy is obtained when the shell is divided into 300 segments. However, it should be noted that 300 segments is an arbitrary number that was selected at the beginning of the comparison studies, and in practice number of segments can be decreased to low values and still accurate results can be obtained. Because in the multi-segment numerical integration technique by decreasing the number of segments one does not actually reduce the accuracy as in finite element analysis. Solutions at the ends of the shell segments will still have sufficient accuracy but the resolution will be lowered. Therefore, one has to calculate the fundamental variables at the intermediate locations afterwards by making use of the fundamental variables determined at the end of the shell segments.

The behaviour of the axial variations of the variables must be considered while deciding the number of segments the shell is divided into for the solution. For these particular problems, solutions performed for less than 300 segments along the shell axial direction may cause peaks existing in the solution curves due to the bending boundary layers nearby the boundaries be missed and therefore prevent to obtain the correct variations in the axial direction.

CHAPTER 5

CASE STUDIES FOR CIRCULAR CYLINDRICAL SHELLS OF REVOLUTION

5.1. Introduction

The analysis method developed in the present study is explained in detail in Chapter 3 and its implementation is carried out by developing a computer code, which is verified using the finite element method solver NASTRAN in Chapter 4. In this chapter, a number of cases are analysed by using the code developed and the results obtained are discussed. As it was mentioned previously, one of the most commonly occurring shells of revolution geometries is circular cylinder and many engineering problems involve this geometry. Therefore, circular cylindrical shells are analysed in the cases studied in this chapter.

The case studies begin with the investigation of temperature change effects through the thickness, where a temperature difference varying with thickness is applied as a thermal load to the body analysed. Next, a problem in which the effects of variable mechanical loads in axial direction is considered by applying pressure to a specific region along the cylinder axis. The analyses continue with the examination of a cylindrical shell under temperature loading, which is unsymmetrical in the circumferential direction and with the study of transverse shear effects on the body under a given type of loading. This

chapter ends with a specific application of the method to an aerospace structure, namely a solid propellant rocket motor body.

5.2. Effect of Temperature Change through the Thickness

In Section 2.3.2, it is explained that for shells of revolution it is very probable to have a varying temperature difference across the thickness depending on the exposure of the shell to the external environment. In this section, a cylindrical pipe which is subject to different temperatures inside and outside the cylinder is analysed. In order to demonstrate the effect of temperature change with thickness clearly, temperature differences in axial and tangential directions are kept constant.

For this problem, four different cases in terms of loading are compared. In the first case, a temperature difference of 100°C, which is constant through the thickness, is considered. Physically, this problem can be an example for a thin cylindrical shell after the steady state is reached and constant temperature distribution is attained.

However, consider a case in which a pipe shaped cylindrical laminated shell is manufactured at room temperature and exposed to a sudden temperature change subsequently. If there is a heat source or heat sink inside the cylinder, the temperature difference will be less inside compared to the outside. For such a case, linearly varying temperature change through the thickness may be assumed. As the second, third and fourth cases, a cylindrical pipe subject to varying temperature differences through the thickness are considered. These cases are given in Table 5.1

Table 5.1 Temperature Difference Values for Analysis Cases 1 – 4

Cases	**Temperature Differences**
Case 1 $(\Delta T1)$	$\Delta T_{in} = \Delta T_{out} = 100°C$
Case 2 $(\Delta T2)$	$\Delta T_{in} = 100°C$, $\Delta T_{out} = 200°C$
Case 3 $(\Delta T3)$	$\Delta T_{in} = 100°C$, $\Delta T_{out} = 250°C$
Case 4 $(\Delta T4)$	$\Delta T_{in} = 100°C$, $\Delta T_{out} = 300°C$

As it was explained in Section 2.3.2, thermal loads were derived by assuming linear variation of the temperature across the shell thickness. The thickness coordinate ζ is equal to zero at the mid-surface of the laminate, and its positive direction is towards outer surface of the shell. Thus, temperature difference can be written as a linear function of ζ, using

$$\Delta T(\zeta) = \frac{\Delta T_{out} - \Delta T_{in}}{\zeta_{out} - \zeta_{in}}(\zeta - \zeta_{in}) + \Delta T_{in} \tag{5.2.1}$$

where ζ_{in} and ζ_{out} are the ζ values at the inner and outer surfaces of the laminate, respectively. The temperature variation across the thickness, material data used, geometric properties, and boundary conditions are summarized in Table 5.2. Change of temperature difference with the thickness coordinate ζ is also shown in Figure 5.1.

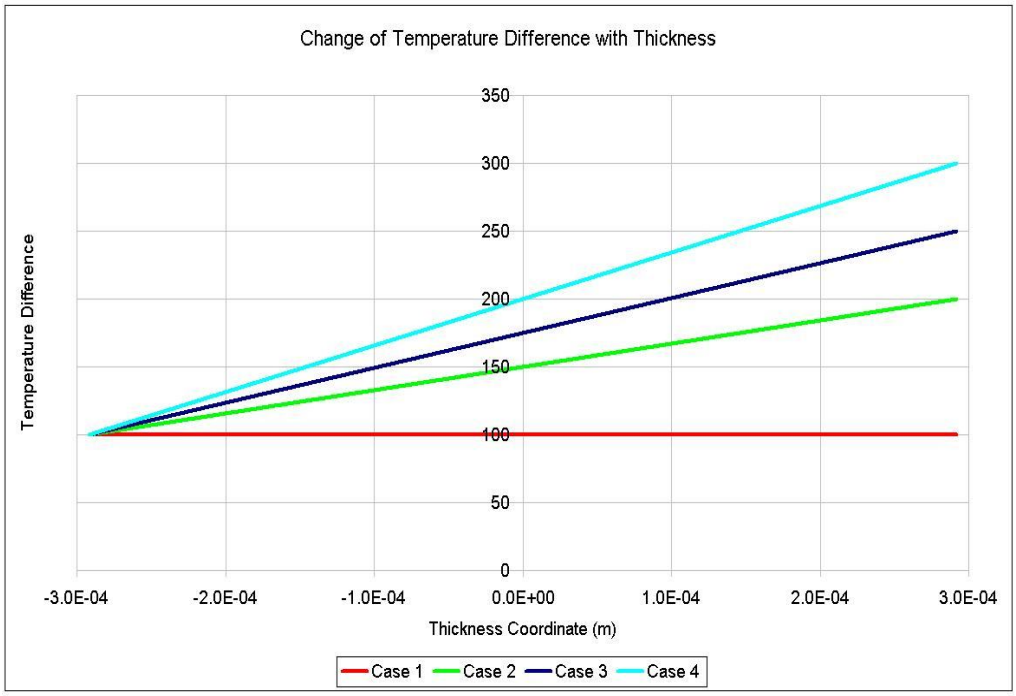

Figure 5.1 Change of Temperature Difference with Thickness for Cases 1 – 4

Table 5.2 Analysis Data for the Problem 5.2

Geometry	**Circular Cylinder**
Radius	0.2 m
Axial Length	1.0 m
Number of segments	300
Material	
Ply Material	MR50/LTM25 Carbon Epoxy Prepreg [23]
E_{11}	155 GPa
E_{22}	7.31 GPa
υ_{12}	0.345

Table 5.2 (continued)

G_{12}	4.19 GPa
G_{13}	4.19 GPa
G_{23}	3 GPa
Ply thickness	0.146 mm
Ply density (ρ)	1520 kg/m^3
α_{11}	-0.43 x 10^{-6} 1/°C
α_{22}	37.4 x 10^{-6} 1/°C
Laminate	
Number of Layers	4
Ply Orientation	[0°/45°/90°/0°]
Loads	
$\Delta T1$ (constant along ζ)	100°C
$\Delta T2 = \Delta T2(\zeta)$	$\Delta T2(\zeta) = 150 + 1.7123 \times 10^5 \times \zeta$
$\Delta T3 = \Delta T3(\zeta)$	$\Delta T3(\zeta) = 175 + 2.56849 \times 10^5 \times \zeta$
$\Delta T4 = \Delta T4(\zeta)$	$\Delta T4(\zeta) = 200 + 3.4247 \times 10^5 \times \zeta$
Boundary Conditions	clamped-clamped
left end	$(u_\zeta^0)_c, (u_\zeta^0)_s, (u_x^0)_c, (u_x^0)_s, (u_\theta^0)_c, (u_\theta^0)_s, (\beta_x^0)_c, (\beta_x^0)_s, (\beta_\theta^0)_c, (\beta_\theta^0)_s = 0$
right end	$(u_\zeta^0)_c, (u_\zeta^0)_s, (u_x^0)_c, (u_x^0)_s, (u_\theta^0)_c, (u_\theta^0)_s, (\beta_x^0)_c, (\beta_x^0)_s, (\beta_\theta^0)_c, (\beta_\theta^0)_s = 0$

In Figure 5.2, change of u_ζ^0 with the axial coordinate at the tangential position $\theta = 0°$ is given for the cases described above.

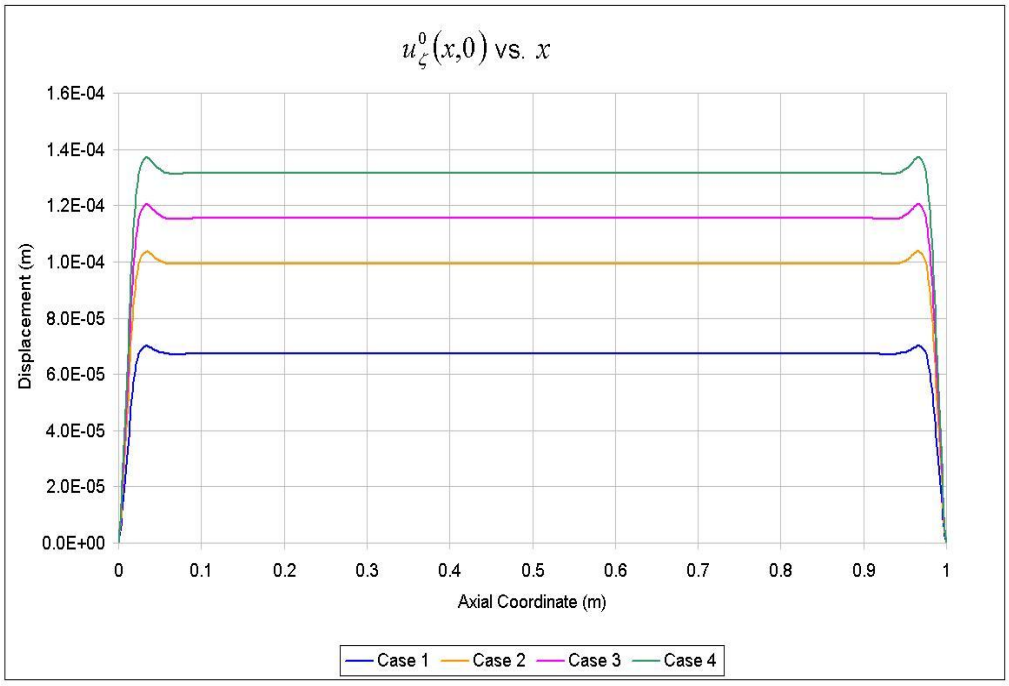

Figure 5.2 Comparison of Solutions for Variation of u_ζ^0 with x for Cases 1 – 4

In Figure 5.3, change of u_x^0 with the axial coordinate at the tangential position $\theta = 0°$ is given for the Cases 1 – 4.

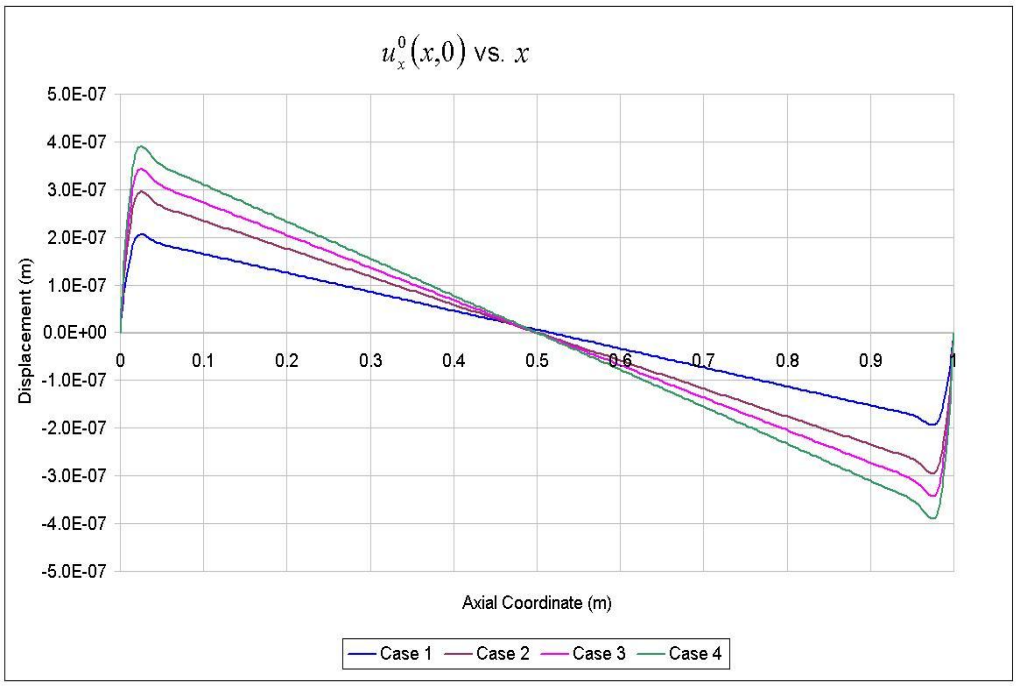

Figure 5.3 Comparison of Solutions for Variation of u_x^0 with x for Cases 1 – 4

It should be recalled that the displacements u_ζ^0 and u_x^0 are defined at the mid-plane of the laminate. It is seen from these figures that the maximum values of both u_ζ^0 and u_x^0 increase with increasing case number, i.e. as the temperature difference increase going from inside to the outside the shell. In addition to that, u_ζ^0 displacements are greater for the cases with higher temperature differences throughout the shell; and the same conclusion is also true for the absolute values of u_x displacements, i.e. the absolute values of u_x^0 displacements are greater for the cases with higher temperature differences throughout the shell as expected. It should also be noted the bending boundary layer near the boundary edges is clearly seen.

In Figure 5.4, change of σ_{xx} at layer 4 with the axial coordinate at the tangential position $\theta = 0°$ is given for the Cases 1 – 4. For the current

analysis, thermal loads are mainly dominated by the temperature difference outside the shell. Naturally, the effect of this is seen on the layer adjacent to the outer surface of the laminate more clearly. Therefore, layer 4 is chosen for the output location of results. The variation of σ_{xx} with the axial coordinate is symmetrical in the axial direction and reaches a stable value at some distance from the boundary. This stable value is reached around $x = 0.08$ m. The variation of σ_{xx} with axial coordinate is given in the interval [0, 0.1] for the cases 1 – 4. For all the load cases, it should be stressed that the stresses are calculated at the mid-plane of each layer.

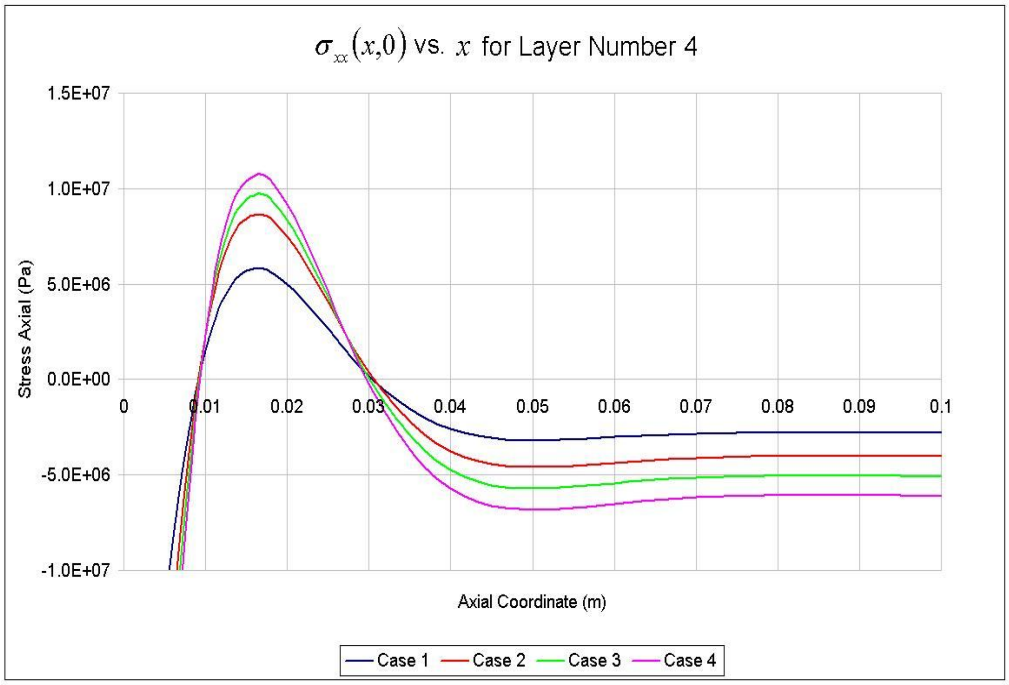

Figure 5.4 Comparison of Solutions for Variation of σ_{xx} at layer 4 with x for Cases 1 – 4

It can be seen from Figure 5-4 that, as expected, the maximum value of σ_{xx} increase with increasing case number, i.e. as the temperature difference

increases. Also the absolute values of axial stresses σ_{xx} are greater for the cases with higher temperature differences throughout the shell. It is again seen that besides the shell boundary, the axial stress exhibits a peak value at a section which is short distance away from boundary. This behaviour is typical for shells of revolution.

In Figure 5.5, solutions for variation of σ_{xx} with layer number for Cases 1 – 4 are compared. It is seen in Figure 5.4 that the axial stress is nearly constant with the axial coordinate x in the interval [0.1, 0.9]. Therefore, for the output of results an axial location in this interval is chosen at $x = 0.333$. Since the problem and the loading is axisymmetric, tangential location is again taken as $\theta = 0°$.

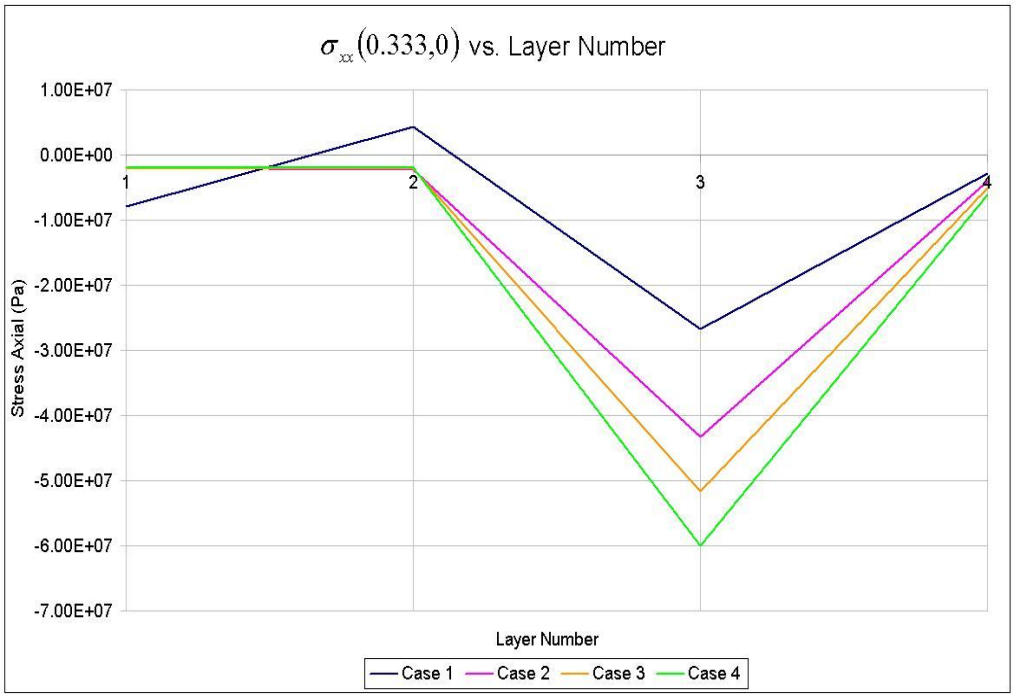

Figure 5.5 Comparison of Solutions for Variation of σ_{xx} with Layer Number for Cases 1 – 4

The graphs of Cases 2 – 4 exhibit very similar behaviour and they can be said to be shifted up or down with respect to each other. In Figure 5.5, it is seen that cases with higher temperature differences have higher axial stress values at each layer and this result is in agreement with the results deduced from previous figures. In case 1, loading is constant through the thickness and therefore it differs from the other load cases. Consequently, the variation of axial stress with the layer number is slightly different from the results of other cases.

Absolute value of the axial stress is almost the same at layer 1 for cases 2 – 4, while it is higher for case 1. This character is also true at layer 2. However, at layers 3 and 4 effect of variable temperature difference with the thickness is seen more clearly. Since the temperature difference increases at the outer layers as the case number is increased, the axial stresses also increase at the outer layers as the case number is increased.

5.3. Effect of Pressure on a Specific Region in the Axial Direction

One of the advantages of the multi-segment method of Integration is that loads can be defined as a function of the meridional coordinate by specifying mechanical and thermal loads at the end points of the shell segments, as previously emphasized in Section 3.5. In addition, any analytical function can be used to define the meridional variation of the loads. This has been shown for a general case in Section 4.2.2.

In many engineering problems, cylindrical shells are subject to mechanical loads exerted on a specific region along the body, such as bearing loads. For the current problem, a ring pressure is applied on the cylinder. In order to demonstrate the effect of local pressure as a function of axial coordinate

clearly, pressure in tangential direction is kept constant. Region where the pressure is applied at is given in Table 5.3, along with the other data used in the analysis.

Table 5.3 Analysis Data for the Problem 5.3

Geometry	**Circular Cylinder**
Radius	0.2 m
Axial Length	1.0 m
Number of segments	300
Material	
Ply Material	MR50/LTM25 Carbon Epoxy Prepreg [23]
E_{11}	155 GPa
E_{22}	7.31 GPa
υ_{12}	0.345
G_{12}	4.19 GPa
G_{13}	4.19 GPa
G_{23}	3 GPa
Ply thickness	0.146 mm
Ply density (ρ)	1520 kg/m^3
α_{11}	-0.43 x 10^{-6} 1/°C
α_{22}	37.4 x 10^{-6} 1/°C
Laminate	
Number of Layers	4
Ply Orientation	[0°/45°/90°/0°]

Table 5.3 (continued)

Loads	
p_ζ	$= \begin{cases} 0 & if \quad x < 0.3 \\ 200\,kPa & if \quad 0.3 \le x \le 0.5 \\ 0 & if \quad 0.5 < x \end{cases}$
Boundary Conditions	clamped-clamped
left end	$\left(u_\zeta^0\right)_c, \left(u_\zeta^0\right)_s, \left(u_x^0\right)_c, \left(u_x^0\right)_s, \left(u_\theta^0\right)_c, \left(u_\theta^0\right)_s, \left(\beta_x^0\right)_c,$ $\left(\beta_x^0\right)_s, \left(\beta_\theta^0\right)_c, \left(\beta_\theta^0\right)_s = 0$
right end	$\left(u_\zeta^0\right)_c, \left(u_\zeta^0\right)_s, \left(u_x^0\right)_c, \left(u_x^0\right)_s, \left(u_\theta^0\right)_c, \left(u_\theta^0\right)_s, \left(\beta_x^0\right)_c,$ $\left(\beta_x^0\right)_s, \left(\beta_\theta^0\right)_c, \left(\beta_\theta^0\right)_s = 0$

In addition, the same problem is also analysed with NASTRAN by the linear static solver sol 101, in order to make a comparison. Same finite element mesh is generated as in the analyses of the problems given in Sections 4.2.1 and 4.2.2.

The effect of pressure applied at a local region can best be visualized by the variation of u_ζ^0 with the axial coordinate. This is given in Figure 5.6 at the tangential position $\theta = 0°$. The results of both NASTRAN and the code are given in this figure for comparison

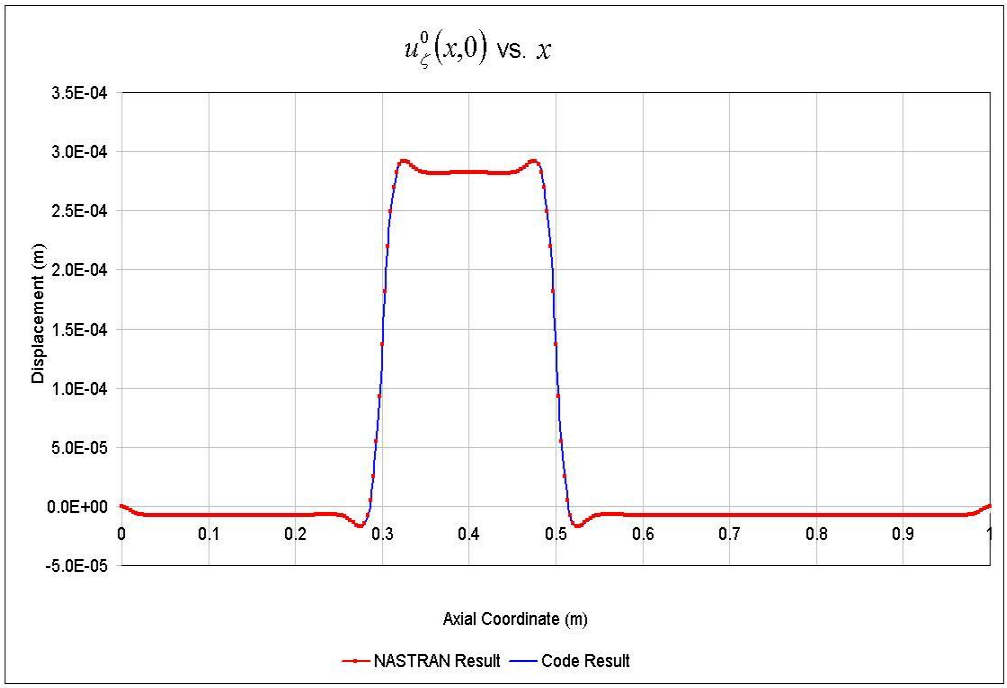

Figure 5.6 Comparison of Solutions for variation of u_ζ^0 with x for the Problem in Section 5.3

In Figure 5.6, the effect of applied pressure between $x = 0.3$ and $x = 0.5$ is seen very clearly, which causes higher deformations in the ζ direction in that area. In addition, the results of NASTRAN and the code overlap and are seen as one curve. In order to compare the results more clearly, percent difference given by equation (4.2.1.1) is calculated for each grid point in the axial direction. This is given in Figure 5.7.

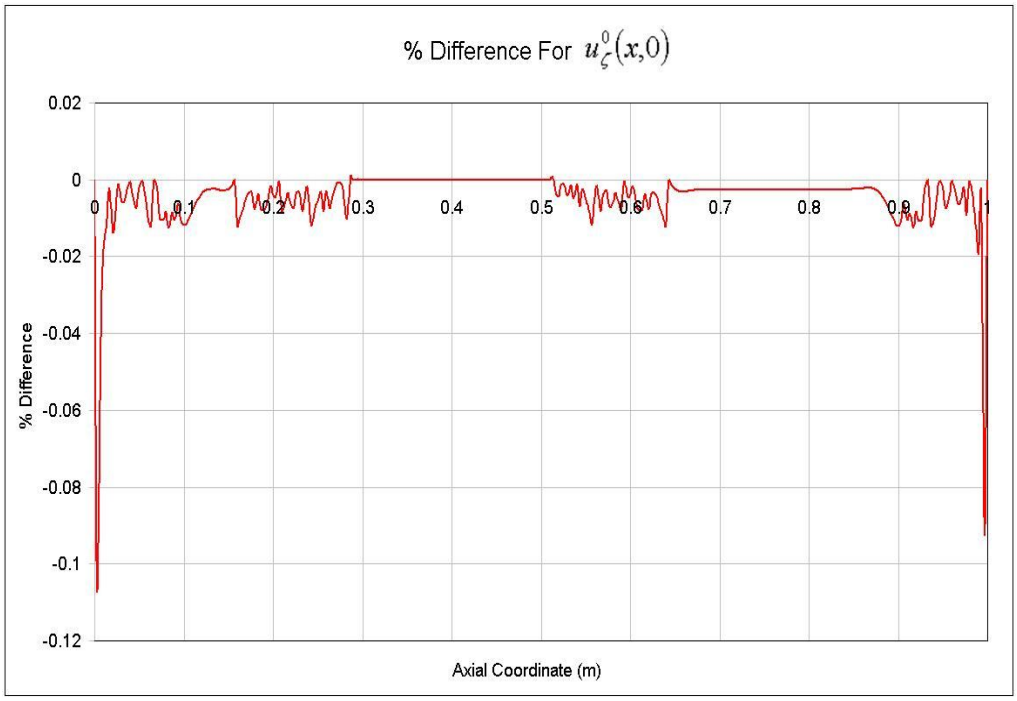

Figure 5.7 Change of Percent Difference with Axial Coordinate for u_ζ^0 the Problem in Section 5.3

Maximum percent difference between the results of NASTRAN and the code is 0.1%, and the percent difference is below 0.02% at most grid points. This shows that NASTRAN and the code find almost the same values, and the difference is most probably due to numerical calculations, similar to the results found in 4.2.1 and 4.2.2.

In Figure 5.8, variation of u_x^0 with the axial coordinate at the tangential position $\theta = 0°$ is given. The axial displacement calculated by the present code and NASTRAN are overlaid on the same figure.

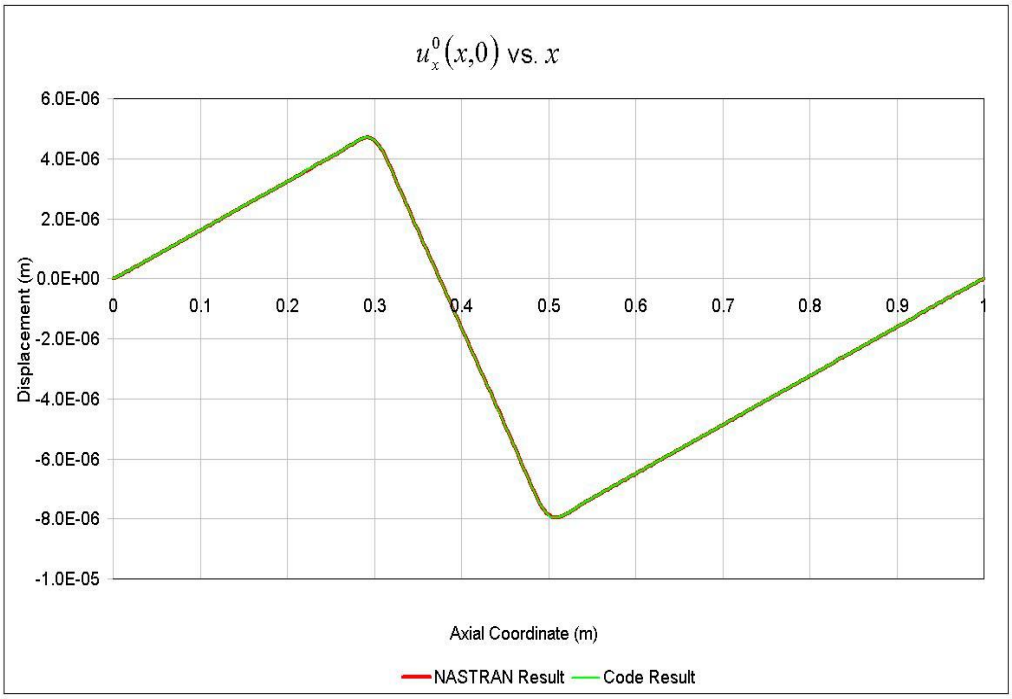

Figure 5.8 Variation of u_x^0 with x for the Problem in Section 5.3, solved by the code and NASTRAN

Effect of pressure applied to the local region is revealed in this figure by the change in the slope of displacement values when approaching the interval [0.3, 0.5] from the left and right. Also it should be noted that u_x^0 values are much lower than u_ζ^0 values as far as the orders of magnitude are considered. Similar to the previous results, code results and NASTRAN results match perfectly.

In Figure 5.9, variation of the stress in the axial direction (σ_{xx}) with axial coordinate at the tangential position $\theta = 0$ and for layer 4 (layer adjacent to the outer surface of the cylinder) is given both for the code and NASTRAN solutions.

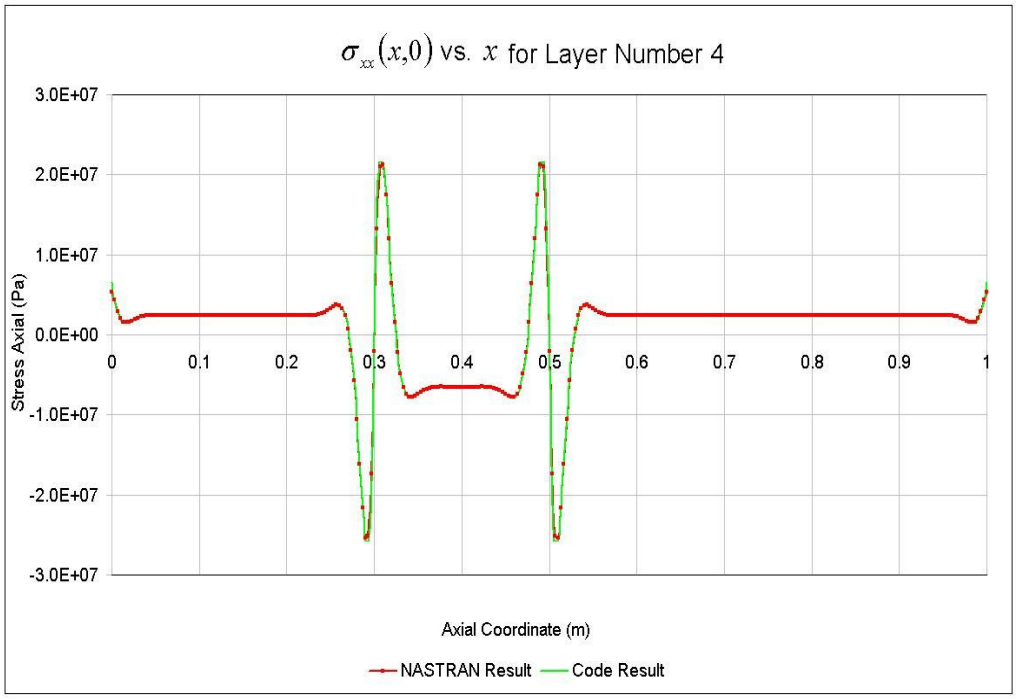

Figure 5.9 Variation of σ_{xx} with x for the Problem in Section 5.3, solved by the code and NASTRAN

Effect of locally exerted pressure on a region along the axis is also seen clearly in Figure 5.9. Besides the jumps in the axial stress at the boundaries of the interval where the stress is applied, stresses in the interval [0.3, 0.5] are also higher than the stresses elsewhere on the cylinder, as expected. Similar to the previous results, code results and NASTRAN results match perfectly.

In Figure 5.10, variation of the stress in the tangential direction $(\sigma_{\theta\theta})$ with axial coordinate at the tangential position $\theta = 0$ and for layer 4 (layer adjacent to the outer surface of the cylinder) is given both for the code and NASTRAN solutions

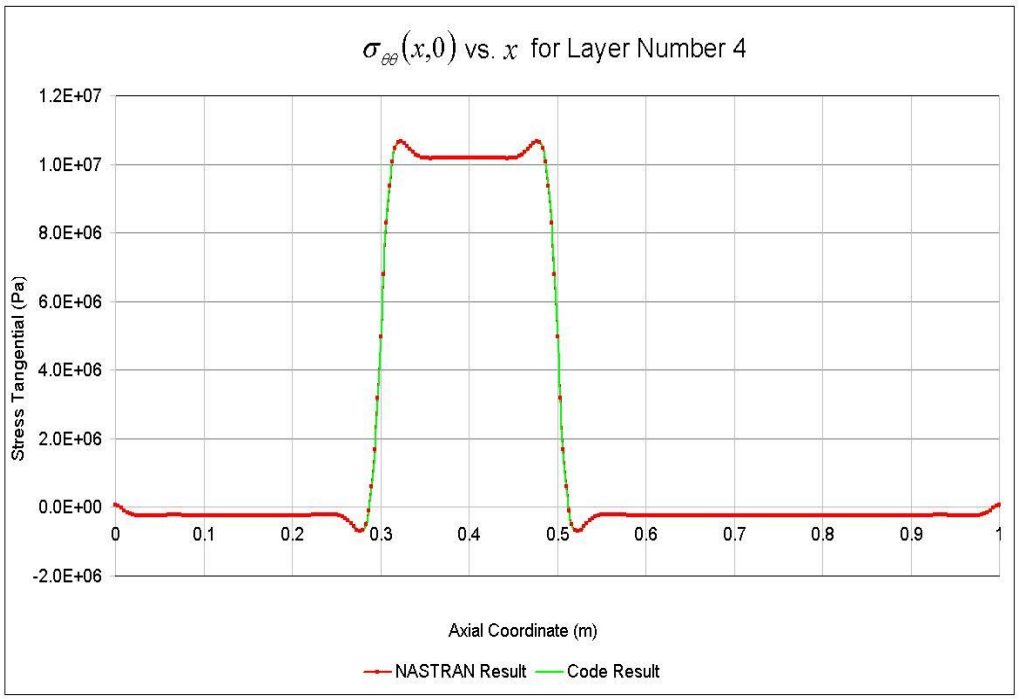

Figure 5.10 Variation of $\sigma_{\theta\theta}$ with x for the Problem in Section 5.3, solved by the code and NASTRAN

Comparing Figure 5.10 with Figure 5.6, it is seen that behaviour of $u_\zeta(x)$ and $\sigma_{\theta\theta}(x,0)$ curves are very similar. This can be explained as follows. In Equation (2.2.3.13), $\varepsilon^0_{\theta\theta}$ is given as a linear function of u_ζ and $\partial u^0_\theta/\partial\theta$. Current problem is axisymmetric, so $\partial u^0_\theta/\partial\theta = 0$. Therefore $\varepsilon^0_{\theta\theta}$ is linearly related to u_ζ only. On the other hand, in Equation (2.3.2.7), $\sigma_{\theta\theta}$ is given as a linear function of ε_{xx}, $\varepsilon_{\theta\theta}$, and $\varepsilon_{x\theta}$, which are also linearly related to ε^0_{xx}, $\varepsilon^0_{\theta\theta}$, and $\varepsilon^0_{x\theta}$ through the Equations (3.7.1) – (3.7.3), respectively. In Figure 5.8, it is seen that u_x is very small compared to u_ζ, and it can be shown that u_θ is also negligibly small compared to u_ζ. Therefore, u_ζ is the dominant term in the calculation of the strains ε^0_{xx}, $\varepsilon^0_{\theta\theta}$, and $\varepsilon^0_{x\theta}$, and consequently $\sigma_{\theta\theta}$. And

since for the particular problem $\sigma_{\theta\theta}$ is linearly related to u_ζ, $\sigma_{\theta\theta}$ curve in Figure 5.10 and u_ζ curve in Figure 5.6 show similar behaviour.

5.4. Cylinder under Unsymmetrical Loading

In order to apply unsymmetrical loads to the shell of revolution, loads that are given as functions of circumferential coordinate θ are expanded using Fourier series, as explained in Section 3.3. In this section, temperature difference is applied as a function of θ to the laminated circular cylindrical shell, whose material and geometrical properties are given in Table 5.4. Table 5.4 also summarizes the temperature load applied and the boundary conditions. In order to demonstrate the effect of temperature difference as a function of θ clearly, temperature difference is taken as constant along the axial direction and also kept constant in thickness direction.

Table 5.4 Analysis Data for the Problem 5.4

Geometry	**Circular Cylinder**
Radius	0.2 m
Axial Length	1.0 m
Number of segments	300
Material	
Ply Material	MR50/LTM25 Carbon Epoxy Prepreg [23]
E_{11}	155 GPa
E_{22}	7.31 GPa

Table 5.4 (continued)

υ_{12}	0.345
G_{12}	4.19 GPa
G_{13}	4.19 GPa
G_{23}	3 GPa
Ply thickness	0.146 mm
Ply density (ρ)	1520 kg/m^3
α_{11}	-0.43 x 10^{-6} 1/°C
α_{22}	37.4 x 10^{-6} 1/°C
Laminate	
Number of Layers	4
Ply Orientation	[0°/45°/90°/0°]
Loads	
ΔT	$= \begin{cases} 300 \times \sin(\theta) & if \quad \theta \in [0, \pi] \\ 70 \times \sin(\theta) & if \quad \theta \in (\pi, 2\pi) \end{cases}$
Boundary Conditions	clamped-clamped
left end	$(u_\zeta^0)_c, (u_\zeta^0)_s, (u_x^0)_c, (u_x^0)_s, (u_\theta^0)_c, (u_\theta^0)_s, (\beta_x^0)_c, (\beta_x^0)_s, (\beta_\theta^0)_c, (\beta_\theta^0)_s = 0$
right end	$(u_\zeta^0)_c, (u_\zeta^0)_s, (u_x^0)_c, (u_x^0)_s, (u_\theta^0)_c, (u_\theta^0)_s, (\beta_x^0)_c, (\beta_x^0)_s, (\beta_\theta^0)_c, (\beta_\theta^0)_s = 0$

Temperature difference given as a function of circumferential coordinate θ is shown in Figure 5.11. Temperature differences caused by convective flows around the body can be modelled by sinusoidal functions. And this load case can physically be an example to a cylindrical pipe subject to different temperatures differences from both sides.

For the expansion of this function using Fourier series, a final circumferential wave number needs to be determined. Mathematically, in Fourier series expansion, circumferential wave number starts from 0 and goes to infinity, as shown by Equation (3.3.41). However, Fourier series converges to the original function after a certain circumferential wave number is reached. For the temperature difference function given in Table 5.4, this number is found to be 14, as depicted in Figure 5.11.

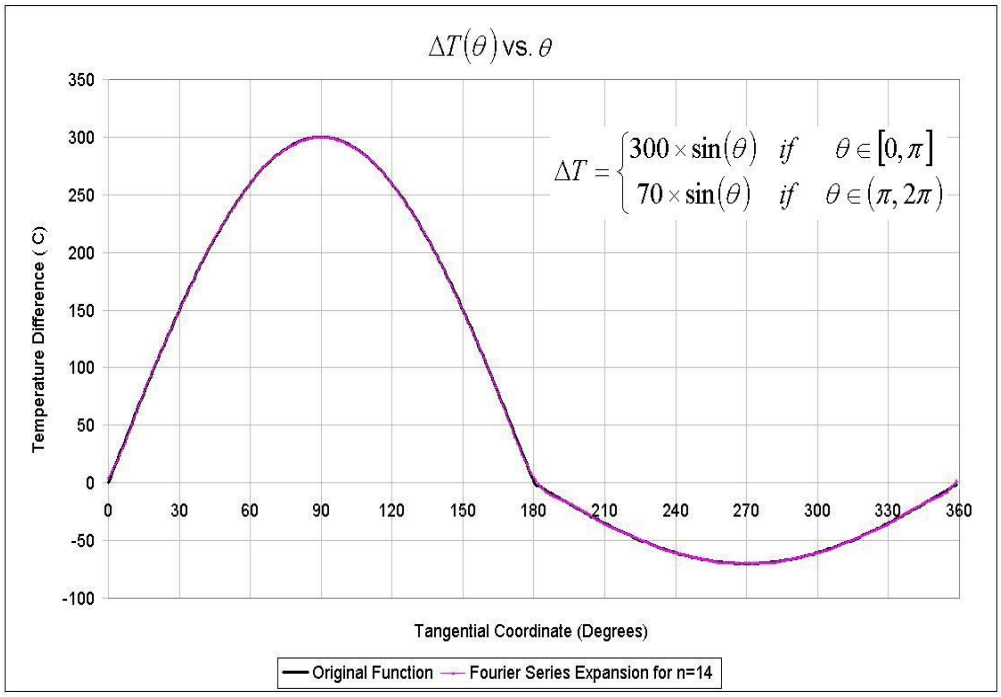

Figure 5.11 Original Temperature Difference Function and its Fourier Series Expansion at n=14 in Problem 5.4

The Fourier series is expanded by Equation (5.4.1) and using the engineering calculation software Mathcad [29].

$$f(\theta) = f_0 + \sum_{n=1}^{14} f_{nc} \cos(n\theta) + f_{ns} \sin(n\theta) \tag{5.4.1}$$

Coefficients f_0, f_{nc} and f_{ns} $(n = 1,2,...,14)$ are calculated as explained in Section 3.3 and by using Equations (3.3.46) – (3.3.48). Fourier components are summarized are in Table 5.5.

Table 5.5 Coefficients of the Temperature Difference Function Expanded using Fourier Series

$f_0 = 73.211$	
$f_{1c} = 0$	$f_{1s} = -185$
$f_{2c} = -48.8$	$f_{2s} = 0$
$f_{3c} = 0$	$f_{3s} = 0$
$f_{4c} = -9.762$	$f_{4s} = 0$
$f_{5c} = 0$	$f_{5s} = 0$
$f_{6c} = -4.184$	$f_{6s} = 0$
$f_{7c} = 0$	$f_{7s} = 0$
$f_{8c} = -2.324$	$f_{8s} = 0$
$f_{9c} = 0$	$f_{9s} = 0$
$f_{10c} = -1.479$	$f_{10s} = 0$
$f_{11c} = 0$	$f_{11s} = 0$
$f_{12c} = -1.024$	$f_{12s} = 0$
$f_{13c} = 0$	$f_{13s} = 0$
$f_{14c} = -0.751$	$f_{14s} = 0$

Convergence of the Fourier series to the original function as the circumferential wave number increases is shown in Figure 5.12. In order to distinguish graphics from each other visually, they are given in the interval [170°, 190°]

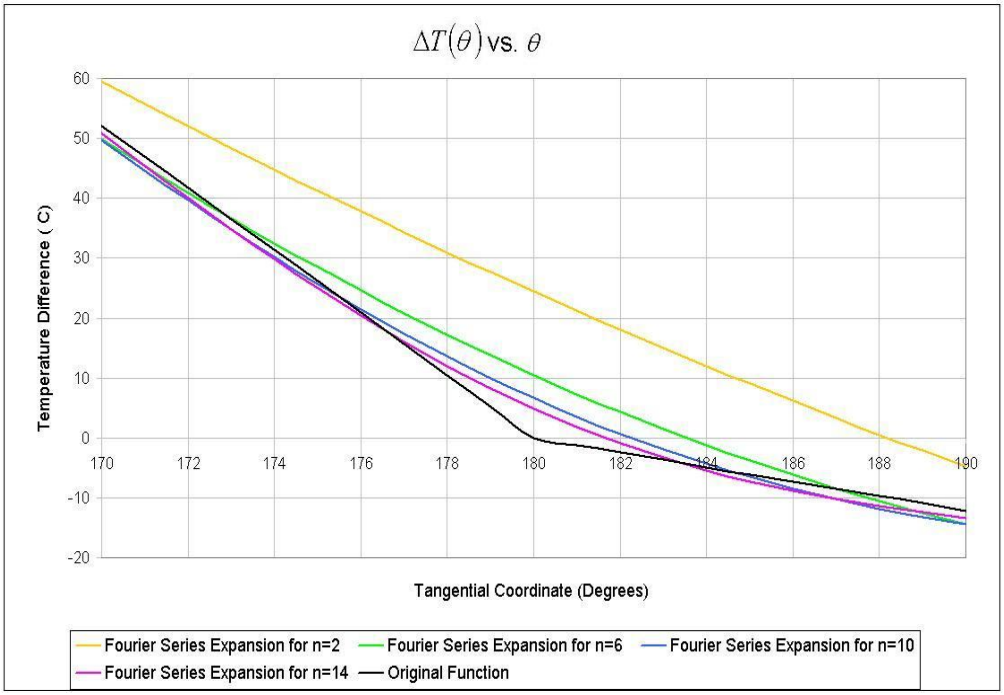

Figure 5.12 Fourier Series Expansion of the Temperature Difference for Various Circumferential Wave Numbers

In this section, effect of circumferential wave number on the results when modelling the unsymmetrical loading with Fourier series is also investigated. Therefore, although the results are primarily given for the final circumferential wave number $n = 14$, results for the circumferential wave numbers less than 14 are also given to demonstrate the change of results with circumferential wave number n. In Figure 5.13, variation of u_ζ^0 with axial coordinate x is given for the tangential location $\theta = 0$ for a number of circumferential wave numbers.

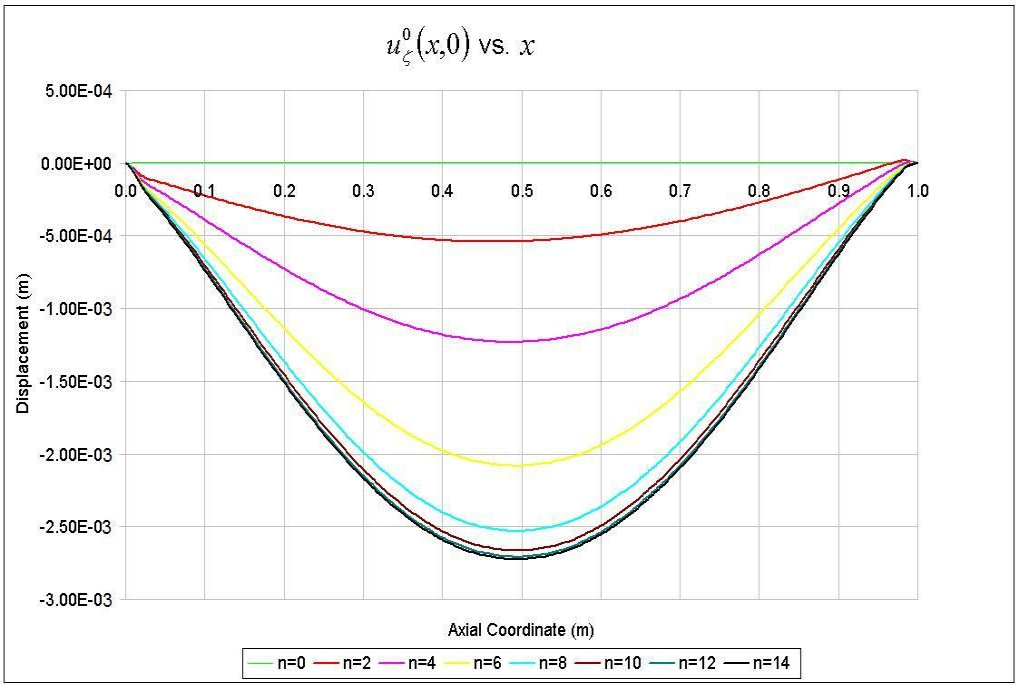

Figure 5.13 Variation of u_ς^0 with x for Various Circumferential Wave Numbers in Problem 5.4

As it is shown in Figure 5.13, the displacement in the thickness direction u_ς^0 converges as the circumferential wave number approaches $n=14$. This behaviour is in accordance with the actual Fourier series representation of the temperature variation given in Figure 5.11. Figure 5.13 also shows that maximum displacement is obtained at $x=0.5$. Therefore, Figure 5.14, which shows the variation of u_ς^0 with θ for various circumferential wave numbers, is plotted for $x=0.5$.

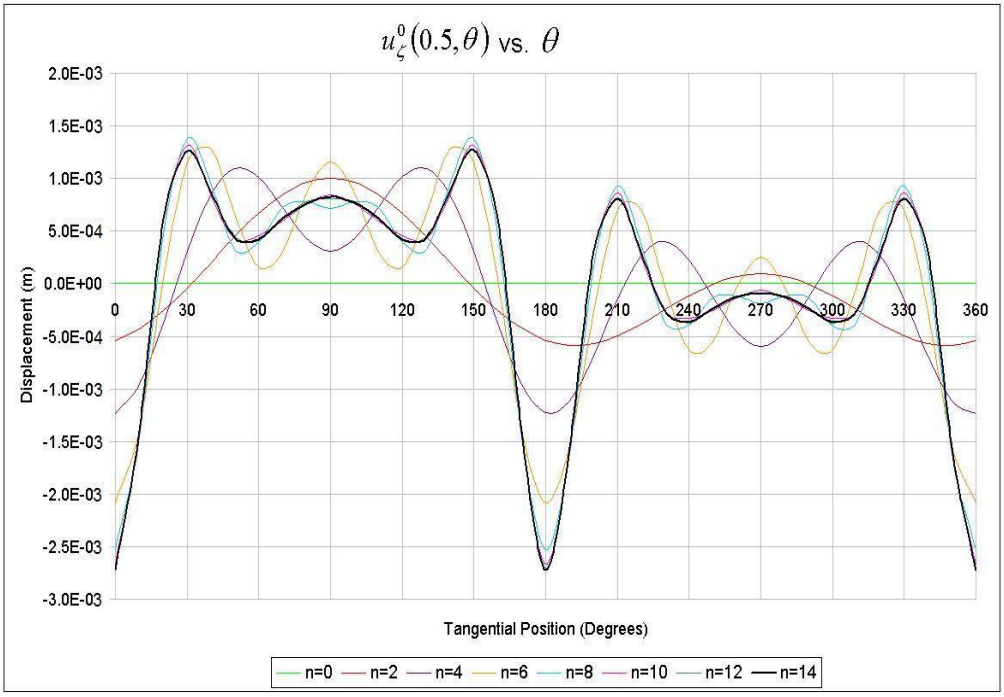

Figure 5.14 Variation of u_ζ^0 with θ for Various Circumferential Wave Numbers in Problem 5.4

Again, it is seen that thickness displacement u_ζ values converge to the solution as the circumferential wave number approaches $n=14$. Maximum percent difference of the solutions for $n=12$ and for $n=14$ is less than 5%. And also since the solution for $n=14$ can not be graphically distinguished from the solution for $n=12$ and can barely be distinguished from the solution for $n=10$, it is concluded that at $n=14$ solution converges. Moreover, it was also shown in Figure 5.11 and Figure 5.12 that the Fourier series of the loading function converges to the original function at a circumferential wave number of 14.

From Figure 5.11 and Figure 5.14, it is apparent that the maximum lateral displacement locations coincides with the angular positions $\theta=0^\circ$ (and $360°$)

and $\theta = 180°$, where the temperature difference changes sign. In Figure 5.15, the variation of tangential displacement u_θ with tangential coordinate θ for various circumferential wave numbers is given at $x = 0.5$.

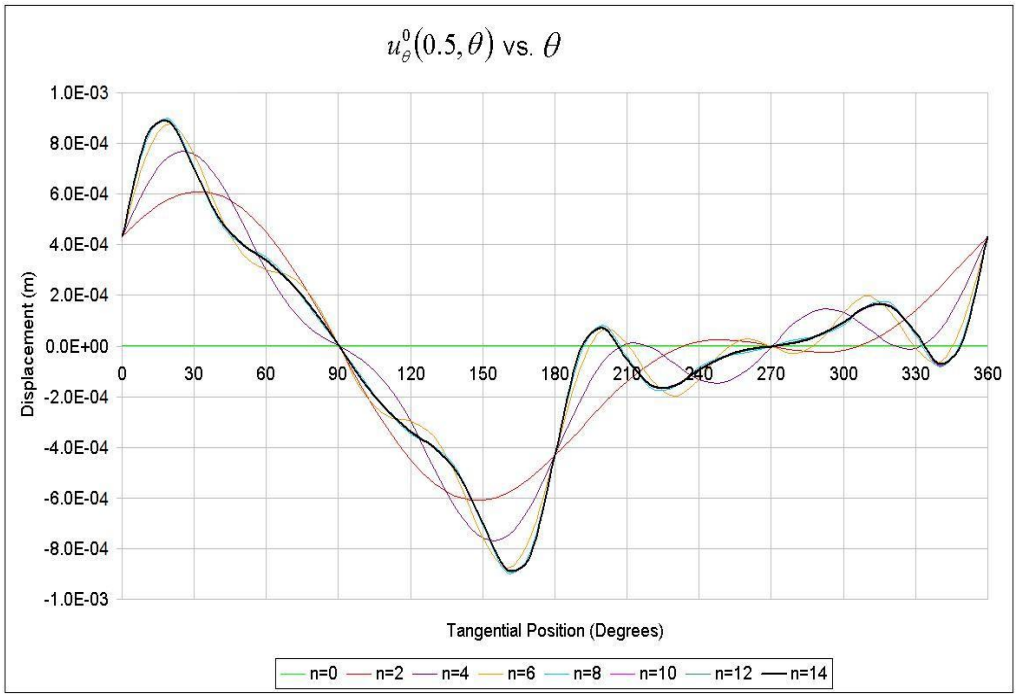

Figure 5.15 Variation of u_θ^0 with θ for Various Circumferential Wave Numbers in Problem 5.4

In Figure 5.15, it is also seen that tangential displacement u_θ^0 values converge at about $n = 14$. After the solution is completed, by using the axial, tangential and thickness displacements, the displaced positions of the grids around the circumference of the cylinder can be calculated in three dimensional space. However, since the loading is constant in axial direction and axial displacement u_x^0 is small compared to u_θ^0 and u_ζ^0, axial displacements are

neglected. Thus, the displaced positions of the grids around the circumference are calculated in two dimensions, at the semi span location, $x = 0.5$.

New positions of the grids constitute the deformed shape of the body at $x = 0.5$. The deformed shape is given in Figure 5.16, along with the undeformed shape. However, since the magnitude of the displacements are on the order of millimetres and therefore the deformed shape cannot be distinguished from the undeformed shape, the displacements are multiplied by 10 and consequently the deformed shape is scaled up to 1/10 in order to exhibit the deformation clearly. It also should be noted that Figure 5.16 shows the mid-plane displacements.

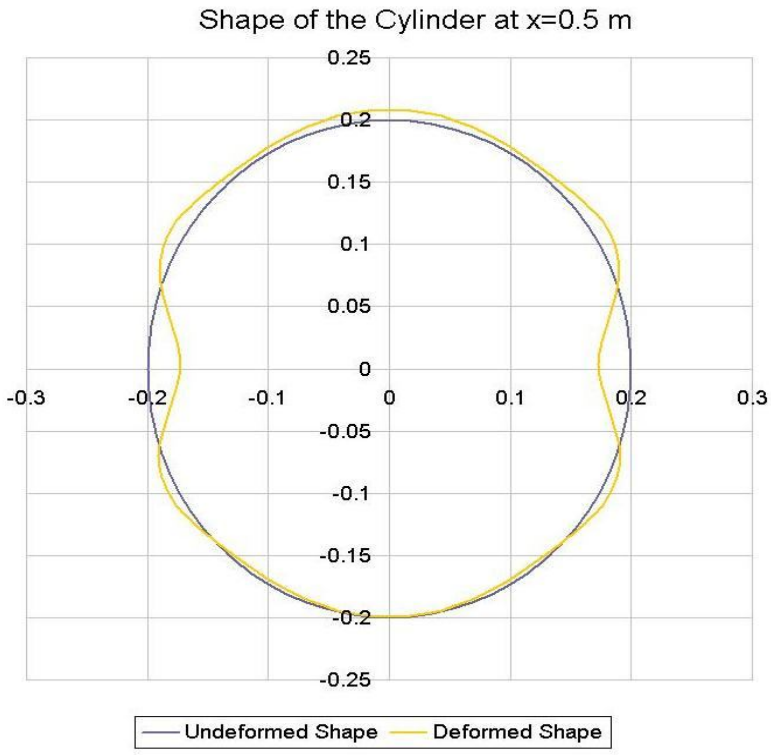

Figure 5.16 Deformed and Undeformed Shape of the Cylinder Cross-Section at $x = 0.5$ (Displacement Scale: 1/10)

In conjunction with Figure 5.14, it is seen that maximum displacements occur near the transition regions ($\theta = 0°, 180°, 360°$) where temperature difference changes from positive to negative values. It should also be noted that the current case studies are analysed under linear elasticity assumptions. The magnitudes of the loads imposed should be checked to see if the resulting displacements can be regarded as small displacements and linear analysis is still applicable. However, in this section the aim was to demonstrate the application of the multi-segment numerical integration technique in the static solution of cylindrical shell of revolution subject to different load types including non-symmetric loads.

In Figure 5.17, the variation of axial stress σ_{xx} with the axial coordinate x is given for various circumferential wave numbers. The stress results are given at $\theta = 0°$ and in layer 4 (layer adjacent to the outer surface of the cylinder).

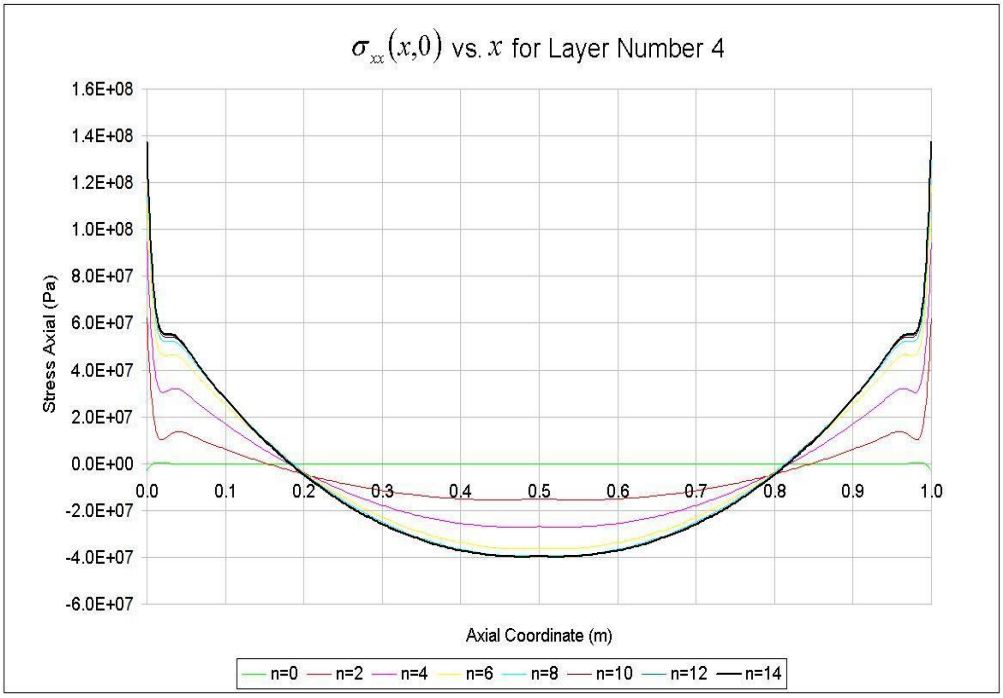

Figure 5.17 Variation of σ_{xx} with x for Various Circumferential Wave Numbers in Problem 5.4

It is seen that axial stress σ_{xx} values also converge to the solution at about $n=14$ as the circumferential wave number n increases. Maximum stress is obtained at the boundaries and the variations are symmetric with respect to $x=0.5$ plane. Figure 5.18 and Figure 5.19 show the variation of σ_{xx} and $\sigma_{\theta\theta}$ respectively with θ for the same circumferential wave numbers, at $x=0.5$ and in layer 4 (layer adjacent to the outer surface of the cylinder).

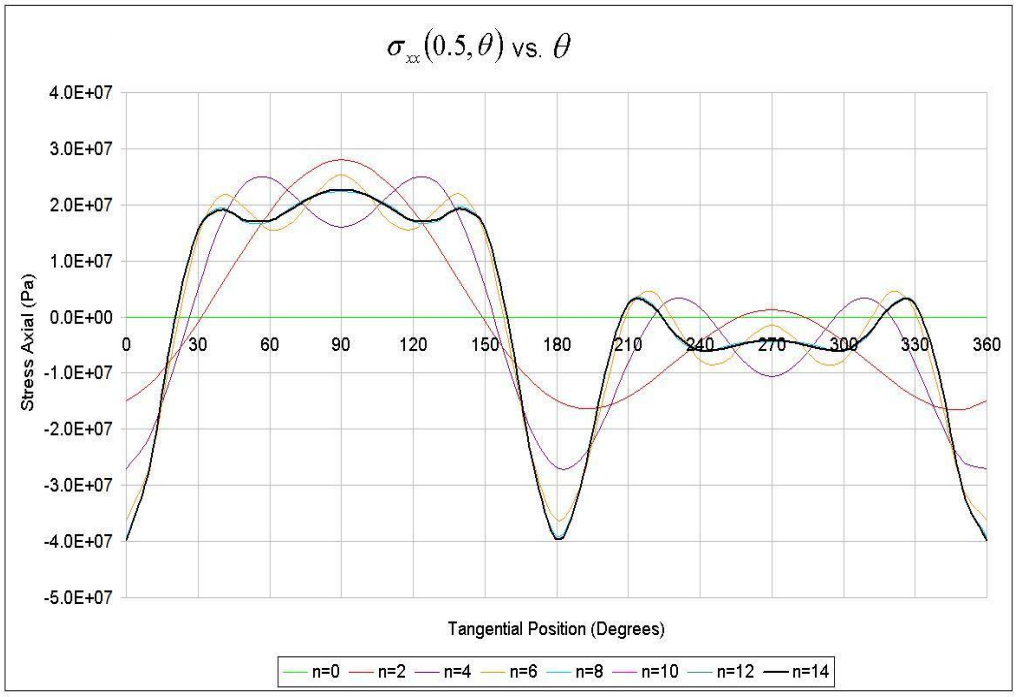

Figure 5.18 Variation of σ_{xx} with θ for Various Circumferential Wave Numbers in Problem 5.4

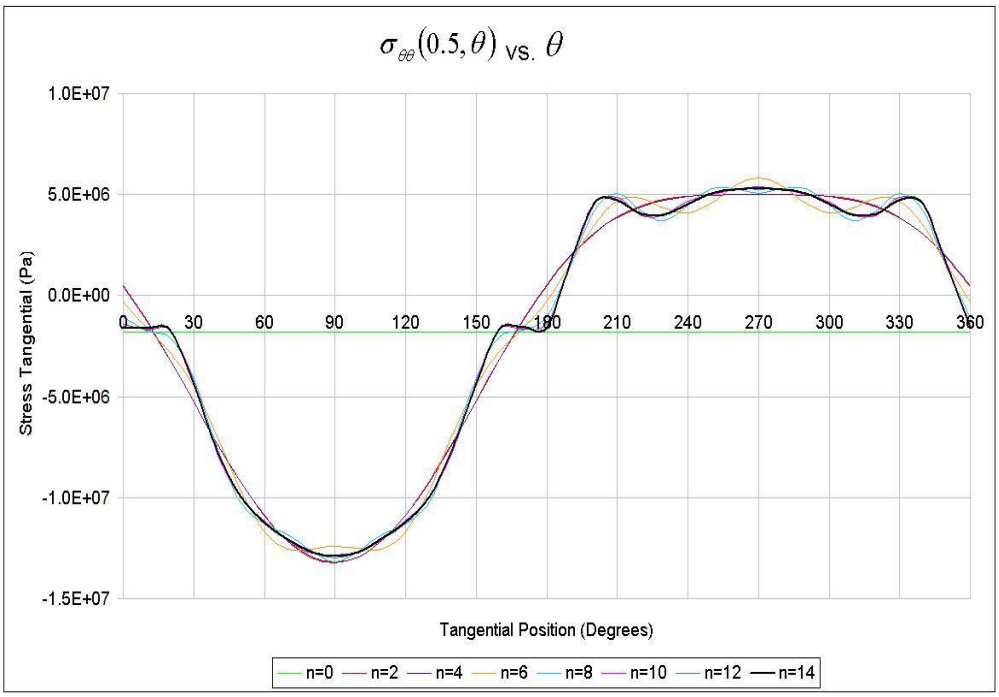

Figure 5.19 Variation of $\sigma_{\theta\theta}$ with θ for Various Circumferential Wave Numbers in Problem 5.4

It is seen in Figure 5.18 that axial stress σ_{xx} is maximum in magnitude at $\theta = 0°$ and at $\theta = 180°$, where positive temperature difference to negative temperature difference transitions occur, similar to the variation of u_ζ with θ. Also σ_{xx} distribution curve has a local maximum at $\theta = 90°$ where the temperature difference is maximum $(300°C)$ around the circumference and has a local minimum at $\theta = 270°$ where the temperature difference is minimum $(-70°C)$ around the circumference of the cylindrical shell.

As opposed to u_θ variation, which is zero at $\theta = 90°$ and at $\theta = 270°$, $\sigma_{\theta\theta}$ values take the minimum and maximum values at these coordinates respectively, as shown by Figure 5.19.

5.5. Transverse Shear Effects

In Chapter 2, classical shell theory equations are modified such that transverse shear strains $\gamma_{\xi\zeta}$ and $\gamma_{\eta\zeta}$ are taken non-zero in order to include the transverse shear effects in the formulation. Therefore, stresses and strains arising from the existence of transverse shear effects can be found. In this section, these results are demonstrated.

In order to obtain not-too-low transverse shear stress values, a laminate consisting of two different lamina materials is analyzed, with a temperature loading, which is changing linearly along the shell in the meridional direction. The material data used, geometric properties, loads and boundary conditions are given together in Table 5.6.

Table 5.6 Analysis Data for the Problem 5.5

Geometry	**Circular Cylinder**
Radius	0.2 m
Axial Length	1.0 m
Number of segments	300
Material	**Laminate Consisting of Two Different Lamina materials**
Ply Material 1	MR50/LTM25 Carbon Epoxy Prepreg [23]
E_{11}	155 GPa
E_{22}	7.31 GPa

Table 5.6 (continued)

υ_{12}	0.345
G_{12}	4.19 GPa
G_{13}	4.19 GPa
G_{23}	3 GPa
Ply thickness	0.146 mm
Ply density (ρ)	1520 kg/m3
α_{11}	-0.43 x 10-6 1/°C
α_{22}	37.4 x 10-6 1/°C
Ply Material 2	CFS003/LTM25 Carbon Epoxy Fabric Prepreg [23]
E_{11}	53.6 GPa
E_{22}	55.2 GPa
υ_{12}	0.042
G_{12}	2.85 GPa
G_{13}	2.85 GPa
G_{23}	2.15 GPa
Ply thickness	0.230 mm
Ply density (ρ)	1450 kg/m3
α_{11}	3.83 x 10-6 1/°C
α_{22}	3.80 x 10-6 1/°C
Laminate	
Number of Layers	5
Ply Materials	Material 1/ Material 2/ Material 1/ Material 2 /Material 1
Ply Orientation	[0°/30°/-30°/45°/60°]

Table 5.6 (continued)

Loads	
ΔT (constant along θ and ζ, variable in x)	$\Delta T = 1000°C$ at $x = 0$, $= 0°C$ at $x = 1$, changing linearly in between
Boundary Conditions	clamped-free
left end	$\left(u_\zeta^0\right)_c, \left(u_\zeta^0\right)_s, \left(u_x^0\right)_c, \left(u_x^0\right)_s, \left(u_\theta^0\right)_c, \left(u_\theta^0\right)_s, \left(\beta_x^0\right)_c,$ $\left(\beta_x^0\right)_s, \left(\beta_\theta^0\right)_c, \left(\beta_\theta^0\right)_s = 0$
right end	$\left(Q_{\phi\zeta}\right)_c, \left(Q_{\phi\zeta}\right)_s, \left(N_{xx}\right)_c, \left(N_{xx}\right)_s, \left(N_{x\theta}\right)_c, \left(N_{x\theta}\right)_s, \left(M_{xx}\right)_c,$ $\left(M_{xx}\right)_s, \left(M_{x\theta}\right)_c, \left(M_{x\theta}\right)_s = 0$

In Figure 5.20 and Figure 5.21, variation of the mid-surface displacements in the thickness direction $\left(u_\zeta^0\right)$ and in the axial direction $\left(u_x^0\right)$ respectively with axial coordinate at $\theta = 0$ is given in order to demonstrate the deformation of the shell.

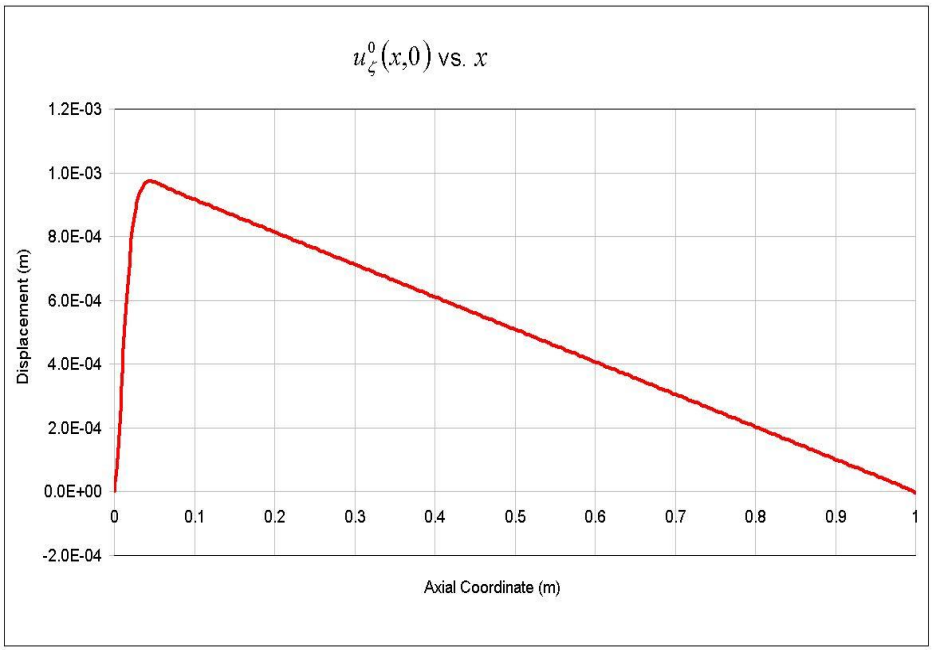

Figure 5.20 Variation of u_ζ^0 with x for Problem 5.5

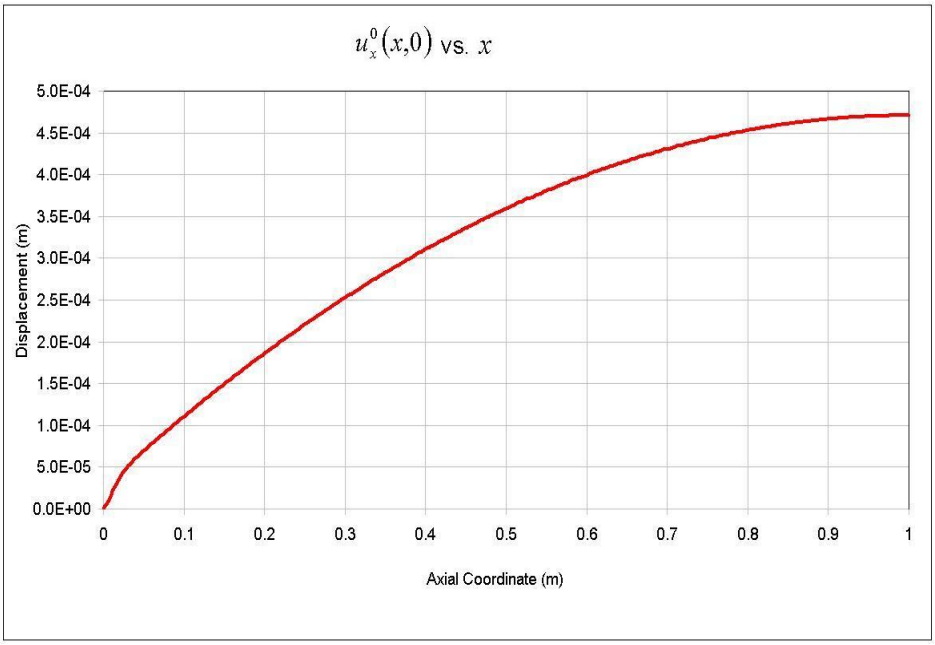

Figure 5.21 Variation of u_x^0 with x for Problem 5.5

It is seen from Figure 5.21 that since the boundary at the right is free, cylinder expands in that direction. u_x^0 is observed to increase quadratically along the cylinder axis. In addition to that, since the temperature difference decreases linearly from the left boundary to the right boundary, mid-surface displacement in the thickness direction $\left(u_\zeta^0\right)$ also decreases linearly in the axial direction, subsequent to reaching a peak value near the fixed boundary.

In Figure 5.22 and Figure 5.23, variation of the transverse force resultant per unit length $\left(Q_{x\zeta}\right)$ with axial coordinate is given at $\theta = 0$. In order to display the results clearly, the cylinder axis is divided into two intervals and given in two separate figures.

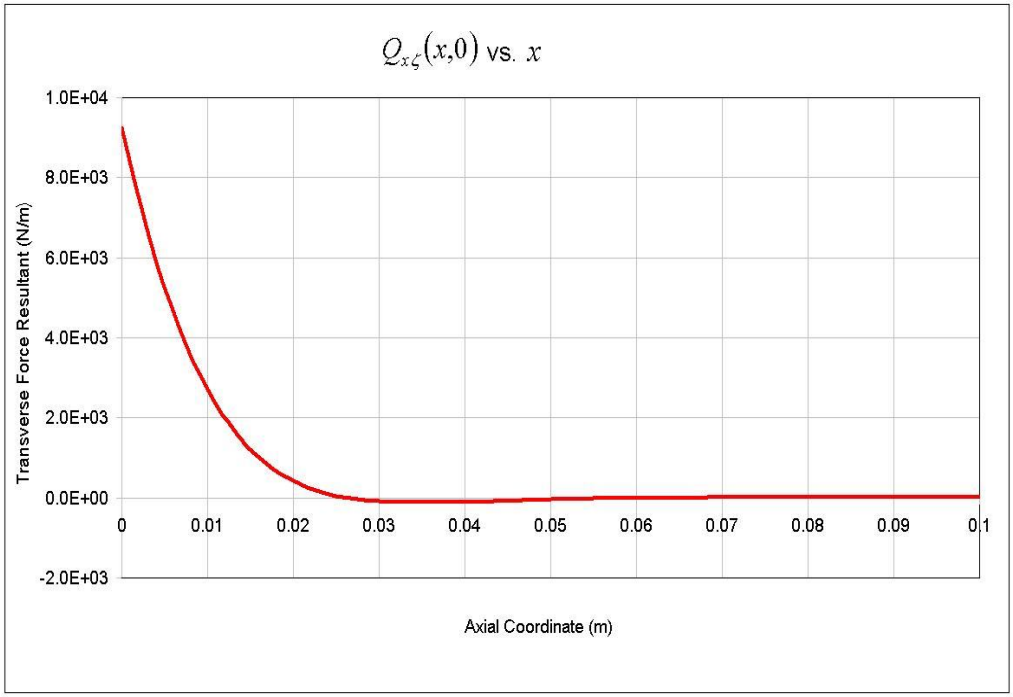

Figure 5.22 Variation of $Q_{x\zeta}$ with x in the Interval [0, 0.1] for Problem 5.5

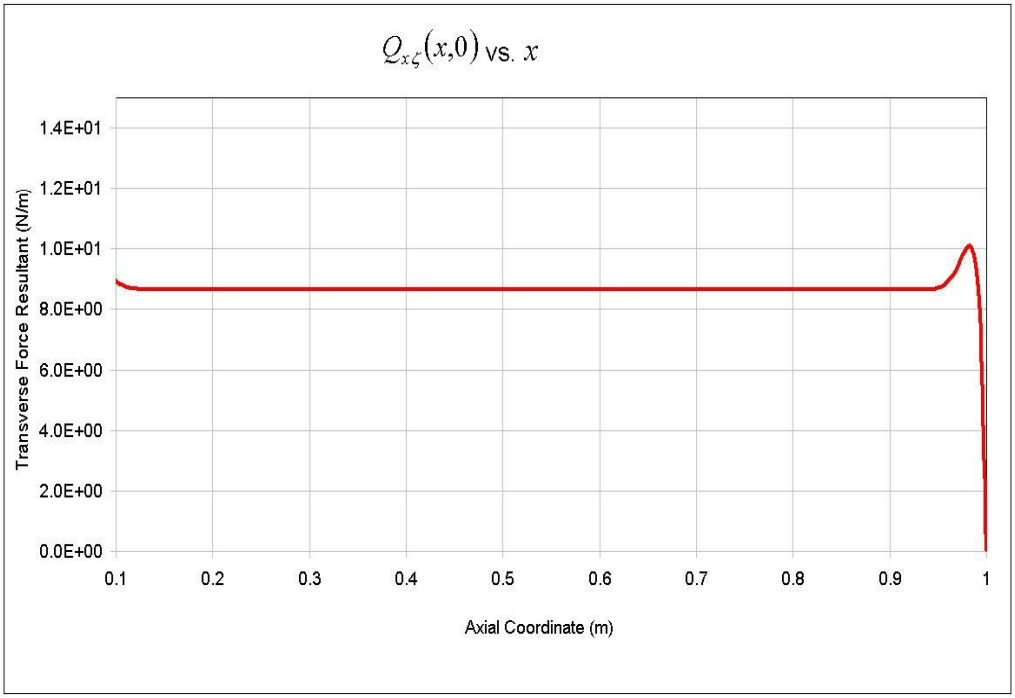

Figure 5.23 Variation of $Q_{x\zeta}$ with x in the Interval [0.1, 1] for Problem 5.5

It should be emphasized that $Q_{x\zeta} = 0$ at the right boundary because that boundary is not constrained and therefore all force and moment resultants are zero. Apart from that, transverse force resultant variation is almost constant away from the boundaries with a value of approximately 8.65 N/m. At the fixed boundary, $Q_{x\zeta}$ is maximum and decreases steeply to its constant value. At the other end, it makes a small peak before its final value at the boundary.

In Figure 5.24 and Figure 5.25 variation of transverse shear stress $\sigma_{x\zeta}$ with the axial coordinate x at $\theta = 0$ is given. Figure 5.26 and Figure 5.27 give the variation of transverse shear stress $\sigma_{\theta\zeta}$ with the axial coordinate x at $\theta = 0$. The transverse shear stresses are plotted for layer 3 which is the middle layer of the laminated shell wall. Once again it should be stressed that stresses are calculated at the mid-surface of the third layer, as shown in Figure 2.6.

Similar to the plots for transverse shear force resultant $Q_{x\zeta}$, in order to display the variation of the transverse shear stresses clearly, the cylinder axis is divided into two intervals and stress results are given in two separate figures for each transverse shear stress.

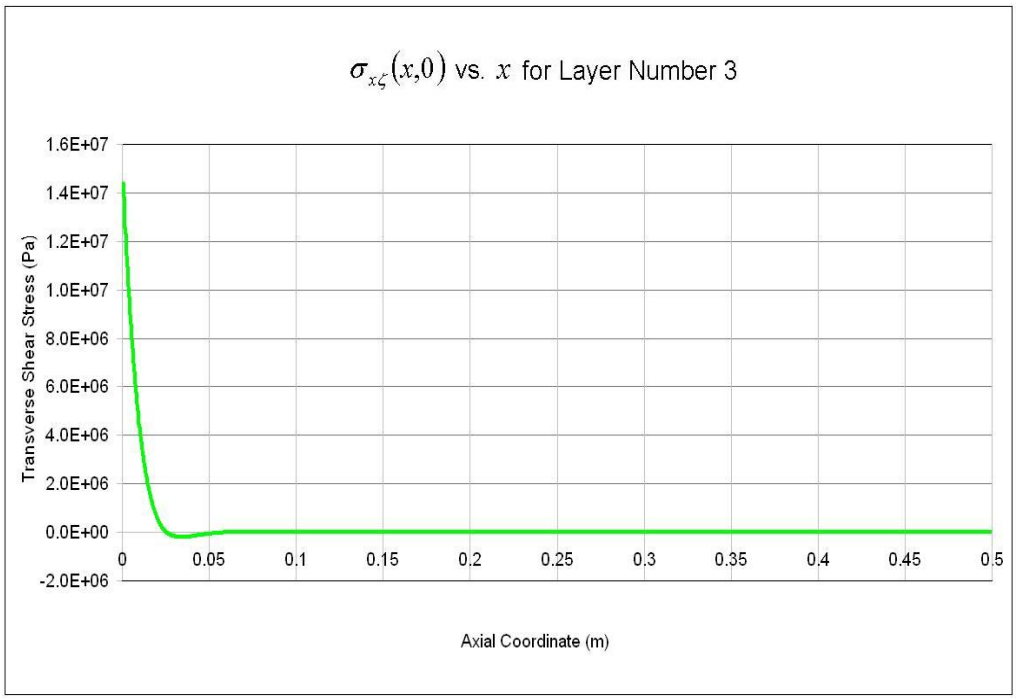

Figure 5.24 Variation of $\sigma_{x\zeta}$ with x in the Interval [0, 0.5] for Problem 5.5

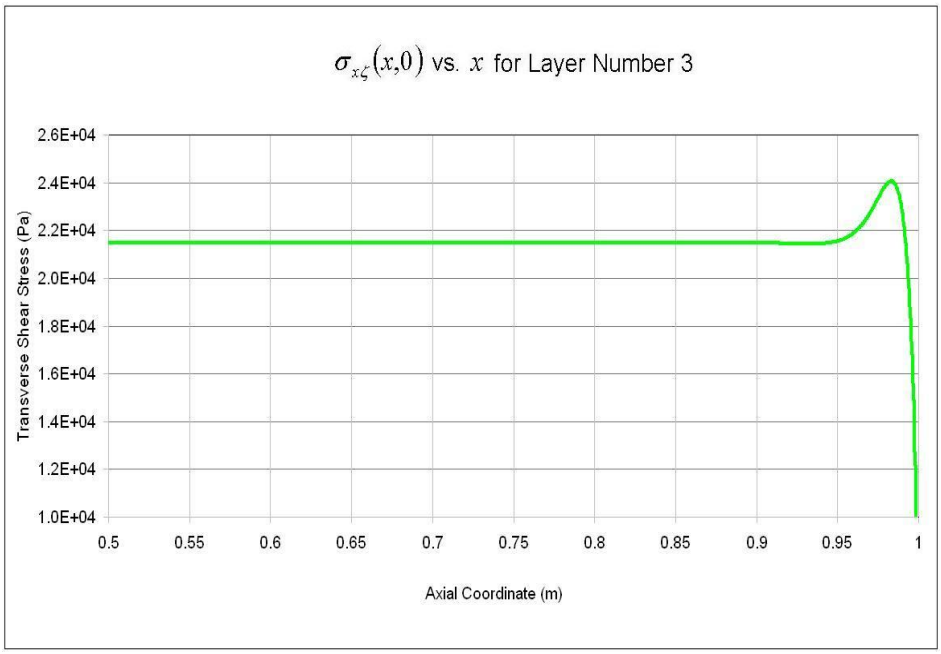

Figure 5.25 Variation of $\sigma_{x\zeta}$ with x in the Interval [0.5, 1] for Problem 5.5

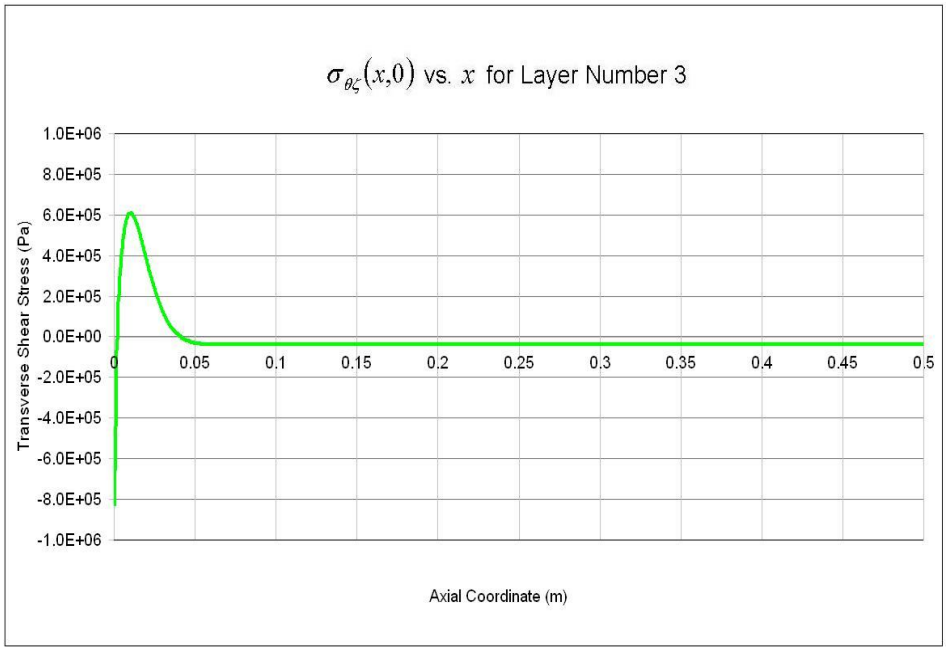

Figure 5.26 Variation of $\sigma_{\theta\zeta}$ with x in the Interval [0, 0.5] for Problem 5.5

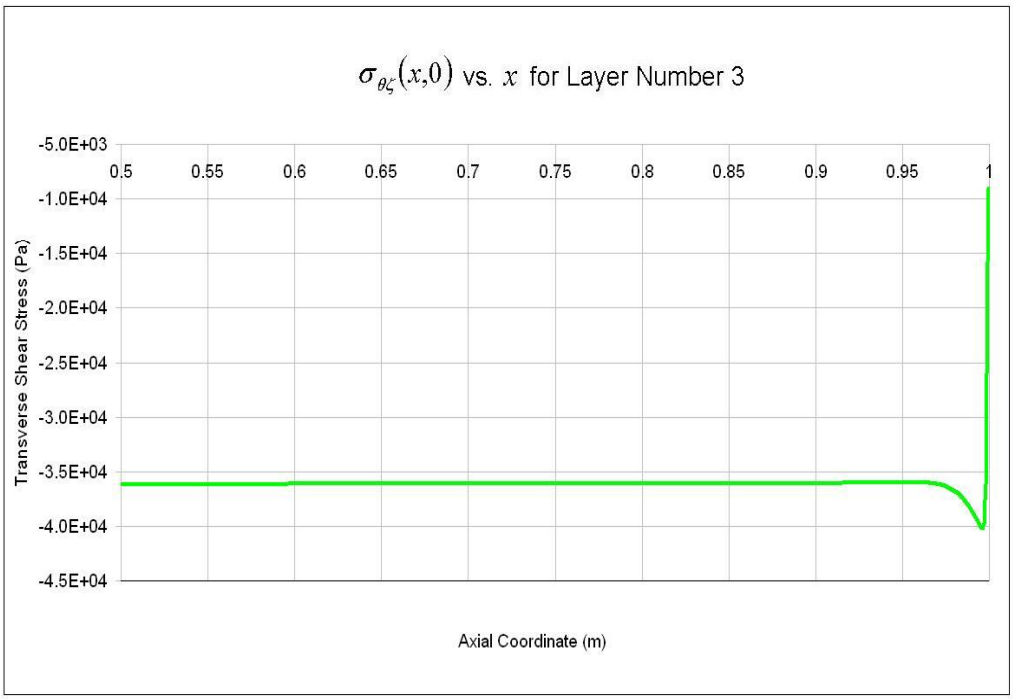

Figure 5.27 Variation of $\sigma_{\theta\zeta}$ with x in the Interval [0.5, 1] for Problem 5.5

The variation of transverse shear stresses $\sigma_{x\zeta}$ and $\sigma_{\theta\zeta}$ are similar to each other and they also show similar behaviour with the transverse force resultant per unit length $Q_{x\zeta}$. However, transverse shear stresses do not vanish at the right boundary, since transverse shear strains are not zero. Transverse shear stresses are maximum at the fixed boundary and make a small peak before the free boundary. Away from the boundaries transverse shear stresses change slightly, with average values of 21500 Pa and -36200 Pa, respectively. However, it should be noted that the transverse shear stresses at the free end show sharp drops. Furthermore, transverse shear strains show similar variations, i.e. they also show sharp drops at the free end and change slightly away from the boundaries, as expected.

It should also be noted that in the present study first order transverse shear deformation theory is used. As it is explained in Section 2.3.3, first order

theory assumes constant transverse shear strain through the thickness and consequently, for each layer a constant transverse shear stress is calculated. Therefore, the first order theory is not adequate to represent the variation of the transverse shear stress through the thickness, because for free inner and outer surfaces the transverse shear stresses must vanish at the inner and outer surfaces. However, in layers near the middle surface of the shell wall the transverse shear stresses calculated based on the first order shear deformation theory is quite satisfactory. And the stress results given in this section are for the 3rd layer, which contains the middle surface. One future work that might be worked on could be to derive the transverse shear stresses from the in-plane stresses that are already determined. This would be a similar approach used in the derivation of the famous transverse shear stress formula for a beam under transverse loading. Since the transverse shear stiffness is already incorporated in the analysis, the fundamental shell variables and the in-plane stresses are more accurate compared to the case in which transverse shear deformation is neglected. After determining the in-plane stresses the transverse shear stresses can be determined by imposing the equilibrium of the infinitesimal shell element. This point is further discussed in Chapter 7.

5.6. An Aerospace Structures Application

Laminated circular cylinders have a vast usage area in aerospace structures, as it is stated earlier. On of the most common applications is the solid propellant rocket motor. A solid-propellant rocket motor consists of a casing, filled with a solid propellant charge, called the grain, which contains all the chemical constituents (fuel plus oxidizer) for complete burning. When ignited, the propellant compounds burn rapidly, expelling hot gases from a nozzle to produce thrust. The propellant burns from the center out toward the sides of the casing. The shape of the center channel determines the rate and pattern of the burn, thus providing a means to control thrust. Unlike liquid-propellant

engines, solid-propellant motors can't be shut down. Once ignited, they burn until all the propellant is exhausted.

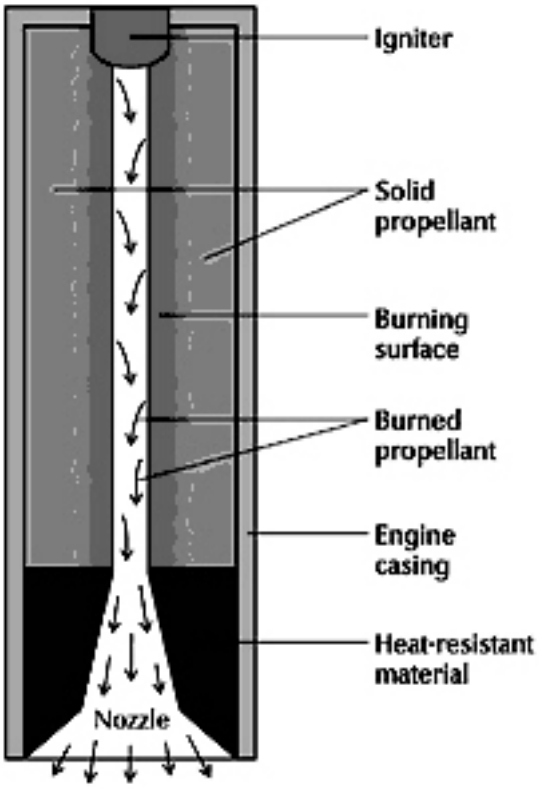

Figure 5.28 A solid Propellant Rocket Motor

Solid propellant rocket motors can be used in long range ballistic missiles as well as short range ballistic missiles. In any case, motors can be analysed statically when they reach steady state during the cruise phase of the mission profiles.

In steady flight, two major types of loading are exerted on the rocket motor: pressure and temperature. In the present study other loads, which can depend on many factors such as the rocket motor and mission profile, are neglected.

Maximum expected operating pressure of a rocket motor also depends on many factors such as the rocket motor geometry and grain size [39], and therefore it is determined by ballistic analyses, which is beyond the scope of this thesis. Therefore, in the present study, pressure exerted on the rocket motor in steady flight is assumed to be 50 bars (5×10^6 Pa).

Another type of loading to be considered is the one arising from the temperature. Like pressure, temperature inside the rocket motor depends on a number of factors such as grain and oxidizer [39], which is again determined by thermal analyses and therefore is a design parameter. However, in some references such as [40] it is stated that temperature inside a rocket motor can reach 3000 K. It should be noted that in real cases this temperature is expected to be on the solid propellant surface and on the motor body this value decreases to lower values due to thermal insulation. For the present case, existence of thermal insulation and the nozzle is ignored and temperature is assumed to be uniformly distributed inside the rocket motor.

Consider a case in which the rocket motor is assembled at 25°C at sea level and cruising at an altitude of 10000 m, where the ambient temperature is about -50°C [41]. Also, if the temperature inside the cylinder is assumed to be 2727°C (3000 K), there exists a sharp temperature difference between inside and outside the cylinder, inside with a temperature difference of 2702°C and outside with a temperature difference of -75° This can be modelled with linear change of temperature difference across the thickness, which is developed in this study.

Such a solid propellant rocket motor can be assumed to be clamped at one end, where it is attached to the other parts of the missile and free at the other end.

In this section, four laminate alternatives, each with a different ply orientation (symmetric and anti-symmetric) is analysed and the results are compared. The

laminate alternatives and ply orientations for each laminate is given in Table 5.7.

Table 5.7 Laminate Alternatives

Laminate	**Material**	**Number of Layers**	**Ply Orientation**
Laminate 1	MR50/LTM25 Carbon Epoxy Prepreg See Table 5.8	4	[45/-45/-45/45]
Laminate 2	MR50/LTM25 Carbon Epoxy Prepreg See Table 5.8	4	[0/90/90/0]
Laminate 3	MR50/LTM25 Carbon Epoxy Prepreg See Table 5.8	4	[30/45/-45/-30]
Laminate 4	MR50/LTM25 Carbon Epoxy Prepreg See Table 5.8	4	[60/30/-30/-30]

Note that Laminate 1 and Laminate 2 are symmetric whereas Laminate 3 and Laminate 4 are anti-symmetric. The geometry, loads, boundary conditions and material data used in the problem is summarized in Table 5.8.

Table 5.8 Analysis Data For Problem 5.6

Geometry	**Circular Cylinder**
Radius	0.04 m
Axial Length	0.5 m
Number of segments	300
Material	
Ply Material	MR50/LTM25 Carbon Epoxy Prepreg [23]
E_{11}	155 GPa
E_{22}	7.31 GPa
υ_{12}	0.345
G_{12}	4.19 GPa
G_{13}	4.19 GPa
G_{23}	3 GPa
Ply thickness	0.146 mm
Ply density (ρ)	1520 kg/m^3
α_{11}	-0.43 x 10^{-6} 1/°C
α_{22}	37.4 x 10^{-6} 1/°C
Laminate	See Table 5.8
Loads	
ΔT (constant along ϕ and θ, changing in ζ)	$\Delta T(\zeta) = 1313.5 - 4.75514 \times 10^5 \times \zeta$
p_ζ (constant along x and θ)	5 MPa
Boundary Conditions	clamped-free
left end	$(u_\zeta^0)_c, (u_\zeta^0)_s, (u_x^0)_c, (u_x^0)_s, (u_\theta^0)_c, (u_\theta^0)_s, (\beta_x^0)_c,$ $(\beta_x^0)_s, (\beta_\theta^0)_c, (\beta_\theta^0)_s = 0$
right end	$(Q_{\phi\zeta})_c, (Q_{\phi\zeta})_s, (N_{xx})_c, (N_{xx})_s, (N_{x\theta})_c,$ $(N_{x\theta})_s, (M_{xx})_c, (M_{xx})_s, (M_{x\theta})_c, (M_{x\theta})_s = 0$

In Figure 5.29, axial variation of u_ζ^0 at $\theta = 0°$ is given for the laminates described in Table 5.7.

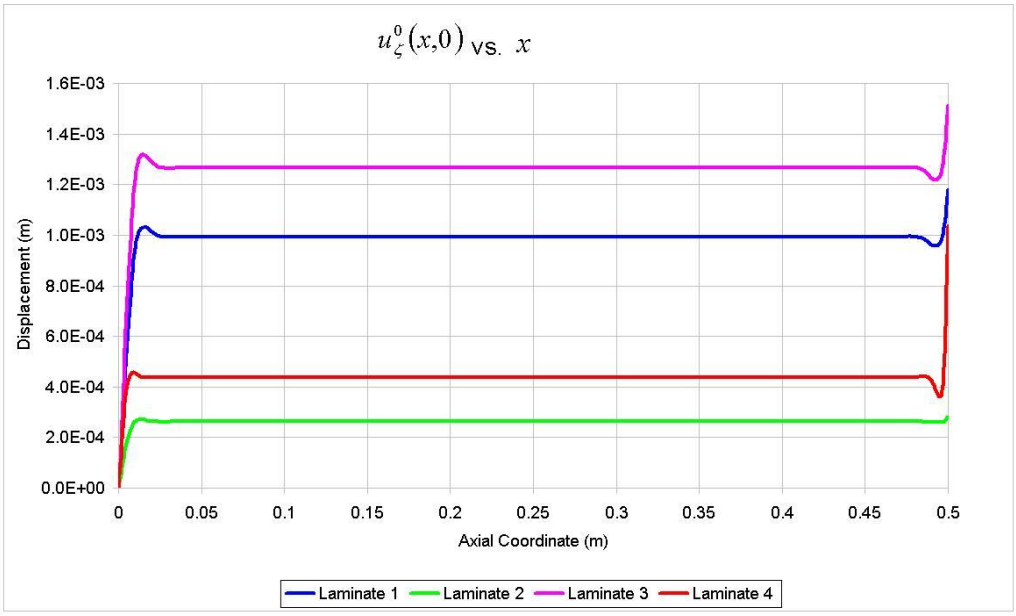

Figure 5.29 Comparison of Solutions for variation of u_ζ^0 with x for Problem 5.6

It is seen that of all the laminates analysed, shell made of laminate 2 deforms least in the thickness direction, followed by the shell made of laminate 4. Figure 5.30 shows the axial variation of u_x^0 at $\theta = 0°$ for laminates 1 – 4.

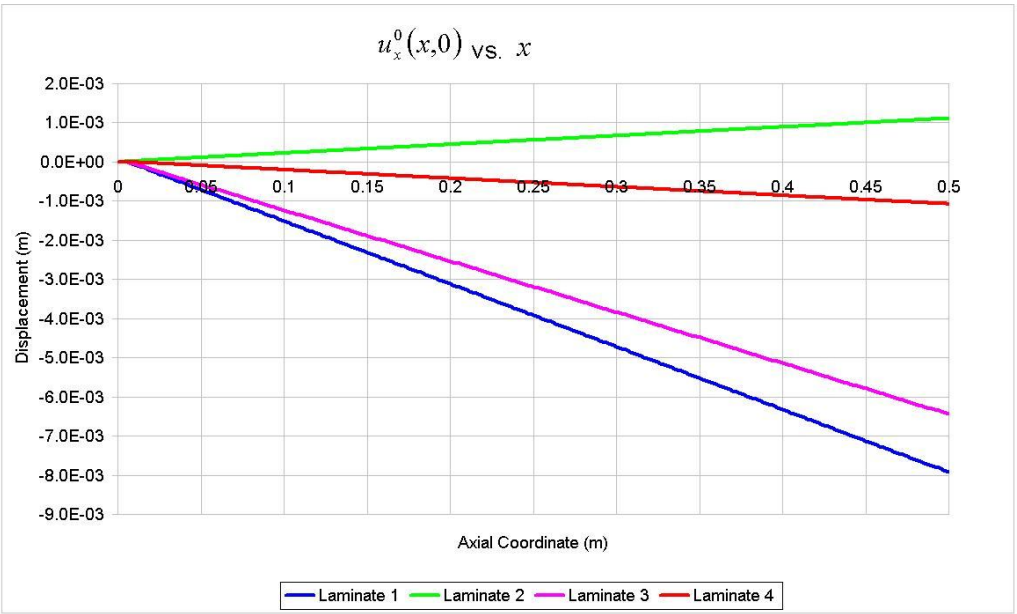

Figure 5.30 Comparison of Solutions for variation of u_x^0 with x for Problem 5.6

Since the ply orientations are different for each laminate, laminate 2 expands while laminates 1, 3 and 4 contract. As far as the orders of magnitude are concerned, axial displacement of shell made of laminate 4 is the least, followed by the shell made of laminate 2. Depending on the design requirements, motor may be desired to expand or contract under such loading conditions. If minimum contraction is desirable, Figure 5.29 and Figure 5.30 together reveal that shell made of laminate 4 can be chosen over the other three alternatives, since it contracts least in the axial direction and also deforms less than twice as much as laminates 1 and 3.

As it is stated in Section 5.4, it should also be noted that the current case studies are analysed under linear elasticity assumptions. The magnitudes of the loads imposed should be checked to see if the resulting displacements can be regarded as small displacements and linear analysis is still applicable. However, in this section the aim was to demonstrate the application of the

multi-segment numerical integration technique in the static solution of a solid propellant rocket motor under the specified steady flight loading conditions.

In addition, the ply orientations chosen here for the analysis of the laminated shell of revolution are also arbitrary, since the aim is again the demonstration of the method. The optimum ply orientation can be determined by a stacking sequence optimization, such as the generic algorithm developed in [42], and the method developed in the present study may be used as a solver subsequent to the optimization of stacking sequence.

Axial variations of axial and tangential stresses for the shell made of laminate 4 are given in Figure 5.31, at $\theta = 0°$ and for layers 1 and 4 (layers adjacent to the inner and outer surfaces of the cylinder, respectively)

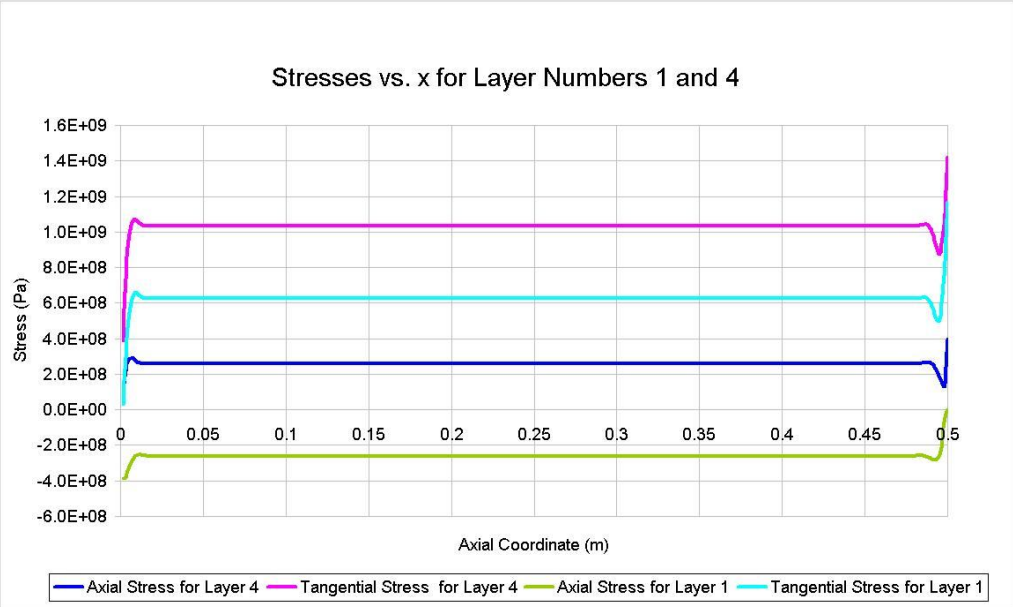

Figure 5.31 Axial Variations of Axial and Tangential Stresses for Laminate 4

As it is seen clearly, behaviours of axial and tangential stresses are similar, with tangential stress being almost three times greater than the axial stress in terms of magnitudes. It can also be concluded that [60°/30°/-30°/-30°] sequence causes the tangential stresses be higher than axial stresses in magnitude.

It should be recalled that during the analyses, temperature difference is modelled to be linearly changing throughout the thickness. In Figure 5.32, variation of axial and tangential stresses with thickness at the mid-span location (x = 0.25 m) and $\theta = 0°$ is given for laminate 4.

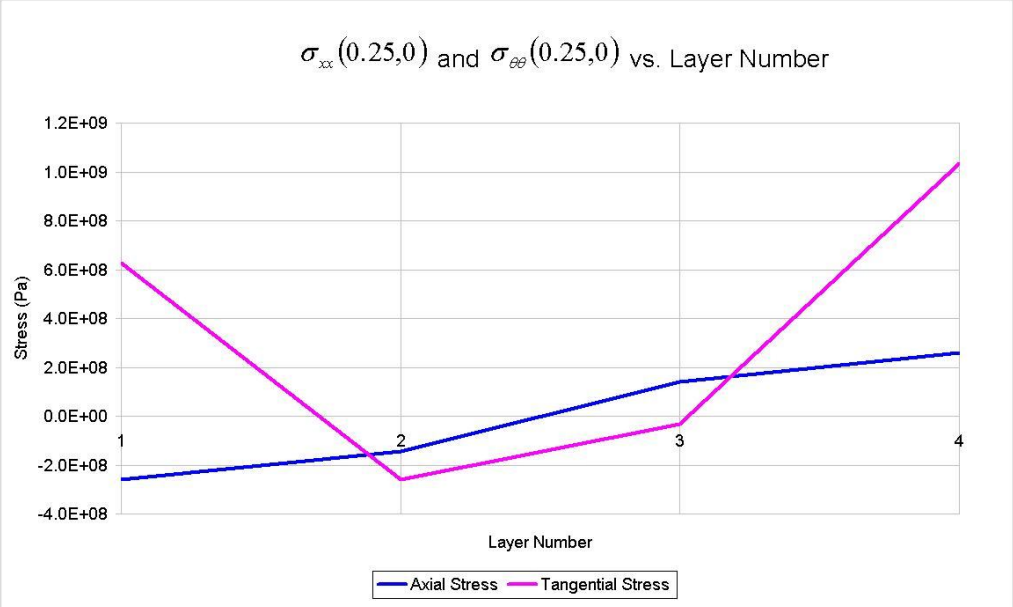

Figure 5.32 Thickness Variation of Axial and Tangential Stresses for Laminate 4

Variation of axial stress exhibits a smoother behaviour throughout the thickness whereas tangential stress variation shows steeper changes especially in the layers adjacent to the inner and outer surfaces of the cylinder.

For both axial and tangential stresses, maximum values occur at layer 4, and this is also the reason to why layer 4 is chosen as one of the thickness positions for the axial variation of axial and tangential stresses. It is also seen that Figure 5.32 is in agreement with Figure 5.31: For axial stress variation, values are negative for layer 1 and positive for layer 4, which can be seen in both figures.

Using the stress values obtained from the analyses, laminates can further be analysed for failure. Laminate strength analysis procedure for failure by itself is another subject of interest, in which various failure algorithms and failure criteria such as Tsai-Hill or maximum stress failure criterion may be employed [4], therefore it is not studied further in the present thesis.

CHAPTER 6

CASE STUDIES FOR GENERAL SHELLS OF REVOLUTION

6.1. Introduction

In Chapter 5, analyses are carried out with various loading cases for circular cylindrical shells. In this chapter, the multisegment numerical integration technique is applied to a shell of revolution geometry other than circular cylinder. In order to achieve this, a truncated spherical shell, which is shown in Figure 6.1, is analysed. As seen in Figure 6.1, the geometrical parameters used for the definition of the shell are:

- The radii in meridional and tangential directions, which are constant and equal to the spherical radius of 1 metre;
- Initial and final meridional positions in terms of the angles measured from the axis of revolution. It should be kept in mind that centres of radii of curvature in meridional and tangential coordinates R_ϕ and R_θ coincide for this geometry.

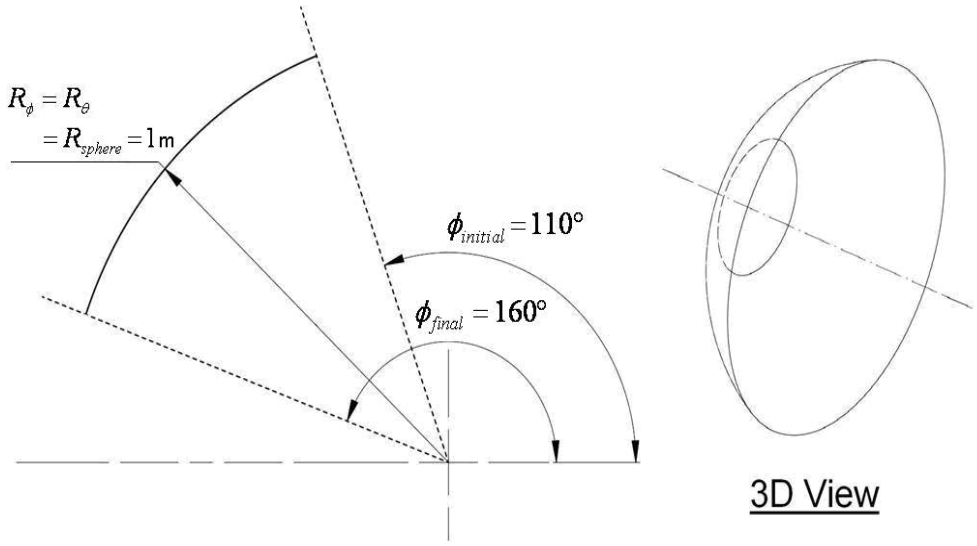

Figure 6.1 Truncated Spherical Shell Geometry Analysed in Chapter 6

In the succeeding sections, the effects of various loading conditions on this truncated spherical shell are examined. In Section 6.2, constant pressure is applied to the shell, and in Section 6.3 spherical truncated shell of revolution is subjected to a number of temperature loads, including the case in which the temperature is linearly changing within the thickness.

In general, in a spherical shell, orientation of fibers in the laminate may be a function of the meridional direction, which depends on the manufacturing process of the laminate. Especially, when the shell is manufactured by the filament winding process, the winding angle and thickness of the shell varies along the meridian of the shell. However, in the present study, in order to demonstrate the application of the multi-segment numerical integration technique to the static analysis of a truncated spherical shell of revolution, orientation of the fibers is assumed to be constant in the meridional direction.

6.2. Pressure Loading

Consider the laminated truncated spherical shell described in Section 6.1 clamped at one end and free at the other is exposed to an internal pressure of 150 kPa which is axisymmetrically and uniformly distributed throughout the shell. The laminate is made of MR50/LTM25 Carbon Epoxy Unidirectional Prepreg [23]. The material data used, geometric properties, loads and boundary conditions are given in Table 6.1

Table 6.1 Analysis Data for Problem 6.2

Geometry	**Truncated Spherical Shell** (See Figure 6.1)
Radii	$R_\phi = R_\theta = R_{sphere} = 1\,\text{m}$
Starting Meridional Position ϕ_{in}	$110°$
Final Meridional Position ϕ_{final}	$160°$
Number of segments	400
Material	
Ply Material	MR50/LTM25 Carbon Epoxy Prepreg [23]
E_{11}	155 GPa
E_{22}	7.31 GPa
υ_{12}	0.345
G_{12}	4.19 GPa
G_{13}	4.19 GPa

Table 6.1 (continued)

G_{23}	3 GPa
Ply thickness	0.146 mm
Ply density (ρ)	1520 kg/m^3
α_{11}	-0.43 x 10^{-6} 1/°C
α_{22}	37.4 x 10^{-6} 1/°C
Laminate	
Number of Layers	4
Ply Orientation	[0°/45°/90°/0°]
Loads	
p_ζ (constant along x and θ)	100 kPa
Boundary Conditions	clamped-free
Starting boundary	$\left(u_\zeta^0\right)_c,\left(u_\zeta^0\right)_s,\left(u_x^0\right)_c,\left(u_x^0\right)_s,\left(u_\theta^0\right)_c,\left(u_\theta^0\right)_s,\left(\beta_x^0\right)_c,$ $\left(\beta_x^0\right)_s,\left(\beta_\theta^0\right)_c,\left(\beta_\theta^0\right)_s=0$
End boundary	$\left(Q_{\phi\zeta}\right)_c,\left(Q_{\phi\zeta}\right)_s,\left(N_{xx}\right)_c,\left(N_{xx}\right)_s,\left(N_{x\theta}\right)_c,\left(N_{x\theta}\right)_s,\left(M_{xx}\right)_c,$ $\left(M_{xx}\right)_s,\left(M_{x\theta}\right)_c,\left(M_{x\theta}\right)_s=0$

In Figure 6.2, change of mid-surface displacement in the thickness direction u_ζ^0 with the meridional coordinate at the tangential position $\theta=0°$ is given.

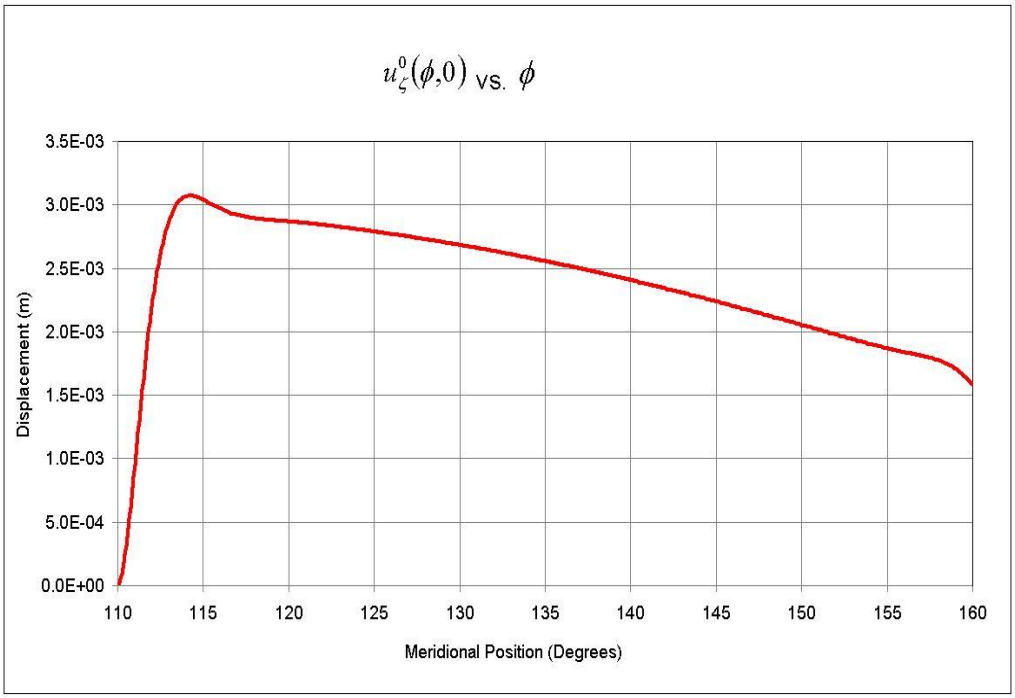

Figure 6.2 Variation of u_ζ^0 with ϕ in Problem 6.2

The variation of u_ζ^0 is similar to that for circular cylinder given in Section 4.2.1 near the starting boundary, increasing to a peak value from zero. However, since the end boundary is free in the current problem, $u_\zeta^0(160°,0)$ is non-zero, therefore u_ζ^0 decreases with an almost constant slope to its value at the end boundary. For the particular load case, the maximum u_ζ^0 displacement is found to be approximately 3.0 mm.

In Figure 6.3, change of mid-surface displacement in the meridional direction u_ϕ^0 with the meridional coordinate at the tangential position $\theta = 0°$ is given.

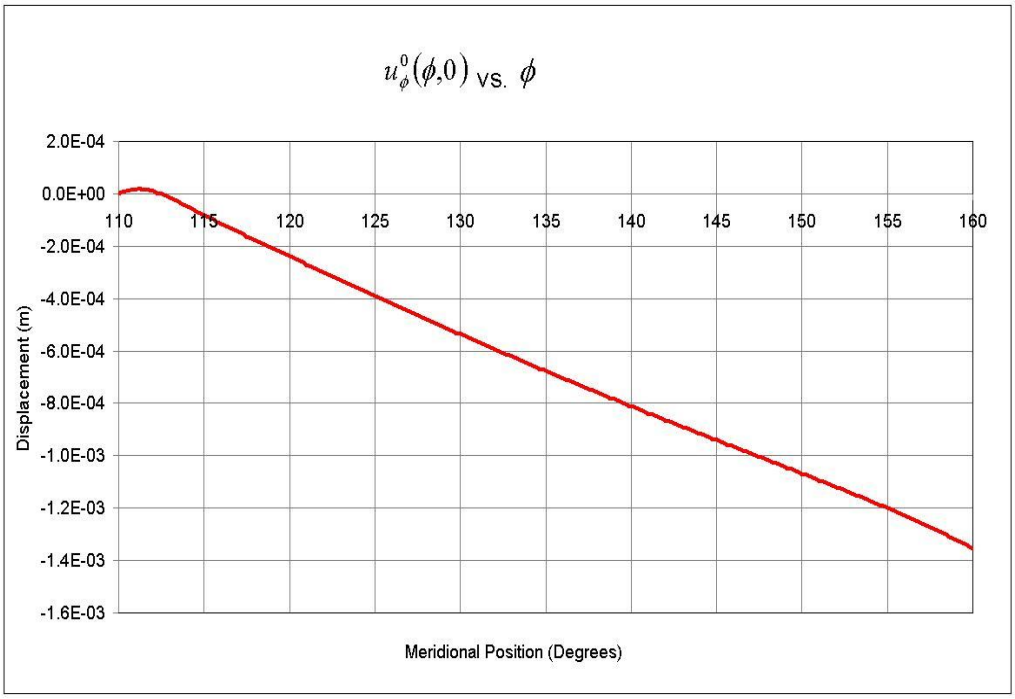

Figure 6.3 Variation of u_ϕ^0 with ϕ in Problem 6.2

Mid-surface displacement in the meridional direction has a quasi-linear change, starting from the clamped boundary until the free boundary. It also should be noted that mid-surface displacements in the meridional direction are smaller than mid-surface displacement in the thickness direction as far as the order of magnitudes are concerned.

In Figure 6.4, change of meridional stress $\sigma_{\phi\phi}$ with the meridional coordinate at the tangential position $\theta = 0°$ and for layer 1 (first layer inside the cylinder) is given. It should be noted that as shown in Figure 2.6, stresses are calculated at the mid-surface of each layer.

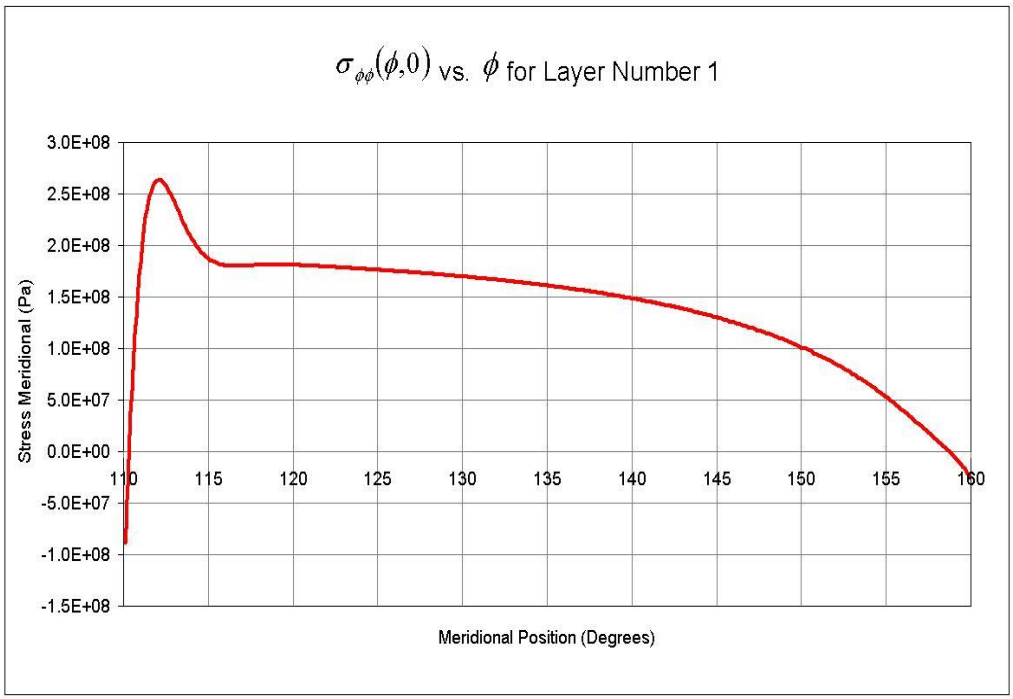

Figure 6.4 Variation of $\sigma_{\phi\phi}$ with ϕ in Problem 6.2

Meridional stress variation is also similar to that for circular cylinder given in Section 4.2.1 near the starting boundary, increasing to a peak value from zero. Then it decreases gradually since the end boundary is free.

In Figure 6.5, change of meridional stress $\sigma_{\phi\phi}$ with layer number at the mid-span location, which is $\phi = 135°$ and tangential position $\theta = 0°$ is given.

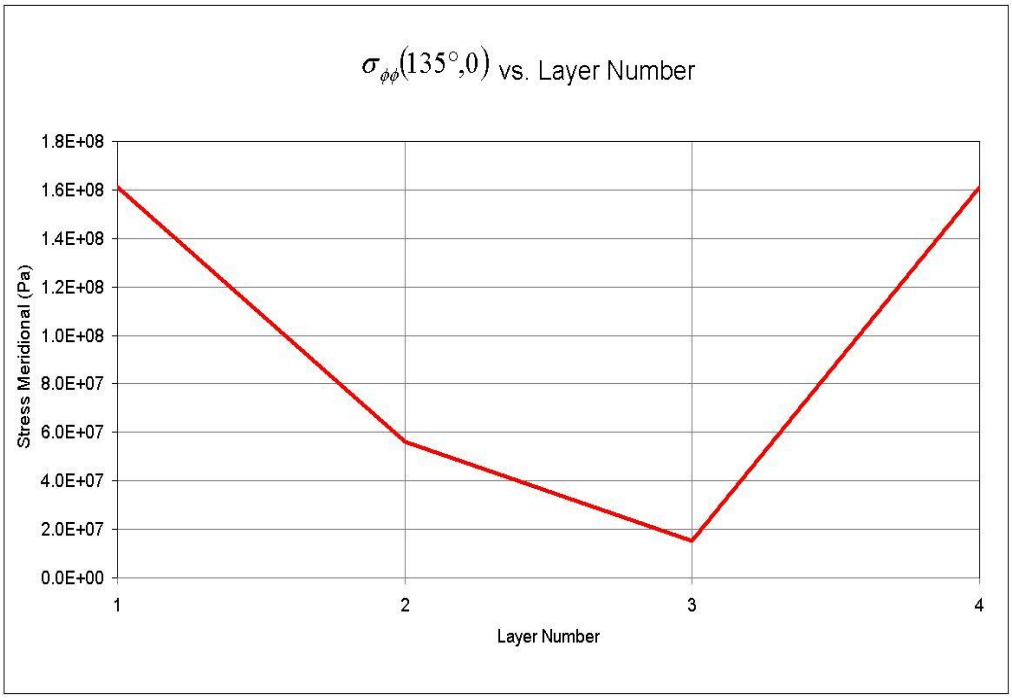

Figure 6.5 Variation of $\sigma_{\phi\phi}$ with Layer Number in Problem 6.2

In Figure 6.5, first point (point at layer number = 1) refers to the meridional stress at mid-surface location of the 1st layer. The same is true for the other layers, ranging from 2 to 4. In this sense, the linear variation between layer number 1 and layer number 2 refers to the linear change of meridional stress between the mid-surface locations of the first and second layers. Again the same argument is applicable to the other layers from 2 to 4.

Meridional stress is highest at the layers next to the inner and outer surfaces of the shell and they have smaller values at the layers near the mid-surface. Stress variation is linear since stresses are linearly connected to overall strains through Equation (3.7.28) and overall strains change linearly through the thickness, as shown in Equations (3.7.1) – (3.7.3).

6.3. Temperature Loading

In this section, the response of the truncated spherical shell to various temperature loads is given. For this problem, four different load cases are compared.

In the first and second cases, temperature differences of 50°C and 200°C, which are constant through the thickness, are considered respectively. For the third case, a varying temperature difference through the thickness is considered such that the inner temperature difference is taken as 50°C and the outside temperature difference is taken as 200°C. Thus, this load case can easily be compared with first and second cases. In the fourth load case, a temperature difference twice as big as the third case is exerted. Load conditions for all cases are given together in Table 6.2. In order to demonstrate the effect of temperature change with thickness clearly, temperature differences in meridional and tangential directions are kept constant.

Table 6.2 Temperature Difference Values for the Load Cases 1 – 4

Cases	**Temperature Differences**
Case 1 $(\Delta T1)$	$\Delta T_{in} = \Delta T_{out} = 50°C$
Case 2 $(\Delta T2)$	$\Delta T_{in} = \Delta T_{out} = 200°C$
Case 3 $(\Delta T3)$	$\Delta T_{in} = 50°C$, $\Delta T_{out} = 200°C$
Case 4 $(\Delta T4)$	$\Delta T_{in} = 100°C$, $\Delta T_{out} = 400°C$

As it was explained in Section 2.3.2, and Section 5.2, thermal loads were derived by assuming linear variation of the temperature across the shell

thickness. The thickness coordinate ζ is equal to zero at the mid-surface of the laminate, and its positive direction is towards outer surface of the shell. Thus, by using Equation (5.2.1), temperature difference can be written as a linear function of ζ. The temperature variation across the thickness, material data used, geometric properties, and boundary conditions are summarized in Table 6.3.

Table 6.3 Analysis Data for the Problem 6.3

Geometry	**Truncated Spherical Shell** (See Figure 6.1)
Radii	$R_\phi = R_\theta = R_{sphere} = 1\,\text{m}$
Starting Meridional Position ϕ_{in}	$110°$
Final Meridional Position ϕ_{final}	$160°$
Number of segments	400
Material	
Ply Material	MR50/LTM25 Carbon Epoxy Prepreg [23]
E_{11}	155 GPa
E_{22}	7.31 GPa
υ_{12}	0.345
G_{12}	4.19 GPa
G_{13}	4.19 GPa
G_{23}	3 GPa
Ply thickness	0.146 mm
Ply density (ρ)	1520 kg/m^3
α_{11}	-0.43 x 10^{-6} 1/°C

Table 6.3 (continued)

α_{22}	37.4 x 10^{-6} 1/°C
Laminate	
Number of Layers	4
Ply Orientation	[0°/45°/90°/0°]
Load Cases	
$\Delta T1$ (constant along ζ) (Case 1)	50°C
$\Delta T2$ (constant along ζ) (Case 2)	200°C
$\Delta T3 = \Delta T3(\zeta)$ (Case 3)	$\Delta T3(\zeta) = 125 + 2.56849 \times 10^5 \times \zeta$
$\Delta T4 = \Delta T4(\zeta)$ (Case 4)	$\Delta T4(\zeta) = 250 + 5.13698 \times 10^5 \times \zeta$
Boundary Conditions	clamped-clamped
Starting boundary	$(u_\zeta^0)_c, (u_\zeta^0)_s, (u_x^0)_c, (u_x^0)_s, (u_\theta^0)_c, (u_\theta^0)_s, (\beta_x^0)_c, (\beta_x^0)_s, (\beta_\theta^0)_c, (\beta_\theta^0)_s = 0$
End boundary	$(u_\zeta^0)_c, (u_\zeta^0)_s, (u_x^0)_c, (u_x^0)_s, (u_\theta^0)_c, (u_\theta^0)_s, (\beta_x^0)_c, (\beta_x^0)_s, (\beta_\theta^0)_c, (\beta_\theta^0)_s = 0$

In Figure 6.6 change of u_ζ^0 with the meridional coordinate at the tangential position $\theta = 0°$ is given for the cases described above

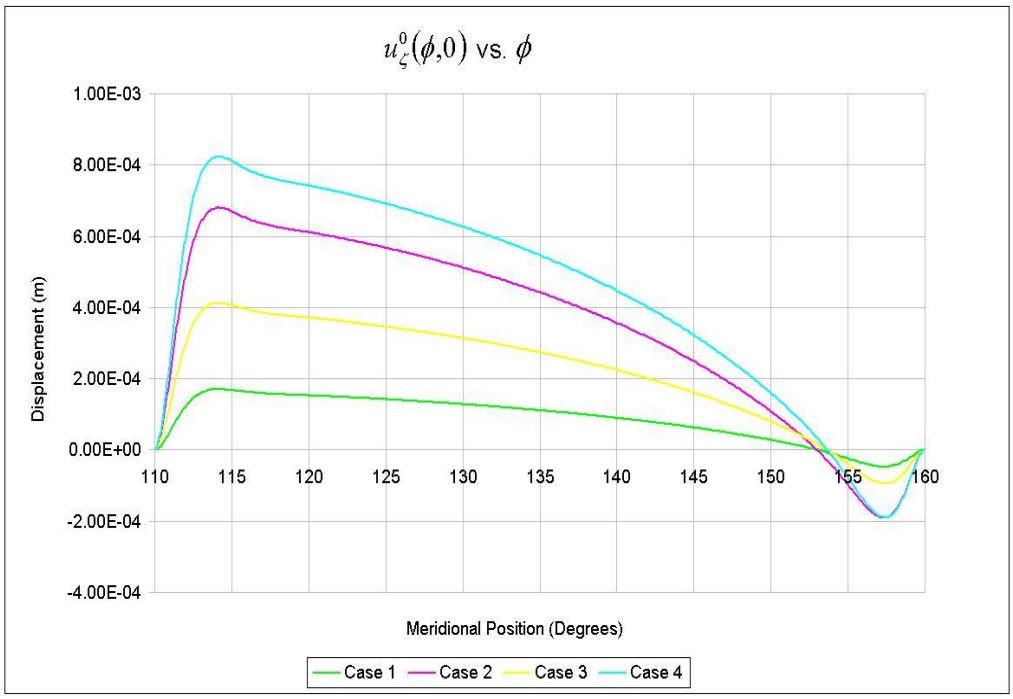

Figure 6.6 Comparison of Solutions for Variation of u_ζ^0 with ϕ for Cases 1 – 4

It is seen that general behaviour of the four load cases are the nearly same with each other. Unlike the cylindrical shell geometry used in Chapter 5, the truncated shell of revolution is not symmetric with respect to a tangential plane and therefore the results are not symmetric with respect to $\phi = 135°$ plane

Another observation is that lateral displacement response for Case 3 is between the responses for Case 1 and Case 2. If it is recalled that $\Delta T = 50°$ for Case 1; $\Delta T = 200°$ for Case 2 and ΔT is linearly changing between 50° and 200° through the thickness for Case 3, this result is expected.

It should also be recalled that temperature difference ΔT for Case 4 is twice as high as the temperature difference ΔT for Case 3. Since the solution method developed in this study uses linear elasticity relations, displacements are also expected to be twice as high. In Figure 6.6, it is clearly seen that

absolute values of displacements at Case 4 are indeed twice as high as those at Case 3.

In Figure 6.7, change of $\sigma_{\phi\phi}$ at layer 4 (outer layer) with the meridional coordinate at the tangential position $\theta = 0°$ is given for the Cases 1 – 4. Stresses are calculated at the mid-plane of the layer.

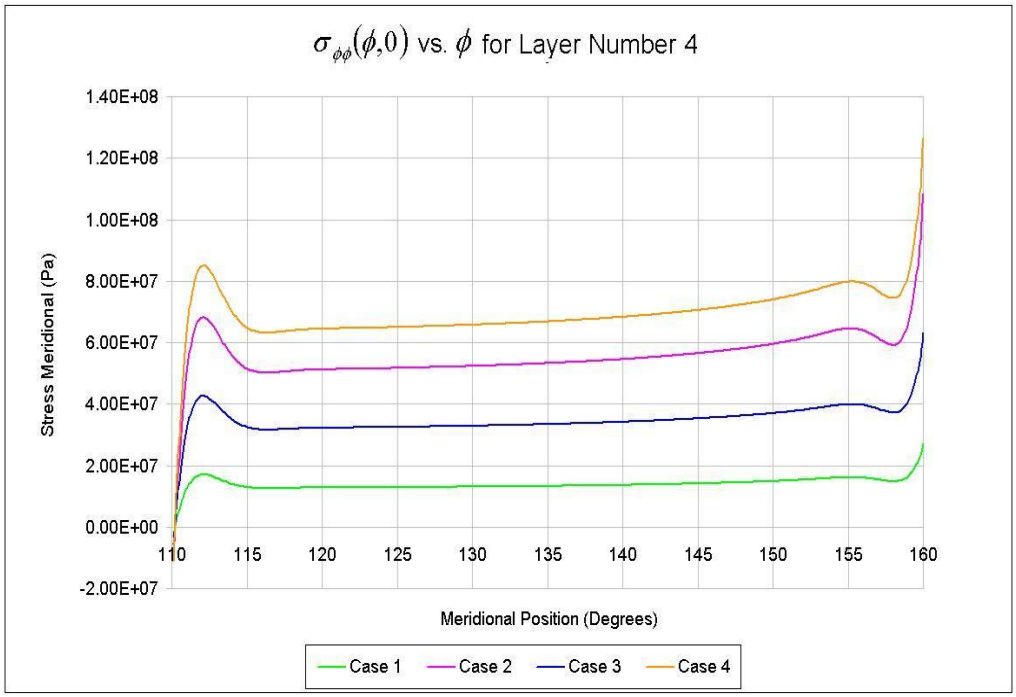

Figure 6.7 Comparison of Solutions for Variation of $\sigma_{\phi\phi}$ at layer 4 with ϕ for Cases 1 – 4

The meridional variations of $\sigma_{\phi\phi}$ are seen to be similar to the variation of axial stress, σ_{xx} for the circular cylinder which is subjected to similar loads (in Figure 5.4). However, for the truncated spherical shell case the meridional

stress is not symmetric with respect to a tangential plane since the geometry is not symmetric with respect to a tangential plane.

Another observation is that, like in Figure 6.6, it is seen that stress response curve for Case 3 is between the stress response curves for Case 1 and Case 2. However it should be noted that these variations are at layer 4 and stresses in Case 2 are higher than stresses in Case 3, although ΔT is equal for Cases 2 and 3 at that layer. Examining the loading condition of Case 3 reveals that in layers 1, 2 and 3 temperature differences ΔT are lower than the constant temperature difference ΔT of Case 4, which causes the lower stresses at layer 4 than the stress in Case 2.

In addition, similar to the case in the displacements, stresses are also expected to be twice as high in Case 4 as in Case 3, since ΔT for Case 4 is twice as high as ΔT for Case 3. Figure 6.7 shows that stress values at Case 4 are twice as high as stress values at Case 3, in agreement with the theory.

In Figure 6.8, solutions for variation of $\sigma_{\phi\phi}$ with layer number for Cases 1 – 4 are compared. It is seen in Figure 6.7 that the meridional stress does not change steeply with the meridional coordinate ϕ in the interval [115°, 155°]. Therefore, for the output of results a meridional location in this interval is chosen as $\phi = 135°$. Tangential location is again taken as $\theta = 0°$.

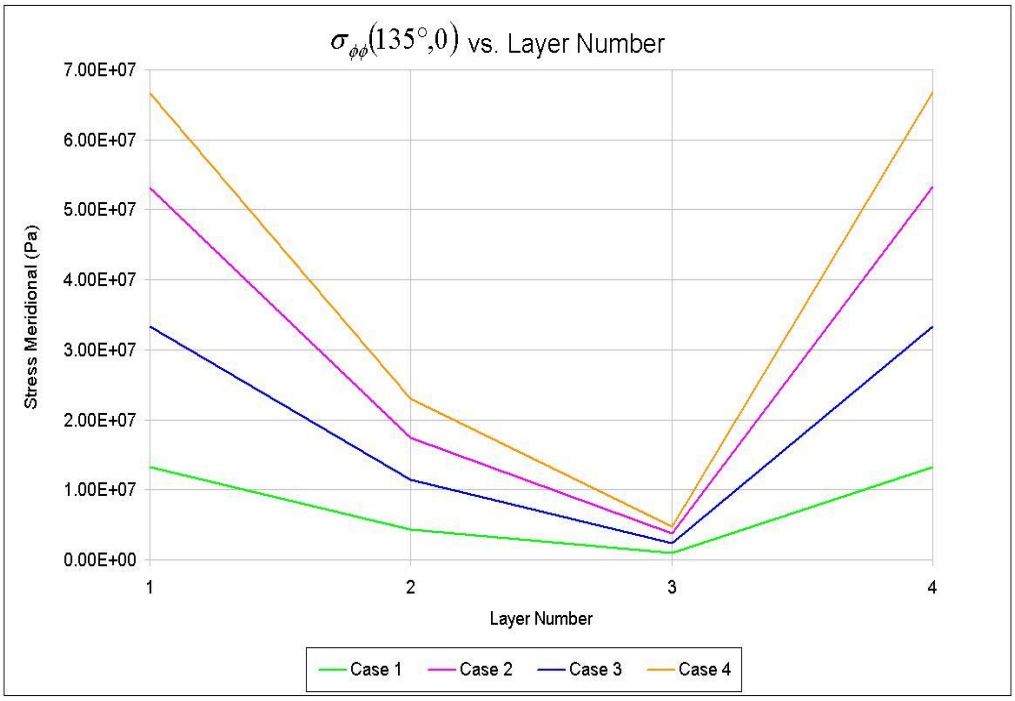

Figure 6.8 Comparison of Solutions for Variation of $\sigma_{\phi\phi}$ with Layer Number for Cases 1 – 4

The effect of temperature difference on the variation of the meridional stresses in the layers of the truncated spherical shell for the load cases 1, 2 and 3 shows the following behaviour. As expected, stresses for the load Case 3 are between stresses for load Cases 1 and 2 in each layer. In addition, meridional stresses in each layer for Case 4 are twice as high as the stresses for Case 3. This result again proves the correct use of linear elasticity relations throughout the multi-segment numerical integration technique that is developed for the static analysis of macroscopically anisotropic general shells of revolution including transverse shear deformation.

Also it is seen that stresses for load Case 4 are higher than stresses for Case 2 in layer 1, although the temperature difference is higher for Case 2 in that layer. This behaviour shows that the local temperature difference is not very

significant in the stress variation, but the variation of the temperature difference throughout the whole thickness is more effective.

CHAPTER 7

CONCLUSIONS & FUTURE WORK

A number of sample cases are analyzed using both the code developed in this study and the finite element analysis tool NASTRAN, as it is explained in Chapter 4. The results are compared and excellent agreement is found for fundamental variables. Since NASTRAN is a displacement based finite element analysis solver; similar to the method developed in this study, the displacements are calculated primarily and the stresses and strains are found consecutively using the displacements, by post-processing. Therefore, although still less than 10% at maximum, the percent difference of stress results between two methods is higher compared to the fundamental variable results, especially at the boundaries.

Consequently, the present technique, besides providing an alternative solution methodology to study the stress and deformation behaviour of anisotropic shells of revolution under non-symmetric loading, can be reliably used as an alternative computational tool to compare against the other solution methodologies.

It should be stressed that the methodologies used in the present study are based on analytical methods, except the numerical integration scheme used in multisegment method of integration and the finite difference method used for the calculation of strains as a first iteration step only in the post-processing of circular cylindrical shells.

It has been shown in Sections 4.2.1 and 4.2.2 that the code developed in this study solves the problems in the sections mentioned about 49 times faster compared to the finite element analysis solver NASTRAN when the shell is divided into 300 segments along the meridian of the shell. Obviously, it should be kept in mind that in the finite element model when 300 elements are placed along the meridian of the shell, the element length in the circumferential direction cannot be arbitrary in order not to end up with an element configuration with a high aspect ratio. Therefore, finite element model becomes very crowded in terms of element and node numbers. For a particular problem one could get reliable results with a much coarser mesh, and in that case the solution times of the present method and finite element method could approach each other. However, in this examples solved in Chapter 4 the comparison is made for 300 segments along the meridian of the shell, and for this size the present method is much faster than the finite element method.

It also should be noted that although it is not quantified, the initial preparation time of the input files for the present method is also much less compared to the pre-processing time of the finite element model. To reduce the finite element solution time further, finite element mesh can be made much coarser in the regions where there are no significant gradients, and the solution time by the finite element solver can be reduced down. However, in that case the pre-processing time would increase. Based on the case studies performed, especially for problems in which gradients of the field quantities are high, the numerical integration based method used in the present study has less solution time compared to the finite element method.

In the present study, extension of the multisegment numerical integration method due to Kalnins [7] is extended to the solution of stress and deformation analysis of anisotropic shells of revolution through the use of finite exponential transform of the fundamental system of equations

It can be deduced from the results of Section 4.2.4 that the results obtained by the multisegment integration method do not change significantly beyond a particular number of segments. 300 segments, which was selected at the beginning of the comparison studies in Chapter 4, is an arbitrary number and in practice number of segments can be decreased to lower values and still accurate results can be obtained. Because as stated earlier, in the multisegment numerical integration technique by decreasing the number of segments one does not actually reduce the accuracy as in finite element analysis. Solutions at the ends of the shell segments will still have sufficient accuracy but the resolution will be lowered. Therefore, one has to calculate the fundamental variables at the intermediate locations afterwards by making use of the fundamental variables determined at the end of the shell segments.

It should be added that by using the multisegment method of integration, concentrated (point) loads can also be exerted on the shell, by defining the distributed loads only at a single segment along the meridional direction. However, the load should be modelled accordingly in the tangential direction using the Fourier series, since it will be an unsymmetrical loading case.

In this study, the applicability of the method of solution is further extended to include the first order transverse shear deformation. However, the first order transverse shear deformation theory has certain drawbacks as indicated in the text. Since the first order shear deformation theory assumes constant transverse shear strain through the thickness, the variation of the transverse shear stresses cannot be obtained accurately if the constant shear strain is multiplied by the reduced stiffness coefficients to determine the transverse shear stresses in each layer of the shell wall.

More correct way to calculate the transverse shear stresses could be accomplished by integrating the stress equilibrium equations for the shell of revolution type studied. By making use of the already determined in-plane stresses along with the continuity relations of the transverse shear stresses at the ply interfaces, and bottom and top surface conditions on the transverse

shear stresses, through-the thickness variation of the transverse shear stresses can be calculated more accurately. Nevertheless, transverse shear stresses calculated based on the first order shear deformation theory is quite satisfactory in layers near the middle surface of the shell wall.

It should be noted since transverse shear stiffness coefficients are included in the initial numerical integration based solution strategy, the in-plane stresses are calculated accurately within the borders of the shell theory used, compared to the theories in which transverse shear deformations are neglected.

In Sections 5.2 and 6.3, the effect of temperature difference linearly changing throughout the thickness is examined and its results are compared with the results of the case in which temprature difference is constant throughout the thickness. In the end it is seen that although shell thickness is very small compared to its other dimensions, the results are effected significantly with respect to the case where no temperature difference change occurs throughout the thickness.

The derivation of the transverse shear stresses from the in-plane stresses which are already determined can be considered as a future work. As stated in Section 5.5, this would be a similar approach used in the derivation of the famous transverse shear stress formula for a beam under transverse loading. After determining the in-plane stresses the transverse shear stresses can be determined by imposing the equilibrium of the infinitesimal shell element, as stated above.

Furthermore, in order to predict the transverse shear effects more accurately throughout the thickness and satisfy traction conditions on top and bottom surfaces, numerical integration based method of solution can be used in conjunction with higher order transverse shear deformation theories, such as those mentioned in [37] and [38].

The method can further be extended to the analysis of filament wound shells of revolution with general meridional curvature. Filament winding is the most commonly used technique to manufacture shells of revolution. In case of filament wound shells of revolution the winding angle and the thickness vary along the meridional coordinate only if the fibers are placed along the geodesic or semi-geodesic paths on the surface of the shell of revolution. Therefore, the change of the winding angle and the thickness must be included in the analysis.

Extension of the numerical integration based method of solution to geometrically non-linear problems and thermoelastic analyses can also be worked on as a future work.

Loads due to moisture can be included in the formulation of loads, for the cases in which moisture effects become dominant.

Finally, the method developed in this thesis can be used as a solver in an extended solution algorithm in which additional solution procedures such as stacking sequence optimization and laminate failure analysis are included.

REFERENCES

[1] Kayran A., *Free vibration analysis of laminated composite shells of revolution including transverse shear deformation*, PhD Thesis, Department of Mechanical Engineering, University of Delaware, 1990.

[2] Yavuzbalkan E., *Free vibration analysis of anisotropic laminated composite shells of revolution*, MSc Thesis, Department of Aerospace Engineering, Middle East Technical University, 2005.

[3] Soedel W., *Vibration of Shells and Plates*, Marcel Dekker, New York, 1993.

[4] Jones R. M., *Mechanics of Composite Materials*, Hemisphere, New York,1975.

[5] Dym C. L., Shames I. H., *Solid Mechanics A Variational Approach*, McGraw-Hill, New York, 1973

[6] Leissa A. W., *Vibration of Shells*, NASA SP-288, Washington, D.C., 1973

[7] Kalnins A., *Analysis of Shells of Revolution Subjected to Symmetrical and Nonsymmetrical Loads*, J. Appl. Mech. 31, 467-476 (1964).

[8] Lestingi J., Padovan J., *Numerical analysis of anisotropic rotational shells subjected to nonsymmetric loads*, Computers and Structures 3 (1974) 133-147.

[9] Reissner E., *A new derivation of the Equations for the deformation of elastic shells*, American Journal of Mathematics 63 (1941) 177-184.

[10] Mindlin R.D., *Influence of rotatory inertia and shear on flexural motions of isotropic, elastic plates*, Journal of Applied Mechanics 18 (1951) 31-38.

[11] Reddy J. N., *Mechanics of Laminated Composite Plates – Theory and Analysis*, Boca Raton, USA, CRC Press, 1997.

[12] Vinson J. R., and Sierakowski, R. L., *The Behaviour of Structures Composed of Composite Materials*, Martinus Nijhoff, Hingham, Massachutsetts, 1986

[13] Reissner E., *On a Variational Theorem In Elasticity, Journal of Mathematics and Physics*, 29:90-95, 1950

[14] Whitney J.M., *The effect of transverse shear deformation on the bending of laminated plates*, *Journal of Composite Materials* 3 (1969) 534-547.

[15] Kreyszig E., *Advanced Engineering Mathematics*, Wiley, New York, 1999

[16] Chapra S.C., Canale R.P., Numerical Methods For Engineers, McGraw-Hill, New York, 2002

[17] Lestingi J., Padovan J., *Complex Numerical Integration Procedure For Static Loading of Anisotropic Shells of Revolution*, Computers and Structures 4 (1974) 1159-1172.

[18] Visual Numerics Inc., http://www.vni.com, last accessed date: 30/08/2008

[19] MacNeal-Schwendler Corporation (MSC), http://www.mscsoftware. com, last accessed date: 30/08/2008

[20] Tyson, H. N. Jr., *Caltech Direct Analog Computer and the Development of Nastran*, http://www.me.caltech.edu/centennial/history/nastran.htm,

last accessed date: 30/08/2008

[21] Sparrow, W. V., *Fuzzy Structures Analysis of Aircraft Panels in NASTRAN,* AIAA-2001-1320, AIAA/ASME/ASCE/AHS/ASC Structures, Structural Dynamics, and Materials Conference and Exhibit, 42nd, Seattle, WA, Apr. 16-19, 2001.

[22] Allman, D. J., *Implementation of a Flat Facet Shell Finite Element for Applications in Structural Dynamics,* Computers and Structures 59, (1996) 657-663.

[23] Cruz, J. R., Shah, C. H., Postyn, A. S., *Properties of Two Carbon Composite Materials using LTM25 Epoxy Resin*, NASA Techical Memorandum 110286, 1996.

[24] A.K. Noor, J.M. Peters, *Vibration analysis of laminated anisotropic shells of Revolution*, Computer Methods in Applied Mechanics and Engineering 61 (1987) 277-301.

[25] Toorani, M.H., Lakis A.A., *General Equations of anisotropic plates and shells including transverse shear deformations, rotatory inertia and initial curvature effects*, Journal of Sound and Vibration 237 (2000) 561-615.

[26] The Mathworks Inc., http://www.mathworks.com, last accessed date: 30/08/2008

[27] Reddy, J.N., *An Introduction to the Finite Element Method*, McGraw-Hill, New York, 2006.

[28] MacNeal, Richard H., *The NASTRAN Theoretical Manual*, December 1972

[29] Parametric Technology Corporation,

http://www.ptc.com/products/mathcad, last accessed date: 30/08/2008

[30] Ugural, A. C., Fenster, S. K., *Advanced Strength and Applied Elasticity*, Prentice Hall, New Jersey, 1995

[31] Beer, F. P., Johnston, E. R., *Vector Mechanics for Engineers*, McGraw-Hill, Toronto, 1998.

[32] Flügge, W., *Stresses in Shells*, Springer-Verlag, Berlin, 1973

[33] Hoskin, B. C., Baker, A. A., *Composite Materials for Aircraft Structures*, AIAA, New York, 1986

[34] Felippa, C. A., *Advanced Finite Element Methods,* Graduate Course Material, University of Colorado, Boulder, 2006

[35] Gürdal, Z., Haftka, R. T., Hajela, P., *Design And Optimization of Laminated Composite Materials,* Wiley, New York, 1999

[36] Armstrong, K. B., Barret, R. T., *Care and Repair of Advanced Composites*, SAE International, 1997

[37] Cook, G. M., *A Higher-Order Bending Theory for Laminated Composite and Sandwich Beams*, NASA Contractor Report 201674, March 1997

[38] Tessler, A., *An Improved Plate Theory of {1,2}-Order for Thick Composite Laminates*, Int'l J. Solids and Structures, 30, pp. 981-1000, 1993.

[39] Sutton, G. P., *Rocket Propulsion Elements,* Wiley-Interscience, 2000

[40] Gudu, T., Ak, M. A., Vural, H., *Estimation of erosive combustion in solid propellant rocket motor by detailed strain gage measurement,* AIAA-1997-

3108 AIAA/ASME/SAE/ASEE Joint Propulsion Conference and Exhibit, 33rd, Seattle, WA, July 6-9, 1997

[41] Anderson, J. D., *Aircraft Performance and Design*, McGraw-Hill International 1999.

[42] Kutay H., *Stacking Sequence Optimization Of A Composite Pressure Vessel By Genetic Algorithm,* MSc Thesis, Department of Aerospace Engineering, Middle East Technical University, 2007.

APPENDIX A

COEFFICIENTS OF THE HOMOGENEOUS PART IN THE FUNDAMENTAL SYSTEM OF EQUATIONS DERIVED IN SECTION 3.2

Coefficients of $\frac{\partial u_\zeta}{\partial \phi}$ equation, i.e. Equation (3.2.5)

$$cp_{11} = -\frac{R_\phi A_{45}}{R_\theta \sin\phi \cdot A_{55}} \tag{A.1}$$

$$c_{12} = 1 \tag{A.2}$$

$$c_{13} = \frac{R_\phi A_{45}}{R_\theta A_{55}} \tag{A.3}$$

$$c_{14} = -R_\phi \tag{A.4}$$

$$c_{15} = -\frac{A_{45} R_\phi}{A_{55}} \tag{A.5}$$

$$c_{16} = \frac{R_\phi}{A_{55}} \tag{A.6}$$

Coefficients of $\frac{\partial u_\phi}{\partial \phi}$ equation, i.e. Equation (3.2.8)

$$c_{21} = \left(\frac{1}{\Delta}\right)\left\{\begin{array}{l}\left(\frac{1}{R_\phi}\right)\left[(-A_{11})(U1)+(-A_{16})(U2)+(-B_{11})(U3)+(-B_{16})(U4)\right] \\ +\left(\frac{1}{R_\theta}\right)\left[(-A_{12})(U1)+(-A_{26})(U2)+(-B_{12})(U3)+(-B_{26})(U4)\right]\end{array}\right\} \quad \text{(A.7)}$$

$$c_{22} = \left(\frac{1}{\Delta}\right)\left(\frac{1}{R_\theta}\frac{\cos\phi}{\sin\phi}\right)\left\{\begin{array}{l}(-A_{12})(U1)+(-A_{26})(U2) \\ +(-B_{12})(U3)+(-B_{26})(U4)\end{array}\right\} \quad \text{(A.8)}$$

$$cp_{22} = \left(\frac{1}{\Delta}\right)\left(\frac{1}{R_\theta}\frac{1}{\sin\phi}\right)\left\{\begin{array}{l}(-A_{16})(U1)+(-A_{66})(U2) \\ +(-B_{16})(U3)+(-B_{66})(U4)\end{array}\right\} \quad \text{(A.9)}$$

$$c_{23} = \left(\frac{1}{\Delta}\right)\left(\frac{1}{R_\theta}\frac{\cos\phi}{\sin\phi}\right)\left\{\begin{array}{l}(A_{16})(U1)+(A_{66})(U2) \\ +(B_{16})(U3)+(B_{66})(U4)\end{array}\right\} \quad \text{(A.10)}$$

$$cp_{23} = \left(\frac{1}{\Delta}\right)\left(\frac{1}{R_\theta}\frac{1}{\sin\phi}\right)\left\{\begin{array}{l}(-A_{12})(U1)+(-A_{26})(U2) \\ +(-B_{12})(U3)+(-B_{26})(U4)\end{array}\right\} \quad \text{(A.11)}$$

$$c_{24} = \left(\frac{1}{\Delta}\right)\left(\frac{1}{R_\theta}\frac{\cos\phi}{\sin\phi}\right)\left\{\begin{array}{l}(-B_{12})(U1)+(-B_{26})(U2) \\ +(-D_{12})(U3)+(-D_{26})(U4)\end{array}\right\} \quad \text{(A.12)}$$

$$cp_{24} = \left(\frac{1}{\Delta}\right)\left(\frac{1}{R_\theta}\frac{1}{\sin\phi}\right)\left\{\begin{array}{l}(-B_{16})(U1)+(-B_{66})(U2) \\ +(-D_{16})(U3)+(-D_{66})(U4)\end{array}\right\} \quad \text{(A.13)}$$

$$c_{25} = \left(\frac{1}{\Delta}\right)\left(\frac{1}{R_\theta}\frac{\cos\phi}{\sin\phi}\right)\left\{\begin{array}{l}(B_{16})(U1)+(B_{66})(U2) \\ +(D_{16})(U3)+(D_{66})(U4)\end{array}\right\} \quad \text{(A.14)}$$

$$cp_{25} = \left(\frac{1}{\Delta}\right)\left(\frac{1}{R_\theta}\frac{1}{\sin\phi}\right)\left\{\begin{array}{l}(-B_{12})(U1)+(-B_{26})(U2) \\ +(-D_{12})(U3)+(-D_{26})(U4)\end{array}\right\} \quad \text{(A.15)}$$

$$c_{27} = \left(\frac{1}{\Delta}\right)\{U1\} \quad \text{(A.16)}$$

$$c_{28} = \left(\frac{1}{\Delta}\right)\{U2\} \quad \text{(A.17)}$$

$$c_{29} = \left(\frac{1}{\Delta}\right)\{U3\} \quad \text{(A.18)}$$

$$c_{210} = \left(\frac{1}{\Delta}\right)\{U4\} \quad \text{(A.19)}$$

where

$$\Delta = \left(\frac{1}{R_\phi}\right)\begin{bmatrix} (A_{11}A_{66}D_{11}D_{66}) - (A_{11}A_{66}D_{16}D_{16}) - (A_{11}B_{16}B_{16}D_{66}) + (A_{11}B_{16}B_{66}D_{16}) \\ + (A_{11}B_{66}B_{16}D_{16}) - (A_{11}B_{66}B_{66}D_{11}) - (A_{16}A_{16}D_{11}D_{66}) + (A_{16}A_{16}D_{16}D_{16}) \\ + (A_{16}B_{16}B_{11}D_{66}) - (A_{16}B_{16}B_{16}D_{16}) - (A_{16}B_{66}B_{11}D_{16}) + (A_{16}B_{66}B_{16}D_{11}) \\ + (B_{11}A_{16}B_{16}D_{66}) - (B_{11}A_{16}B_{66}D_{16}) - (B_{11}A_{66}B_{11}D_{66}) + (B_{11}A_{66}B_{16}D_{16}) \\ + (B_{11}B_{66}B_{11}B_{66}) - (B_{11}B_{66}B_{16}B_{16}) - (B_{16}A_{16}B_{16}D_{16}) + (B_{16}A_{16}B_{66}D_{11}) \\ + (B_{16}A_{66}B_{11}D_{16}) - (B_{16}A_{66}B_{16}D_{11}) - (B_{16}B_{16}B_{11}B_{66}) + (B_{16}B_{16}B_{16}B_{16}) \end{bmatrix} \tag{A.20}$$

$$U1 = \begin{bmatrix} (A_{66}D_{11}D_{66}) - (A_{66}D_{16}D_{16}) - (B_{16}B_{16}D_{66}) \\ + (B_{16}B_{66}D_{16}) + (B_{66}B_{16}D_{16}) - (B_{66}B_{66}D_{11}) \end{bmatrix} \tag{A.21}$$

$$U2 = \begin{bmatrix} (-A_{16}D_{11}D_{66}) + (A_{16}D_{16}D_{16}) + (B_{16}B_{11}D_{66}) \\ -(B_{16}B_{16}D_{16}) - (B_{66}B_{11}D_{16}) + (B_{66}B_{16}D_{11}) \end{bmatrix} \tag{A.22}$$

$$U3 = \begin{bmatrix} (A_{16}B_{16}D_{66}) - (A_{16}B_{66}D_{16}) - (A_{66}B_{11}D_{66}) \\ + (A_{66}B_{16}D_{16}) + (B_{66}B_{11}B_{66}) - (B_{66}B_{16}B_{16}) \end{bmatrix} \tag{A.23}$$

$$U4 = \begin{bmatrix} (-A_{16}B_{16}D_{16}) + (A_{16}B_{66}D_{11}) + (A_{66}B_{11}D_{16}) \\ -(A_{66}B_{16}D_{11}) - (B_{16}B_{11}B_{66}) + (B_{16}B_{16}B_{16}) \end{bmatrix} \tag{A.24}$$

Coefficients of $\frac{\partial u_\theta}{\partial \phi}$ equation, i.e. Equation (3.2.9)

$$c_{31} = \left(\frac{1}{\Delta}\right)\begin{Bmatrix} \left(\frac{1}{R_\phi}\right)\left[(-A_{11})(V1) + (-A_{16})(V2) + (-B_{11})(V3) + (-B_{16})(V4)\right] \\ + \left(\frac{1}{R_\theta}\right)\left[(-A_{12})(V1) + (-A_{26})(V2) + (-B_{12})(V3) + (-B_{26})(V4)\right] \end{Bmatrix} \tag{A.25}$$

$$c_{32} = \left(\frac{1}{\Delta}\right)\left(\frac{1}{R_\theta}\frac{\cos\phi}{\sin\phi}\right)\begin{Bmatrix} (-A_{12})(V1) + (-A_{26})(V2) \\ + (-B_{12})(V3) + (-B_{26})(V4) \end{Bmatrix} \tag{A.26}$$

$$cp_{32} = \left(\frac{1}{\Delta}\right)\left(\frac{1}{R_\theta}\frac{1}{\sin\phi}\right)\begin{Bmatrix} (-A_{16})(V1) + (-A_{66})(V2) \\ + (-B_{16})(V3) + (-B_{66})(V4) \end{Bmatrix} \tag{A.27}$$

$$c_{33} = \left(\frac{1}{\Delta}\right)\left(\frac{1}{R_\theta}\frac{\cos\phi}{\sin\phi}\right)\begin{Bmatrix}(A_{16})(V1)+(A_{66})(V2)\\+(B_{16})(V3)+(B_{66})(V4)\end{Bmatrix} \quad \text{(A.28)}$$

$$cp_{33} = \left(\frac{1}{\Delta}\right)\left(\frac{1}{R_\theta}\frac{1}{\sin\phi}\right)\begin{Bmatrix}(-A_{12})(V1)+(-A_{26})(V2)\\+(-B_{12})(V3)+(-B_{26})(V4)\end{Bmatrix} \quad \text{(A.29)}$$

$$c_{34} = \left(\frac{1}{\Delta}\right)\left(\frac{1}{R_\theta}\frac{\cos\phi}{\sin\phi}\right)\begin{Bmatrix}(-B_{12})(V1)+(-B_{26})(V2)\\+(-D_{12})(V3)+(-D_{26})(V4)\end{Bmatrix} \quad \text{(A.30)}$$

$$cp_{34} = \left(\frac{1}{\Delta}\right)\left(\frac{1}{R_\theta}\frac{1}{\sin\phi}\right)\begin{Bmatrix}(-B_{16})(V1)+(-B_{66})(V2)\\+(-D_{16})(V3)+(-D_{66})(V4)\end{Bmatrix} \quad \text{(A.31)}$$

$$c_{35} = \left(\frac{1}{\Delta}\right)\left(\frac{1}{R_\theta}\frac{\cos\phi}{\sin\phi}\right)\begin{Bmatrix}(B_{16})(V1)+(B_{66})(V2)\\+(D_{16})(V3)+(D_{66})(V4)\end{Bmatrix} \quad \text{(A.32)}$$

$$cp_{35} = \left(\frac{1}{\Delta}\right)\left(\frac{1}{R_\theta}\frac{1}{\sin\phi}\right)\begin{Bmatrix}(-B_{12})(V1)+(-B_{26})(V2)\\+(-D_{12})(V3)+(-D_{26})(V4)\end{Bmatrix} \quad \text{(A.33)}$$

$$c_{37} = \left(\frac{1}{\Delta}\right)\{V1\} \quad \text{(A.34)}$$

$$c_{38} = \left(\frac{1}{\Delta}\right)\{V2\} \quad \text{(A.35)}$$

$$c_{39} = \left(\frac{1}{\Delta}\right)\{V3\} \quad \text{(A.36)}$$

$$c_{310} = \left(\frac{1}{\Delta}\right)\{V4\} \quad \text{(A.37)}$$

where

$$V1 = \begin{bmatrix}(-A_{16}D_{11}D_{66})+(A_{16}D_{16}D_{16})+(B_{11}B_{16}D_{66})\\-(B_{11}B_{66}D_{16})-(B_{16}B_{16}D_{16})+(B_{16}B_{66}D_{11})\end{bmatrix} \quad \text{(A.38)}$$

$$V2 = \begin{bmatrix}(A_{11}D_{11}D_{66})-(A_{11}D_{16}D_{16})-(B_{11}B_{11}D_{66})\\+(B_{11}B_{16}D_{16})+(B_{16}B_{11}D_{16})-(B_{16}B_{16}D_{11})\end{bmatrix} \quad \text{(A.39)}$$

$$V3 = \begin{bmatrix}(-A_{11}B_{16}D_{66})+(A_{11}B_{66}D_{16})+(A_{16}B_{11}D_{66})\\-(A_{16}B_{16}D_{16})-(B_{16}B_{11}B_{66})+(B_{16}B_{16}B_{16})\end{bmatrix} \quad \text{(A.40)}$$

$$V4 = \begin{bmatrix} (A_{11}B_{16}D_{16}) - (A_{11}B_{66}D_{11}) - (A_{16}B_{11}D_{16}) \\ + (A_{16}B_{16}D_{11}) + (B_{11}B_{11}B_{66}) - (B_{11}B_{16}B_{16}) \end{bmatrix} \quad \text{(A.41)}$$

and Δ is given by Equation (A20).

Coefficients of $\frac{\partial \beta_\phi}{\partial \phi}$ equation, i.e. Equation (3.2.10)

$$c_{41} = \left(\frac{1}{\Delta}\right)\left\{\begin{array}{l} \left(\frac{1}{R_\phi}\right)\left[(-A_{11})(Y1) + (-A_{16})(Y2) + (-B_{11})(Y3) + (-B_{16})(Y4)\right] \\ + \left(\frac{1}{R_\theta}\right)\left[(-A_{12})(Y1) + (-A_{26})(Y2) + (-B_{12})(Y3) + (-B_{26})(Y4)\right] \end{array}\right\} \quad \text{(A.42)}$$

$$c_{42} = \left(\frac{1}{\Delta}\right)\left(\frac{1}{R_\theta}\frac{\cos\phi}{\sin\phi}\right)\left\{\begin{array}{l} (-A_{12})(Y1) + (-A_{26})(Y2) \\ + (-B_{12})(Y3) + (-B_{26})(Y4) \end{array}\right\} \quad \text{(A.43)}$$

$$cp_{42} = \left(\frac{1}{\Delta}\right)\left(\frac{1}{R_\theta}\frac{1}{\sin\phi}\right)\left\{\begin{array}{l} (-A_{16})(Y1) + (-A_{66})(Y2) \\ + (-B_{16})(Y3) + (-B_{66})(Y4) \end{array}\right\} \quad \text{(A.44)}$$

$$c_{43} = \left(\frac{1}{\Delta}\right)\left(\frac{1}{R_\theta}\frac{\cos\phi}{\sin\phi}\right)\left\{\begin{array}{l} (A_{16})(Y1) + (A_{66})(Y2) \\ + (B_{16})(Y3) + (B_{66})(Y4) \end{array}\right\} \quad \text{(A.45)}$$

$$cp_{43} = \left(\frac{1}{\Delta}\right)\left(\frac{1}{R_\theta}\frac{1}{\sin\phi}\right)\left\{\begin{array}{l} (-A_{12})(Y1) + (-A_{26})(Y2) \\ + (-B_{12})(Y3) + (-B_{26})(Y4) \end{array}\right\} \quad \text{(A.46)}$$

$$c_{44} = \left(\frac{1}{\Delta}\right)\left(\frac{1}{R_\theta}\frac{\cos\phi}{\sin\phi}\right)\left\{\begin{array}{l} (-B_{12})(Y1) + (-B_{26})(Y2) \\ + (-D_{12})(Y3) + (-D_{26})(Y4) \end{array}\right\} \quad \text{(A.47)}$$

$$cp_{44} = \left(\frac{1}{\Delta}\right)\left(\frac{1}{R_\theta}\frac{1}{\sin\phi}\right)\left\{\begin{array}{l} (-B_{16})(Y1) + (-B_{66})(Y2) \\ + (-D_{16})(Y3) + (-D_{66})(Y4) \end{array}\right\} \quad \text{(A.48)}$$

$$c_{45} = \left(\frac{1}{\Delta}\right)\left(\frac{1}{R_\theta}\frac{\cos\phi}{\sin\phi}\right)\left\{\begin{array}{l} (B_{16})(Y1) + (B_{66})(Y2) \\ + (D_{16})(Y3) + (D_{66})(Y4) \end{array}\right\} \quad \text{(A.49)}$$

$$cp_{45} = \left(\frac{1}{\Delta}\right)\left(\frac{1}{R_\theta}\frac{1}{\sin\phi}\right)\left\{\begin{array}{l} (-B_{12})(Y1) + (-B_{26})(Y2) \\ + (-D_{12})(Y3) + (-D_{26})(Y4) \end{array}\right\} \quad \text{(A.50)}$$

$$c_{47} = \left(\frac{1}{\Delta}\right)\{Y1\} \tag{A.51}$$

$$c_{48} = \left(\frac{1}{\Delta}\right)\{Y2\} \tag{A.52}$$

$$c_{49} = \left(\frac{1}{\Delta}\right)\{Y3\} \tag{A.53}$$

$$c_{410} = \left(\frac{1}{\Delta}\right)\{Y4\} \tag{A.54}$$

where

$$Y1 = \begin{bmatrix} (A_{16}B_{16}D_{66}) - (A_{16}D_{16}B_{66}) - (B_{11}A_{66}D_{66}) \\ + (B_{11}B_{66}B_{66}) + (B_{16}A_{66}D_{16}) - (B_{16}B_{66}B_{16}) \end{bmatrix} \tag{A.55}$$

$$Y2 = \begin{bmatrix} (-A_{11}B_{16}D_{66}) + (A_{11}D_{16}B_{66}) + (B_{11}A_{16}D_{66}) \\ - (B_{11}B_{16}B_{66}) - (B_{16}A_{16}D_{16}) + (B_{16}B_{16}B_{16}) \end{bmatrix} \tag{A.56}$$

$$Y3 = \begin{bmatrix} (A_{11}A_{66}D_{66}) - (A_{11}B_{66}B_{66}) - (A_{16}A_{16}D_{66}) \\ + (A_{16}B_{16}B_{66}) + (B_{16}A_{16}B_{66}) - (B_{16}B_{16}A_{66}) \end{bmatrix} \tag{A.57}$$

$$Y4 = \begin{bmatrix} (-A_{11}A_{66}D_{16}) + (A_{11}B_{66}B_{16}) + (A_{16}A_{16}D_{16}) \\ - (A_{16}B_{16}B_{16}) - (B_{11}A_{16}B_{66}) + (B_{11}B_{16}A_{66}) \end{bmatrix} \tag{A.58}$$

and Δ is given by Equation (A20).

Coefficients of $\frac{\partial \beta_\theta}{\partial \phi}$ equation, i.e. Equation (3.2.11)

$$c_{51} = \left(\frac{1}{\Delta}\right)\left\{\begin{array}{l} \left(\frac{1}{R_\phi}\right)\left[(-A_{11})(Z1) + (-A_{16})(Z2) + (-B_{11})(Z3) + (-B_{16})(Z4)\right] \\ + \left(\frac{1}{R_\theta}\right)\left[(-A_{12})(Z1) + (-A_{26})(Z2) + (-B_{12})(Z3) + (-B_{26})(Z4)\right] \end{array}\right\} \tag{A.59}$$

$$c_{52} = \left(\frac{1}{\Delta}\right)\left(\frac{1}{R_\theta}\frac{\cos\phi}{\sin\phi}\right)\begin{Bmatrix}(-A_{12})(Z1)+(-A_{26})(Z2)\\+(-B_{12})(Z3)+(-B_{26})(Z4)\end{Bmatrix} \tag{A.60}$$

$$cp_{52} = \left(\frac{1}{\Delta}\right)\left(\frac{1}{R_\theta}\frac{1}{\sin\phi}\right)\begin{Bmatrix}(-A_{16})(Z1)+(-A_{66})(Z2)\\+(-B_{16})(Z3)+(-B_{66})(Z4)\end{Bmatrix} \tag{A.61}$$

$$c_{53} = \left(\frac{1}{\Delta}\right)\left(\frac{1}{R_\theta}\frac{\cos\phi}{\sin\phi}\right)\begin{Bmatrix}(A_{16})(Z1)+(A_{66})(Z2)\\+(B_{16})(Z3)+(B_{66})(Z4)\end{Bmatrix} \tag{A.62}$$

$$cp_{53} = \left(\frac{1}{\Delta}\right)\left(\frac{1}{R_\theta}\frac{1}{\sin\phi}\right)\begin{Bmatrix}(-A_{12})(Z1)+(-A_{26})(Z2)\\+(-B_{12})(Z3)+(-B_{26})(Z4)\end{Bmatrix} \tag{A.63}$$

$$c_{54} = \left(\frac{1}{\Delta}\right)\left(\frac{1}{R_\theta}\frac{\cos\phi}{\sin\phi}\right)\begin{Bmatrix}(-B_{12})(Z1)+(-B_{26})(Z2)\\+(-D_{12})(Z3)+(-D_{26})(Z4)\end{Bmatrix} \tag{A.64}$$

$$cp_{54} = \left(\frac{1}{\Delta}\right)\left(\frac{1}{R_\theta}\frac{1}{\sin\phi}\right)\begin{Bmatrix}(-B_{16})(Z1)+(-B_{66})(Z2)\\+(-D_{16})(Z3)+(-D_{66})(Z4)\end{Bmatrix} \tag{A.65}$$

$$c_{55} = \left(\frac{1}{\Delta}\right)\left(\frac{1}{R_\theta}\frac{\cos\phi}{\sin\phi}\right)\begin{Bmatrix}(B_{16})(Z1)+(B_{66})(Z2)\\+(D_{16})(Z3)+(D_{66})(Z4)\end{Bmatrix} \tag{A.66}$$

$$cp_{55} = \left(\frac{1}{\Delta}\right)\left(\frac{1}{R_\theta}\frac{1}{\sin\phi}\right)\begin{Bmatrix}(-B_{12})(Z1)+(-B_{26})(Z2)\\+(-D_{12})(Z3)+(-D_{26})(Z4)\end{Bmatrix} \tag{A.67}$$

$$c_{57} = \left(\frac{1}{\Delta}\right)\{Z1\} \tag{A.68}$$

$$c_{58} = \left(\frac{1}{\Delta}\right)\{Z2\} \tag{A.69}$$

$$c_{59} = \left(\frac{1}{\Delta}\right)\{Z3\} \tag{A.70}$$

$$c_{510} = \left(\frac{1}{\Delta}\right)\{Z4\} \tag{A.71}$$

where

$$Z1 = \begin{bmatrix}(-A_{16}B_{16}D_{16})+(A_{16}D_{11}B_{66})+(B_{11}A_{66}D_{16})\\-(B_{11}B_{16}B_{66})-(B_{16}A_{66}D_{11})+(B_{16}B_{16}B_{16})\end{bmatrix} \tag{A.72}$$

$$Z2 = \begin{bmatrix} (A_{11}B_{16}D_{16}) - (A_{11}D_{11}B_{66}) - (B_{11}A_{16}D_{16}) \\ + (B_{11}B_{11}B_{66}) + (B_{16}A_{16}D_{11}) - (B_{16}B_{11}B_{16}) \end{bmatrix} \quad \text{(A.73)}$$

$$Z3 = \begin{bmatrix} (-A_{11}A_{66}D_{16}) + (A_{11}B_{16}B_{66}) + (A_{16}A_{16}D_{16}) \\ - (A_{16}B_{11}B_{66}) - (B_{16}A_{16}B_{16}) + (B_{16}B_{11}A_{66}) \end{bmatrix} \quad \text{(A.74)}$$

$$Z4 = \begin{bmatrix} (A_{11}A_{66}D_{11}) - (A_{11}B_{16}B_{16}) - (A_{16}A_{16}D_{11}) \\ + (A_{16}B_{11}B_{16}) + (B_{11}A_{16}B_{16}) - (B_{11}B_{11}A_{66}) \end{bmatrix} \quad \text{(A.75)}$$

and Δ is given by Equation (A20).

Coefficients of $\frac{\partial Q_{\phi\zeta}}{\partial \phi}$ equation, i.e. Equation (3.2.12)

$$c_{61} = \left\{ \left(\frac{1}{R_\theta} \right) \begin{bmatrix} (A_{12})(c_{21}) + (A_{12}) + (A_{26})(c_{31}) \\ + (B_{12})(c_{41}) + (B_{26})(c_{51}) \end{bmatrix} + \left(\frac{R_\phi}{R_\theta^2} \right)(A_{22}) \right\} \quad \text{(A.76)}$$

$$cdp_{61} = \left\{ \left(-\frac{1}{R_\theta} \right) \left(\frac{A_{45}}{\sin\phi} \right)(cp_{11}) + \left(-\frac{R_\phi}{R_\theta^2} \right) \left(\frac{A_{44}}{\sin^2\phi} \right) \right\} \quad \text{(A.77)}$$

$$c_{62} = \left\{ \left(\frac{1}{R_\theta} \right) \left[(A_{12})(c_{22}) + (A_{22}) \left(\frac{\cos\phi}{\sin\phi} \right) + (A_{26})(c_{32}) + (B_{12})(c_{42}) + (B_{26})(c_{52}) \right] \right\} \quad \text{(A.78)}$$

$$cp_{62} = \left\{ \left(\frac{1}{R_\theta} \right) \begin{bmatrix} \left(\frac{A_{45}}{\sin\phi} \right) + \left(-\frac{A_{45}}{\sin\phi} \right)(c_{12}) + (A_{12})(cp_{22}) + \left(\frac{R_\phi}{R_\theta} \right) \left(\frac{A_{26}}{\sin\phi} \right) \\ + (A_{26})(cp_{32}) + (B_{12})(cp_{42}) + (B_{26})(cp_{52}) \end{bmatrix} \right\} \quad \text{(A.79)}$$

$$c_{63} = \left\{ \left(\frac{1}{R_\theta} \right) \left[(A_{12})(c_{23}) + (A_{26})(c_{33}) + (-A_{26}) \left(\frac{\cos\phi}{\sin\phi} \right) + (B_{12})(c_{43}) + (B_{26})(c_{53}) \right] \right\} \quad \text{(A.80)}$$

$$cp_{63} = \left\{ \left(\frac{1}{R_\theta} \right) \begin{bmatrix} \left(-\frac{A_{45}}{\sin\phi} \right)(c_{13}) + \left(\frac{R_\phi}{R_\theta} \right) \left(\frac{A_{44}}{\sin\phi} \right) + (A_{12})(cp_{23}) + \left(\frac{R_\phi}{R_\theta} \right) \left(\frac{A_{22}}{\sin\phi} \right) \\ + (A_{26})(cp_{33}) + (B_{12})(cp_{43}) + (B_{26})(cp_{53}) \end{bmatrix} \right\} \quad \text{(A.81)}$$

$$c_{64} = \left\{ \left(\frac{1}{R_\theta} \right) \left[(A_{12})(c_{24}) + (A_{26})(c_{34}) + (B_{12})(c_{44}) + (B_{26})(c_{54}) + (B_{22}) \left(\frac{\cos\phi}{\sin\phi} \right) \right] \right\} \tag{A.82}$$

$$cp_{64} = \left\{ \left(\frac{1}{R_\theta} \right) \left[\begin{array}{l} \left(-R_\phi \left(\frac{A_{45}}{\sin\phi} \right) + \left(-\frac{A_{45}}{\sin\phi} \right) (c_{14}) + (A_{12})(cp_{24}) + (A_{26})(cp_{34}) \right. \\ \left. + (B_{12})(cp_{44}) + \left(\frac{R_\phi}{R_\theta} \right) \left(\frac{B_{26}}{\sin\phi} \right) + (B_{26})(cp_{54}) \right] \end{array} \right\} \tag{A.83}$$

$$c_{65} = \left\{ \left(\frac{1}{R_\theta} \right) \left[(A_{12})(c_{25}) + (A_{26})(c_{35}) + (B_{12})(c_{45}) + (B_{26})(c_{55}) + (-B_{26}) \left(\frac{\cos\phi}{\sin\phi} \right) \right] \right\} \tag{A.84}$$

$$cp_{65} = \left\{ \left(\frac{1}{R_\theta} \right) \left[\begin{array}{l} \left(-\frac{A_{45}}{\sin\phi} \right) (c_{15}) + \left(-R_\phi \left(\frac{A_{44}}{\sin\phi} \right) + (A_{12})(cp_{25}) + (A_{26})(cp_{35}) \right. \\ \left. + (B_{12})(cp_{45}) + \left(\frac{R_\phi}{R_\theta} \right) \left(\frac{B_{22}}{\sin\phi} \right) + (B_{26})(cp_{55}) \right] \end{array} \right\} \tag{A.85}$$

$$c_{66} = \left\{ \left(-\frac{R_\phi}{R_\theta} \right) \left(\frac{\cos\phi}{\sin\phi} \right) \right\} \tag{A.86}$$

$$cp_{66} = \left\{ \left(-\frac{1}{R_\theta} \right) \left[\left(\frac{A_{45}}{\sin\phi} \right) (c_{16}) \right] \right\} \tag{A.87}$$

$$c_{67} = \left\{ \left(\frac{1}{R_\theta} \right) \left[(A_{12})(c_{27}) + (A_{26})(c_{37}) + (B_{12})(c_{47}) + (B_{26})(c_{57}) \right] + (1) \right\} \tag{A.88}$$

$$c_{68} = \left\{ \left(\frac{1}{R_\theta} \right) \left[(A_{12})(c_{28}) + (A_{26})(c_{38}) + (B_{12})(c_{48}) + (B_{26})(c_{58}) \right] \right\} \tag{A.89}$$

$$c_{69} = \left\{ \left(\frac{1}{R_\theta} \right) \left[(A_{12})(c_{29}) + (A_{26})(c_{39}) + (B_{12})(c_{49}) + (B_{26})(c_{59}) \right] \right\} \tag{A.90}$$

$$c_{610} = \left\{ \left(\frac{1}{R_\theta} \right) \left[(A_{12})(c_{210}) + (A_{26})(c_{310}) + (B_{12})(c_{410}) + (B_{26})(c_{510}) \right] \right\} \tag{A.91}$$

Coefficients of $\frac{\partial N_{\phi\phi}}{\partial \phi}$ equation, i.e. Equation (3.2.13)

$$c_{71} = \left\{ \left(\frac{1}{R_\theta} \right) \left(\frac{\cos\phi}{\sin\phi} \right) \left[\begin{array}{l} (A_{12})(c_{21}) + (A_{12}) + (A_{26})(c_{31}) + (B_{12})(c_{41}) \\ + (B_{26})(c_{51}) + \left(\frac{R_\phi}{R_\theta} \right)(A_{22}) \end{array} \right] \right\} \tag{A.92}$$

$$c_{72} = \left\{ \left(\frac{1}{R_\theta} \right) \left(\frac{\cos\phi}{\sin\phi} \right) \left[\begin{array}{l} (A_{12})(c_{22}) + \left(\frac{R_\phi}{R_\theta} \right)(A_{22}) \left(\frac{\cos\phi}{\sin\phi} \right) + (A_{26})(c_{32}) \\ + (B_{12})(c_{42}) + (B_{26})(c_{52}) \end{array} \right] \right\} \tag{A.93}$$

$$cp_{72} = \left\{ \left(\frac{1}{R_\theta} \right) \left(\frac{\cos\phi}{\sin\phi} \right) \left[\begin{array}{l} (A_{12})(cp_{22}) + (A_{26})(cp_{32}) + (B_{12})(cp_{42}) \\ + \left(\frac{R_\phi}{R_\theta} \right) \left(\frac{1}{\sin\phi} \right)(A_{26}) + (B_{26})(cp_{52}) \end{array} \right] \right\} \tag{A.94}$$

$$c_{73} = \left\{ \left(\frac{1}{R_\theta} \right) \left(\frac{\cos\phi}{\sin\phi} \right) \left[\begin{array}{l} (A_{12})(c_{23}) + (A_{26})(c_{33}) + (-A_{26}) \left(\frac{\cos\phi}{\sin\phi} \right) \\ + (B_{12})(c_{43}) + (B_{26})(c_{53}) \end{array} \right] \right\} \tag{A.95}$$

$$cp_{73} = \left\{ \left(\frac{1}{R_\theta} \right) \left(\frac{\cos\phi}{\sin\phi} \right) \left[\begin{array}{l} (A_{12})(cp_{23}) + \left(\frac{R_\phi}{R_\theta} \right)(A_{22}) \left(\frac{1}{\sin\phi} \right) + (A_{26})(cp_{33}) \\ + (B_{12})(cp_{43}) + (B_{26})(cp_{53}) \end{array} \right] \right\} \tag{A.96}$$

$$c_{74} = \left\{ \left(\frac{1}{R_\theta} \right) \left(\frac{\cos\phi}{\sin\phi} \right) \left[\begin{array}{l} (A_{12})(c_{24}) + (A_{26})(c_{34}) + (B_{12})(c_{44}) \\ + (B_{22}) \left(\frac{\cos\phi}{\sin\phi} \right) + (B_{26})(c_{54}) \end{array} \right] \right\} \tag{A.97}$$

$$cp_{74} = \left\{ \left(\frac{1}{R_\theta} \right) \left(\frac{\cos\phi}{\sin\phi} \right) \left[\begin{array}{l} (A_{12})(cp_{24}) + (A_{26})(cp_{34}) + (B_{12})(cp_{44}) \\ + \left(\frac{R_\phi}{R_\theta} \right)(B_{26}) \left(\frac{1}{\sin\phi} \right) + (B_{26})(cp_{54}) \end{array} \right] \right\} \tag{A.98}$$

$$c_{75} = \left\{ \left(\frac{1}{R_\theta} \right) \left(\frac{\cos\phi}{\sin\phi} \right) \left[\begin{array}{l} (A_{12})(c_{25}) + (A_{26})(c_{35}) + (B_{12})(c_{45}) \\ + (B_{26})(c_{55}) + (-B_{26}) \left(\frac{\cos\phi}{\sin\phi} \right) \end{array} \right] \right\} \tag{A.99}$$

$$cp_{75} = \left\{ \left(\frac{1}{R_\theta} \right) \left(\frac{\cos\phi}{\sin\phi} \right) \left[\begin{array}{l} (A_{12})(cp_{25}) + (A_{26})(cp_{35}) + (B_{12})(cp_{45}) \\ + \left(\frac{R_\phi}{R_\theta} \right)(B_{22}) \left(\frac{1}{\sin\phi} \right) + (B_{26})(cp_{55}) \end{array} \right] \right\} \tag{A.100}$$

$$c_{76} = \{-1\} \tag{A.101}$$

$$c_{77} = \left\{ \left(\frac{1}{R_\theta} \right) \left(\frac{\cos\phi}{\sin\phi} \right) \left[\left(-R_\phi \right) + \left(A_{12} \right)\left(c_{27} \right) + \left(A_{26} \right)\left(c_{37} \right) + \left(B_{12} \right)\left(c_{47} \right) + \left(B_{26} \right)\left(c_{57} \right) \right] \right\} \tag{A.102}$$

$$c_{78} = \left\{ \left(\frac{1}{R_\theta} \right) \left(\frac{\cos\phi}{\sin\phi} \right) \left[\left(A_{12} \right)\left(c_{28} \right) + \left(A_{26} \right)\left(c_{38} \right) + \left(B_{12} \right)\left(c_{48} \right) + \left(B_{26} \right)\left(c_{58} \right) \right] \right\} \tag{A.103}$$

$$cp_{78} = \left\{ \left(-\frac{R_\phi}{R_\theta} \right) \left(\frac{1}{\sin\phi} \right) \right\} \tag{A.104}$$

$$c_{79} = \left\{ \left(\frac{1}{R_\theta} \right) \left(\frac{\cos\phi}{\sin\phi} \right) \left[\left(A_{12} \right)\left(c_{29} \right) + \left(A_{26} \right)\left(c_{39} \right) + \left(B_{12} \right)\left(c_{49} \right) + \left(B_{26} \right)\left(c_{59} \right) \right] \right\} \tag{A.105}$$

$$c_{710} = \left\{ \left(\frac{1}{R_\theta} \right) \left(\frac{\cos\phi}{\sin\phi} \right) \left[\left(A_{12} \right)\left(c_{210} \right) + \left(A_{26} \right)\left(c_{310} \right) + \left(B_{12} \right)\left(c_{410} \right) + \left(B_{26} \right)\left(c_{510} \right) \right] \right\} \tag{A.106}$$

Coefficients of $\frac{\partial N_{\phi\theta}}{\partial\phi}$ equation, i.e. Equation (3.2.14)

$$cp_{81} = \left\{ \begin{array}{l} \left(\frac{1}{R_\theta} \right) \left[\left(-A_{45} \right)\left(cp_{11} \right) + \left(-\frac{R_\phi}{R_\theta \sin\phi} \right)\left(A_{44} \right) \right] \\ + \left(\frac{1}{R_\theta} \right) \left(\frac{1}{\sin\phi} \right) \left[\begin{array}{l} \left(-A_{12} \right)\left(c_{21} \right) + \left(-A_{12} \right) + \left(-\frac{R_\phi}{R_\theta} \right)\left(A_{22} \right) + \left(-A_{26} \right)\left(c_{31} \right) \\ + \left(-B_{12} \right)\left(c_{41} \right) + \left(-B_{26} \right)\left(c_{51} \right) \end{array} \right] \end{array} \right\} \tag{A.107}$$

$$c_{82} = \left\{ \left(\frac{1}{R_\theta} \right) \left[\left(A_{45} \right) + \left(-A_{45} \right)\left(c_{12} \right) \right] \right\} \tag{A.108}$$

$$cp_{82} = \left\{ \left(\frac{1}{R_\theta} \right) \left(\frac{1}{\sin\phi} \right) \left[\begin{array}{l} \left(-A_{12} \right)\left(c_{22} \right) + \left(-A_{22} \right)\left(\frac{\cos\phi}{\sin\phi} \right) + \left(-A_{26} \right)\left(c_{32} \right) \\ + \left(-B_{12} \right)\left(c_{42} \right) + \left(-B_{26} \right)\left(c_{52} \right) \end{array} \right] \right\} \tag{A.109}$$

$$cdp_{82} = \left\{ \left(\frac{1}{R_\theta} \right) \left(\frac{1}{\sin\phi} \right) \left[\begin{array}{l} (-A_{12})(cp_{22}) + \left(-\frac{R_\phi}{R_\theta} \right) (A_{26}) \left(\frac{1}{\sin\phi} \right) + (-A_{26})(cp_{32}) \\ + (-B_{12})(cp_{42}) + (-B_{26})(cp_{52}) \end{array} \right] \right\} \tag{A.110}$$

$$c_{83} = \left\{ \left(\frac{1}{R_\theta} \right) \left[(-A_{45})(c_{13}) + \left(\frac{R_\phi}{R_\theta} \right) (A_{44}) \right] \right\} \tag{A.111}$$

$$cp_{83} = \left\{ \left(\frac{1}{R_\theta} \right) \left(\frac{1}{\sin\phi} \right) \left[\begin{array}{l} (-A_{12})(c_{23}) + (-A_{26})(c_{33}) + (A_{26}) \left(\frac{\cos\phi}{\sin\phi} \right) \\ + (-B_{12})(c_{43}) + (-B_{26})(c_{53}) \end{array} \right] \right\} \tag{A.112}$$

$$cdp_{83} = \left\{ \left(\frac{1}{R_\theta} \right) \left(\frac{1}{\sin\phi} \right) \left[\begin{array}{l} (-A_{12})(cp_{23}) + \left(-\frac{R_\phi}{R_\theta} \right) (A_{22}) \left(\frac{1}{\sin\phi} \right) + (-A_{26})(cp_{33}) \\ + (-B_{12})(cp_{43}) + (-B_{26})(cp_{53}) \end{array} \right] \right\} \tag{A.113}$$

$$c_{84} = \left\{ \left(\frac{1}{R_\theta} \right) \left[(-R_\phi)(A_{45}) + (-A_{45})(c_{14}) \right] \right\} \tag{A.114}$$

$$cp_{84} = \left\{ \left(\frac{1}{R_\theta} \right) \left(\frac{1}{\sin\phi} \right) \left[\begin{array}{l} (-A_{12})(c_{24}) + (-A_{26})(c_{34}) + (-B_{12})(c_{44}) \\ + (-B_{22}) \left(\frac{\cos\phi}{\sin\phi} \right) + (-B_{26})(c_{54}) \end{array} \right] \right\} \tag{A.115}$$

$$cdp_{84} = \left\{ \left(\frac{1}{R_\theta} \right) \left(\frac{1}{\sin\phi} \right) \left[\begin{array}{l} (-A_{12})(cp_{24}) + (-A_{26})(cp_{34}) + (-B_{12})(cp_{44}) \\ + \left(-\frac{R_\phi}{R_\theta} \right) (B_{26}) \left(\frac{1}{\sin\phi} \right) + (-B_{26})(cp_{54}) \end{array} \right] \right\} \tag{A.116}$$

$$c_{85} = \left\{ \left(\frac{1}{R_\theta} \right) \left[(-A_{45})(c_{15}) + (-R_\phi)(A_{44}) \right] \right\} \tag{A.117}$$

$$cp_{85} = \left\{ \left(\frac{1}{R_\theta} \right) \left(\frac{1}{\sin\phi} \right) \left[\begin{array}{l} (-A_{12})(c_{25}) + (-A_{26})(c_{35}) + (-B_{12})(c_{45}) \\ + (-B_{26})(c_{55}) + (B_{26}) \left(\frac{\cos\phi}{\sin\phi} \right) \end{array} \right] \right\} \tag{A.118}$$

$$cdp_{85} = \left\{ \left(\frac{1}{R_\theta} \right) \left(\frac{1}{\sin\phi} \right) \left[\begin{array}{l} (-A_{12})(cp_{25}) + (-A_{26})(cp_{35}) + (-B_{12})(cp_{45}) \\ + \left(-\frac{R_\phi}{R_\theta} \right) (B_{22}) \left(\frac{1}{\sin\phi} \right) + (-B_{26})(cp_{55}) \end{array} \right] \right\} \tag{A.119}$$

$$c_{86} = \left\{ \left(\frac{1}{R_\theta} \right) \left[(-A_{45})(c_{16}) \right] \right\} \tag{A.120}$$

$$cp_{87} = \left\{ \left(\frac{1}{R_\theta} \right) \left(\frac{1}{\sin\phi} \right) \left[(-A_{12})(c_{27}) + (-A_{26})(c_{37}) + (-B_{12})(c_{47}) + (-B_{26})(c_{57}) \right] \right\} \tag{A.121}$$

$$c_{88} = \left\{ \left(\frac{1}{R_\theta} \right) \left[(-2R_\phi) \left(\frac{\cos\phi}{\sin\phi} \right) \right] \right\} \tag{A.122}$$

$$cp_{88} = \left\{ \left(\frac{1}{R_\theta} \right) \left(\frac{1}{\sin\phi} \right) \left[(-A_{12})(c_{28}) + (-A_{26})(c_{38}) + (-B_{12})(c_{48}) + (-B_{26})(c_{58}) \right] \right\} \tag{A.123}$$

$$cp_{89} = \left\{ \left(\frac{1}{R_\theta} \right) \left(\frac{1}{\sin\phi} \right) \left[(-A_{12})(c_{29}) + (-A_{26})(c_{39}) + (-B_{12})(c_{49}) + (-B_{26})(c_{59}) \right] \right\} \tag{A.124}$$

$$cp_{810} = \left\{ \left(\frac{1}{R_\theta} \right) \left(\frac{1}{\sin\phi} \right) \left[(-A_{12})(c_{210}) + (-A_{26})(c_{310}) + (-B_{12})(c_{410}) + (-B_{26})(c_{510}) \right] \right\} \tag{A.125}$$

Coefficients of $\frac{\partial M_{\phi\phi}}{\partial \phi}$ equation, i.e. Equation (3.2.15)

$$c_{91} = \left\{ \left(\frac{1}{R_\theta} \right) \left(\frac{\cos\phi}{\sin\phi} \right) \left[\begin{array}{l} (B_{12}) + \left(\frac{R_\phi}{R_\theta} \right)(B_{22}) + (B_{12})(c_{21}) + (B_{26})(c_{31}) \\ + (D_{12})(c_{41}) + (D_{26})(c_{51}) \end{array} \right] \right\} \tag{A.126}$$

$$cp_{91} = \left\{ \left(\frac{1}{R_\theta} \right) \left(\frac{1}{\sin\phi} \right) \left[\begin{array}{l} (-B_{16})(c_{21}) + (-B_{16}) + \left(-\frac{R_\phi}{R_\theta} \right)(B_{26}) + (-B_{66})(c_{31}) \\ + (-D_{16})(c_{41}) + (-D_{66})(c_{51}) \end{array} \right] \right\} \tag{A.127}$$

$$c_{92} = \left\{ \left(\frac{1}{R_\theta} \right) \left(\frac{\cos\phi}{\sin\phi} \right) \left[\begin{array}{l} (B_{12})(c_{22}) + (B_{22}) \left(\frac{\cos\phi}{\sin\phi} \right) + (B_{26})(c_{32}) \\ + (D_{12})(c_{42}) + (D_{26})(c_{52}) \end{array} \right] \right\} \tag{A.128}$$

$$cp_{92} = \left\{ \begin{array}{l} \left(\frac{1}{R_\theta}\right)\left(\frac{1}{\sin\phi}\right)\left[\begin{array}{l} (-B_{16})(c_{22}) + \left(-\frac{R_\phi}{R_\theta}\right)(B_{26})\left(\frac{\cos\phi}{\sin\phi}\right) + (-B_{66})(c_{32}) \\ +(-D_{16})(c_{42}) + (-D_{66})(c_{52}) \end{array} \right] \\ +\left(\frac{1}{R_\theta}\right)\left(\frac{\cos\phi}{\sin\phi}\right)\left[\begin{array}{l} (B_{12})(cp_{22}) + \left(\frac{R_\phi}{R_\theta}\right)\left(\frac{1}{\sin\phi}\right)(B_{26}) + (B_{26})(cp_{32}) \\ +(D_{12})(cp_{42}) + (D_{26})(cp_{52}) \end{array} \right] \end{array} \right\} \quad \text{(A.129)}$$

$$cdp_{92} = \left\{ \left(\frac{1}{R_\theta}\right)\left(\frac{1}{\sin\phi}\right)\left[\begin{array}{l} (-B_{16})(cp_{22}) + \left(-\frac{R_\phi}{R_\theta}\right)\left(\frac{1}{\sin\phi}\right)(B_{66}) + (-B_{66})(cp_{32}) \\ +(-D_{16})(cp_{42}) + (-D_{66})(cp_{52}) \end{array} \right] \right\} \quad \text{(A.130)}$$

$$c_{93} = \left\{ \left(\frac{1}{R_\theta}\right)\left(\frac{\cos\phi}{\sin\phi}\right)\left[\begin{array}{l} (B_{12})(c_{23}) + (B_{26})(c_{33}) + (-B_{26})\left(\frac{\cos\phi}{\sin\phi}\right) \\ +(D_{12})(c_{43}) + (D_{26})(c_{53}) \end{array} \right] \right\} \quad \text{(A.131)}$$

$$cp_{93} = \left\{ \begin{array}{l} \left(\frac{1}{R_\theta}\right)\left(\frac{1}{\sin\phi}\right)\left[\begin{array}{l} (-B_{16})(c_{23}) + (-B_{66})(c_{33}) + \left(-\frac{R_\phi}{R_\theta}\right)(-B_{66})\left(\frac{\cos\phi}{\sin\phi}\right) \\ +(-D_{16})(c_{43}) + (-D_{66})(c_{53}) \end{array} \right] \\ +\left(\frac{1}{R_\theta}\right)\left(\frac{\cos\phi}{\sin\phi}\right)\left[\begin{array}{l} (B_{12})(cp_{23}) + \left(\frac{R_\phi}{R_\theta}\right)\left(\frac{1}{\sin\phi}\right)(B_{22}) + (B_{26})(cp_{33}) \\ +(D_{12})(cp_{43}) + (D_{26})(cp_{53}) \end{array} \right] \end{array} \right\} \quad \text{(A.132)}$$

$$cdp_{93} = \left\{ \left(\frac{1}{R_\theta}\right)\left(\frac{1}{\sin\phi}\right)\left[\begin{array}{l} (-B_{16})(cp_{23}) + \left(-\frac{R_\phi}{R_\theta}\right)\left(\frac{1}{\sin\phi}\right)(B_{26}) + (-B_{66})(cp_{33}) \\ +(-D_{16})(cp_{43}) + (-D_{66})(cp_{53}) \end{array} \right] \right\} \quad \text{(A.133)}$$

$$c_{94} = \left\{ \left(\frac{1}{R_\theta}\right)\left(\frac{\cos\phi}{\sin\phi}\right)\left[\begin{array}{l} (B_{12})(c_{24}) + (B_{26})(c_{34}) + (D_{12})(c_{44}) \\ +(D_{22})\left(\frac{\cos\phi}{\sin\phi}\right) + (D_{26})(c_{54}) \end{array} \right] \right\} \quad \text{(A.134)}$$

$$cp_{94} = \left\{ \begin{array}{l} \left(\frac{1}{R_\theta}\right)\left(\frac{1}{\sin\phi}\right)\left[\begin{array}{l} (-B_{16})(c_{24}) + (-B_{66})(c_{34}) + (-D_{16})(c_{44}) \\ + \left(-\frac{R_\phi}{R_\theta}\right)(D_{26})\left(\frac{\cos\phi}{\sin\phi}\right) + (-D_{66})(c_{54}) \end{array} \right] \\ + \left(\frac{1}{R_\theta}\right)\left(\frac{\cos\phi}{\sin\phi}\right)\left[\begin{array}{l} (B_{12})(cp_{24}) + (B_{26})(cp_{34}) + (D_{12})(cp_{44}) \\ + \left(\frac{R_\phi}{R_\theta}\right)\left(\frac{1}{\sin\phi}\right)(D_{26}) + (D_{26})(cp_{54}) \end{array} \right] \end{array} \right\} \quad \text{(A.135)}$$

$$cdp_{94} = \left\{ \left(\frac{1}{R_\theta}\right)\left(\frac{1}{\sin\phi}\right)\left[\begin{array}{l} (-B_{16})(cp_{24}) + (-B_{66})(cp_{34}) + (-D_{16})(cp_{44}) \\ + \left(-\frac{R_\phi}{R_\theta}\right)\left(\frac{1}{\sin\phi}\right)(D_{66}) + (-D_{66})(cp_{54}) \end{array} \right] \right\} \quad \text{(A.136)}$$

$$c_{95} = \left\{ \left(\frac{1}{R_\theta}\right)\left(\frac{\cos\phi}{\sin\phi}\right)\left[\begin{array}{l} (B_{12})(c_{25}) + (B_{26})(c_{35}) + (D_{12})(c_{45}) \\ + (D_{26})(c_{55}) + (-D_{26})\left(\frac{\cos\phi}{\sin\phi}\right) \end{array} \right] \right\} \quad \text{(A.137)}$$

$$cp_{95} = \left\{ \begin{array}{l} \left(\frac{1}{R_\theta}\right)\left(\frac{1}{\sin\phi}\right)\left[\begin{array}{l} (-B_{16})(c_{25}) + (-B_{66})(c_{35}) + (-D_{16})(c_{45}) \\ + (-D_{66})(c_{55}) + \left(-\frac{R_\phi}{R_\theta}\right)(-D_{66})\left(\frac{\cos\phi}{\sin\phi}\right) \end{array} \right] \\ + \left(\frac{1}{R_\theta}\right)\left(\frac{\cos\phi}{\sin\phi}\right)\left[\begin{array}{l} (B_{12})(cp_{25}) + (B_{26})(cp_{35}) + (D_{12})(cp_{45}) \\ + \left(\frac{R_\phi}{R_\theta}\right)\left(\frac{1}{\sin\phi}\right)(D_{22}) + (D_{26})(cp_{55}) \end{array} \right] \end{array} \right\} \quad \text{(A.138)}$$

$$cdp_{95} = \left\{ \left(\frac{1}{R_\theta}\right)\left(\frac{1}{\sin\phi}\right)\left[\begin{array}{l} (-B_{16})(cp_{25}) + (-B_{66})(cp_{35}) + (-D_{16})(cp_{45}) \\ + \left(-\frac{R_\phi}{R_\theta}\right)\left(\frac{1}{\sin\phi}\right)(D_{26}) + (-D_{66})(cp_{55}) \end{array} \right] \right\} \quad \text{(A.139)}$$

$$c_{96} = \{R_\phi\} \quad \text{(A.140)}$$

$$c_{97} = \left\{ \left(\frac{1}{R_\theta}\right)\left(\frac{\cos\phi}{\sin\phi}\right)\left[(B_{12})(c_{27}) + (B_{26})(c_{37}) + (D_{12})(c_{47}) + (D_{26})(c_{57})\right] \right\} \quad \text{(A.141)}$$

$$c_{98} = \left\{ \left(\frac{1}{R_\theta}\right)\left(\frac{\cos\phi}{\sin\phi}\right)\left[(B_{12})(c_{28}) + (B_{26})(c_{38}) + (D_{12})(c_{48}) + (D_{26})(c_{58})\right] \right\} \quad \text{(A.142)}$$

$$c_{99} = \left\{ \left(-\frac{R_\phi}{R_\theta}\right)\left(\frac{\cos\phi}{\sin\phi}\right) + \left(\frac{1}{R_\theta}\right)\left(\frac{\cos\phi}{\sin\phi}\right)\left[\begin{array}{l} (B_{12})(c_{29}) + (B_{26})(c_{39}) \\ + (D_{12})(c_{49}) + (D_{26})(c_{59}) \end{array} \right] \right\} \quad \text{(A.143)}$$

$$c_{910} = \left\{ \left(\frac{1}{R_\theta} \right) \left(\frac{\cos\phi}{\sin\phi} \right) \left[(B_{12})(c_{210}) + (B_{26})(c_{310}) + (D_{12})(c_{410}) + (D_{26})(c_{510}) \right] \right\} \quad \text{(A.144)}$$

$$cp_{910} = \left\{ \left(-\frac{R_\phi}{R_\theta} \right) \left(\frac{1}{\sin\phi} \right) \right\} \quad \text{(A.145)}$$

Coefficients of $\frac{\partial M_{\phi\theta}}{\partial \phi}$ equation, i.e. Equation (3.2.16)

$$cp_{101} = \left\{ \begin{array}{l} \left(\frac{1}{R_\theta} \right) \left(\frac{1}{\sin\phi} \right) \left[\begin{array}{l} (-B_{12})(c_{21}) + (-B_{12}) + \left(-\frac{R_\phi}{R_\theta} \right)(B_{22}) \\ + (-B_{26})(c_{31}) + (-D_{12})(c_{41}) + (-D_{26})(c_{51}) \end{array} \right] \\ + \left[(A_{45})(cp_{11}) + \left(\frac{R_\phi}{R_\theta} \right) \left(\frac{A_{44}}{\sin\phi} \right) \right] \end{array} \right\} \quad \text{(A.146)}$$

$$c_{102} = \{ [(-A_{45}) + (A_{45})(c_{12})] \} \quad \text{(A.147)}$$

$$cp_{102} = \left\{ \left(\frac{1}{R_\theta} \right) \left(\frac{1}{\sin\phi} \right) \left[\begin{array}{l} (-B_{12})(c_{22}) + (-B_{22}) \left(\frac{\cos\phi}{\sin\phi} \right) + (-B_{26})(c_{32}) \\ + (-D_{12})(c_{42}) + (-D_{26})(c_{52}) \end{array} \right] \right\} \quad \text{(A.148)}$$

$$cdp_{102} = \left\{ \left(\frac{1}{R_\theta} \right) \left(\frac{1}{\sin\phi} \right) \left[\begin{array}{l} (-B_{12})(cp_{22}) + \left(-\frac{R_\phi}{R_\theta} \right) (B_{26}) \left(\frac{1}{\sin\phi} \right) + (-B_{26})(cp_{32}) \\ + (-D_{12})(cp_{42}) + (-D_{26})(cp_{52}) \end{array} \right] \right\} \quad \text{(A.149)}$$

$$c_{103} = \left\{ \left[(A_{45})(c_{13}) + \left(-\frac{R_\phi}{R_\theta} \right)(A_{44}) \right] \right\} \quad \text{(A.150)}$$

$$cp_{103} = \left\{ \left(\frac{1}{R_\theta} \right) \left(\frac{1}{\sin\phi} \right) \left[\begin{array}{l} (-B_{12})(c_{23}) + (-B_{26})(c_{33}) + (B_{26}) \left(\frac{\cos\phi}{\sin\phi} \right) \\ + (-D_{12})(c_{43}) + (-D_{26})(c_{53}) \end{array} \right] \right\} \quad \text{(A.151)}$$

$$cdp_{103} = \left\{ \left(\frac{1}{R_\theta} \right) \left(\frac{1}{\sin\phi} \right) \left[\begin{array}{l} (-B_{12})(cp_{23}) + \left(-\frac{R_\phi}{R_\theta} \right) (B_{22}) \left(\frac{1}{\sin\phi} \right) + (-B_{26})(cp_{33}) \\ + (-D_{12})(cp_{43}) + (-D_{26})(cp_{53}) \end{array} \right] \right\} \tag{A.152}$$

$$c_{104} = \left\{ \left[(A_{45})(c_{14}) + (A_{45})(R_\phi) \right] \right\} \tag{A.153}$$

$$cp_{104} = \left\{ \left(\frac{1}{R_\theta} \right) \left(\frac{1}{\sin\phi} \right) \left[\begin{array}{l} (-B_{12})(c_{24}) + (-B_{26})(c_{34}) + (-D_{12})(c_{44}) \\ + (-D_{22}) \left(\frac{\cos\phi}{\sin\phi} \right) + (-D_{26})(c_{54}) \end{array} \right] \right\} \tag{A.154}$$

$$cdp_{104} = \left\{ \left(\frac{1}{R_\theta} \right) \left(\frac{1}{\sin\phi} \right) \left[\begin{array}{l} (-B_{12})(cp_{24}) + (-B_{26})(cp_{34}) + (-D_{12})(cp_{44}) \\ + \left(-\frac{R_\phi}{R_\theta} \right) (D_{26}) \left(\frac{1}{\sin\phi} \right) + (-D_{26})(cp_{54}) \end{array} \right] \right\} \tag{A.155}$$

$$c_{105} = \left\{ \left[(A_{45})(c_{15}) + (A_{44})(R_\phi) \right] \right\} \tag{A.156}$$

$$cp_{105} = \left\{ \left(\frac{1}{R_\theta} \right) \left(\frac{1}{\sin\phi} \right) \left[\begin{array}{l} (-B_{12})(c_{25}) + (-B_{26})(c_{35}) + (-D_{12})(c_{45}) \\ + (-D_{26})(c_{55}) + (D_{26}) \left(\frac{\cos\phi}{\sin\phi} \right) \end{array} \right] \right\} \tag{A.157}$$

$$cdp_{105} = \left\{ \left(\frac{1}{R_\theta} \right) \left(\frac{1}{\sin\phi} \right) \left[\begin{array}{l} (-B_{12})(cp_{25}) + (-B_{26})(cp_{35}) + (-D_{12})(cp_{45}) \\ + (-D_{26})(cp_{55}) + \left(-\frac{R_\phi}{R_\theta} \right) (D_{22}) \left(\frac{1}{\sin\phi} \right) \end{array} \right] \right\} \tag{A.158}$$

$$c_{106} = \left\{ \left[(A_{45})(c_{16}) \right] \right\} \tag{A.159}$$

$$cp_{107} = \left\{ \left(\frac{1}{R_\theta} \right) \left(\frac{1}{\sin\phi} \right) \left[(-B_{12})(c_{27}) + (-B_{26})(c_{37}) + (-D_{12})(c_{47}) + (-D_{26})(c_{57}) \right] \right\} \tag{A.160}$$

$$cp_{108} = \left\{ \left(\frac{1}{R_\theta} \right) \left(\frac{1}{\sin\phi} \right) \left[(-B_{12})(c_{28}) + (-B_{26})(c_{38}) + (-D_{12})(c_{48}) + (-D_{26})(c_{58}) \right] \right\} \tag{A.161}$$

$$cp_{109} = \left\{ \left(\frac{1}{R_\theta} \right) \left(\frac{1}{\sin\phi} \right) \left[(-B_{12})(c_{29}) + (-B_{26})(c_{39}) + (-D_{12})(c_{49}) + (-D_{26})(c_{59}) \right] \right\} \tag{A.162}$$

$$c_{1010} = \left\{ (-2) \left(\frac{R_\phi}{R_\theta} \right) \left(\frac{\cos\phi}{\sin\phi} \right) \right\} \tag{A.163}$$

$$cp_{1010} = \left\{ \left(\frac{1}{R_\theta} \right) \left(\frac{1}{\sin\phi} \right) \left[(-B_{12})(c_{210}) + (-B_{26})(c_{310}) + (-D_{12})(c_{410}) + (-D_{26})(c_{510}) \right] \right\} \tag{A.164}$$

APPENDIX B

COEFFICIENTS OF THE NONHOMOGENEOUS PART IN THE FUNDAMENTAL SYSTEM OF EQUATIONS DERIVED IN SECTION 3.2

The nonhomogeneous coefficients $B_i \quad (i = 1,2,...,10)$ of the fundamental system of equations given in Section 3.2 can be related to the loading terms through

$$\begin{Bmatrix} B_1 \\ B_2 \\ B_3 \\ B_4 \\ B_5 \\ B_6 \\ B_7 \\ B_8 \\ B_9 \\ B_{10} \end{Bmatrix} = \begin{bmatrix} 0 & 0 & 0 & 0 & 0 & 0 & 0 & 0 & 0 \\ 0 & 0 & 0 & CB_{24} & 0 & CB_{26} & CB_{27} & 0 & CB_{29} \\ 0 & 0 & 0 & CB_{34} & 0 & CB_{36} & CB_{37} & 0 & CB_{39} \\ 0 & 0 & 0 & CB_{44} & 0 & CB_{46} & CB_{47} & 0 & CB_{49} \\ 0 & 0 & 0 & CB_{54} & 0 & CB_{56} & CB_{57} & 0 & CB_{59} \\ CB_{61} & 0 & 0 & CB_{64} & CB_{65} & CB_{66} & CB_{67} & 0 & CB_{69} \\ 0 & CB_{72} & 0 & CB_{74} & CB_{75} & CB_{76} & CB_{77} & 0 & CB_{79} \\ 0 & 0 & CB_{83} & 0 & 0 & 0 & 0 & 0 & 0 \\ 0 & 0 & 0 & CB_{94} & 0 & CB_{96} & CB_{97} & CB_{98} & CB_{99} \\ 0 & 0 & 0 & 0 & 0 & 0 & 0 & 0 & 0 \end{bmatrix} \begin{Bmatrix} p_\zeta \\ p_\phi \\ p_\theta \\ N_\phi^T \\ N_\theta^T \\ N_{\phi\theta}^T \\ M_\phi^T \\ M_\theta^T \\ M_{\phi\theta}^T \end{Bmatrix} \tag{B.1}$$

where

the nonhomogeneous coefficients (B_1) of $\dfrac{\partial u_\zeta}{\partial \phi}$ equation, i.e. Equation (3.2.5) are given as:

$$CB_{1j} = 0 \qquad (j = 1,2,...9) \tag{B.2}$$

the nonhomogeneous coefficients (B_2) of $\frac{\partial u_\phi}{\partial \phi}$ equation, i.e. Equation (3.2.8) are given as:

$$CB_{24} = c_{27} \tag{B.3}$$

$$CB_{26} = c_{28} \tag{B.4}$$

$$CB_{27} = c_{29} \tag{B.5}$$

$$CB_{29} = c_{210} \tag{B.6}$$

the nonhomogeneous coefficients (B_3) of $\frac{\partial u_\theta}{\partial \phi}$ equation, i.e. Equation (3.2.9) are given as:

$$CB_{34} = c_{37} \tag{B.7}$$

$$CB_{36} = c_{38} \tag{B.8}$$

$$CB_{37} = c_{39} \tag{B.9}$$

$$CB_{39} = c_{310} \tag{B.10}$$

the nonhomogeneous coefficients (B_4) of $\frac{\partial \beta_\phi}{\partial \phi}$ equation, i.e. Equation (3.2.10) are given as:

$$CB_{44} = c_{47} \tag{B.11}$$

$$CB_{46} = c_{48} \tag{B.12}$$

$$CB_{47} = c_{49} \tag{B.13}$$

$$CB_{49} = c_{410} \tag{B.14}$$

the nonhomogeneous coefficients (B_5) of $\frac{\partial \beta_\theta}{\partial \phi}$ equation, i.e. Equation (3.2.11) are given as:

$$CB_{54} = c_{57} \tag{B.15}$$

$$CB_{56} = c_{58} \tag{B.16}$$

$$CB_{57} = c_{59} \tag{B.17}$$

$$CB_{59} = c_{510} \tag{B.18}$$

the nonhomogeneous coefficients (B_6) of $\frac{\partial Q_{\phi\zeta}}{\partial \phi}$ equation, i.e. Equation (3.2.12) are given as:

$$CB_{61} = -R_\phi \tag{B.19}$$

$$CB_{64} = \frac{1}{R_\theta}\left(A_{12}c_{27} + A_{26}c_{37} + B_{12}c_{47} + B_{26}c_{57}\right) \tag{B.20}$$

$$CB_{65} = -\frac{R_\phi}{R_\theta} \tag{B.21}$$

$$CB_{66} = \frac{1}{R_\theta}\left(A_{12}c_{28} + A_{26}c_{38} + B_{12}c_{48} + B_{26}c_{58}\right) \tag{B.22}$$

$$CB_{67} = \frac{1}{R_\theta}\left(A_{12}c_{29} + A_{26}c_{39} + B_{12}c_{49} + B_{26}c_{59}\right) \tag{B.23}$$

$$CB_{69} = \frac{1}{R_\theta}\left(A_{12}c_{210} + A_{26}c_{310} + B_{12}c_{410} + B_{26}c_{510}\right) \tag{B.24}$$

the nonhomogeneous coefficients (B_7) of $\frac{\partial N_{\phi\phi}}{\partial \phi}$ equation, i.e. Equation (3.2.13) are given as:

$$CB_{72} = -R_\phi \tag{B.25}$$

$$CB_{74} = \frac{1}{R_\theta}\frac{\cos\phi}{\sin\phi}\left(A_{12}c_{27} + A_{26}c_{37} + B_{12}c_{47} + B_{26}c_{57}\right) \tag{B.26}$$

$$CB_{75} = -\frac{R_\phi}{R_\theta}\frac{\cos\phi}{\sin\phi} \tag{B.27}$$

$$CB_{76} = \frac{1}{R_\theta}\frac{\cos\phi}{\sin\phi}\left(A_{12}c_{28} + A_{26}c_{38} + B_{12}c_{48} + B_{26}c_{58}\right) \tag{B.28}$$

$$CB_{77} = \frac{1}{R_\theta}\frac{\cos\phi}{\sin\phi}\left(A_{12}c_{29} + A_{26}c_{39} + B_{12}c_{49} + B_{26}c_{59}\right) \tag{B.29}$$

$$CB_{79} = \frac{1}{R_\theta}\frac{\cos\phi}{\sin\phi}\left(A_{12}c_{210} + A_{26}c_{310} + B_{12}c_{410} + B_{26}c_{510}\right) \tag{B.30}$$

the nonhomogeneous coefficients $\left(B_8\right)$ of $\frac{\partial N_{\phi\theta}}{\partial\phi}$ equation, i.e. Equation (3.2.14) are given as:

$$CB_{83} = -R_\phi \tag{B.31}$$

the nonhomogeneous coefficients $\left(B_9\right)$ of $\frac{\partial M_{\phi\phi}}{\partial\phi}$ equation, i.e. Equation (3.2.15) are given as:

$$CB_{94} = \frac{1}{R_\theta}\frac{\cos\phi}{\sin\phi}\left(B_{12}c_{27} + B_{26}c_{37} + D_{12}c_{47} + D_{26}c_{57}\right) \tag{B.32}$$

$$CB_{96} = \frac{1}{R_\theta}\frac{\cos\phi}{\sin\phi}\left(B_{12}c_{28} + B_{26}c_{38} + D_{12}c_{48} + D_{26}c_{58}\right) \tag{B.33}$$

$$CB_{97} = \frac{1}{R_\theta}\frac{\cos\phi}{\sin\phi}\left(B_{12}c_{29} + B_{26}c_{39} + D_{12}c_{49} + D_{26}c_{59}\right) \tag{B.34}$$

$$CB_{98} = -\frac{R_\phi}{R_\theta}\frac{\cos\phi}{\sin\phi} \tag{B.35}$$

$$CB_{99} = \frac{1}{R_\theta}\frac{\cos\phi}{\sin\phi}\left(B_{12}c_{210} + B_{26}c_{310} + D_{12}c_{410} + D_{26}c_{510}\right) \tag{B.36}$$

the nonhomogeneous coefficients $\left(B_{10}\right)$ of $\frac{\partial M_{\phi\theta}}{\partial \phi}$ equation, i.e. Equation (3.2.16) are given as:

$$CB_{10j} = 0 \qquad \left(j = 1,2,...9\right) \tag{B.37}$$

In the Equations (B.3) – (B.36), c_{ij} are the coefficients of the homogeneous part in the fundamental system of equations derived in Section 3.2, and given in detail in Appendix A.

A_{ij} are the extensional stiffness coefficients, B_{ij} are the bending stretching coupling stiffness coefficients, and D_{ij} are the bending stiffness coefficients given by Equations (2.3.2.24) – (2.3.2.26).

It should be stressed that B_i $\left(i = 1,2,...,10\right)$ is the vector of nonhomogeneous coefficients in the fundamental system of equations; whereas B_{ij} $\left(i, j = 1,2,6\right)$ are the bending stretching coupling stiffness coefficients given by Equation (2.3.2.25) and they should not be confused.

APPENDIX C

FINITE EXPONENTIAL FOURIER TRANSFORM OF EQUATION (3.2.12)

Equation (3.2.12) is given in Section 3.2 as

$$\begin{aligned}\frac{\partial Q_\phi}{\partial \phi} &= c_{61}u_\zeta^0 + cdp_{61}\frac{\partial^2 u_\zeta^0}{\partial \theta^2} + c_{62}u_\phi^0 + cp_{62}\frac{\partial u_\phi^0}{\partial \theta} + c_{63}u_\theta^0 + cp_{63}\frac{\partial u_\theta^0}{\partial \theta} + c_{64}\beta_\phi \\ &+ cp_{64}\frac{\partial \beta_\phi}{\partial \theta} + c_{65}\beta_\theta + cp_{65}\frac{\partial \beta_\theta}{\partial \theta} + c_{66}Q_\phi + cp_{66}\frac{\partial Q_\phi}{\partial \theta} + c_{67}N_{\phi\phi} \\ &+ c_{68}N_{\phi\theta} + c_{69}M_{\phi\phi} + c_{610}M_{\phi\theta} + B_6\end{aligned} \tag{C.1}$$

Applying the finite exponential Fourier transform to Equation (C.1), along with using the expansion given in Appendix B,

$$\frac{1}{2\pi}\int_0^{2\pi}\left[\frac{\partial Q_\phi(\phi,\theta)}{\partial\phi}e^{-in\theta}\right]d\theta=(c_{61})\frac{1}{2\pi}\int_0^{2\pi}\left[u_\zeta^0(\phi,\theta)e^{-in\theta}\right]d\theta+$$

$$(cdp_{61})\frac{1}{2\pi}\int_0^{2\pi}\left[\frac{\partial^2 u_\zeta^0(\phi,\theta)}{\partial\theta^2}e^{-in\theta}\right]d\theta+(c_{62})\frac{1}{2\pi}\int_0^{2\pi}\left[u_\phi^0(\phi,\theta)e^{-in\theta}\right]d\theta+$$

$$(cp_{62})\frac{1}{2\pi}\int_0^{2\pi}\left[\frac{\partial u_\phi^0(\phi,\theta)}{\partial\theta}e^{-in\theta}\right]d\theta+(c_{63})\frac{1}{2\pi}\int_0^{2\pi}\left[u_\theta^0(\phi,\theta)e^{-in\theta}\right]d\theta+$$

$$(cp_{63})\frac{1}{2\pi}\int_0^{2\pi}\left[\frac{\partial u_\theta^0(\phi,\theta)}{\partial\theta}e^{-in\theta}\right]d\theta+(c_{64})\frac{1}{2\pi}\int_0^{2\pi}\left[\beta_\phi(\phi,\theta)e^{-in\theta}\right]d\theta+$$

$$(cp_{64})\frac{1}{2\pi}\int_0^{2\pi}\left[\frac{\partial\beta_\phi(\phi,\theta)}{\partial\theta}e^{-in\theta}\right]d\theta+(c_{65})\frac{1}{2\pi}\int_0^{2\pi}\left[\beta_\theta(\phi,\theta)e^{-in\theta}\right]d\theta+$$

$$(cp_{65})\frac{1}{2\pi}\int_0^{2\pi}\left[\frac{\partial\beta_\theta(\phi,\theta)}{\partial\theta}e^{-in\theta}\right]d\theta+(c_{66})\frac{1}{2\pi}\int_0^{2\pi}\left[Q_\phi(\phi,\theta)e^{-in\theta}\right]d\theta+$$

$$(cp_{66})\frac{1}{2\pi}\int_0^{2\pi}\left[\frac{\partial Q_\phi(\phi,\theta)}{\partial\theta}e^{-in\theta}\right]d\theta+(c_{67})\frac{1}{2\pi}\int_0^{2\pi}\left[N_\phi(\phi,\theta)e^{-in\theta}\right]d\theta+$$

$$(c_{68})\frac{1}{2\pi}\int_0^{2\pi}\left[N_{\phi\theta}(\phi,\theta)e^{-in\theta}\right]d\theta+(c_{69})\frac{1}{2\pi}\int_0^{2\pi}\left[M_\phi(\phi,\theta)e^{-in\theta}\right]d\theta+$$

$$(c_{610})\frac{1}{2\pi}\int_0^{2\pi}\left[M_{\phi\theta}(\phi,\theta)e^{-in\theta}\right]d\theta+(CB_{61})\frac{1}{2\pi}\int_0^{2\pi}\left[p_\zeta(\phi,\theta)e^{-in\theta}\right]d\theta$$

$$+(CB_{64})\frac{1}{2\pi}\int_0^{2\pi}\left[N_\phi^T(\phi,\theta)e^{-in\theta}\right]d\theta+(CB_{65})\frac{1}{2\pi}\int_0^{2\pi}\left[N_\theta^T(\phi,\theta)e^{-in\theta}\right]d\theta \qquad \text{(C.2)}$$

$$+(CB_{66})\frac{1}{2\pi}\int_0^{2\pi}\left[N_{\phi\theta}^T(\phi,\theta)e^{-in\theta}\right]d\theta+(CB_{67})\frac{1}{2\pi}\int_0^{2\pi}\left[M_\phi^T(\phi,\theta)e^{-in\theta}\right]d\theta$$

$$+(CB_{69})\frac{1}{2\pi}\int_0^{2\pi}\left[M_{\phi\theta}^T(\phi,\theta)e^{-in\theta}\right]d\theta$$

Utilizing Equation (3.3.2) in Equation (C.2),

$$\int_0^{2\pi}\begin{bmatrix}\dfrac{\partial Q_\phi(\phi,\theta)}{\partial\phi}\cos n\theta\\ -i\sin n\theta\dfrac{\partial Q_\phi(\phi,\theta)}{\partial\phi}\end{bmatrix}d\theta=(c_{61})\int_0^{2\pi}\begin{bmatrix}u_\zeta^0(\phi,\theta)\cos n\theta\\ -iu_\zeta^0(\phi,\theta)\sin n\theta\end{bmatrix}d\theta$$
$$+(cdp_{61})\int_0^{2\pi}(in)^2\begin{bmatrix}u_\zeta^0(\phi,\theta)\cos n\theta\\ -iu_\zeta^0(\phi,\theta)\sin n\theta\end{bmatrix}d\theta+(c_{62})\int_0^{2\pi}\begin{bmatrix}u_\phi^0(\phi,\theta)\cos n\theta\\ -iu_\phi^0(\phi,\theta)\sin n\theta\end{bmatrix}d\theta$$
$$+(cp_{62})\int_0^{2\pi}(in)\begin{bmatrix}u_\phi^0(\phi,\theta)\cos n\theta\\ -iu_\phi^0(\phi,\theta)\sin n\theta\end{bmatrix}d\theta+(c_{63})\int_0^{2\pi}\begin{bmatrix}u_\theta^0(\phi,\theta)\cos n\theta\\ -iu_\theta^0(\phi,\theta)\sin n\theta\end{bmatrix}d\theta$$
$$+(cp_{63})\int_0^{2\pi}(in)\begin{bmatrix}u_\theta^0(\phi,\theta)\cos n\theta\\ -iu_\theta^0(\phi,\theta)\sin n\theta\end{bmatrix}d\theta+(c_{64})\int_0^{2\pi}\begin{bmatrix}\beta_\phi(\phi,\theta)\cos n\theta\\ -i\beta_\phi(\phi,\theta)\sin n\theta\end{bmatrix}d\theta$$
$$+(cp_{64})\int_0^{2\pi}(in)\begin{bmatrix}\beta_\phi(\phi,\theta)\cos n\theta\\ -i\beta_\phi(\phi,\theta)\sin n\theta\end{bmatrix}d\theta+(c_{65})\int_0^{2\pi}\begin{bmatrix}\beta_\theta(\phi,\theta)\cos n\theta\\ -i\beta_\theta(\phi,\theta)\sin n\theta\end{bmatrix}d\theta$$
$$+(cp_{65})\int_0^{2\pi}(in)\begin{bmatrix}\beta_\theta(\phi,\theta)\cos n\theta\\ -i\beta_\theta(\phi,\theta)\sin n\theta\end{bmatrix}d\theta+(c_{66})\int_0^{2\pi}\begin{bmatrix}Q_\phi(\phi,\theta)\cos n\theta\\ -iQ_\phi(\phi,\theta)\sin n\theta\end{bmatrix}d\theta$$
$$+(cp_{66})\int_0^{2\pi}(in)\begin{bmatrix}Q_\phi(\phi,\theta)\cos n\theta\\ -iQ_\phi(\phi,\theta)\sin n\theta\end{bmatrix}d\theta+(c_{67})\int_0^{2\pi}\begin{bmatrix}N_\phi(\phi,\theta)\cos n\theta\\ -iN_\phi(\phi,\theta)\sin n\theta\end{bmatrix}d\theta$$
$$+(c_{68})\int_0^{2\pi}\begin{bmatrix}N_{\phi\theta}(\phi,\theta)\cos n\theta\\ -iN_{\phi\theta}(\phi,\theta)\sin n\theta\end{bmatrix}d\theta+(c_{69})\int_0^{2\pi}\begin{bmatrix}M_\phi(\phi,\theta)\cos n\theta\\ -iM_\phi(\phi,\theta)\sin n\theta\end{bmatrix}d\theta$$
$$+(c_{610})\int_0^{2\pi}\begin{bmatrix}M_{\phi\theta}(\phi,\theta)\cos n\theta\\ -iM_{\phi\theta}(\phi,\theta)\sin n\theta\end{bmatrix}d\theta+CB_{61}\int_0^{2\pi}\begin{bmatrix}p_\zeta(\phi,\theta)\cos n\theta\\ -ip_\zeta(\phi,\theta)\sin n\theta\end{bmatrix}d\theta$$
$$+CB_{64}\int_0^{2\pi}\begin{bmatrix}N_\phi^T(\phi,\theta)\cos n\theta\\ -iN_\phi^T(\phi,\theta)\sin n\theta\end{bmatrix}d\theta+CB_{65}\int_0^{2\pi}\begin{bmatrix}N_\theta^T(\phi,\theta)\cos n\theta\\ -iN_\theta^T(\phi,\theta)\sin n\theta\end{bmatrix}d\theta$$
$$+CB_{66}\int_0^{2\pi}\begin{bmatrix}N_{\phi\theta}^T(\phi,\theta)\cos n\theta\\ -iN_{\phi\theta}^T(\phi,\theta)\sin n\theta\end{bmatrix}d\theta+CB_{67}\int_0^{2\pi}\begin{bmatrix}M_\phi^T(\phi,\theta)\cos n\theta\\ -iM_\phi^T(\phi,\theta)\sin n\theta\end{bmatrix}d\theta$$
$$+CB_{69}\int_0^{2\pi}\begin{bmatrix}M_{\phi\theta}^T(\phi,\theta)\cos n\theta\\ -iM_{\phi\theta}^T(\phi,\theta)\sin n\theta\end{bmatrix}d\theta \qquad \text{(C.3)}$$

Note that expansion of N_ϕ^T, N_θ^T, $N_{\phi\theta}^T$, M_ϕ^T, M_θ^T and $M_{\phi\theta}^T$ terms have further been explained in detail in Section 3.3. Expanding Equation (C.3) by using Equation (3.3.2),

$$\left[\frac{dQ_\phi(\phi)}{d\phi}\right]_{nc} - i\left[\frac{dQ_\phi(\phi)}{d\phi}\right]_{ns} = (c_{61})\left\{\left[u_\zeta^0(\phi)\right]_{nc} - i\left[u_\zeta^0(\phi)\right]_{ns}\right\}$$

$$-(n^2)(cdp_{61})\left\{\left[u_\zeta^0(\phi)\right]_{nc} - i\left[u_\zeta^0(\phi)\right]_{ns}\right\} + (c_{62})\left\{\left[u_\phi^0(\phi)\right]_{nc} - i\left[u_\phi^0(\phi)\right]_{ns}\right\}$$

$$+(cp_{62})(n)\left\{i\left[u_\phi^0(\phi)\right]_{nc} + \left[u_\phi^0(\phi)\right]_{ns}\right\} + (c_{63})\left\{\left[u_\theta^0(\phi)\right]_{nc} - i\left[u_\theta^0(\phi)\right]_{ns}\right\}$$

$$+(cp_{63})(n)\left\{i\left[u_\theta^0(\phi)\right]_{nc} + \left[u_\theta^0(\phi)\right]_{ns}\right\} + (c_{64})\left\{\left[\beta_\phi(\phi)\right]_{nc} - i\left[\beta_\phi(\phi)\right]_{ns}\right\}$$

$$+(cp_{64})(n)\left\{i\left[\beta_\phi(\phi)\right]_{nc} + \left[\beta_\phi(\phi)\right]_{ns}\right\} + (c_{65})\left\{\left[\beta_\theta(\phi)\right]_{nc} - i\left[\beta_\theta(\phi)\right]_{ns}\right\}$$

$$+(cp_{65})(n)\left\{i\left[\beta_\theta(\phi)\right]_{nc} + \left[\beta_\theta(\phi)\right]_{ns}\right\} + (c_{66})\left\{\left[Q_\phi(\phi)\right]_{nc} - i\left[Q_\phi(\phi)\right]_{ns}\right\}$$

$$+(cp_{66})(n)\left\{i\left[Q_\phi(\phi)\right]_{nc} + \left[Q_\phi(\phi)\right]_{ns}\right\} + (c_{67})\left\{\left[N_\phi(\phi)\right]_{nc} - i\left[N_\phi(\phi)\right]_{ns}\right\}$$

$$+(c_{68})\left\{\left[N_{\phi\theta}(\phi)\right]_{nc} - i\left[N_{\phi\theta}(\phi)\right]_{ns}\right\} + (c_{69})\left\{\left[M_\phi(\phi)\right]_{nc} - i\left[M_\phi(\phi)\right]_{ns}\right\}$$

$$+(c_{610})\left\{\left[M_{\phi\theta}(\phi)\right]_{nc} - i\left[M_{\phi\theta}(\phi)\right]_{ns}\right\} + CB_{61}\left\{\left[p_\zeta(\phi)\right]_{nc} - i\left[p_\zeta(\phi)\right]_{ns}\right\}$$

$$+CB_{64}\left\{\left[N_\phi^T(\phi)\right]_{nc} - i\left[N_\phi^T(\phi)\right]_{ns}\right\} + CB_{65}\left\{\left[N_\theta^T(\phi)\right]_{nc} - i\left[N_\theta^T(\phi)\right]_{ns}\right\} \quad \text{(C.4)}$$

$$+CB_{66}\left\{\left[N_{\phi\theta}^T(\phi)\right]_{nc} - i\left[N_{\phi\theta}^T(\phi)\right]_{ns}\right\} + CB_{67}\left\{\left[M_\phi^T(\phi)\right]_{nc} - i\left[M_\phi^T(\phi)\right]_{ns}\right\}$$

$$+CB_{69}\left\{\left[M_{\phi\theta}^T(\phi)\right]_{nc} - i\left[M_{\phi\theta}^T(\phi)\right]_{ns}\right\}$$

Now separating the real and imaginary terms of Equation (C.4) and writing the parts involving the real and imaginary terms in two equations as follows:

$$\left[\frac{dQ_\phi(\phi)}{d\phi}\right]_{nc} = (c_{61})\left[u_\zeta^0(\phi)\right]_{nc} - (n^2)(cdp_{61})\left[u_\zeta^0(\phi)\right]_{nc} + (c_{62})\left[u_\phi^0(\phi)\right]_{nc}$$

$$+ (cp_{62})(n)\left[u_\phi^0(\phi)\right]_{ns} + (c_{63})\left[u_\theta^0(\phi)\right]_{nc} + (cp_{63})(n)\left[u_\theta^0(\phi)\right]_{ns} + (c_{64})\left[\beta_\phi(\phi)\right]_{nc}$$

$$+ (cp_{64})(n)\left[\beta_\phi(\phi)\right]_{ns} + (c_{65})\left[\beta_\theta(\phi)\right]_{nc} + (cp_{65})(n)\left[\beta_\theta(\phi)\right]_{ns} + (c_{66})\left[Q_\phi(\phi)\right]_{nc} \quad \text{(C.5)}$$

$$+ (cp_{66})(n)\left[Q_\phi(\phi)\right]_{ns} + (c_{67})\left[N_\phi(\phi)\right]_{nc} + (c_{68})\left[N_{\phi\theta}(\phi)\right]_{nc} + (c_{69})\left[M_\phi(\phi)\right]_{nc}$$

$$+ (c_{610})\left[M_{\phi\theta}(\phi)\right]_{nc} + CB_{61}\left[p_\zeta(\phi)\right]_{nc} + CB_{64}\left[N_\phi^T(\phi)\right]_{nc} + CB_{65}\left[N_\theta^T(\phi)\right]_{nc}$$

$$+ CB_{66}\left[N_{\phi\theta}^T(\phi)\right]_{nc} + CB_{67}\left[M_\phi^T(\phi)\right]_{nc} + CB_{69}\left[M_{\phi\theta}^T(\phi)\right]_{nc}$$

and imaginary terms,

$$\left[\frac{dQ_\phi(\phi)}{d\phi}\right]_{ns} = (c_{61})\left[u_\zeta^0(\phi)\right]_{ns} - (n^2)(cdp_{61})\left[u_\zeta^0(\phi)\right]_{ns} + (c_{62})\left[u_\phi^0(\phi)\right]_{ns}$$

$$- (cp_{62})(n)\left[u_\phi^0(\phi)\right]_{nc} + (c_{63})\left[u_\theta^0(\phi)\right]_{ns} - (cp_{63})(n)\left[u_\theta^0(\phi)\right]_{nc} + (c_{64})\left[\beta_\phi(\phi)\right]_{ns}$$

$$- (cp_{64})(n)\left[\beta_\phi(\phi)\right]_{nc} + (c_{65})\left[\beta_\theta(\phi)\right]_{ns} - (cp_{65})(n)\left[\beta_\theta(\phi)\right]_{nc} + (c_{66})\left[Q_\phi(\phi)\right]_{ns} \quad \text{(C.6)}$$

$$- (cp_{66})(n)\left[Q_\phi(\phi)\right]_{nc} + (c_{67})\left[N_\phi(\phi)\right]_{ns} + (c_{68})\left[N_{\phi\theta}(\phi)\right]_{ns} + (c_{69})\left[M_\phi(\phi)\right]_{ns}$$

$$+ (c_{610})\left[M_{\phi\theta}(\phi)\right]_{ns} + CB_{61}\left[p_\zeta(\phi)\right]_{ns} + CB_{64}\left[N_\phi^T(\phi)\right]_{ns} + CB_{65}\left[N_\theta^T(\phi)\right]_{ns}$$

$$+ CB_{66}\left[N_{\phi\theta}^T(\phi)\right]_{ns} + CB_{67}\left[M_\phi^T(\phi)\right]_{ns} + CB_{69}\left[M_{\phi\theta}^T(\phi)\right]_{ns}$$

APPENDIX D

THE ELEMENTS OF COEFFICIENT MATRIX K

The elements of the coefficient matrix $[K]_{20\times 20}$ given in Equation (3.3.59) are listed below.

The elements of 1st row are:

$$K_{11}=0;\ K_{12}=ncp_{11};\ K_{13}=c_{12};\ K_{14}=0;\ K_{15}=c_{13};$$

$$K_{16}=0;\ K_{17}=c_{14};\ K_{18}=0;\ K_{19}=c_{15};\ K_{110}=0; \qquad \text{(D.1-10)}$$

$$K_{111}=c_{16};\ K_{112}=0;\ K_{113}=0;\ K_{114}=0;\ K_{115}=0;$$

$$K_{116}=0;\ K_{117}=0;\ K_{118}=0;\ K_{119}=0;\ K_{120}=0;$$

The elements of 2nd row are:

$$K_{21}=-ncp_{11};\ K_{22}=0;\ K_{23}=0;\ K_{24}=c_{12};\ K_{25}=0;$$

$$K_{26}=c_{13};\ K_{27}=0;\ K_{28}=c_{14};\ K_{29}=0;\ K_{210}=c_{15}; \qquad \text{(D.11-20)}$$

$$K_{211}=0;\ K_{212}=c_{16};\ K_{213}=0;\ K_{214}=0;\ K_{215}=0;$$

$$K_{216}=0;\ K_{217}=0;\ K_{218}=0;\ K_{219}=0;\ K_{220}=0$$

The elements of 3rd row are:

$$K_{31} = c_{21};\ K_{32} = 0;\ K_{33} = c_{22};\ K_{34} = ncp_{22};\ K_{35} = c_{23};$$

$$K_{36} = ncp_{23};\ K_{37} = c_{24};\ K_{38} = ncp_{24};\ K_{39} = c_{25};\ K_{310} = ncp_{25};$$

$$K_{311} = 0;\ K_{312} = 0;\ K_{313} = c_{27};\ K_{314} = 0;\ K_{315} = c_{28};$$

$$K_{316} = 0;\ K_{317} = c_{29};\ K_{318} = 0;\ K_{319} = c_{210};\ K_{320} = 0$$

(D.21-30)

The elements of 4th row are:

$$K_{41} = 0;\ K_{42} = c_{21};\ K_{43} = -ncp_{22};\ K_{44} = c_{22};\ K_{45} = -ncp_{23};$$

$$K_{46} = c_{23};\ K_{47} = -ncp_{24};\ K_{48} = c_{24};\ K_{49} = -ncp_{25};\ K_{410} = c_{25};$$

$$K_{411} = 0;\ K_{412} = 0;\ K_{413} = 0;\ K_{414} = c_{27};\ K_{415} = 0;$$

$$K_{416} = c_{28};\ K_{417} = 0;\ K_{418} = c_{29};\ K_{419} = 0;\ K_{420} = c_{210}$$

(D.31-40)

The elements of 5th row are:

$$K_{51} = c_{31};\ K_{52} = 0;\ K_{53} = c_{32};\ K_{54} = ncp_{32};\ K_{55} = c_{33};$$

$$K_{56} = ncp_{33};\ K_{57} = c_{34};\ K_{58} = ncp_{34};\ K_{59} = c_{35};\ K_{510} = ncp_{35};$$

$$K_{511} = 0;\ K_{512} = 0;\ K_{513} = c_{37};\ K_{514} = 0;\ K_{515} = c_{38};$$

$$K_{516} = 0;\ K_{517} = c_{39};\ K_{518} = 0;\ K_{519} = c_{310};\ K_{520} = 0$$

(D.41-50)

The elements of 6th row are:

$$K_{61}=0;\ K_{62}=c_{31};\ K_{63}=-ncp_{32};\ K_{64}=c_{32};\ K_{65}=-ncp_{33};$$

$$K_{66}=c_{33};\ K_{67}=-ncp_{34};\ K_{68}=c_{34};\ K_{69}=-ncp_{35};\ K_{610}=c_{35};$$

$$K_{611}=0;\ K_{612}=0;\ K_{613}=0;\ K_{614}=c_{37};\ K_{615}=0; \qquad \text{(D.51-60)}$$

$$K_{616}=c_{38};\ K_{617}=0;\ K_{618}=c_{39};\ K_{619}=0;\ K_{620}=c_{310}$$

The elements of 7th row are:

$$K_{71}=c_{41};\ K_{72}=0;\ K_{73}=c_{42};\ K_{74}=ncp_{42};\ K_{75}=c_{43};$$

$$K_{76}=ncp_{43};\ K_{77}=c_{44};\ K_{78}=ncp_{43};\ K_{79}=c_{45};\ K_{710}=ncp_{45};$$

$$K_{711}=0;\ K_{712}=0;\ K_{713}=c_{47};\ K_{714}=0;\ K_{715}=c_{48}; \qquad \text{(D.61-70)}$$

$$K_{716}=0;\ K_{717}=c_{49};\ K_{718}=0;\ K_{719}=c_{410};\ K_{720}=0$$

The elements of 8th row are:

$$K_{81}=0;\ K_{82}=c_{41};\ K_{83}=-ncp_{42};\ K_{84}=c_{42};\ K_{85}=-ncp_{43};$$

$$K_{86}=c_{43};\ K_{87}=-ncp_{44};\ K_{88}=c_{44};\ K_{89}=-ncp_{45};\ K_{810}=c_{45};$$

$$K_{811}=0;\ K_{812}=0;\ K_{813}=0;\ K_{814}=c_{47};\ K_{815}=0; \qquad \text{(D.71-80)}$$

$$K_{816}=c_{48};\ K_{817}=0;\ K_{818}=c_{49};\ K_{819}=0;\ K_{820}=c_{410}$$

The elements of 9th row are:

$$K_{91} = c_{51};\ K_{92} = 0;\ K_{93} = c_{52};\ K_{94} = ncp_{52};\ K_{95} = c_{53};$$

$$K_{96} = ncp_{53};\ K_{97} = c_{54};\ K_{98} = ncp_{54};\ K_{99} = c_{55};\ K_{910} = ncp_{55};$$

(D.81-90)

$$K_{911} = 0;\ K_{912} = 0;\ K_{913} = c_{57};\ K_{914} = 0;\ K_{915} = c_{58};$$

$$K_{916} = 0;\ K_{917} = c_{59};\ K_{918} = 0;\ K_{919} = c_{510};\ K_{920} = 0$$

The elements of 10th row are:

$$K_{101} = 0;\ K_{102} = c_{51};\ K_{103} = -ncp_{52};\ K_{104} = c_{52};\ K_{105} = -ncp_{53};$$

$$K_{106} = c_{53};\ K_{107} = -ncp_{54};\ K_{108} = c_{54};\ K_{109} = -ncp_{55};\ K_{1010} = c_{55};$$

(D.91-100)

$$K_{1011} = 0;\ K_{1012} = 0;\ K_{1013} = 0;\ K_{1014} = c_{57};\ K_{1015} = 0;$$

$$K_{1016} = c_{58};\ K_{1017} = 0;\ K_{1018} = c_{59};\ K_{1019} = 0;\ K_{1020} = c_{510}$$

The elements of 11th row are:

$$K_{111} = c_{61} - n^2 cdp_{61};\ K_{112} = 0;\ K_{113} = c_{62};\ K_{114} = ncp_{62};\ K_{115} = c_{63};$$

$$K_{116} = ncp_{63};\ K_{117} = c_{64};\ K_{118} = ncp_{64};\ K_{119} = c_{65};\ K_{1110} = ncp_{65};$$

$$K_{1111} = c_{66};\ K_{1112} = ncp_{66};\ K_{1113} = c_{67};\ K_{1114} = 0;\ K_{1115} = c_{68};$$

$$K_{1116} = 0;\ K_{1117} = c_{69};\ K_{1118} = 0;\ K_{1119} = c_{610};\ K_{1120} = 0$$

(D.101-110)

The elements of 12th row are:

$$K_{121}=0;\ K_{122}=c_{61}-n^2cdp_{61};\ K_{123}=-ncp_{62};\ K_{124}=c_{62};\ K_{125}=-ncp_{63};$$

$$K_{126}=c_{63};\ K_{127}=-ncp_{64};\ K_{128}=c_{64};\ K_{129}=-ncp_{65};\ K_{1210}=c_{65};$$

$$K_{1211}=-ncp_{66};\ K_{1212}=c_{66};\ K_{1213}=0;\ K_{1214}=c_{67};\ K_{1215}=0;$$

$$K_{1216}=c_{68};\ K_{1217}=0;\ K_{1218}=c_{69};\ K_{1219}=0;\ K_{1220}=c_{610}$$

(D.111-120)

The elements of 13th row are:

$$K_{131}=c_{71};\ K_{132}=0;\ K_{133}=c_{72};\ K_{134}=ncp_{72};\ K_{135}=c_{73};$$

$$K_{136}=ncp_{73};\ K_{137}=c_{74};\ K_{138}=ncp_{74};\ K_{139}=c_{75};\ K_{1310}=ncp_{75};$$

(D.121-130)

$$K_{1311}=c_{76};\ K_{1312}=0;\ K_{1313}=c_{77};\ K_{1314}=0;\ K_{1315}=c_{78};$$

$$K_{1316}=ncp_{78};\ K_{1317}=c_{79};\ K_{1318}=0;\ K_{1319}=c_{710};\ K_{1320}=0$$

The elements of 14th row are:

$$K_{141}=0;\ K_{142}=c_{71};\ K_{143}=-ncp_{72};\ K_{144}=c_{72};\ K_{145}=-ncp_{73};$$

$$K_{146}=c_{73};\ K_{147}=-ncp_{74};\ K_{148}=c_{74};\ K_{149}=-ncp_{75};\ K_{1410}=c_{75};$$

(D.131-140)

$$K_{1411}=0;\ K_{1412}=c_{76};\ K_{1413}=0;\ K_{1414}=c_{77};\ K_{1415}=-ncp_{78};$$

$$K_{1416}=c_{78};\ K_{1417}=0;\ K_{1418}=c_{79};\ K_{1419}=0;\ K_{1420}=c_{710}$$

The elements of 15th row are:

$$K_{151}=0;\ K_{152}=ncp_{81};\ K_{153}=c_{82}-n^2cdp_{82};\ K_{154}=ncp_{82};$$

$$K_{155}=c_{83}-n^2cdp_{83};K_{156}=ncp_{83};\ K_{157}=c_{84}-n^2cdp_{84};\ K_{158}=ncp_{84};$$

$$K_{159}=c_{85}-n^2cdp_{85};\ K_{1510}=ncp_{85};\ K_{1511}=c_{86};\ K_{1512}=0;$$

$$K_{1513}=0;\ K_{1514}=ncp_{87};\ K_{1515}=c_{88};K_{1516}=ncp_{88};$$

$$K_{1517}=0;\ K_{1518}=ncp_{89};\ K_{1519}=0;\ K_{1520}=ncp_{810}$$

(D.141-150)

The elements of 16th row are:

$$K_{161}=-ncp_{81};\ K_{162}=0;\ K_{163}=-ncp_{82};\ K_{164}=c_{82}-n^2cdp_{82};$$

$$K_{165}=-ncp_{83};K_{166}=c_{83}-n^2cdp_{83};\ K_{167}=-ncp_{84};\ K_{168}=c_{84}-n^2cdp_{84};$$

$$K_{169}=-ncp_{85};\ K_{1610}=c_{85}-n^2cdp_{85};\ K_{1611}=0;\ K_{1612}=c_{86};$$

$$K_{1613}=-ncp_{87};\ K_{1614}=0;\ K_{1615}=-ncp_{88};\ K_{1616}=c_{88};$$

$$K_{1617}=-ncp_{89};\ K_{1618}=0;\ K_{1619}=-ncp_{810};\ K_{1620}=0$$

(D.151-160)

The elements of 17th row are:

$$K_{171}=c_{91};\ K_{172}=0;\ K_{173}=c_{92};\ K_{174}=ncp_{92};\ K_{175}=c_{93};$$

$$K_{176}=ncp_{93};\ K_{177}=c_{94};\ K_{178}=ncp_{94};\ K_{179}=c_{95};\ K_{1710}=ncp_{95};$$

(D.161-170)

$$K_{1711}=c_{96};\ K_{1712}=0;\ K_{1713}=c_{97};\ K_{1714}=0;\ K_{1715}=c_{98};$$

$$K_{1716}=0;\ K_{1717}=c_{99};\ K_{1718}=0;\ K_{1719}=c_{910};\ K_{1720}=ncp_{910}$$

The elements of 18th row are:

$$K_{181}=0;\ K_{182}=c_{91};\ K_{183}=-ncp_{92};\ K_{184}=c_{92};\ K_{185}=-ncp_{93};$$

$$K_{186}=c_{93};\ K_{187}=-ncp_{94};\ K_{188}=c_{94};\ K_{189}=-ncp_{95};\ K_{1810}=c_{95};$$

$$K_{1811}=0;\ K_{1812}=c_{96};\ K_{1813}=0;\ K_{1814}=c_{97};\ K_{1815}=0; \qquad \text{(D.171-180)}$$

$$K_{1816}=c_{98};\ K_{1817}=0;\ K_{1818}=c_{99};\ K_{1819}=-ncp_{910};\ K_{1820}=c_{910}$$

The elements of 19th row are:

$$K_{191}=0;\ K_{192}=ncp_{101};\ K_{193}=c_{102}-n^2cdp_{102};\ K_{194}=ncp_{102};$$

$$K_{195}=c_{103}-n^2cdp_{103};K_{196}=ncp_{103};\ K_{197}=c_{104}-n^2cdp_{104};\ K_{198}=ncp_{104};$$

$$K_{199}=c_{105}-n^2cdp_{105};\ K_{1910}=ncp_{105};K_{1911}=c_{106};\ K_{1912}=0;$$

$$K_{1913}=0;\ K_{1914}=ncp_{107};\ K_{1915}=0;K_{1916}=ncp_{108};$$

$$K_{1917}=0;\ K_{1918}=ncp_{109};\ K_{1919}=c_{1010};\ K_{1920}=ncp_{1010} \qquad \text{(D.181-190)}$$

The elements of 20th row are:

$$K_{201} = -ncp_{101};\ K_{202} = 0;\ K_{203} = -ncp_{102};\ K_{204} = c_{102} - n^2 cdp_{102};$$

$$K_{205} = -ncp_{103};\ K_{206} = c_{103} - n^2 cdp_{103};\ K_{207} = -ncp_{104};\ K_{208} = c_{104} - n^2 cdp_{104};$$

$$K_{209} = -ncp_{105};\ K_{2010} = c_{105} - n^2 cdp_{105};\ K_{2011} = 0;\ K_{2012} = c_{106};$$

$$K_{2013} = -ncp_{107};\ K_{2014} = 0;\ K_{2015} = -ncp_{108};K_{2016} = 0;$$

$$K_{2017} = -ncp_{109};\ K_{2018} = 0;\ K_{2019} = -ncp_{1010};\ K_{2020} = c_{1010}$$

(D.191-200)

In the Equations (D1.1) – (D1.200), n is the circumferential wave number; c_{ij}, cp_{ij} and cdp_{ij} are coefficients of the homogeneous part in the fundamental system of equations derived in Section 3.2 and given in detail in Appendix A

APPENDIX E

THE ELEMENTS OF COEFFICIENT MATRIX KB

The transformed nonhomogeneous coefficients $B^{(1)}$ and $B^{(2)}$ of the fundamental system of equations are given by Equation (3.3.62). This equation can be written as

$$\begin{Bmatrix} B^{(1)} \\ B^{(2)} \end{Bmatrix}_{20\times 1} = [KB]_{20\times 18} \begin{bmatrix} (p_\zeta)_{nc}, (p_\zeta)_{ns}, (p_\phi)_{nc}, (p_\phi)_{ns}, (p_\theta)_{nc}, (p_\theta)_{ns}, \\ (N_\phi^T)_{nc}, (N_\phi^T)_{ns}, (N_\theta^T)_{nc}, (N_\theta^T)_{ns}, (N_{\phi\theta}^T)_{nc}, (N_{\phi\theta}^T)_{ns}, \\ (M_\phi^T)_{nc}, (M_\phi^T)_{ns}, (M_\theta^T)_{nc}, (M_\theta^T)_{ns}, (M_{\phi\theta}^T)_{nc}, (M_{\phi\theta}^T)_{ns} \end{bmatrix}_{18x1}^T \tag{E.1}$$

where the elements of 1st row are

$$KB_{1j} = 0 \qquad (j = 1,2,...18) \tag{E.2}$$

The elements of 2nd row are

$$KB_{2j} = 0 \qquad (j = 1,2,...18) \tag{E.3}$$

The elements of 3rd row are

$$KB_{37} = KB_{38} = CB_{24} \tag{E.4}$$

$$KB_{311} = KB_{312} = CB_{26} \tag{E.5}$$

$$KB_{313} = KB_{314} = CB_{27} \quad \text{(E.6)}$$

$$KB_{317} = KB_{318} = CB_{29} \quad \text{(E.7)}$$

The elements of 4th row are

$$KB_{47} = KB_{48} = CB_{24} \quad \text{(E.8)}$$

$$KB_{411} = KB_{412} = CB_{26} \quad \text{(E.9)}$$

$$KB_{413} = KB_{414} = CB_{27} \quad \text{(E.10)}$$

$$KB_{417} = KB_{418} = CB_{29} \quad \text{(E.11)}$$

The elements of 5th row are

$$KB_{57} = KB_{58} = CB_{34} \quad \text{(E.12)}$$

$$KB_{511} = KB_{512} = CB_{36} \quad \text{(E.13)}$$

$$KB_{513} = KB_{514} = CB_{37} \quad \text{(E.14)}$$

$$KB_{517} = KB_{518} = CB_{39} \quad \text{(E.15)}$$

The elements of 6th row are

$$KB_{57} = KB_{68} = CB_{34} \quad \text{(E.16)}$$

$$KB_{611} = KB_{612} = CB_{36} \quad \text{(E.17)}$$

$$KB_{613} = KB_{614} = CB_{37} \quad \text{(E.18)}$$

$$KB_{617} = KB_{618} = CB_{39} \quad \text{(E.19)}$$

The elements of 7th row are

$$KB_{77} = KB_{78} = CB_{44} \quad \text{(E.20)}$$

$$KB_{711} = KB_{712} = CB_{46} \quad \text{(E.21)}$$

$$KB_{713} = KB_{714} = CB_{47} \quad \text{(E.22)}$$

$$KB_{717} = KB_{718} = CB_{49} \quad \text{(E.23)}$$

The elements of 8th row are

$$KB_{87} = KB_{88} = CB_{44} \quad \text{(E.24)}$$

$$KB_{811} = KB_{812} = CB_{46} \quad \text{(E.25)}$$

$$KB_{813} = KB_{814} = CB_{47} \quad \text{(E.26)}$$

$$KB_{817} = KB_{818} = CB_{49} \quad \text{(E.27)}$$

The elements of 9th row are

$$KB_{97} = KB_{98} = CB_{54} \quad \text{(E.28)}$$

$$KB_{911} = KB_{912} = CB_{56} \quad \text{(E.29)}$$

$$KB_{913} = KB_{914} = CB_{57} \quad \text{(E.30)}$$

$$KB_{917} = KB_{918} = CB_{59} \quad \text{(E.31)}$$

The elements of 10th row are

$$KB_{107} = KB_{108} = CB_{54} \quad \text{(E.32)}$$

$$KB_{1011} = KB_{1012} = CB_{56} \quad \text{(E.33)}$$

$$KB_{1013} = KB_{1014} = CB_{57} \quad \text{(E.34)}$$

$$KB_{1017} = KB_{1018} = CB_{59} \quad \text{(E.35)}$$

The elements of 11th row are

$$KB_{111} = KB_{112} = CB_{61} \quad \text{(E.36)}$$

$$KB_{117} = KB_{118} = CB_{64} \quad \text{(E.37)}$$

$$KB_{119} = KB_{1110} = CB_{65} \quad \text{(E.38)}$$

$$KB_{1111} = KB_{1112} = CB_{66} \quad \text{(E.39)}$$

$$KB_{1113} = KB_{1114} = CB_{67} \quad \text{(E.40)}$$

$$KB_{1117} = KB_{1118} = CB_{69} \quad \text{(E.41)}$$

The elements of 12th row are

$$KB_{121} = KB_{122} = CB_{61} \quad \text{(E.42)}$$

$$KB_{127} = KB_{128} = CB_{64} \quad \text{(E.43)}$$

$$KB_{129} = KB_{1210} = CB_{65} \quad \text{(E.44)}$$

$$KB_{1211} = KB_{1212} = CB_{66} \quad \text{(E.45)}$$

$$KB_{1213} = KB_{1214} = CB_{67} \quad \text{(E.46)}$$

$$KB_{1217} = KB_{1218} = CB_{69} \quad \text{(E.47)}$$

The elements of 13th row are

$$KB_{133} = KB_{134} = CB_{72} \quad \text{(E.48)}$$

$$KB_{137} = KB_{138} = CB_{74} \quad \text{(E.49)}$$

$$KB_{139} = KB_{1310} = CB_{75} \quad \text{(E.50)}$$

$$KB_{1311} = KB_{1312} = CB_{76} \quad \text{(E.51)}$$

$$KB_{1313} = KB_{1314} = CB_{77} \quad \text{(E.52)}$$

$$KB_{1317} = KB_{1318} = CB_{79} \quad \text{(E.53)}$$

The elements of 14th row are

$$KB_{143} = KB_{144} = CB_{72} \quad \text{(E.54)}$$

$$KB_{147} = KB_{148} = CB_{74} \quad \text{(E.55)}$$

$$KB_{149} = KB_{1410} = CB_{75} \quad \text{(E.56)}$$

$$KB_{1411} = KB_{1412} = CB_{76} \quad \text{(E.57)}$$

$$KB_{1413} = KB_{1414} = CB_{77} \quad \text{(E.58)}$$

$$KB_{1417} = KB_{1418} = CB_{79} \quad \text{(E.59)}$$

The elements of 15th row are

$$KB_{155} = KB_{156} = CB_{83} \quad \text{(E.60)}$$

The elements of 16th row are

$$KB_{165} = KB_{166} = CB_{83} \quad \text{(E.61)}$$

The elements of 17th row are

$$KB_{177} = KB_{178} = CB_{94} \quad \text{(E.62)}$$

$$KB_{1711} = KB_{1712} = CB_{96} \quad \text{(E.63)}$$

$$KB_{1713} = KB_{1714} = CB_{97} \quad \text{(E.64)}$$

$$KB_{1715} = KB_{1716} = CB_{98} \quad \text{(E.65)}$$

$$KB_{1717} = KB_{1718} = CB_{99} \quad \text{(E.66)}$$

The elements of 18th row are

$$KB_{187} = KB_{188} = CB_{94} \quad \text{(E.67)}$$

$$KB_{1811} = KB_{1812} = CB_{96} \quad \text{(E.68)}$$

$$KB_{1813} = KB_{1814} = CB_{97} \quad \text{(E.69)}$$

$$KB_{1815} = KB_{1816} = CB_{98} \quad \text{(E.70)}$$

$$KB_{1817} = KB_{1818} = CB_{99} \quad \text{(E.71)}$$

The elements of 19th row are

$$KB_{19\,j} = 0 \qquad (j = 1,2,...18) \tag{E.72}$$

The elements of 20th row are

$$KB_{20\,j} = 0 \qquad (j = 1,2,...18) \tag{E.73}$$

In the Equations (D.4) – (D.71), CB_{ij} are the coefficients that relate the nonhomogeneous coefficients B_i to the loading terms through the Equation (B.1), and they are given in detail in Appendix B.